Fluorescence probes for the detection of biologically relevant species

Gardiner, Jordan

Award date:
2019

Awarding institution:
University of Bath

Copyright Notice

Candidate's signature……..

Restrictions on Use and Licensing

Access to this thesis/portfolio in print or electronically is restricted until……

Signed on behalf of the Doctoral College.....

Declaration of any previous submission of the work

The material presented here for examination for the award of a higher degree by research has been incorporated into a submission for another degree. Two sensors (97 & 103) and the TCF based sensors have been used in the thesis of Dr Adam C. Sedgewick at the University of Bath for the degree of Ph.D.

Candidate's signature……..

Declaration of authorship

I am the author of this thesis, and the work described therein was carried out by myself personally, with the exception of chapters 3 & 4 where 50% of the work was carried out by Dr Adam C. Sedgewick.

Candidate's signature……..

Fluorescent probes for the detection of biologically relevant species

Jordan Edward Gardiner

A thesis submitted for the degree of Doctor of Philosophy

University of bath

Department of Chemistry

May 2019

Table of contents

Abstract

Detection of chemical species in physiological systems is of great importance in the research and investigation of human diseases. Fluorescence spectroscopy has proven itself as an essential tool for the study of targets in biological systems. It is a reliable method for the semi-quantitative analysis of target analytes and provides a near unprecedented level of spatial and temporal resolution. As such, there is a need for increased specificity and new modes of detection within the field of fluorescent probes which drives research and development in the area.

An introduction to the background of fluorescence is given herein, with explanations of the common mechanisms of fluorescence. Then, analytes that are commonly targeted for detection and probes that have been designed to target them are exemplified. Three research chapters follow, describing the design, synthesis and analysis of new probes developed throughout this thesis. Coumarin, fluorescein and TCF fluorophores are used as core units in each of the chapters formed. Probes that have been developed include MLGs for dual analyte "AND" detection, that require the presence of two species for a signal to be released. A coumarin-based triple analyte "AND" probe has also been developed that required the presence of Glutamate, $Zinc^{2+}$ and peroxynitrite ($ONOO^-$), which has the potential to detect diseased neurons in the brain. Single analyte TCF-based probes have also been developed for the detection of $ONOO^-$ and glutathione. A number of these probes have been studied in cellular systems and show great promise for use in the study of human disease and revealing important information between the relationships of chemicals therein.

Acknowledgements

Thanks must first go to Professor Tony D. James, for the supervision and support that has been a constant in the time I have spent at the University of Bath. Steven D. Bull has also provided advice and guidance throughout many difficult projects and challenging syntheses. Thanks must also go to my secondary supervisor Jean Van Den Elsen for the support and help he has offered with regards to the biological projects I have been involved in and support in the prospecting for new ones.

Dr Adam C. Sedgwick has been the lead Ph.D. in the James group for the majority of my time at Bath and we have worked together a huge amount in the synthesis and analysis of the new probes. I thank him massively for his determination and the wisdom he offered me. Group members Maria Odyniec, Maria Weber and Luling Wu are also in reception of great thanks for their help and support in the lab. Dr Liam Stephens, of the Bull group, provided much humour and entertainment in the lab, which always lifted spirits. Daniel Sanz Sharley and I started at the same time and we have spent many lunches together, discussing troublesome syntheses and possible solutions to them, which I thank him for thoroughly. Also, Dr William Cunningham and other members of the Bull group, past and present have always helped with reaction conditions and offered valuable advice, which I am very thankful for.

Bethany Patenall, Lauren Gwynne, Laura Wallace and George Williams, of the Jenkins group at Bath have all aided me at times over the duration of my stay and have been very good friends, offering support and the offer of coffee at a moment's notice.

Thanks must also go to all those whom have collaborated to produce the results in this thesis, including cellular images by Xiao-Peng He, and enzyme studies by Robert Elmes.

Finally I must thank the EPSRC and the University of Bath for the funding and the facilities that have enabled me to carry out this valuable research.

Abbreviations

%	Percent
=N-	Imine group
µM	Micro molar
µmol	Micro moles
$^1O_2$	Singlet Oxygen
2,4-DNBS`	2,4-dinitrobenzene sulfonyl ester
A	Absorbance
Å	Angstrom
AAPH	2, 2'-azobis (2-amidinopropane) dihydrochloride
AAs	Amino acids
Ac_2O	Acetic anhydride
AcOH	Acetic acid
AD	Alzheimer's disease
AIBN	2,2′-Azobis(2-methylpropionitrile)
AIE	Aggregation induced emission
BIAB	[acetyloxy(phenyl)-λ_3-iodanyl] acetate
Bpin	Boronic acid pinacol ester
c	Concentration
C=O	Carbonyl group
-C≡N	Cyano group
CA	Caffeic Acid
CFP	Cyan fluorescent protein
$CH_3^{\bullet}$	Methyl radical
$CHCl_3$	Dichloromethane

ClO^-	Hypochlorite anion
CO_2	Carbon dioxide
Cr^{3+}	Chromium 3+ ion
Cu	Copper
CVD	Cardiovascular disease
Cys	Cysteine
DCDHF	Dicyanomethylenedihydrofuran
DCF	Dichlorofluorescein
DCM	Dicyanomethylene-4H-pyran
DIPEA	Diisopropylethyl amine
DMA	Dimethyl anthracene
DMF	Dimethylformamide
DMSO	Dimethyl sulfoxide
DNA	Deoxyribonucleic acid
E_{abs}	Absorbance energy
E_{em}	Emission energy
EMS	Electro-magnetic spectrum
ESI	Electrospray
ESIPT	Excited State Intramolecular Proton Transfer
EtOAc	Ethyl acetate
EtOH	Ethanol
F^-	Fluoride anion
FAD	Flavin adenine dinucleotide
Fe^{2+}	Iron 2+ ion
Fe^{3+}	Iron 3+ Ion
FITC	Fluorescein isothiocyanate
FMN	Flavin mononucleotide

FRET	Förster Resonance Energy Transfer
GLP	Good laboratory practice
Glu	Glutamate
Gly	Glycine
GSH	Glutathione
GSSG	Oxidised GSH dimer
h	Hours
H_2O	Water
H_2O_2	Hydrogen peroxide
H_2O_3	Dihydrogen trioxide
HB	Hydrogen bond
HBT	2-(2-hydroxyphenyl)benzothiazole
HCl	Hydrogen chloride
HClO	Hypochlorous acid
Hcys	Homocystine
Hg	Mercury
Hg^{2+}	Mercury 2+ ion
HMRS	High resolution mass spectrometry
HMTA	Hexamethylene-tetraamine
$HO^{\bullet}$	Hydroxyl radical
HOMO	Highest occupied molecular orbital
HPLC	High pressure liquid chromatography
IC	Internal conversion
ICT	Internal Charge Transfer
IR	Infra-red
ISC	Intersystem crossing
J	Coupling constant

K_2CO_3	Potassium carbonate
KI	Potassium iodide
KNO_2	Potassium nitrite
KO_2	Potassium oxide
K_{tet}	Tetrahedral ester rate formation
K_{trig}	Trigonal planar ester rate formation
l	Path length
L	Litre
LE	Locally excited
LOD	Limit of detection
LPS	Lipopolysaccharide
LUMO	Lowest unoccupied molecular orbital
Lys	Lysine
M	Molar
MeCN	Acetonitrile
MeOH	Methanol
Mg^{2+}	Magnesium 2+ ion
$MgSO_4$	Magnesium sulfate
MHz	Megahertz
min	Minutes
MLG	Molecular logic gate
mM	Milli molar
MPO	Myeloperoxidase
M_R	Molecular weight
MS	Mass spectrometry
N_2H_4	Hydrazine
Na_2SO_4	Sodium sulfate

NAC	*N*-Acetylcysteine
NADH	Nicotinamide adenine dinucleotide
NADPH	Nicotinamide-adenine dinucleotide phosphate
NaOAc	Sodium acetate
NBS	N-bromo succinimide
-NH_2	Amino group
NH_2NH_2•H_2O	Hydrazine hydrate
Ni^{2+}	Nickel 2+ ion
NIR	Near infra-red
NLO	Non-linear optics
nm	Nanometre
NMM	*N*-methylmaleimide
NMR	Nuclear magnetic resonance
$NO^{\bullet}$ / NO	Nitric oxide
NO_2^-	Nitrite anion
-NO_2	Nitro group
NO_3^-	Nitrate
NOS	Nitric oxide synthase
ns	Nanosecond
NTR	Nitroreductase
O_2	Molecular Oxygen
$O_2^{\bullet-}$	Superoxide
O_3	Ozone
^oC	Degrees centigrade
-OH	Hydroxyl group
OLED	Organic light emitting diode
-OMe	Methoxy group

$ONOO^-$	Peroxynitrite
OTBDMS	Tert-butyl di-methyl silyl group
PBS	Phosphate buffered saline
Pd	Palladium
PDT	Photodynamic therapy
PEG	Polyethylene glycol
PET	Photoinduced electron transfer
pK_a	Acid dissociation constant
$POCl_3$	Phosphorus oxychloride
PPM	Parts per million
RA	Rheumatoid arthritis
RBF	Round bottom flask
RNS	Reactive nitrogen species
$ROO^\bullet$	Peroxyl radical
ROS	Reactive oxygen species
RPT	Reverse proton transfer
RSH	Thiol compound
rt	Room temp
S	Singlet
s	Second
SIN-1	3-morpholinosydnoni3-morpholinosydnonimine mine
S_NAr	Nucleophilic aromatic substitution
SO_2	Sulfur dioxide
T	Triplet
TBAF	Tetrabutylammonium fluoride
TCF	Tricyanovinyldihydrofuran
TEMPO	(2,2,6,6-tetramethylpiperidin-1-yl)oxidanyl

THF	Tetrahydrofuran
TICT	Twisted internal charge transfer
TOF	Time of flight
UV	Ultra-violet
wt.	Weight
YFP	Yellow fluorescent protein
$Zn(OAc)_2$	Zinc diacetate
Zn^{2+}	Zinc 2+ ion
$ZnCl_2$	Zinc chloride
α	Alpha
β	Beta
δH / δC	Chemical shift hydrogen / carbon
ε	Molar absorbance coefficient
λ	Wavelength
λ_{abs}	Absorbance wavelength
λ_{em}	Emission wavelength
π	Pi
φ_F	Fluorescence quantum yield

1.0 Introduction

In this thesis, I present some of the work that I have completed while in Professor Tony James' group at the University of Bath, on the development of fluorescent probes for the detection of biologically relevant species. This chapter covers the background concepts of fluorescence and fluorescence spectroscopy. It gives details on the design of fluorescent sensors, examples of important biological analytes and probes that have been developed to detect them.

1.1 Fluorescence

Fluorescence and phosphorescence are two types of photoluminescence.[1] Defined as the emission of light from an electronically excited state, photoluminescence is an umbrella term used to describe many forms of light emission. The processes of fluorescence and phosphorescence are best described using a Jablonski diagram (**Figure 1**).

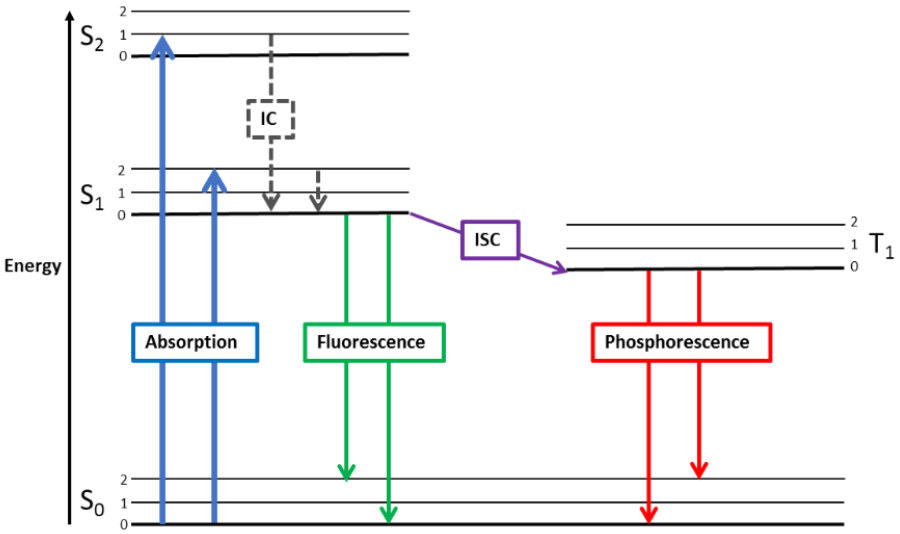

Figure 1 – A Jablonski diagram showing the S_0, S_1 and S_2 singlet energy levels and the T_1 triplet level. Internal conversion (IC), intersystem crossing (ISC) leading to fluorescence and phosphorescence are depicted.

In both processes, there is an initial excitation of an electron *via* an external light source. This promotes an electron into a higher vibrational level (S_1 or S_2). If the electron is in a higher energy state (S_2) it relaxes down to the lowest vibrationally excited state (S_1) *via* the process of internal conversion (IC). In fluorescence, this excited electron is still paired to

the spin of the ground state electron (having an opposite spin) so the relaxation of the electron is allowed and happens very quickly (~10^{-12} s).[2] In phosphorescence, spin conversion of the electron occurs as it undergoes intersystem crossing (ISC) from S_1 to T_1. When in the T_1 state, transition of the electron back to the S_0 state is now forbidden, because both electrons now have the same spin. This means that the process of phosphorescent relaxation from the T_1 state takes significantly longer (~10^{-2} s).[1]

Many substances exhibit fluorescent properties.[2] Once excited at a specific wavelength, the release of a photon at a different wavelength can be used as a reliable tool for semi-quantative analysis of the detection of fluorescent molecules. This has led to the development of a myriad of techniques that harness fluorescent materials as indicators and analytical tools.[3-7]

1.2 Harnessing fluorescence as a tool

The process of fluorescence spectroscopy is defined as the controlled excitement of a chemical species at a specific wavelength (routinely in the UV region) that results in emission of an electron at a longer wavelength (typically in the visible-IR region).[1]

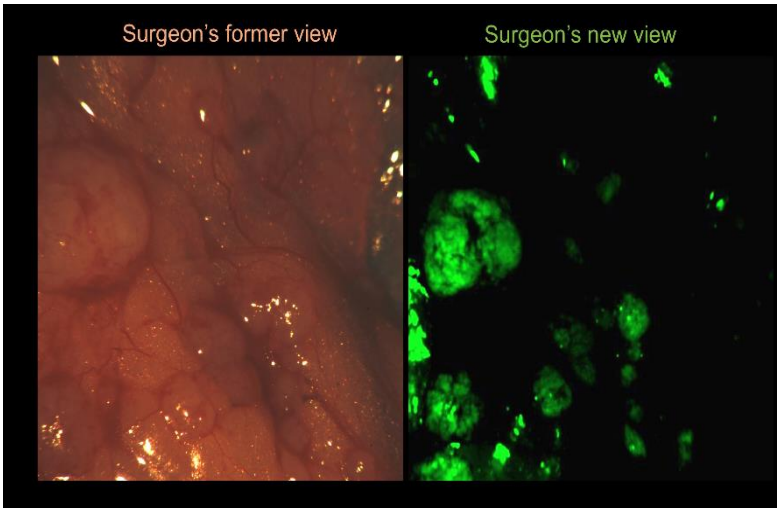

Figure 2 – An image taken from an ovarian surgery operation, with the surgeons' unaided view on the left and the use of a fluorescent surgical marker on the right. The probe is only activated in ovarian cancer cells and visually identifies the cancerous tissue that the surgeon needs to remove.[13]

Fluorescence spectroscopy is an analytical tool that can be employed for the detection of a wide array of chemical species through the use of fluorescent molecular probes.[3] These

probes interact with a target analyte in a defined fashion to cause a fluorescence response. The molecular nature of these probes and our ability to precisely detect light signals using laboratory equipment, means this technology is very well suited for interrogating biological pathways.[8]

Fluorescence analysis presents a non-invasive approach for the detection of specific chemical species in complex mixtures of potential targets. Detecting harmful chemicals within living systems, without destroying the system, offers huge benefits over many other detection methods. For example, mass spectrometry (MS) analysis requires the dissection of samples and their irrevocable alteration *via* the ionisation process.[9] Electrochemical and chromatographic techniques are also destructive methods of analysis that offer limited insight into real time processes in complex systems. In addition, many reactive species are extremely short lived and most other methods of analysis are too slow to detect them.[10] Conversely, a correctly designed fluorescent probe, already present in the biological system, can interact directly with these short-lived species to give a visual response.[10]

Fluorescent probes can provide us with whole sample analysis of living systems, with a near unprecedented level of spatial and temporal resolution being produced, due to their intrinsic sensitivity. It is for these reasons that fluorescent probes have been widely utilised for many biological applications. Fundamental biological research into complex reaction pathways within cells,[5] detection of harmful pollutants,[11] diagnostic tools for clinical analysis in hospitals[12] and targeted surgical aids[13] (**Figure 2**) are all modern uses of fluorescent probes that clearly demonstrate their value.

1.2.1 Fluorescence terminology

There are numerous specific terminologies that are used when analysing and describing fluorescence processes and this section describes some of the most important terms (**in bold**) required to understand the fluorescent process. *

Stokes shift is the difference between the wavelength of excitation (absorbance wavelength, λ_{abs}) and the emission wavelength (λ_{em}) (**Figure 3**). **Stokes fluorescence** can result when the light emitted from the fluorophore occurs at a longer wavelength than the light absorbed (e.g. $\lambda_{em} > \lambda_{abs}$ with $E_{abs} > E_{em}$). **Anti-Stokes fluorescence** results when the

light emitted from the fluorophore occurs at a shorter wavelength than the light absorbed ($\lambda_{em} < \lambda_{abs}$ with $E_{abs} < E_{em}$).

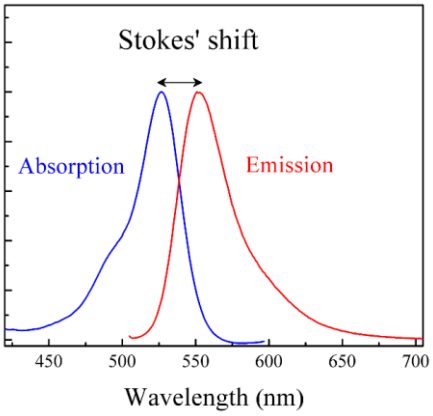

Figure 3 – An example of the absorption and emission of a typical molecule with the Stokes shift highlighted.

Fluorescence quantum yield (φ_F) is defined as the ratio of the number of photons emitted to the number of photons absorbed. A theoretically perfect value for a fluorophore would be 1, where all of the photons absorbed by a probe are re-emitted. However, not all photons are absorbed productively and thus quantum yields are typically lower than 1, fluorophores are typically still considered to be highly fluorescent even when they have a quantum yield as low as 0.1.

Molar absorbance (ε) describes the ability of a compound to absorb light at a specific wavelength. ε is a part of the Beer-Lambert law ($A = \varepsilon cl$), where (A) is absorbance, (c) is analyte concentration and (l) is the path length respectively.

Bathochromic shift is the change in spectral band position in the emission spectra of a molecule to a longer wavelength. **Hypsochromic shift** is the change in shift in spectral band of a molecule to a shorter wavelength. Both these types of shift are normally associated with changes in molecular structure and/or solvent polarity (**solvatochromism**).

*All definitions sourced from ref. 1.

1.3 Design of fluorescent probes

There are numerous ways to design chemical probes for specific fluorescence sensing applications, with a well-engineered probe required, if a targeted biological system is to be interrogated effectively.

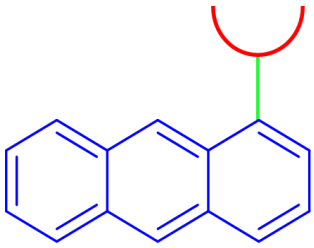

Figure 4 – General scheme of a sensor containing receptor (red), linker (green) and reporter (blue) units.

Classically, a three-component model has been used for the design of fluorescent probes for biological applications,[14] consisting of a receptor unit, a linker unit and a reporting unit (**Figure 4**). The receptor unit binds to the target analyte to produce an interaction that is relayed through a linker unit to modify the fluorescent properties of the reporter unit.

The type of interaction that occurs between the analyte and the receptor unit defines the nomenclature used to describe the probe. If the binding of the analyte to the probe is reversible, for example *via* non-covalent interactions, then the term used to describe the probe is a chemosensor. However, if irreversible changes occur when the analyte interacts with the probe, (e.g. *via* a chemical reaction occurring) then the correct term to describe the probe is a chemidosimeter. These definitions have been used in the literature to describe

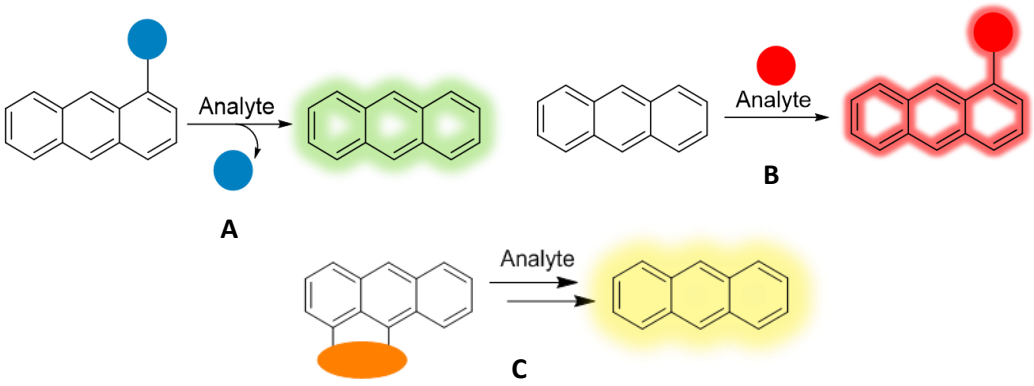

Figure 5 – Diagram showing the mechanism of action of three types of probe interacting with an analyte to produce a fluorescent response.
A = bond cleavage, B = ligand coordination, C = reaction cascade.

many different probes, with descriptions of the two types of sensor often having been used interchangeably in much of the recent literature. Therefore, for the ease of the reader, this thesis describes the former type of sensor as a 'fluorescent probe' and the latter type as a 'reaction based fluorescent probe', respectively. Two sub-sections of reaction-based probes are known as bond cleavage probes and reaction cascade probes. Whereas, bond cleavage probes typically require only a single reaction for the fluorescent signal to be generated (**Figure 5**), a reaction cascade probe requires more than one reaction to take place to produce a fluorescence response. The receptor units used in reactive probes are often described masking units, since they "mask" the fluorophore unit until a cleavage event occurs in the presence of the target analyte.

1.3.1 Receptor unit

The selectivity of the receptor unit is a crucial part of probe design, with a reliable, highly specific and easily modified chemical unit representing the ideal receptor. The receptor should ideally minimise off-target interactions, give a low detection limit and be easily modifiable in case structural alterations are needed. Additionally, the receptor, or reactive

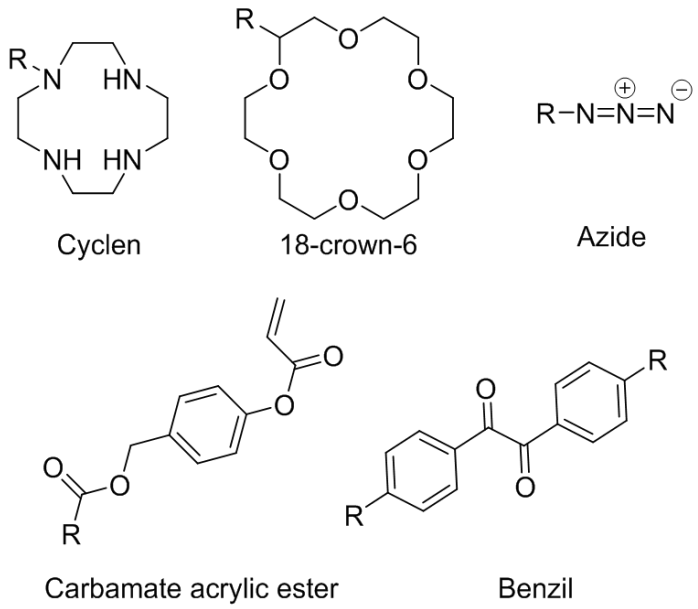

Figure 6 – Structures of a variety of receptor units that have been used as fluorescent probes. Cyclen and 18-crown-6 through metal coordination, azides can react with H_2S, acrylic esters can undergo conjugate addition reactions with cysteine residues, benzil groups react with H_2O_2.

chemical trigger, needs to be non-toxic so that any side products of the binding event (or reaction) that occur, do not interfere with the system being studied.

The design of receptor units varies hugely (**Figure 6**), with many chemical units having been designed to specifically target biologically important species within cellular environments. For example, many cyclic structures have been shown to reliably and reversibly bind metal ions, which occurs through donation of electron density from a heteroatom (typically nitrogen or oxygen) to a positively charged metal ion that results in the formation of a stable metal complex.[15]

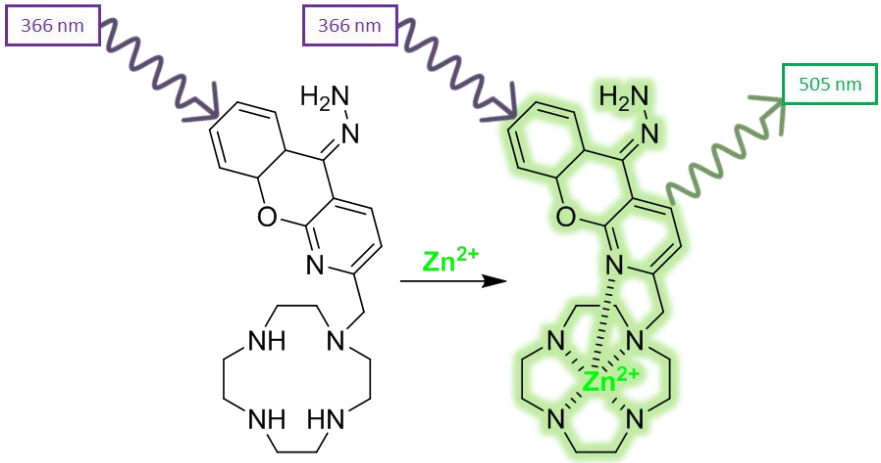

1

Figure 7 – Example of a probe (**1**) developed by Lemercier *et al.* that uses a cyclen receptor group to activate a fluorescent unit.

Two popular examples of macrocyclic sensors are cyclen ring systems containing multiple nitrogen atoms and 18-crown-6 ethers ring systems that contain multiple oxygen atoms. Lemercier has used cyclen for the detection of Zn^{2+} ions using an azaxanthone fluorophore in probe **1** (**Figure 7**).[15]

Alternatively, an azide moiety has been used by Chang *et al.* as a reliable reactive unit for the detection of hydrogen sulfide (H_2S).[16, 17] A chemical reaction occurs between the two groups that results in the reduction of the azide and oxidation of the H_2S. An amino-group is generated, resulting in activation of the fluorophore.

Boronic acids and boronic acid pinacol esters (Bpin) have been used extensively as receptor units for sensing applications *in vivo*.[18] They are capable of binding diol motifs and reacting with reactive oxygen species (e.g. peroxynitrite, **Figure 8**, **A** & **B**).

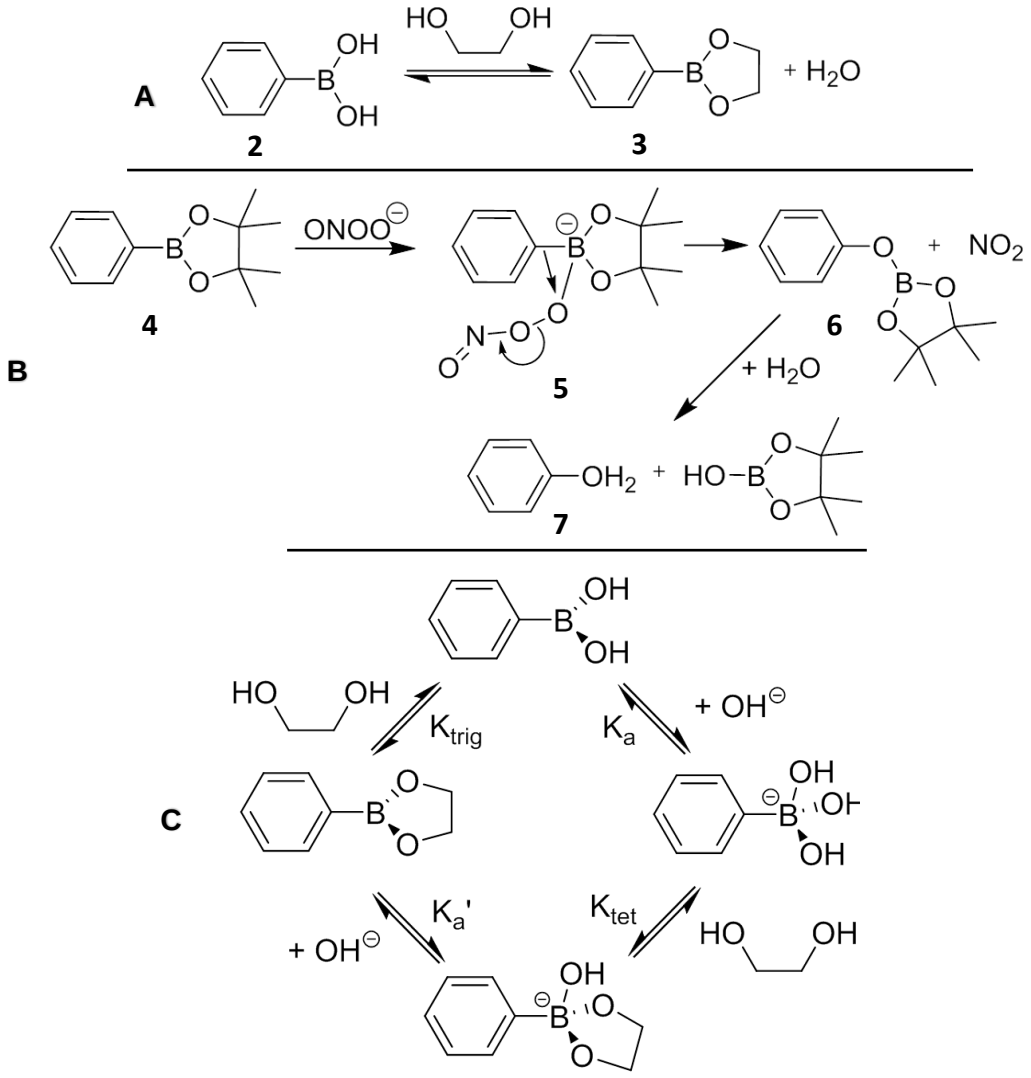

Figure 8 – (a) Coordination of a boronic acid **2** with a 1,2-diol produces a cyclic boronic ester **3**; (b) Reaction of an aryl boronic ester **4** with peroxynitrite affords an 'ate' complex **5** that decomposes through **6** to form phenol **7** and boronic acid pinacol ester. (c) The equilibrium system existing between boronic acid and a diol, forming trigonal and tetrahedral esters.

The coordination of diols to boronic acids has been used for the detection of carbohydrates since the early 1990's.[18] Boronic acid binds to a diol in an equilibrium system consisting of a trigonal planar boronic acid and a tetrahedral boronic acid (**Figure 8**, **C**). These are formed from either the planar neutral boronic acid molecule or the tetrahedral anionic boronic acid. The rate of formation of the tetrahedral ester (K_{tet}) is generally five orders of magnitude larger than that of the planar alternative (K_{trig}).[57] This results in favourable binding between a carbohydrate and boronic acid group occurring at a higher pH level.

Anthracene based sensors **8** and **9** (**Figure 9**) are two early examples of sensors that employed the boron functionality to bind carbohydrates.[18] Binding of the sensor to a vicinal diol unit of a sugar (e.g. glucose) results in their fluorescent anthracene moieties being turned 'on' (mechanism discussed in the following section).

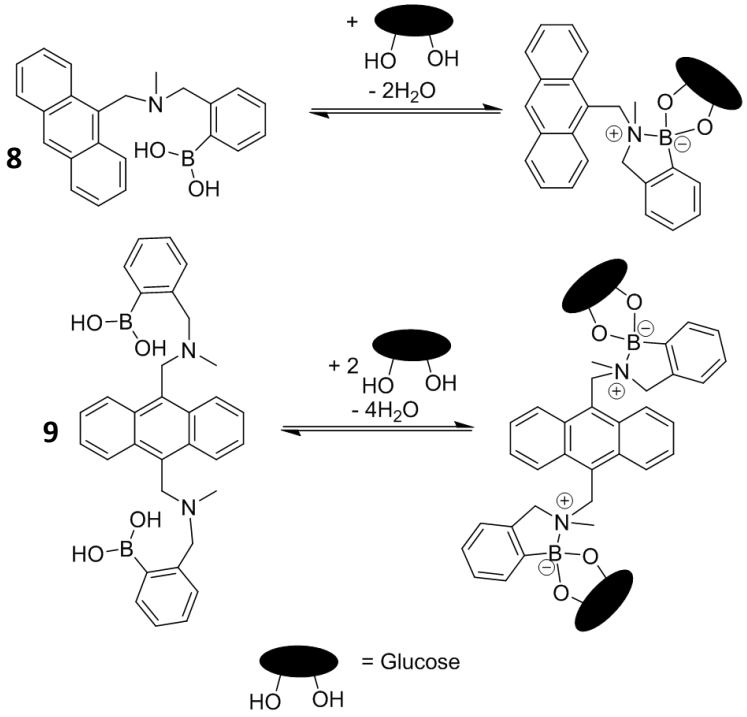

Figure 9 – Carbohydrate sensors **8** and **9**.

1.3.2 Reporter unit

The reporter unit is the fluorophore component of the probe. Numerous variables need to be considered when choosing a suitable fluorophore for a new sensor. Firstly, it is important that the fluorophore is non-toxic at the relevant sensing concentrations, to prevent damage to the biological system. Secondly, a probe with the right excitation / emission wavelengths for non-invasive imaging in cellular systems need to be used, with both parameters normally within the NIR or visible region. Irradiation of tissue with light from other regions of the electromagnetic spectrum (EMS) can potentially cause photo-damage to the tissue being irradiated.[5]

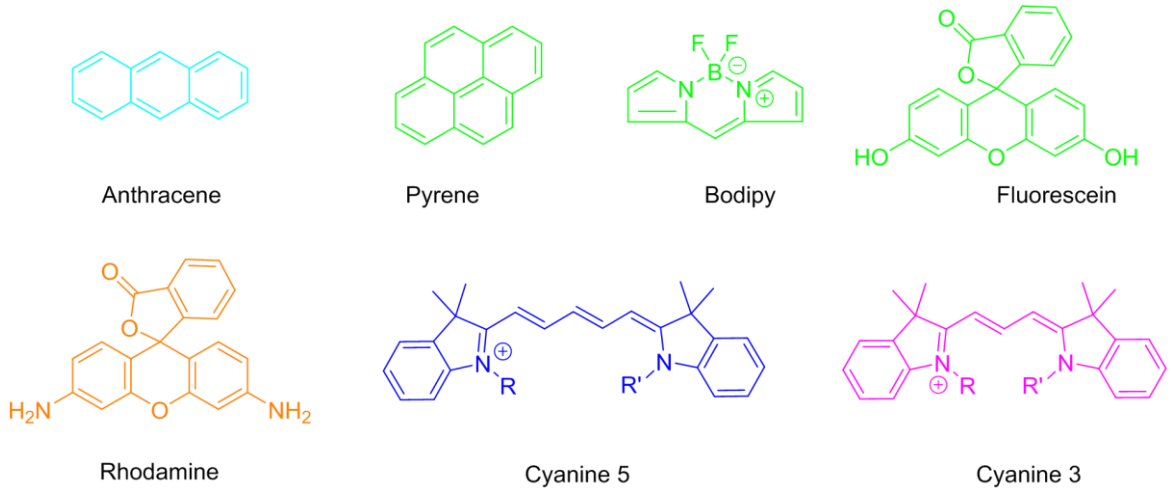

Figure 10 – A selection of commonly used fluorophores that have been used for fluorescent sensor design.

The fluorophore must also have a suitably high level of optical brightness (φ_F), so that the probe is easily distinguishable from any background fluorescence, with a low limit of detection meaning that a small quantity of probe can be used for sensing. Also, to be used in cellular studies, the fluorophore must have the correct balance of hydrophilicity and lipophilicity, ideally exhibiting good 'drug-like' properties. This enables effective transfer of the probe in cellular environments and allows the probe to pass more easily through cell membranes and increase cellular retention times. A wide range of different fluorescent molecules have been harnessed for use as chemical probes (**Figure 10**), whose mechanism of action is included the following sections.[2]

1.3.3 Linker unit

The linker that binds the receptor and the fluorophore must also be precisely designed, with respect to linker length, flexibility and its electronic properties, with an optimal linker required to position the reporter and binding units and modulate its solubility.

1.4 Fluorescence sensing mechanisms

Four important mechanisms that are commonly used as the basis of fluorescent probes will now be described, namely: Photoinduced Electron Transfer (PET), Förster Resonance Energy Transfer (FRET), Internal Charge Transfer (ICT), and Excited State Intramolecular Proton Transfer (ESIPT) sensors.

1.4.1 PET

Photoinduced electron transfer (PET) is one of the most widely utilised mechanisms harnessed for use in fluorescent probes. The process of PET involves excitation of an electron from the highest occupied molecular orbital (HOMO) of a fluorophore to its lowest unoccupied molecular orbital (LUMO). An electron from the HOMO of an 'unbound' receptor then moves to fill the HOMO of the fluorophore,[20] with this transfer event resulting in fluorescence quenching. The excited state electron in the LUMO of the fluorophore can then returns to the ground state *via* a non-radiative pathway (**Figure 11**).

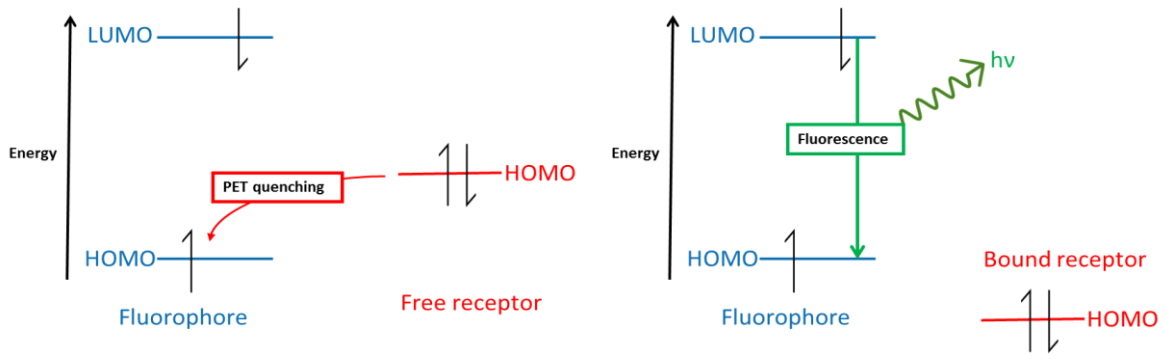

Figure 11 – An electronic diagram of the PET process (left) with the free (unbound) receptor quenching the fluorophore.

An essential requirement for this process to take place is close matching of the HOMO energy levels of the fluorophore and the unbound receptor, with the HOMO of the receptor being at a slightly higher level to allow movement of electrons to the HOMO of the fluorophore. An alternate state for the PET sensor occurs when the receptor is bound to the analyte which lowers the energy of the HOMO receptor and stops the quenching process. This results in radiative relaxation of the excited state electron in the fluorophore resulting in the probes fluorescence being turning 'on'.

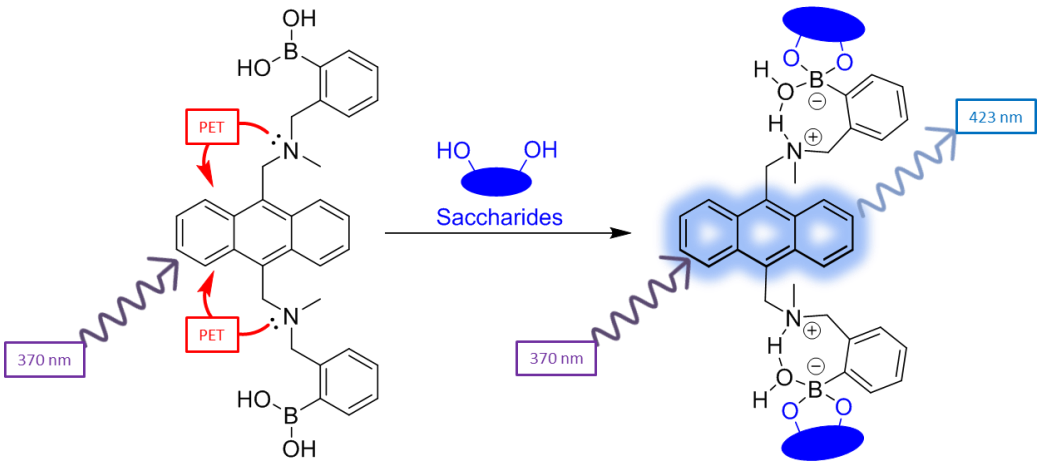

9

Figure 12 – A diagram depicting the mechanism of the PET process responsible for quenching the fluorescence of probe **9** and the PET quenching process that is stopped from binding of a diol saccharide unit to the boronic acid fragment, which turns on, allowing the fluorescence of the anthracene unit.

One of the best examples of a fluorescent probe using a PET mechanism is based on a bis-boronic acid that can be used to sense diol units on saccharides such as glucose or fructose. For example, Shinkai *et al.* developed sensor **9** that employed a PET mechanism for the detection of diol-containing saccharides in the early 1990s (**Figure 12**).[19] The lone pairs of the nitrogen atoms of the sensor **9** were found to quench the fluorescence of the anthracene fluorophore unit in its unbound state. Binding the diol motifs of one or two saccharide units to the boronic acid units of **9** resulted in the lone pair electrons of the nitrogen atoms hydrogen bonding to water molecules to generate their corresponding boronate anions. This results in loss of PET quenching of **9**, permitting the fluorescence of the anthracene

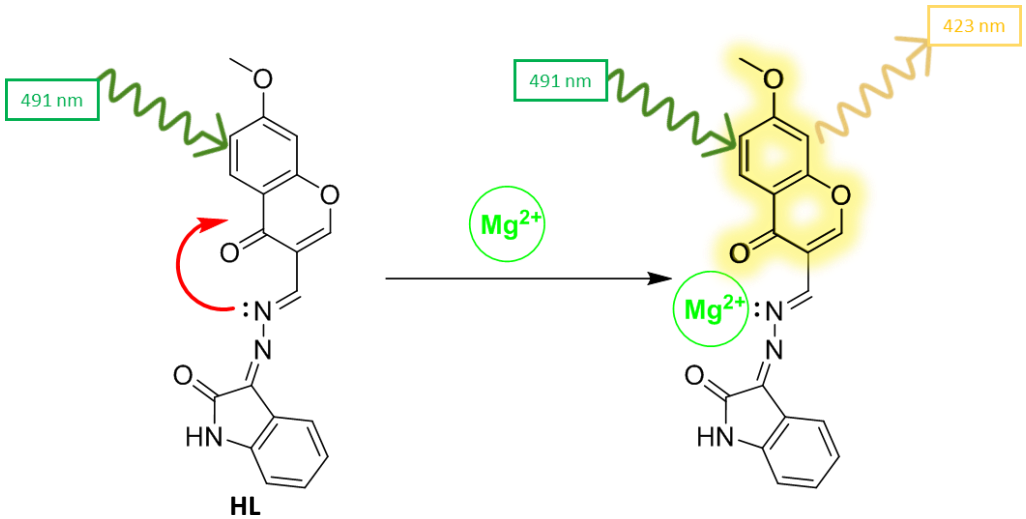

HL

Figure 13 – A diagram depicting the mechanism of the PET quenching process of probe **HL**, with binding of an Mg^{2+} ion resulting in the quenching process being eliminated, which results in fluorescence being turned on.

unit at 423 nm, when the sensor was excited at 370 nm.

In another example of a PET sensor, Yang *et al.* used a Schiff base derivative to develop a turn on fluorescent probe for Mg^{2+} ions (**HL**, **Figure 13**).[21] The nitrogen lone pairs of this sensor result in PET quenching of the fluorophore, with chelation of the Mg^{2+} ion then blocking this quenching event, which results in the fluorescence of the sensor being turned on.

1.4.2 FRET

Förster resonance energy transfer (FRET) is a process where two or more fluorophores can exchange their energies *via* long range dipole-dipole resonance interactions.[20] The main parameter influencing FRET is the ability to close match the energy levels of each of the fluorophores by bringing them together in close proximity (1 – 10 nm) (**Figure 14**).

The FRET process begins with the donor fluorophore being excited to a higher S_1 energy level, with the excited electron then relaxing slightly to the lowest vibrational state of the higher energy level, through ab internal conversion process. When the FRET acceptor is not close enough to the donor, this excited electron then decays back to the ground state, *via* a normal fluorescence process. The FRET acceptor has HOMO and LUMO orbitals

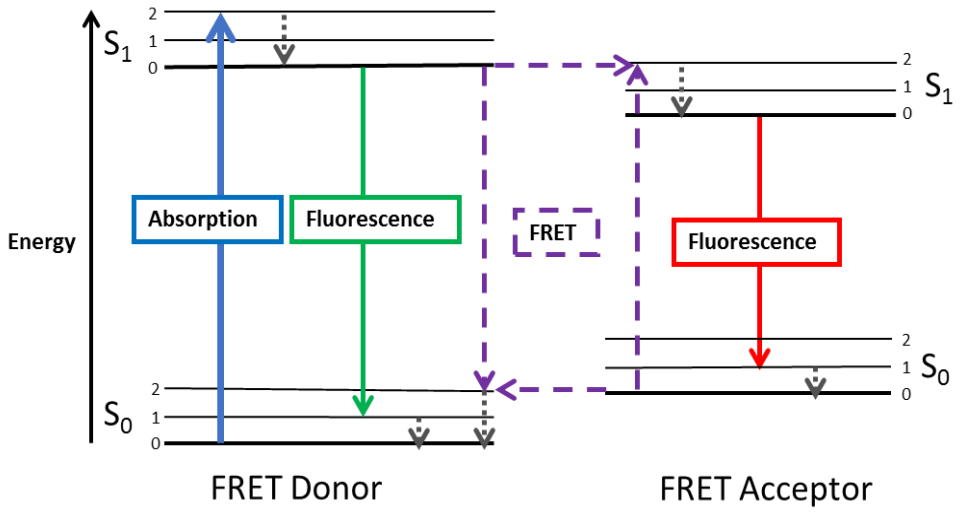

Figure 14 – A diagram depicting the mechanism of the FRET process. Initial excitation of the donor fluorophore is followed by relaxation to the lowest vibrational excited state of S_1 *via* internal conversion. A FRET process can then occur *via* energy transfer from the FRET donor to the FRET acceptor, which is caused by the similarity of their energy levels and their close proximity.

similar in energy to that of the donor. Therefore, once excited, the FRET donor can transfer energy to the FRET acceptor through a non-radiative dipole-dipole coupling mechanism. The efficiency of this energy transfer process is inversely proportional to $\times 10^6$ the distance between the two FRET units. The use of a fluorescence diagram is a popular method to depict the required emission overlap and excitation bands of the two donor-acceptor components (**Figure 15**).

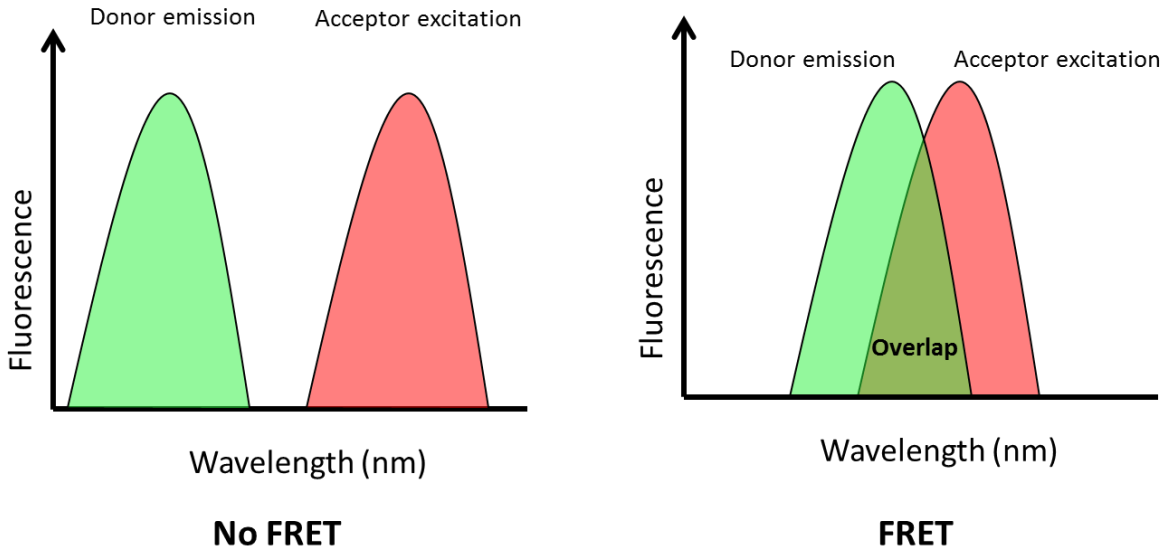

Figure 15 – A pictorial diagram of the spectral overlap required between the donor emission and the acceptor excitation peaks that is required for FRET to occur.

The use of this process is advantageous relative to other probes, since it can be reliably used to detect the distance between the FRET donor & acceptor pair.[22] Also, due to the transfer of energy from the excited state of the donor, the fluorescence intensity of

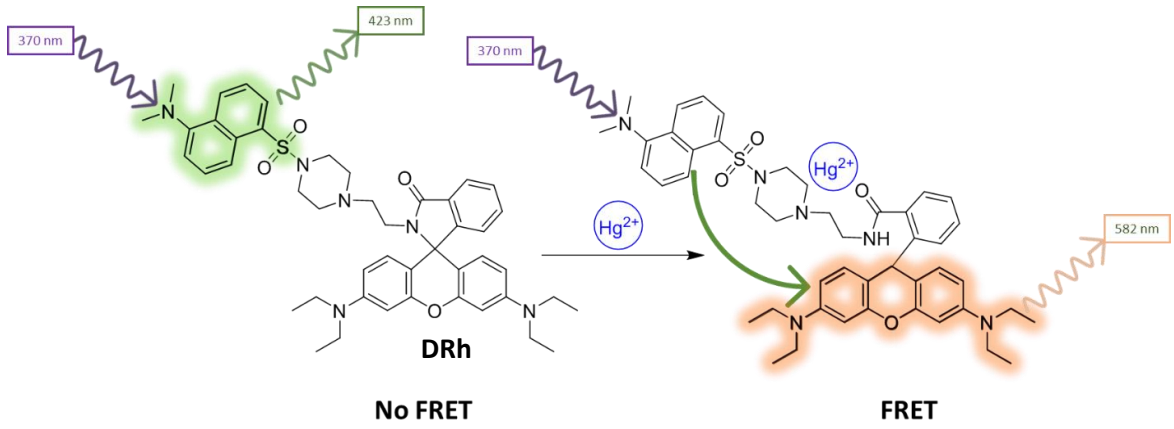

Figure 16 – A diagram of a FRET sensor used for detecting Hg^{2+}, depicting DRh in its unbound FRET off state and DRh-Hg^{2+} in its FRET on states.

emission of the donor decreases, as the excitation and emission of the acceptor increases, which allows a ratiometric relationship between the two emission peaks to be determined.

Li *et al*. used a fluorescent FRET based molecular probe (**DRh**)for the detection of mercury ions (Hg^{2+}) in water and living cells (**Figure 16**). A dansyl group was used as the donor and a rhodamine group as the acceptor, with the presence of Hg^{2+} ion resulting in ring-opening of the spirolactam ring of the rhodamine that results in a FRET process taking place.

Another example of the use of FRET in a fluorescent molecular probe is the work of Xing *et al.* who developed a FRET probe for proteolytic activity on cell surfaces (**MFP**).[23] This probe used a fluorescein donor and a dabcyl (4-(dimethylaminoazo)benzene-4-carboxamide) quencher, linked *via* a hexanoic acid and an enzyme active cleavable peptide (RVRRSVK). Upon enzymatic cleavage of the peptide linker by furin, the two units of the probe are separated, resulting in the fluorescence of the fluorescein unit being turned on (**Figure 17**).

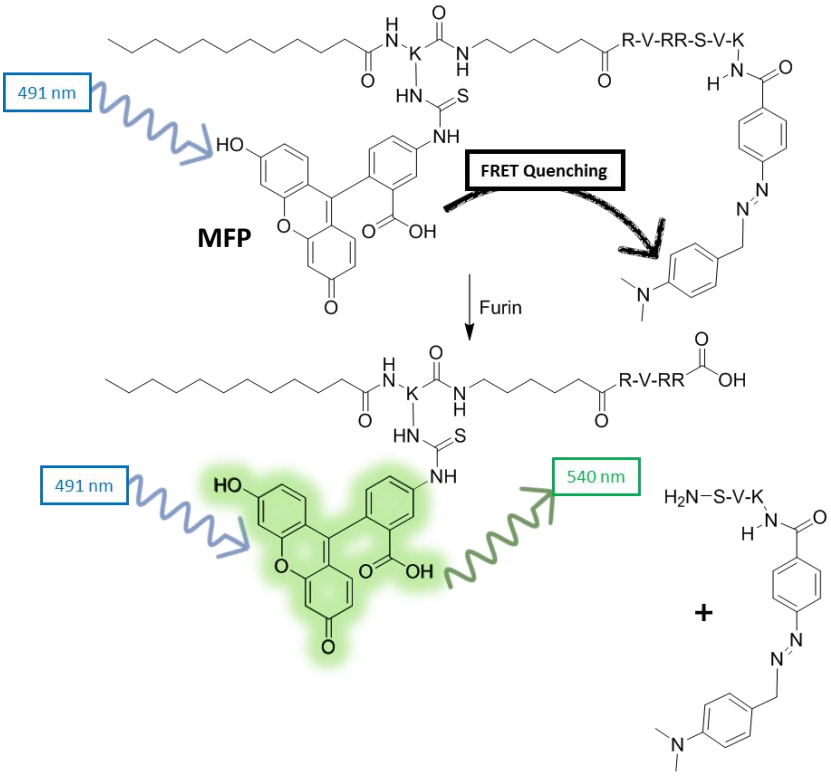

Figure 17 – A diagram of the FRET quenching that occurs in the probe **MFP**, with enzymatic cleavage of the quenching Dabcyl group by Furin, which results in the fluorescence of the fluorescein unit being turned on.

1.4.3 ICT

Internal charge transfer (ICT) is another mechanism used in the production of fluorescent molecular probes, which relies on intramolecular movement of charge. The main requirement for the occurrence of ICT in a system is the presence of both electron donating and electron accepting groups, which are commonly referred to as "push-pull" groups.[20]

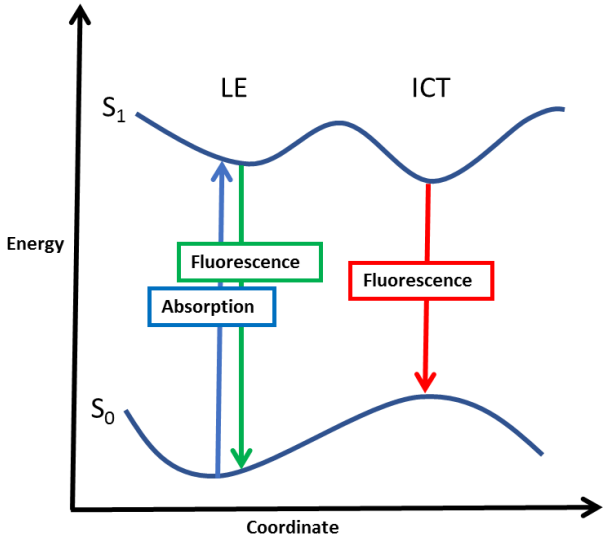

Figure 18 – Representation of the energy potential of the fluorophore in the LE and ICT state, with a bathochromic shift in the ICT state represented by the shorter red emission, relative to a larger green emission.

Excitation causes promotion of an electron in a locally excited state (LE) to an ICT state, which results in a substantial change in the dipole moment of the molecule. The ICT state offers a different, lower energy pathway for relaxation of the electron *via* a longer wavelength emission (**Figure 18**). Charge separated species are very sensitive to their environment, including the polarity of the solvent system, counterions in solution and their ability to participate in hydrogen bonding. Binding a receptor unit to either one of these groups can cause a change in the excitation / emission spectra that results in a ratiometric response to a specific analyte.[24]

Bharadwaj *et al.* employed an ICT process to develop a probe (**LP**) for the detection of Zn^{2+},[25] consisting of a benzothiazole electron acceptor unit and a terpyridine unit as an electron donor (**Figure 19**). The terpyridine unit binds to cationic Zn^{2+} which electron lowers the energy of the ground state, resulting in a blue shift to the probe fluorescence.

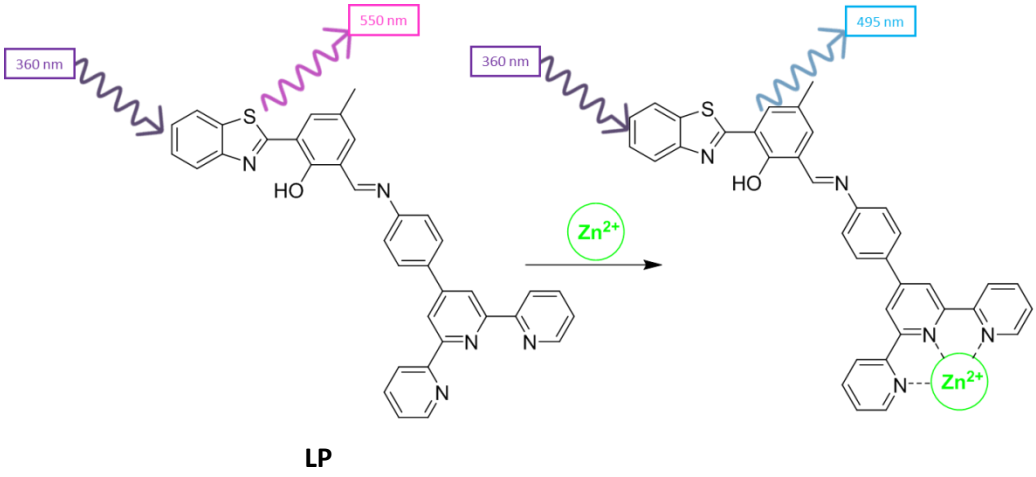

Figure 19 – ITC mode of action of the Zn^{2+} probe **LP**.

Lin *et al.* have recently reported an example of using an ITC fluorescent probe **PBD-FA** for the detection of formaldehyde (**Figure 20**).[26] This probe uses a benzoxadiazole fluorophore as the core unit, which contained an electron deficient homoallylamino group that is reactive towards formaldehyde. This reactive unit undergoes condensation with formaldehyde, followed by a 2-aza-Cope rearrangement and sequential hydrolysis, to form an active aldehyde fluorophore.

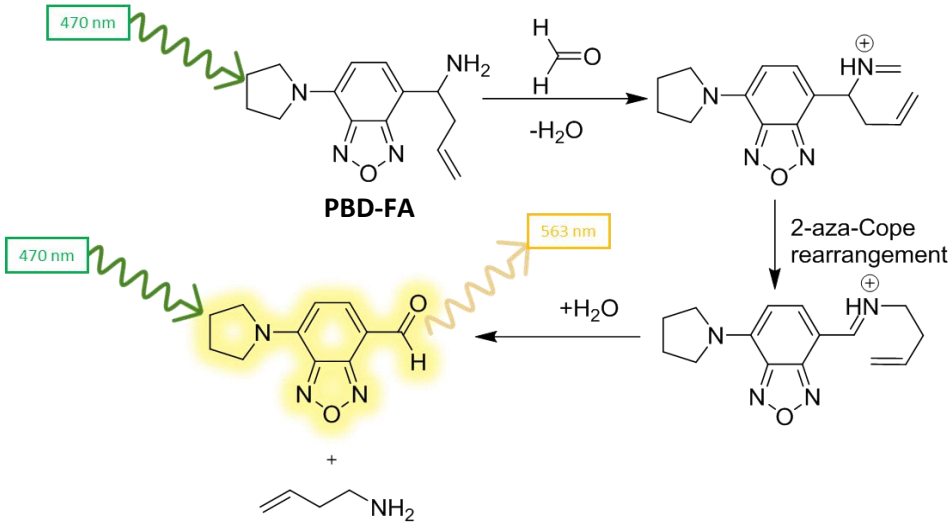

Figure 20 – Schematic of the cascade reactions that occur when the **PBD-FA** probe reacts with formaldehyde to afford a fluorophore.

1.4.4 ESIPT

Excited state intramolecular proton transfer (ESIPT) is a process whereby an electronically excited molecule relaxes through a tautomerisation event involving the movement of protons.[20] Typically, for this to occur, the sensor must contain an intramolecular hydrogen bond (HB) between a hydrogen donor (-OH or -NH_2) and a hydrogen bond acceptor (=N-, C=O). A popular method of incorporating ESIPT, involves the keto-enol tautomerisation of molecules such as 2-(2-hydroxyphenyl)benzothiazole (**HBT**) (**Figure 21**).

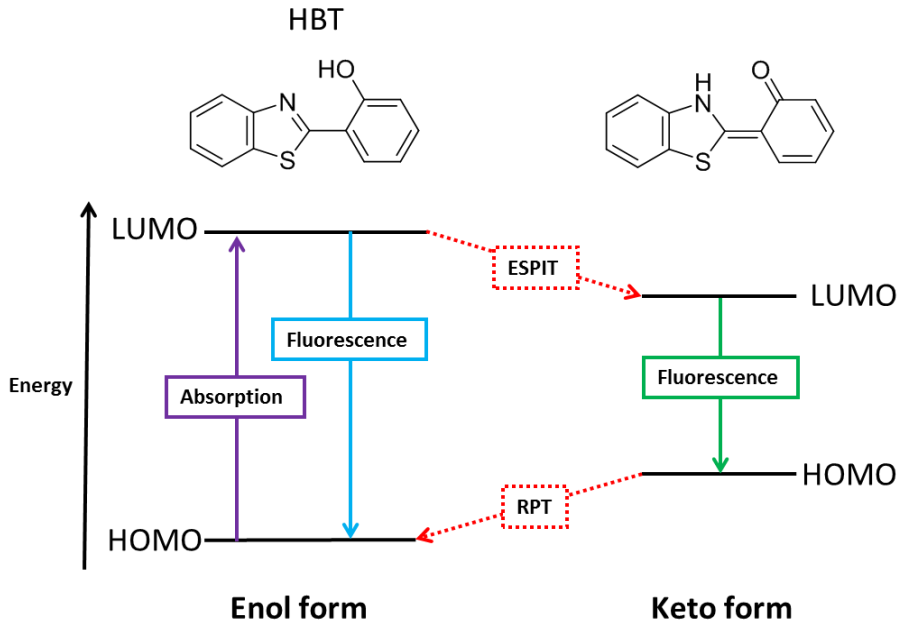

Figure 21 – Diagram of an ESIPT process that relies on the keto-enol tautomerisation of **HBT** with the emission of the keto form lower in energy (longer wavelength) than its enol form.

ESIPT is a four-level electron process, with the lowest energy state existing in the enol form. When excitation occurs, electron density shifts within the molecule resulting in the acidity of the HB donor group increasing, which coincides with a simultaneous increase in the basicity of the HB accepting group. This results in very rapid tautomerisation event between the enol and the keto forms of the fluorophore, with the keto form radiatively decaying to its ground state *via* a process of reverse proton transfer (RPT) to afford the original ground state enol.[20]

These electronic properties give ESIPT distinct advantages over other forms of fluorescence, because they result in a much larger Stokes shift when compared to ICT, whilst the two tautomeric forms also enable a ratiometric response to be determined.[27]

Fluorescent ESIPT probes typically function by blocking the HB donor site with a reactive receptor unit that can be cleaved by an analyte to reveal a fluorophore unit. An example of an ESIPT fluorophore used as a "turn off" probe (**10**) was developed in 2016 by Kim *et al.* with blocking of emission from the ESIPT process occurring through binding of a Zn^{2+} ion (**Figure 22**).[2]

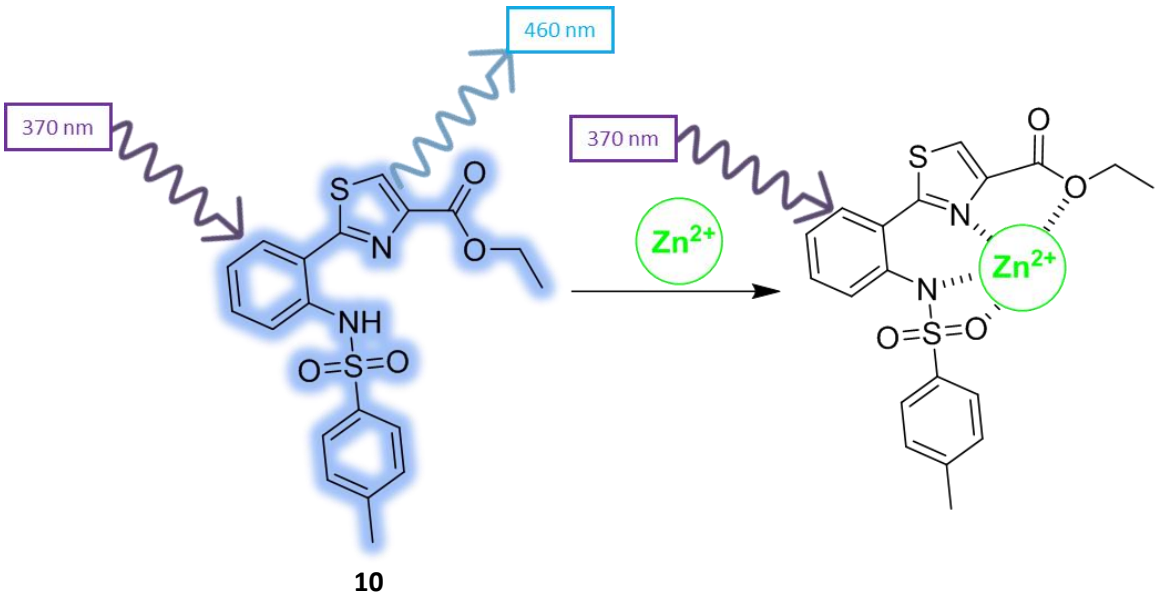

10

Figure 22 – Diagram of the on-off Zn^{2+} sensor **10** where binding action of zinc blocks the ESIPT process.

A second example of an ESIPT probe with a dual output mode was developed by Yang *et al.* for the detection of fluoride ions, probe **11**.[28] Fluoride sensitivity is gained using a tert-butyldiphenyl silyl group to block a HB donor -OH group that is then cleaved upon exposure to fluoride ion (**Figure 23**). The characteristic dual emission of the two tautomers of the fluorophore enabled the probe to be used as a ratiometric sensor. Initially, emission of the unreacted probe occurs at 416 nm, however, addition of aliquots of fluoride ion results in a decrease in this emission. *O*-silyl cleavage results in the emergence of a new longer wavelength emission corresponding to its keto form at 560 nm.

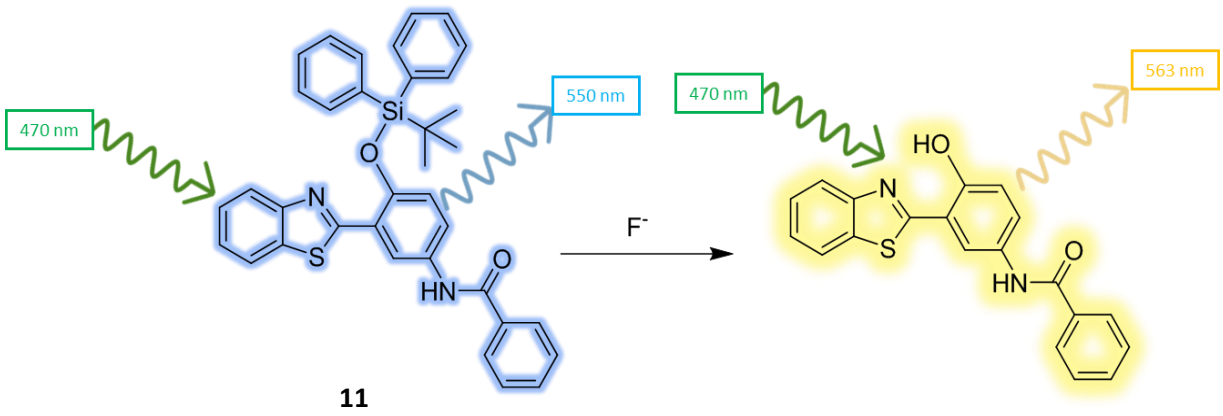

11

Figure 23 – Diagram of the dual emission sensor **11** of for the detection of fluoride.

1.5 Biological targets for fluorescent probes

A myriad of potential targets for fluorescent probes exist in biology, with the need to measure the existence, concentration and movement of specific analytes, ever-present for monitoring human health. Metal ions, amino acids, peptides, small molecules, reactive oxygen and reactive nitrogen species (ROS & RNS) can all serve as analytes that can be detected by chemical probes. In addition to detecting these individual species, cellular and physiological events can also be targeted, including changes in DNA and protein folding and variance in intracellular and extracellular pH levels.

A representative selection of different analytes will be discussed in the following section, with the reasoning and method employed for their detection described.

1.5.1 Metal ions

Metal ions are essential components in biological systems that play vital roles in the healthy functioning of cells.[30] Iron is present in haemoglobin, potassium and calcium are used as signalling ions and the use of manganese as a cofactor in superoxide dismutase are some of the many examples of the roles that metals have in the body.

Tight regulation of the concentration of metals in the body is essential, with lack of a specific metals leading to deficiency, while overabundance leads to toxicity.[30] Dysregulation of metal ions occurs in many diseases, including neurodegenerative diseases (Zn^{2+}),[31] diabetes (Ni^{2+})[32] and cancer (Fe^{2+}),[33] so an understanding of how metals are used and regulated in the cell is of great interest. Accordingly, many fluorescent probes have been successfully developed for the detection of metal ions.

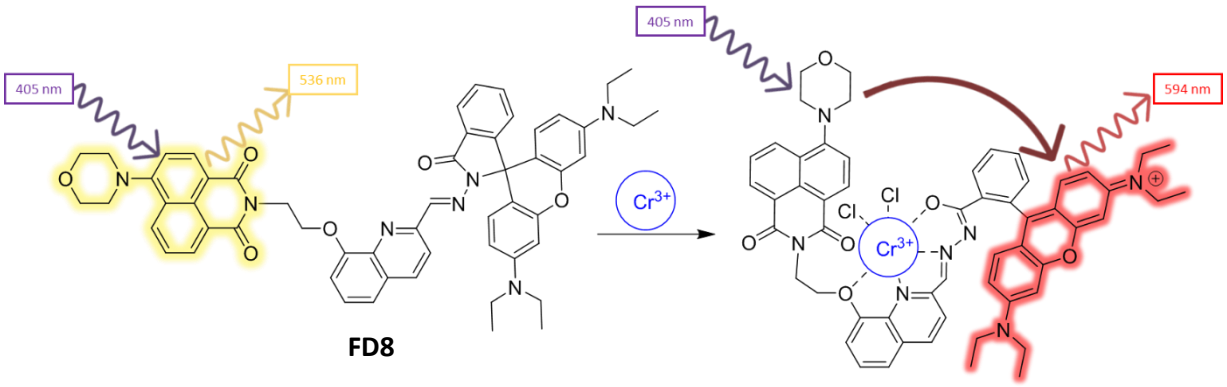

Figure 24 – Detection of Cr^{3+} using the FRET probe **FD8**.

Chromium^{III} (Cr^{3+}) is an essential trace metal that has been found to have an important role in the metabolism of fats, proteins and nucleic acids, with perturbed levels of this metal indicating an increased risk of cardio vascular disease (CVD) and type two diabetes. This has led to the development of a fluorescent probe by Huang *et al.* (**FD8**), that used a FRET based approach using a 1,8-napthalimide donor and a rhodamine acceptor (**Figure 24**).[34] Upon binding of the Cr^{III} ion, the spirolactam unit of the rhodamine ring opens which results in the FRET process being turned on and a ratiometric response.

Mercury (Hg) is well known as being a toxic metal in biological systems, with methylmercurial compounds known to be some of the most toxic organometallic species known. Pitchumani *et al.*, have developed a fluorescent probe **12** for the detection of mercury that employs a twisted internal charged transfer (TICT) based mechanism (**Figure 25**).[35] Binding of the Hg^{2+} ion is achieved *via* a dansyl group which has a quenching effect on the probe, whilst also bathochromically shifting probe emission from 496 nm to 514 nm.

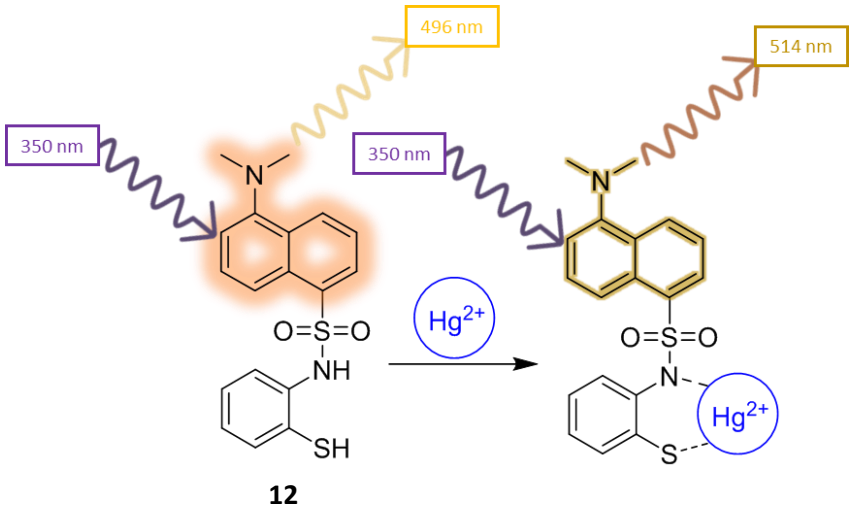

12

Figure 25 – Diagram of the TICT process that occurs when the probe **12** binds to Hg^{2+} which causes a change in fluorescence response.

1.5.2 α-Amino acids

Tracking the presence and localisation of α-amino acids (AAs) within cells can afford important information on their role, and the success of potential treatments, in disease. There are numerous ways that changes in amino acid levels can disturb the healthy functioning of cells. Cysteine (Cys) for example is an amino acid that is known to be deficient in several disease states, including edema,[36] lethargy and liver damage. [37,38] Therefore, there is a desire to study and monitor the presence of specific amino acids in biological settings and many examples of fluorescent probes for this purpose have been developed.

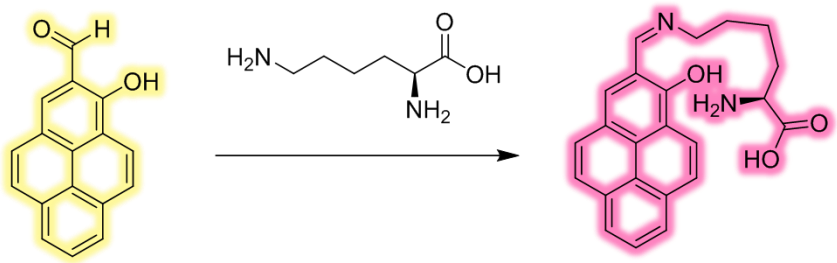

13

Figure 26 – Colour change observed when a pyrene-based sensor is exposed to lysine.

Yoon *et al.* have described the development of a fluorescent sensor **13** for the detection of lysine (Lys) (**Figure 26**),[39] involving a pyrene fluorophore functionalised with aldehyde and phenol groups. Selective reaction of the aldehyde group of the sensor with the amino

group of Lys results in a Schiff base that is stabilised by the α-amino group of the Lys. This binding event results is a colour change of the sensor from yellow to pink, that was seen to be visible to the naked eye.

Glutamate has been observed in unusually high levels in several diseases and health problems, such as stroke, amyotrophic lateral sclerosis and Alzheimer's disease (AD). Lee *et al.* have developed a sensor **14** for the detection of glutamate using an on-off PET quenching mechanism caused by the HB donor activity of the thiourea fragment (**Figure 27**).[40] The unbound sensor has an emission peak at 413 nm that is gradually turned off when it is exposed to glutamate.

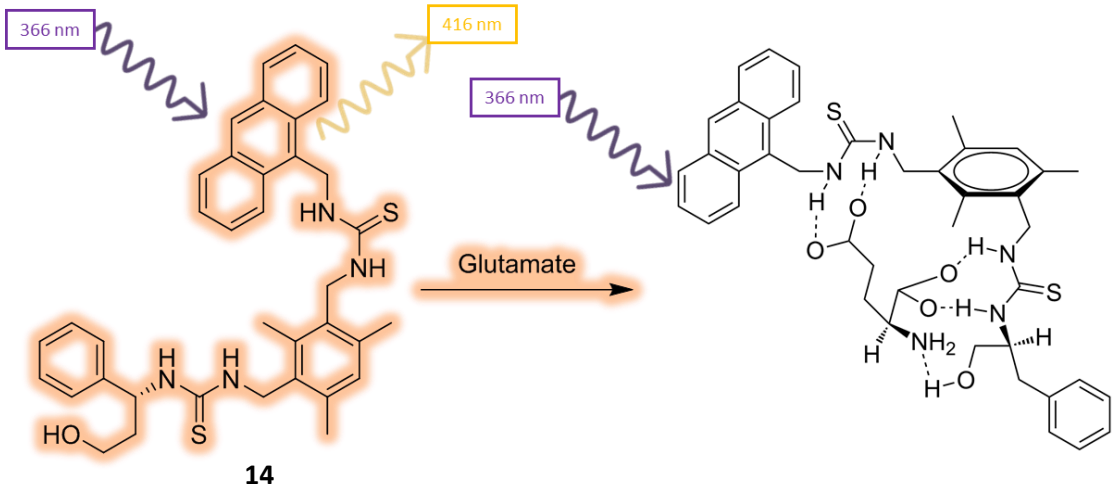

Figure 27 – PET quenching of fluorescent output of sensor **14** by glutamate.

1.5.3 pH sensing

The pH (H^+ concentration) of a cellular environment is an important variable controlling the balance of healthy cell function, playing vital roles in cellular processes such as apoptosis, ion transport and muscle contraction.[41] Fluctuations in pH levels regulate many cellular processes,[42] with abnormal pH levels observed in diseases such as cancer and inflammation. [43,44] Accurate measurement of the pH value within cells and specific organelles is therefore a highly desirable tool in biological research, with fluorescent probes providing a highly efficient method for monitoring the pH in cells and tissues *in vivo*.[42]

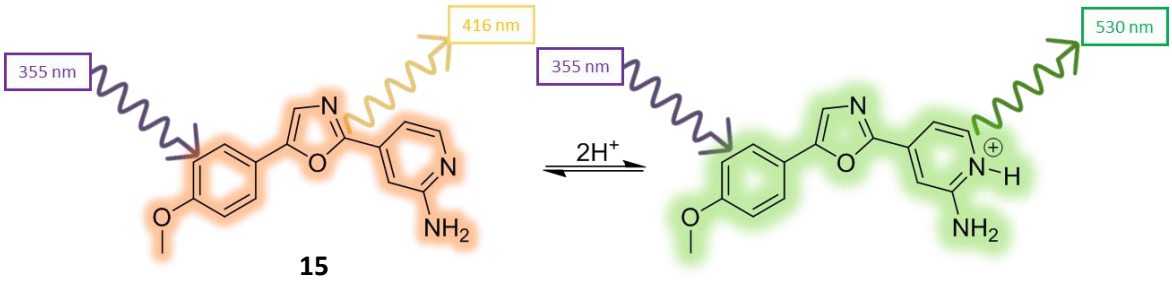

Figure 28 – A ratiometric sensor **15** for determining pH.

One such example was developed by Jullien *et al*, who employed a 2-(4-pyridyl)-5-aryloxazole **15**, appended with donor and acceptor units to allow an ICT type fluorescence mechanism to operate under pH control. The probe contains a central oxazole unit substituted with a methoxy (-OMe) group and a 2-aminopyridyl group that has a pK_a of 6.9 (**Figure 28**).[45] This sensor provided a ratiometric response to change in pH levels, corresponding to the relative amounts of free and protonated amine that exist at different pH levels. Both species were fluorescent and exhibited similar φ_F values, with the free amine sensor having an emission at 465 nm, with the protonated version of the sensor bathochromically shifted to 530 nm, upon excitation at 335 nm.

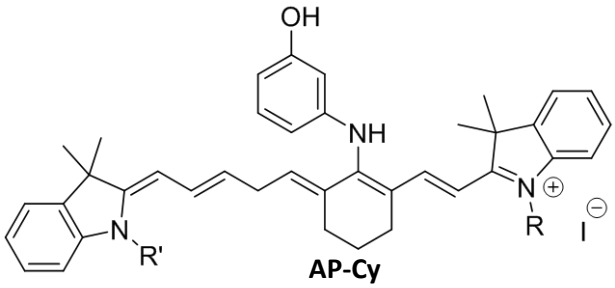

Figure 29 – Structure of the **AP-CY** probe.

An *et al.* have developed a PET based NIR pH probe based on a cyanine structure (**AP-Cy**, **Figure 29**), which incorporates a three amino phenol group into a cyanine core.[48] Varying the pH causes shifts in the absorption spectra of the compound, absorbing at 558 nm at pH 3.58, whilst two absorptions at 453 nm and 750 nm were observed at pH 7.07 and 10.50, respectively. Unlike other fluorescein-based pH probes, a strong increase in fluorescence was observed at low pH values, which is due to protonation of the nitrogen atom blocking the PET process. This sensor was shown to be very useful for the study of acidic organelles, as there was a greater than tenfold increase in fluorescence intensity over a pH range from 4.0-6.5. **AP-Cy** was observed to be cell permeable and so could be used to monitor pH variation in human hepatocellular liver carcinoma cell lines (HepG2).

1.5.4 ROS /RNS

Reactive oxygen species (ROS) and reactive nitrogen species (RNS) are two highly reactive chemical species that are produced in cellular environments as a part of normal cellular life cycle processes.[46] The function of these highly reactive species ranges from cell defence, cell proliferation and regulated cell destruction (apoptosis).[47,48] Due to the reactivity of these chemicals, their production is normally highly regulated, so they are kept at a low concentration. However, when there is an unregulated increase in their production, antioxidants that are responsible for countering their negative effects are overwhelmed and the cell starts to undergo damage. The highly oxidising nature of these ROS / RNS species can result in irreparable damage to other important biomolecules, such as proteins, DNA and carbohydrates.[49] Eventually, this damage can cause mutation, disruption of cellular functions and causes disease. Consequently, oxidative stress has been associated with a wide range of different diseased states. Alzheimer's disease,[50] cancer,[51] type two diabetes[52] and cardio vascular disease[53] are all examples of disease states where ROS / RNS are present in higher concentrations than normal. This gives a compelling driving force for the development of fluorescent probes to detect and quantify their occurrence in healthy and diseased cells. These reactive oxygen species are often very short lived (hydroxyl radical half-life ~10^{-9} s)[46] and are hard to detect *via* non-fluorescent methods (**Section 1.2**). Therefore, fluorescent probes are attractive as a tool specifically for ROS / RNS. A selection of probes for different ROS/RNS species are discussed in the following section.

1.5.4.1 Superoxide

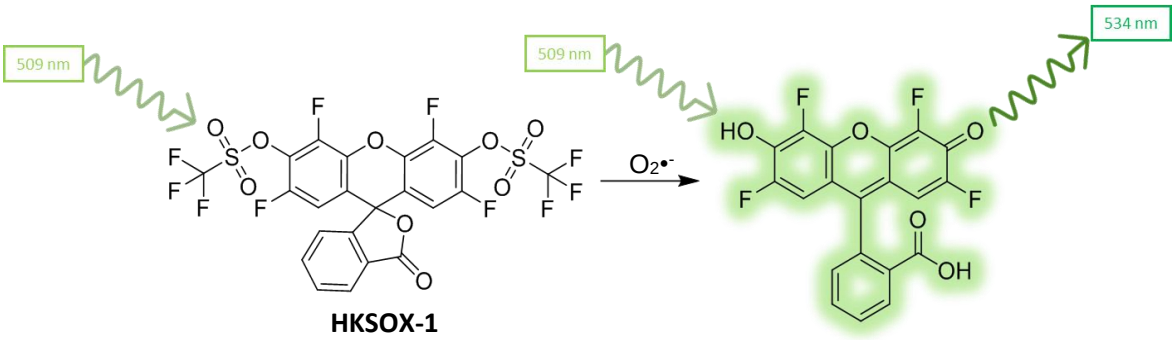

Figure 30 – The fluorescence of probe **HKSOX-1** is turning on upon exposure to $O_2^{\bullet-}$.

Superoxide ($O_2^{\bullet-}$) is a ROS that is commonly referred to as the "primary" ROS, as it reacts quickly in the cellular environment to generate other ROS / RNS. $O_2^{\bullet-}$ is produced mainly in the mitochondria through the reaction between molecular oxygen and respiratory enzymes such as xanthine oxidase.[56] $O_2^{\bullet-}$ can react directly with intracellular biomolecules causing damage that has been implicated in aging[57] and inflammation.[58] Yang *et al.* have developed a fluorescent sensor for the detection of $O_2^{\bullet-}$ using an ICT based tetrafluoro-fluorescein probe containing two -OH groups masked as trifluoromethanesulfonate moieties (**HKSOX-1**).[59] $O_2^{\bullet-}$ undergoes nucleophilic attack at the trifluoromethanesulfonate groups to give free phenol groups (**Figure 30**) which results in ring opening of the fluorescein fragment to turn on its fluorescence.

Another, extremely sensitive and cell permeable fluorescent probe (**Hydro-IR-676**) for the detection of $O_2^{\bullet-}$ was developed by Kundu *et al.* which employs a reduced cyanine dye structure that is both non-fluorescent and cell permeable. Subsequent oxidation of the probe by $O_2^{\bullet-}$ affords a non-cell permeable cyanine dye that is highly fluorescent (**Figure 31**).[60]

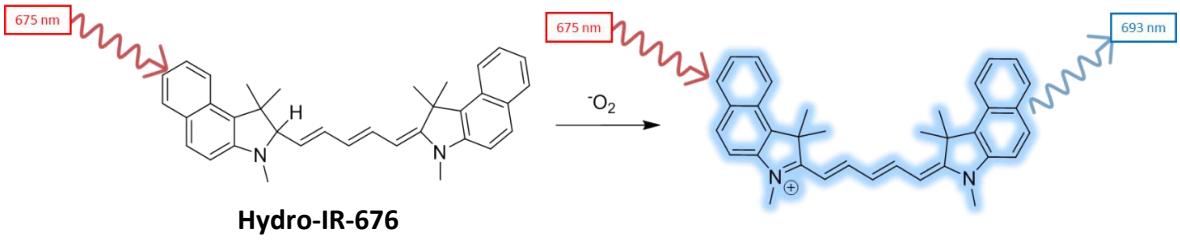

Figure 31 – **Hydro-IR-676** reacting with $O_2^{\bullet-}$ to form the fluorescent cyanine dye.

1.5.4.2 Hypochlorous acid/ hypochlorite

Hypochlorous acid (HClO) and its conjugate base, the hypochlorite anion (ClO^-) are another type of ROS, which exist at physiological pH due to their weak acidic natures. HClO/ClO^- is produced *via* myeloperoxidase (MPO) enzyme[65] in leukocytes, from the reaction between hydrogen peroxide (H_2O_2) and chloride (Cl^-) and is essential for a number of vital cell functions, including cell defence and signalling.[61] However, a number of diseases occur where levels of HClO production are known to be unregulated causing harm, including multiple sclerosis[61] and rheumatoid arthritis (RA).[63]

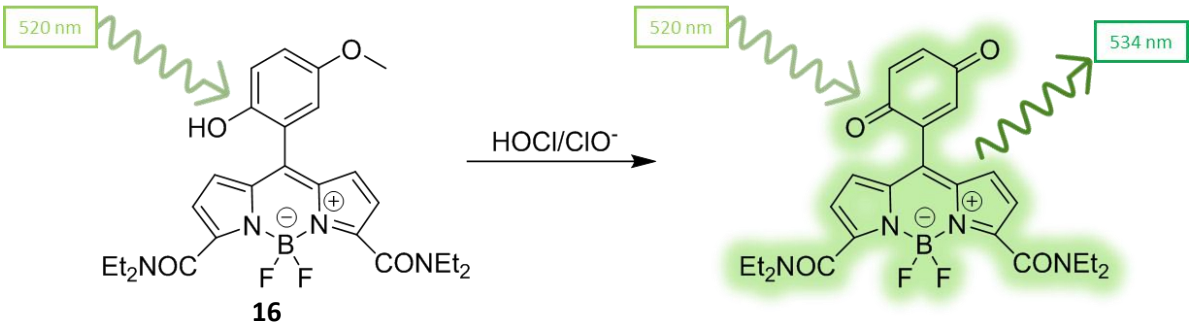

Figure 32 – BODIPY based sensor **16** for the detection of HClO / ClO^- *via* deprotection of the *p*-methoxyphenol group to afford a quinone unit.

HClO/ ClO^- has been shown to have specific reactivity towards *p*-methoxyphenol groups transforming them into benzoquinone units, with Yang *et al.* harnessing this reactivity to develop a fluorescent probe **16** for the detection of HClO/ ClO^-.[64] The sensor, in its deactivated state, is comprised of a *p*-methoxyphenol derived BODIPY (**Section 1.3.2**) which is fluorescence quenched *via* a PET mechanism. HClO/ ClO^- reacts with the *p*-methoxyphenol group to form a benzoquinone bound group which results in the loss of PET process and the fluorescence response of the BODIPY unit being turned on (**Figure 32**).

Yu *et al*. developed another fluorescent probe **17** for the detection of HClO / ClO^- using a coumarin fluorophore appended with an oxime as a reactive unit,[65] with a PET quenching mechanism operating in the parent probe to turn-off its fluorescence. The weakly fluorescent probe then reacts with the HClO/ClO^- which results in its oxime unit being oxidised to a nitrile (C≡N) group. This conversion results in the PET process being blocked and a seven-fold increase in the fluorescence intensity of the BODIPY unit (**Figure 33**). This sensor was found to be effective in stimulated macrophage cell lines that

produce MPO (the precursor of HClO / ClO^- in cells) affording a fluorescence response that was visible in cellular imaging studies.

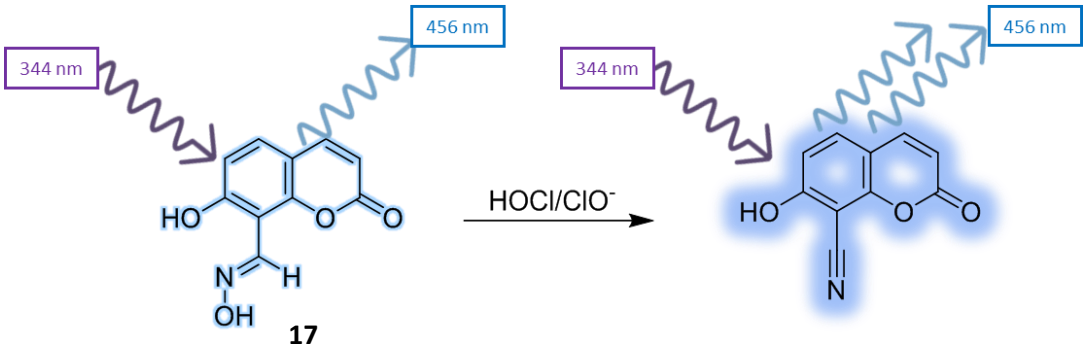

17

Figure 33 – Oxime based coumarin based sensor **17** for detecting HClO / ClO^-.

1.5.4.3 Hydroxyl radical

The hydroxyl radical ($HO^{\bullet}$) is a ROS that is produced biologically *via* the non-enzymatic Fenton reaction of H_2O_2 and Fe^{3+}. Free Fe^{3+} being produced from reaction of $O_2^{\bullet -}$ with [4Fe-S] containing enzymes.[66] The unstable nature of radical species means that the half-life of $HO^{\bullet}$ is very short (<1 ns),[67] which can react proteins and DNA in the immediate vicinity.

One of the effective ways to target $HO^{\bullet}$ is to use a reactive nitroxide unit in the presence of a small amount of dimethyl sulfoxide (DMSO) in the buffer system (0.1 %). The $HO^{\bullet}$ radical reacts quantitatively with the DMSO in solution to produce a methyl radical ($CH_3^{\bullet}$) that can react selectively with a nitroxide group. Bi *et al.* used this reactivity profile to design several probes based on a core rhodamine fluorophore structure, including a mono-nitroxide example (**18**, **Figure 34**).[68] When the $CH_3^{\bullet}$ reacts with the nitroxide radical of the

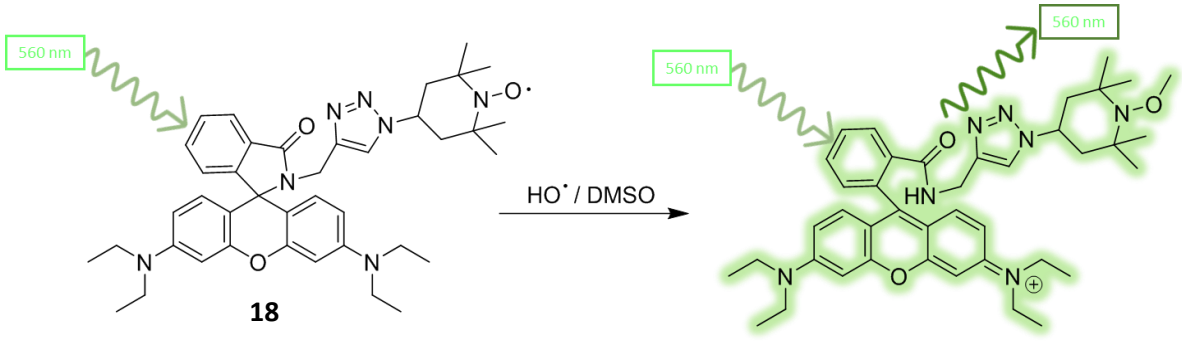

18

Figure 34 – Turn on response of **18** in response of HO• in the presence of DMSO.

probe it causes cessation of an intramolecular quenching process. The low pH of this assay (4.0) then allows the opening of the spirolactam of the rhodamine sensor, resulting in a >400 increase in fluorescence response.

Another interesting example of a probe for the detection of HO• was reported by Song *et al.* based on hybridisation of two fluorophore structures with a coumarin aldehyde being condensed with an indolium fragment to form compound **19** with a fluorescent coumarin fragment (emission at 495 nm),[69] and a cyanine fragment whose fluorescence is deactivated by an ICT mechanism (**Figure 35**). Upon addition of HO• to the system, there is a ratiometric response by the probe, with a decrease in the emission at 495 nm and an increase in emission of a bathochromically shifted peak at 651 nm, resulting from oxidation of the cyanine fragment that results in a fully conjugated system.

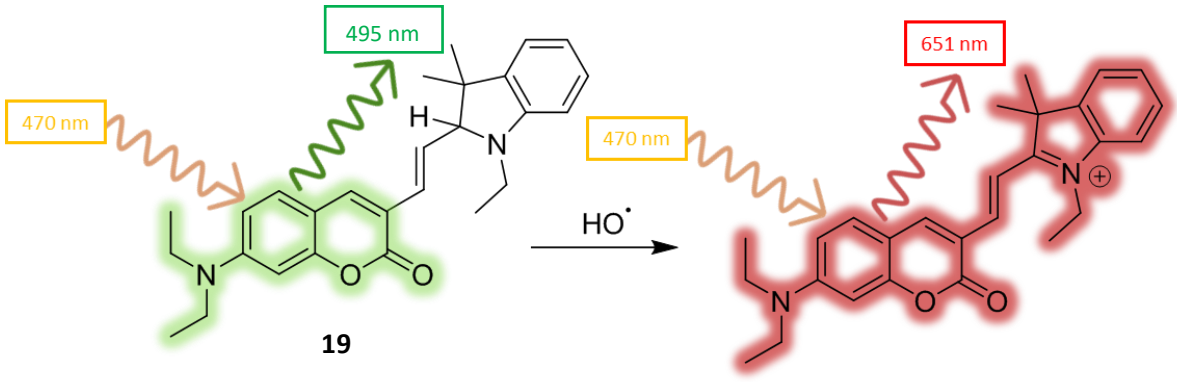

Figure 35 – Oxidation of probe **19** by a hydroxyl radical results in activation of the cyanine segment of the probe and a bathochromic shift in its emission.

1.5.4.4 Singlet oxygen

Singlet oxygen ($^1O_2$) is a molecule of oxygen (O_2) that has been excited to a higher electronic state, which is a ROS species that can cause extensive damage to DNA, proteins and enzymes.[70] In addition, $^1O_2$ is increasingly used as a therapeutic agent in photodynamic therapy (PDT),[71] which is an emerging cancer treatment that uses photo-irradiation and light sensitive molecules (photo-sensitizers) to directly produce $^1O_2$ in cellular environments. Once produced, this $^1O_2$ can cause oxidative damage to the local environment and kill cancerous cells. Probes that can be used to study the mechanism by

which process works, as well as the diffusion of the $^1O_2$ in cells is essential to understand the risk and benefits of this method.

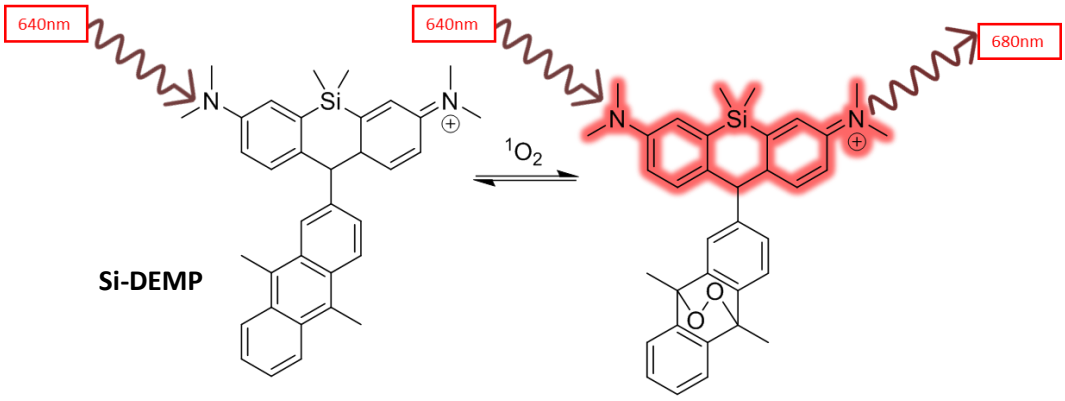

Figure 36 – Trapping of the $^1O_2$ by the sensor **Si-DEMP** and the fluorescence response.

Majima *et al.* have developed a long wavelength $^1O_2$ probe, comprised of a 9,10-dimethylanthrancene (DMA) group bound to a silicon-containing rhodamine (Si-rhodamine) unit (**Si-DMEP**, **Figure 36**). The DMA group acts as a diene receptor unit, with the $^1O_2$ reversibly adding across the central benzene unit *via* a [4+2] cycloaddition reaction. This reaction stops the PET quenching of the DMA to the Si-rhodamine fragment causing a turn-on fluorescence response. Si-DEMP shows a very weak emission at 640 nm and a dramatic increase when exposed to $^1O_2$ in whole cell systems.

1.5.4.5 Ozone

Ozone (O_3) is an allotrope of oxygen that is much more reactive than a standard O_2 molecule, which is produced from the reaction of O_2 with UV light.[72] This process is

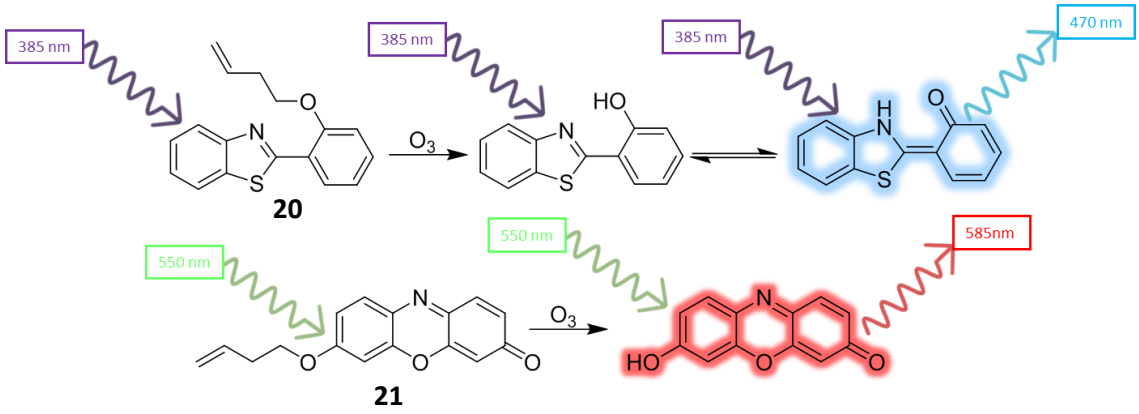

Figure 37 – Wang's (**20**) and Ma's (**21**) probes for O_3 using the reactivity of but-3-enyl group.

known to occur in the upper atmosphere which protects the Earth from harmful UV light emitted by the sun. However, when generated in biological systems, O_3 is known to be highly toxic.[73] It was thought that risk from O_3 to health was minimal, until recent work demonstrated that there was a mechanism for its production in the body. Antibodies in the human immune system have been shown to catalyse the production of O_3 and dihydrogen trioxide (H_2O_3) from $^1O_2$ as cell defence mechanisms.[74]

One of the common methods to detect O_3 is to use but-3-enyl, a terminal homo-allyl branch, that reacts with the O_3 to cleave the butene group, to liberate a free phenolic unit. This approach has been used by Ma *et al.* and Wang *et al.* to produce probes **20** and **21** for O_3 based on ICT and ESIPT based fluorophores, respectively (**Figure 37**).[75]

Another method used by Tang *et al.* for the detection of O_3 employed an L-tryptophan (Trp) fragment as a receptor unit on a probe **22** (**Figure 38**),[76] which produces a ring opened analogue that turns on a TICT process which turns on the fluorescence response of the cyanine fluorophore.

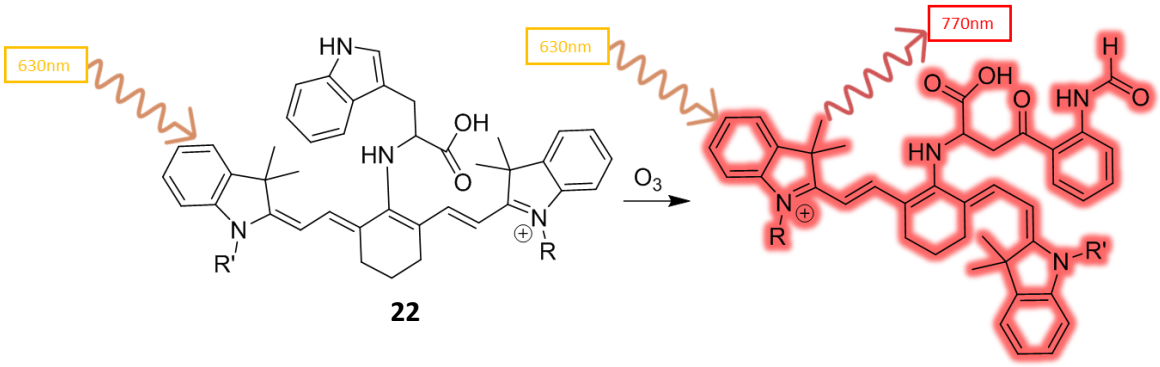

Figure 38 – A non-radiative TICT probe for the detection of O_3.

1.5.4.6 Nitric oxide

Nitric oxide ($NO^{\bullet}$ / NO) or nitrogen monoxide, is a small signalling molecule with a single electron (radical) that has a short half-life (<1 s),[77] which is used throughout the human body in many different environments, including for the control of vascular tone and platelet aggregation.[78] It is primarily produced in the body through a catalytic pathway involving NO synthase (NOS) catalysed reaction of amino acids with oxygen and reduced nicotinamide-adenine dinucleotide phosphate (NADPH).[77]

It may also be produced non-enzymatically, from several pathways that involve the reduction of nitrite (NO_2^-) under acidic conditions, with the importance of NO in so many biological pathways and its short half-life making it an important target for fluorescent probes.

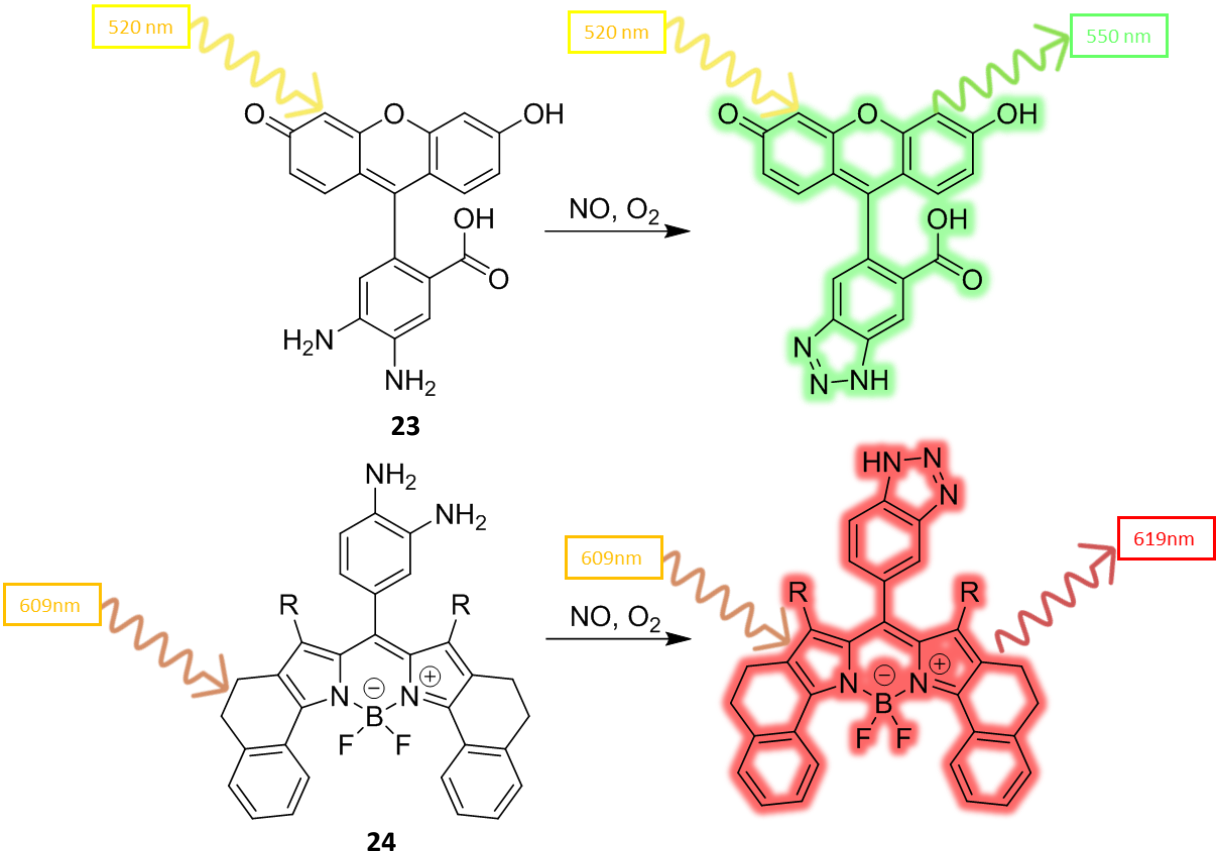

Figure 39 – *o*-Phenylenediamine based nitric oxide sensors **23** and **24**.

The most popular method used to design probes to detect NO involves the use of *o*-phenylenediamine as the receptor group. The di-aniline functionality reacts with NO to produce a benzotriazole ring system with lower electron donating ability that turns off its PET quenching process to an attached fluorophore. Two examples of this type of probe have been developed by Nagano *et al.* and Zhang *et al.* that contain a fluorescein (**23**) and a BODIPY base (**24**), respectively (**Figure 39**).[79] Both probes work based on the selectivity of the *o*-phenylenediamine fragment with the PET process being blocked by reaction with NO to turn on the fluorescence.

Another method for the detection of NO relies on an N-nitrosation reaction between NO and p-phenylenediamine to cause a fluorescence response. The mechanism relies on quenching of the PET process present in the unreacted probe. Lui *et al.* used this mechanism to make a phenyl-coumarin based probe for NO (**25**, **Figure 40**), which was able to detect endogenous and exogenous NO in living cells and a live mouse model.[80]

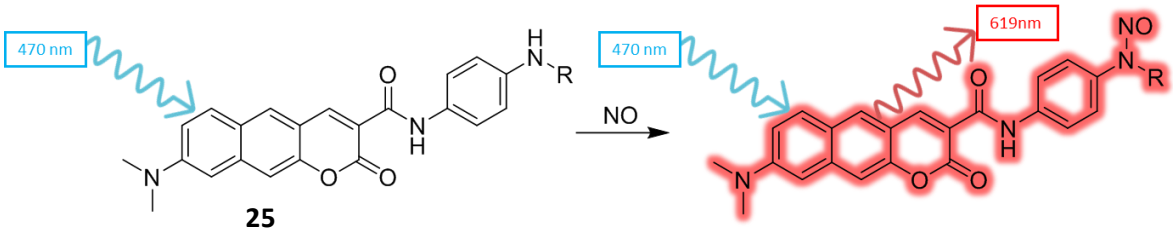

Figure 40 – Nitrosation of **25**.

1.5.4.7 Hydrogen peroxide

Hydrogen peroxide (H_2O_2) is the simplest peroxide compound which in its neutral form is a weak oxidant and as a nucleophile that plays a vital role in numerous cell functions, such as respiration, immune response and cellular signalling.[81] The relatively low reactivity of

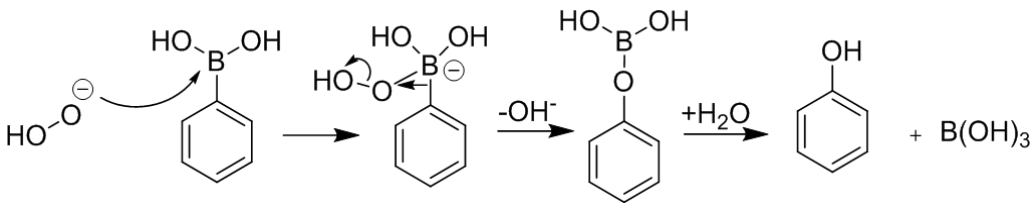

Figure 41 – H_2O_2 reacting with phenylboronic acid to produce phenol and boric acid.

H_2O_2 (relative to other ROS) allows it to move around the cell and permeate through cell membranes allowing for the damage of a larger range of biological structures. Irregular levels of H_2O_2 have been observed in neurodegenerative diseases,[81] inflammatory diseases and cancers.[83,84]

The most widely used mechanism for the detection of H_2O_2 involves the reactivity of peroxide towards aryl boronate moieties (**Figure 41**).[85] HO_2^- is the anionic form of H_2O_2, which is a strong nucleophile that can attack the empty p-orbital of a boron atom to form a tetrahedral anionic boronate species. A bond migration can then occur to transform a carbon-boron bond into a more stable boron-oxygen bond, resulting in an unstable borate species that can be hydrolysed rapidly.

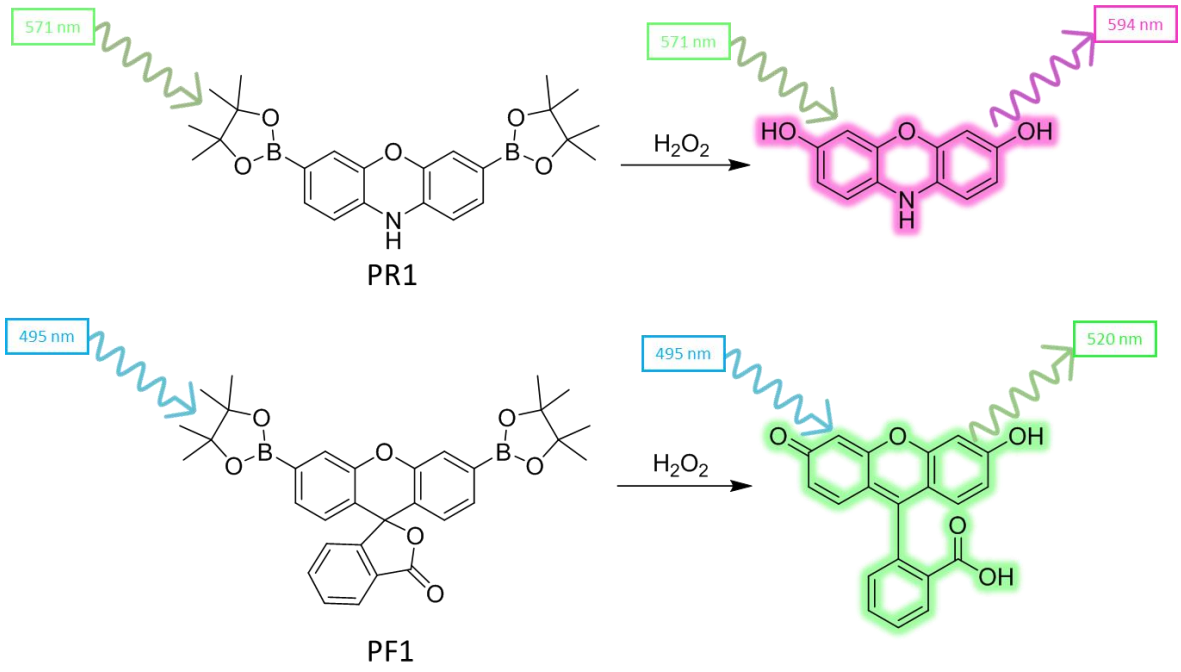

Figure 42 – The sensors **PR1** and **PF1** react with H_2O_2 to turn on the fluorescence of their resorufin and fluorescein fragments, respectively.

Some of the most popular and successful probes for H_2O_2 have been developed by Chang and co-workers, who employed boronic acid pinacol ester groups attached to a range of xanthene-based fluorophores to produce several turn-on probes.[86-89] Two of these probes (**PF1** & **PR1**, **Figure 42**) exhibited a particularly strong response to the presence of H_2O_2, with an increase of over 1000 times relative to the "off" state of the sensor. These probes showed very good cellular permeability and were used to visualize H_2O_2 in mammalian cells.

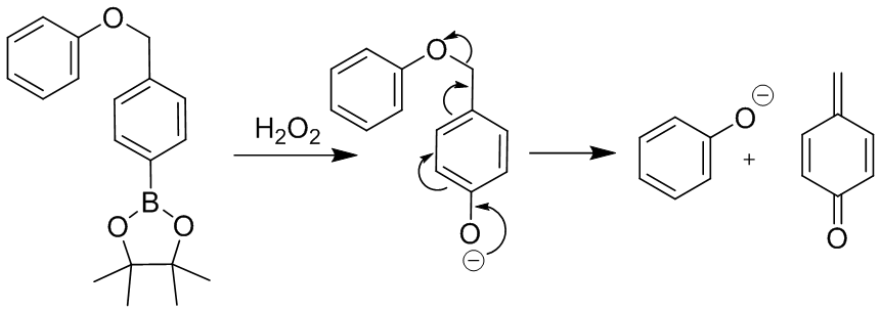

Figure 43 – Reaction of methylphenylboronic acid pinacol ester receptor group with H_2O_2 form an intermediate phenolate that collapses to form another phenolate anion and cyclohexadiene-1-one.

Song *et al.* developed a longer wavelength probe (**26**), with a large fluorescence red shift based on an ESPIT core fragment appended to a cleavable methylphenylboronic acid pinacol fragment. Upon cleavage of the boronic ester by H_2O_2, the resultant phenol self eliminates through a 1,6-benzyl elimination pathway (**Figure 43**) to produce a new phenol group. This activates the donor ability of the phenol group which turns on the ESIPT mechanism of the fluorophore (**Figure 44**).[90]

Other mechanisms for the sensing of H_2O_2 in fluorescent probes also exist, including those that rely on the use of arylsulfonyl esters,[91] diphenyl phosphine,[92] and α-diketone groups.[93]

Yu *et al.* used a selenium containing fluorophore that relies on oxidation of a selenium centre to inhibit a PET process and cause a fluorescence response in solution (1:99 DMSO:

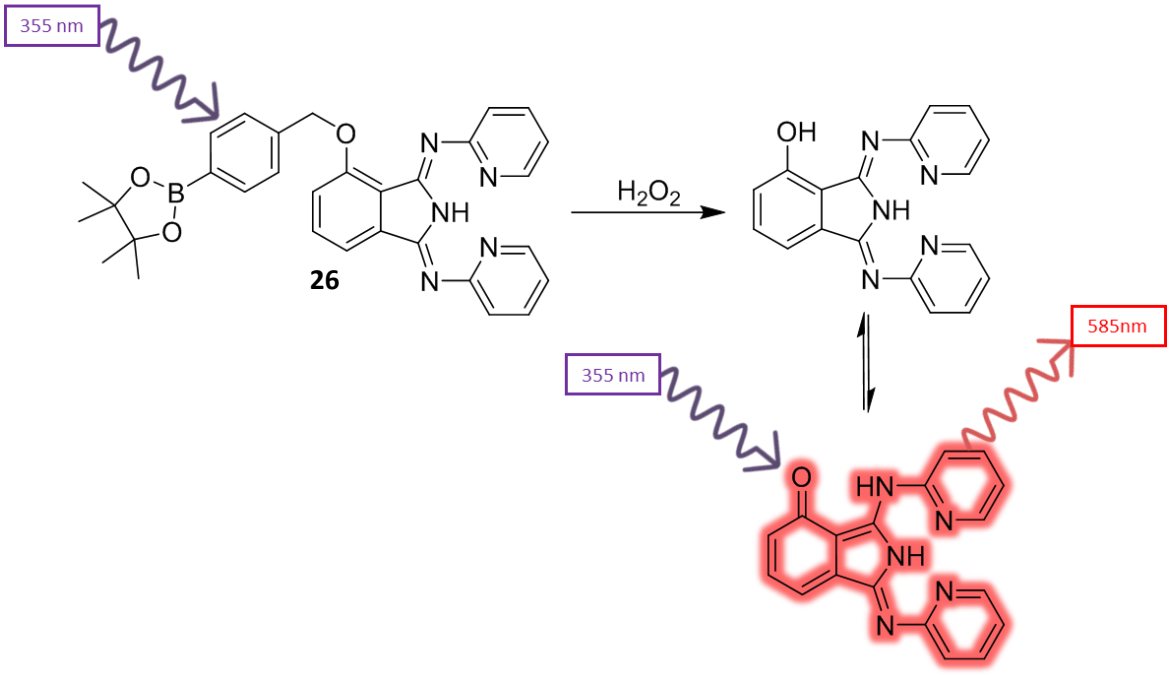

Figure 44 – Reaction of H_2O_2 with probe **26** results in ESPIT fluorescence.

H_2O) and an aggregation induced emission (AIE) in the solid state.[94] This sensor was observed to be highly specific for H_2O_2, however, its propensity to crash out of solution required the presence of DMSO which made it unsuitable for biological studies.

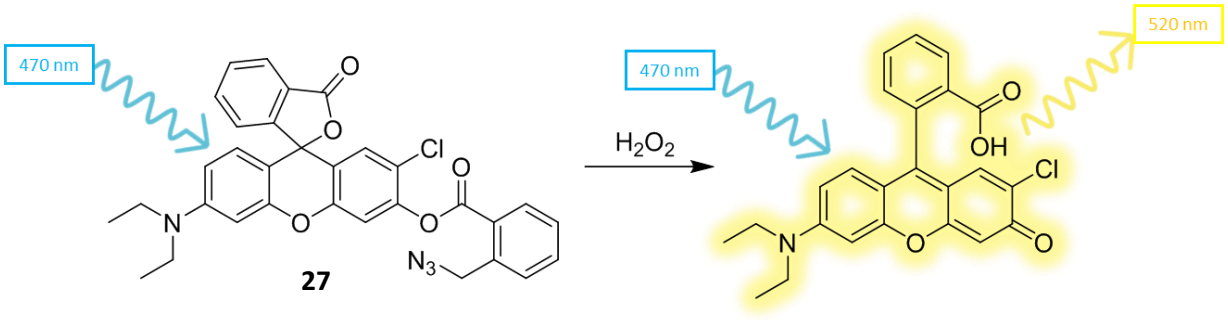

Figure 45 – Reaction of probe **27** with H_2O_2 produces a fluorescent chloro-rhodol compound.

A more successful utilisation method for H_2O_2 detection was developed by Zhan *et al.* who employed a sensor with a reactive unit bound to a 7'-chloro-*N*, *N*-diethylrhodol fluorophore (**27**, **Figure 45**).[95] A 2-(azidomethyl) benzoyl acid unit condensed to a rhodol fluorophore was found to be sensitive to nucleophilic cleavage with H_2O_2 to afford a good fluorescent response.

1.5.4.8 Peroxynitrite

Peroxynitrite ($ONOO^-$) is a structural isomer of nitrate (NO_3^-) that is a highly reactive RNS species formed from the diffusion-controlled reaction between NO and $O_2^{\bullet -}$ in cells.[96] This reaction is incredibly fast and can spontaneously occur throughout the cell, as well as across cellular structures and membranes. Due to its inherent high reactivity, the half-life of $ONOO^-$ is very short (~10-20 ms) and it reacts quickly within biomolecules in cells, causing damage to DNA, proteins and other biological molecules.[96] Additionally, it plays an important role in cell signalling processes, having been observed to cause caspase activation and apoptosis.[97] The majority of the $ONOO^-$ produced in cells breaks down in contact with CO_2 to produce NO_2 and carbonate radicals, which can also go on to damage biomolecules (e.g. tyrosine nitration).[98]

Classically, methods to detect $ONOO^-$ were based on trapping of intermediate species and products of its interactions, rather than methods for its direct observation.[99] However, a reactive trifluoro ketone group appended to a fluorescein-based fluorophore, by Shen *et al.* to make **HKGreen-1**, was found to react with $ONOO^-$ to afford a dioxirane intermediate that decomposes to afford a dienone product and a dichloro fluorescein fluorophore (**Figure 46**).[100]

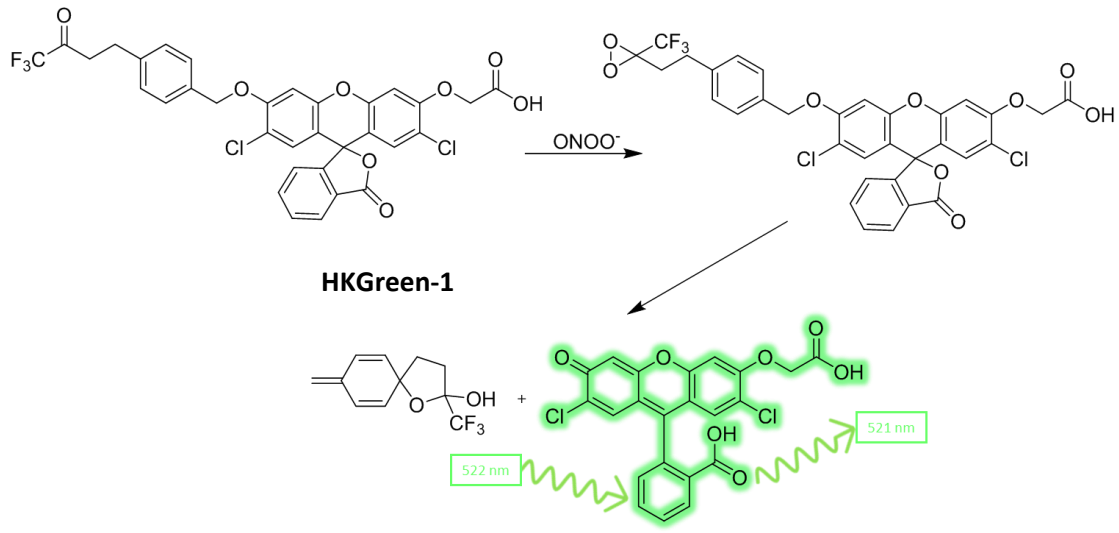

Figure 46 – Reaction of **HKGreen-1** probe with $ONOO^-$ to afford dichloro fluorescein.

Guo *et al.* developed another $ONOO^-$ probe using a methyl(4-hydroxyphenyl) amino group bound to a pyronin fluorophore (**28**, **Figure 47**).[103] The receptor group acts as a PET quenching group for the fluorophore, with exposure of the probe to $ONOO^-$ resulting in a two-electron oxidation of the methyl-(4-hydroxyphenyl) amino group to form an unstable iminium species that is rapidly hydrolysed to yield a fluorescent probe and 1,4-benzoquinone. This sensor showed a rapid and intense fluorescence turn on in the presence of $ONOO^-$, as well as very high specificity over other ROS /RNS.

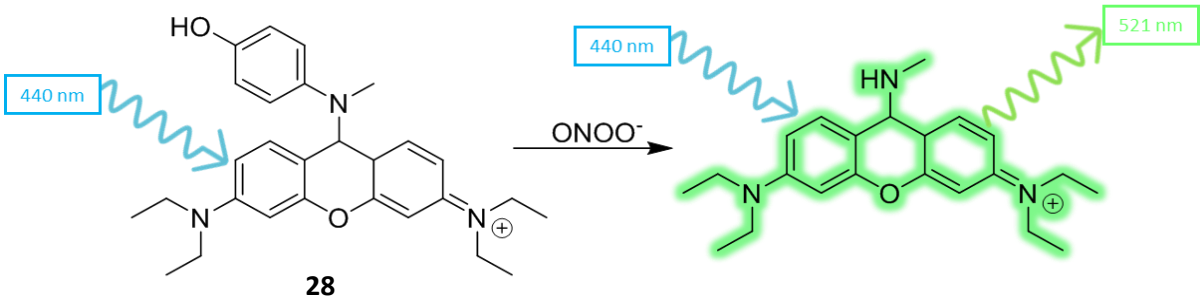

Figure 47 – Turn on mechanism for probe 28 in response to $ONOO^-$.

The development of a new class of fluorescent probe was prompted by the report in 2009 by Kalyanaraman *et al.* of the reactivity of $ONOO^-$ towards phenylboronic acids.[85] The reaction that occurs between the $ONOO^-$ and the boronate species proceeds through the same mechanistic steps as the reaction between H_2O_2 and boronate esters. The key difference between the two reactions is that the $ONOO^-$ reaction proceeds at over a million times ($\times 10^6$) faster than the reaction of H_2O_2. Also, reaction of H_2O_2 with $ONOO^-$ occurs over 200 times faster than the competing reaction between HClO and boronates.

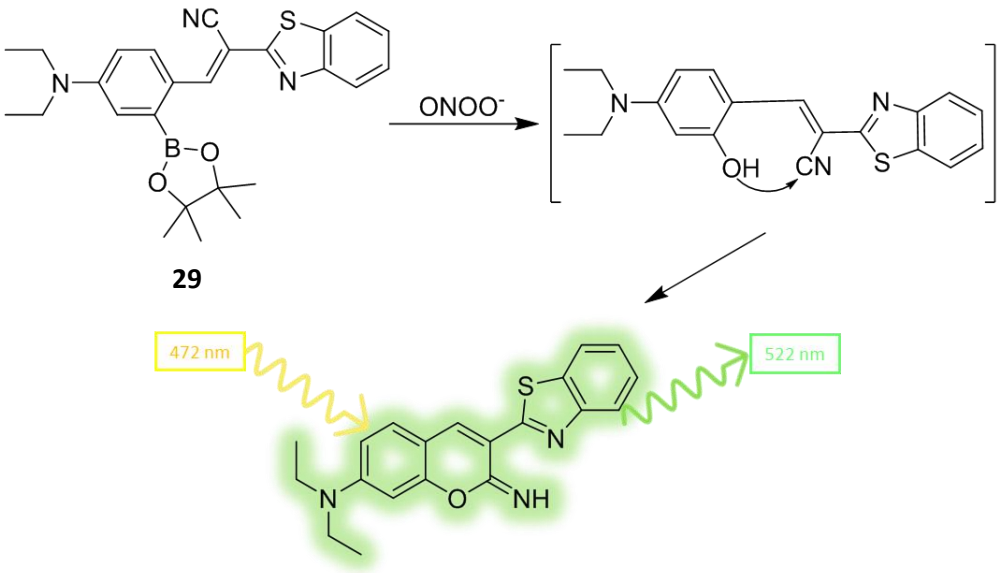

Figure 48 – Reaction of **29** and $ONOO^-$ produces a coumarin fluorophore.

Guo *et al.* have developed an ESIPT based sensor for the detection of $ONOO^-$ based on this methodology, using a probe (**29**, **Figure 48**) based on a benzothiazine appended to a diethyl-amino phenyl boronate group through an alkene bridge containing a nitrile group.[102] Upon reaction with the $ONOO^-$ the boronate fragment is cleaved to afford a

phenol group that then undergoes intramolecular reaction with the nitrile group to form a highly fluorescent coumarin fluorophore.

In another example, Wang *et al.* used a coumarin scaffold based on a 4-methylumbiliferone scaffold for the direct synthesis of a $ONOO^-$ probe **30** containing a phenyl boronic acid pinacol ester group (**Figure 49**).[101] This probe was fluorescent, with excitation at 322 nm resulting in emission at 385 nm, however oxidative cleavage of the boronic acid group by $ONOO^-$ resulted in a bathochromic shift of the emission peak. This probe was successful employed to visualise endogenous $ONOO^-$ in cell lines with minimal cytotoxicity in zebra fish embryos and mice models.

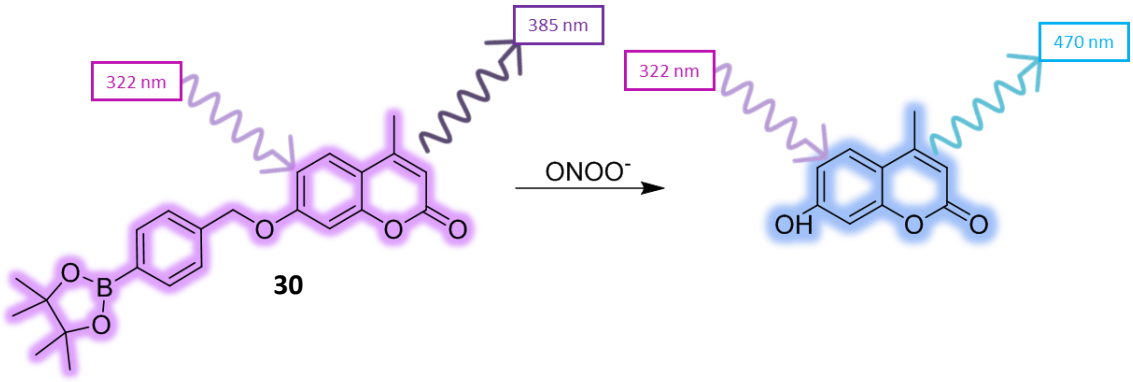

Figure 49 – Change in the fluorescence response of a probe **30** caused by cleavage of the phenylboronic acid pinacol ester group.

Bull & James *et al.* developed a functionalised N-substituted-1,8-napthalamide probe **31** for the detection of $ONOO^-$ (**Figure 50**).[104] This probe was appended with a PET quenching tertiary amine bound to a phenyl boronic ester of fructose, with a water molecule coordinating to the bridging amine to block its PET quenching ability. The strongly nucleophilic $ONOO^-$ reacts with the boronate ester resulting in cleavage to afford a phenol group and a free amino group that then serves as a PET group. This causes an ON-OFF response in the presence of $ONOO^-$, however, a significant turn off of fluorescence was also observed in the presence of ClO^- that lowers the specificity of the probe.

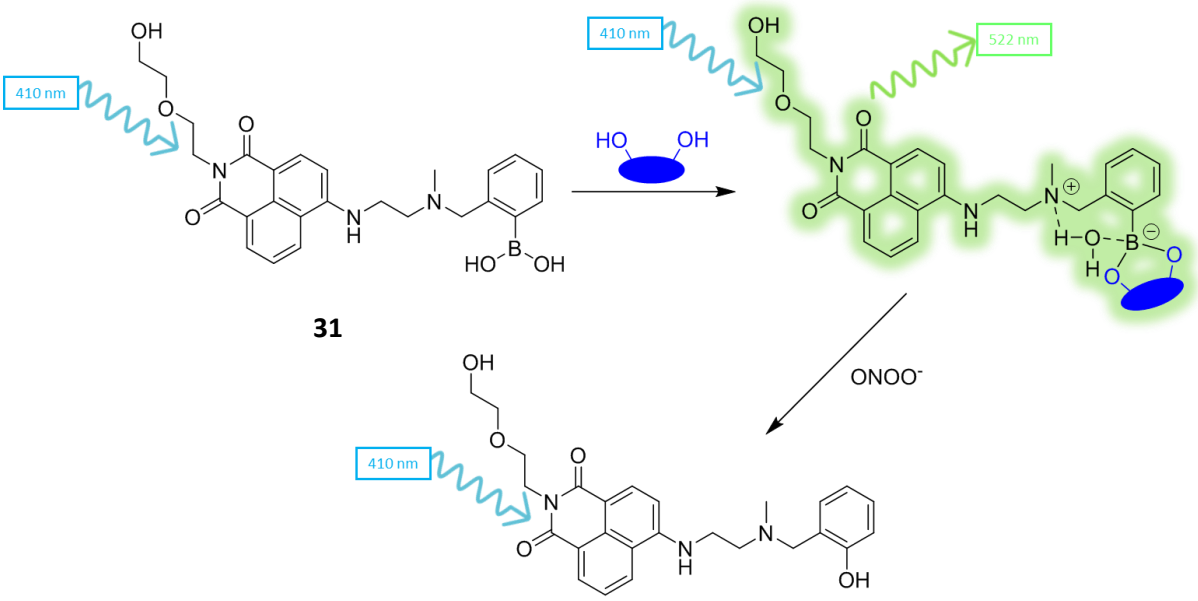

Figure 50 – Mechanics of an ON-OFF naphthalimide based boronate ester sensor **31** for $ONOO^-$.

1.6 Dual analyte probes and molecular logic gates

Traditionally, fluorescent probes only require one analyte to produce a response. However, recently there has been a significant increase in the number of dual or multi-analyte probes developed.[106] This has led to the development of molecules that perform logical operations based on multiple physical or chemical inputs that lead to a single output, in a process referred to as a molecular logic gate (MLG).[105] Dual analyte probes use two receptor groups bound to a fluorophore that require the binding (or reaction) of two independent analytes to produce a fluorescence response (**Figure 51**). This process allows for the simultaneous detection of two analytes in the same system.

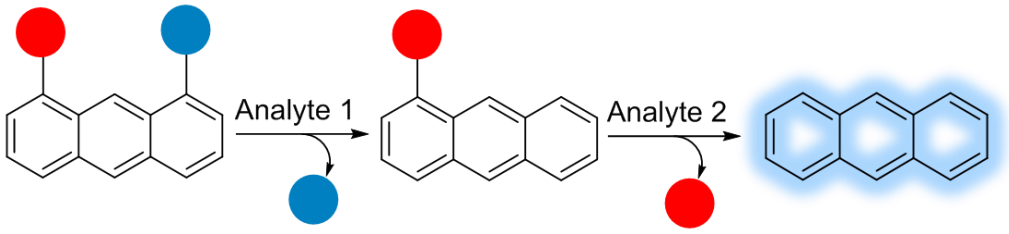

Figure 51 – Dual analyte probe reacting with two analytes to reveal a fluorescent probe.

If detection of two species is required, then the use of a dual activated probe is a much faster and more efficient method than using two individual probes for sequential testing.[107] An example of the need to detect the presence of more than one species is in macrophages, where the production of both NO and H_2O_2 is required for the effective destruction of pathogens.[108-110] These two analytes are relatively short lived and would be hard to detect with two individual probes, due to small 'real-time' differences in uptake, localisation and selectivity that would make it extremely difficult to gather reliable data using individual analytes.

A dual detection probe is normally based on an "AND" MLG system, meaning that both analyte-1 AND analyte-2 need to be present for the fluorescence response to turn on.[105] There are, however, several other types of logic that can be achieved using MLGs, as summarised in the truth table shown in **Figure 52**.[111] An "Or" logic gate gives a positive result if one or both of the analytes is present. An "XOR" system is an exclusive OR gate, where a positive is given in the presence of one analyte only. An "INH" logic gate is positive in the presence of only one analyte, with its response inhibited in the presence of the other analyte. A "NOR" logic gate only gives a positive result when both analytes are absent. A "NAND" logic is positive if neither, or only one of the analytes are present, whilst being negative if both analytes are present. Finally, a "XNOR" logic gate is positive in the absence or presence of both analytes and negative if only one analyte is present.

	OR	AND	XOR	INH	NOR	NAND	XNOR
MLG alone	✘	✘	✘	✘	✔	✔	✔
Analyte 1	✔	✘	✔	✔	✘	✔	✘
Analyte 2	✔	✘	✔	✘	✘	✔	✘
Analyte 1 +2	✔	✔	✘	✘	✘	✘	✔

Figure 52 – Truth table for a two-input logic gate, showing the possible outcomes for the two inputs from analyte 1 and analyte 2.

Numerous reviews have published summarising recent developments in MLGs in recent years, with a few interesting examples of their uses now presented to demonstrate their potential application.[105, 112-115]

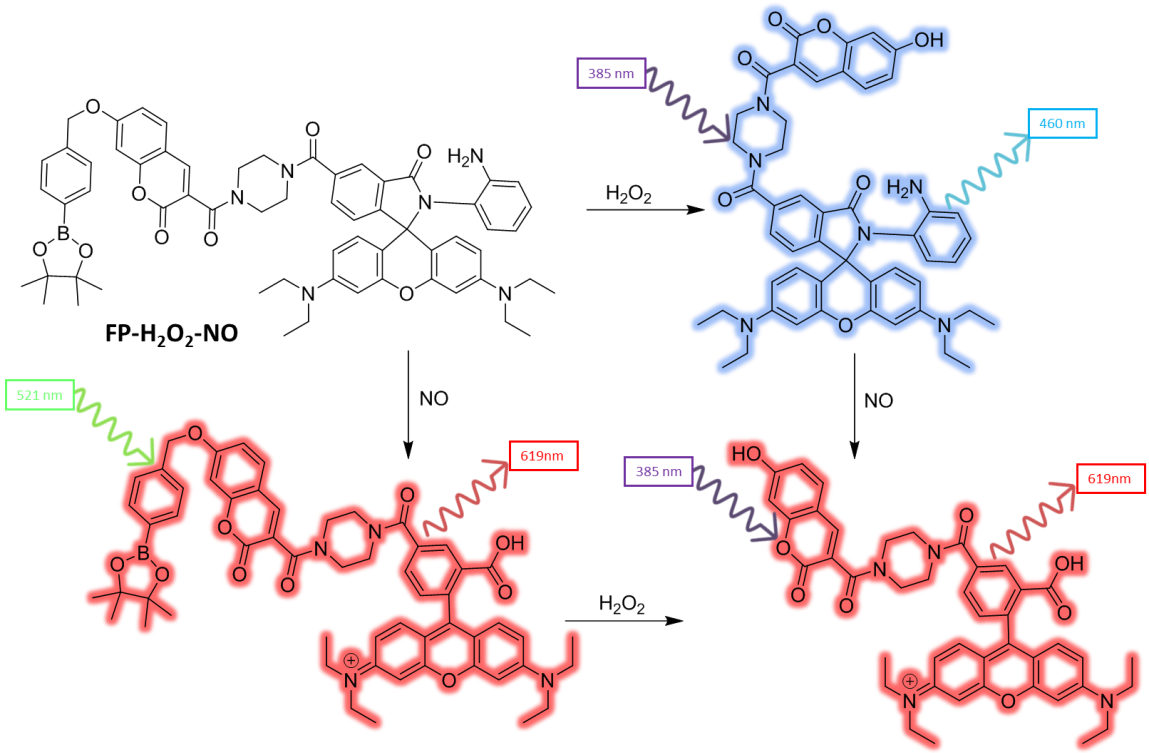

Figure 53 – Representation of the different sensing outputs of the MLG **FP-H_2O_2-NO.**

Zhu *et al.* have developed an MLG probe capable of responding to the presence of both H_2O_2, and NO singularly, as well as in combination (**FP-H_2O_2-NO**, **Figure 53**).[116] This was achieved *via* the use to two distinct masked fluorophores that were connected together using a piperazine linker. The reactive group for the H_2O_2 was a boronic acid pinacol ester group, bound to a 7-hydroxycoumarin fluorophore, whilst the reactive group used for targeting of NO was a phenylenediamine group attached to a rhodamine-fluorophore.

Upon exposure to H_2O_2, the boronic ester is cleaved and the blue fluorescence of the coumarin is turned on for an excitation at 400 nm. Exposure of the probe to NO results in the phenylenediamine group being cleaved to release the rhodamine fluorophore, which gives a red fluorescence response upon excitation of 550 nm. The ability of the probe to detect both species arises from the FRET that can occur between the coumarin (FRET donor) and the rhodamine (FRET acceptor) units after both reactive masking groups have

been cleaved caused by excitation at the coumarin absorption wavelength of 400 nm. This allows a single probe to detect the presence of either or both of the analytes.

In another example, a two-input "AND" logic probe was developed by Song *et al.* for the detection of H_2S and intracellular thiols (RSH).[117] Probe **QME-N_3** is based on a quinolone scaffold containing an azide group that is reduced by H_2S to afford an amino group and an α,β-unsaturated malonate unit that undergoes conjugate addition with a RSH nucleophile, with both events required to elicit a fluorescence response (**Figure 54**).

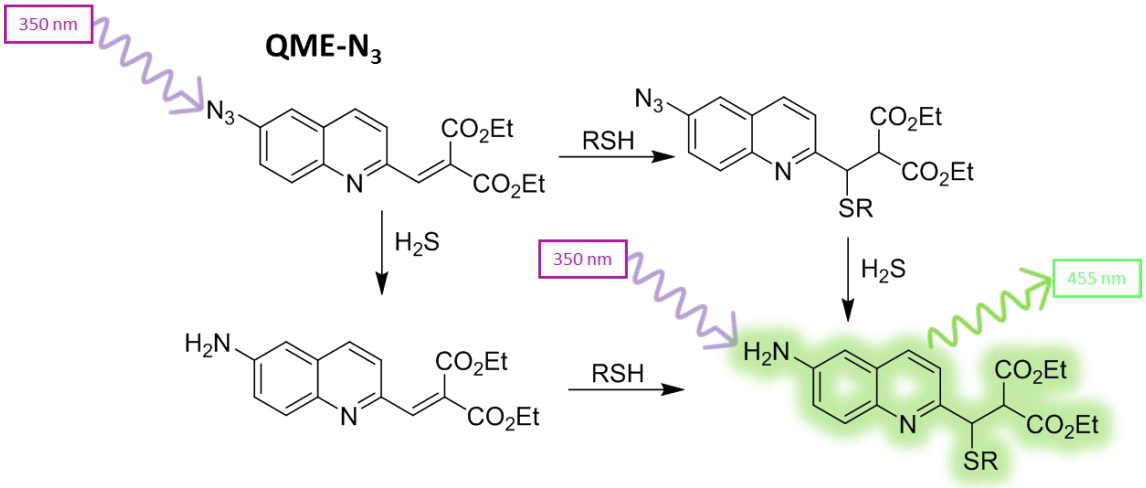

Figure 54 – Reaction scheme of probe **QME-N_3** reacting with H_2S and RSH.

1.7 Summary of introduction

Fluorescence is a very useful tool in the design of sensors that can be used for the study of biological systems. The three main components of a fluorescent probe and details of common fluorescence mechanisms employed in fluorescent probes are discussed and numerous examples where these probes have been used in biological systems presented. An introduction to the principle of MLGs and the development of multi-analyte probes is also provided. Many of the target analytes described in this introduction are linked directly to human illnesses, with new probes still required to interrogate intracellular processes and determine mechanisms of action. Existing fluorescent probes have proven their worth repeatedly; however, ever more precise and sensitive probes with new reactive units and brighter fluorophores are required to push forward limits of detection.

1.8 Introduction references

1: J. R. Lakowicz, *Principles of Fluorescence spectroscopy*, Springer, New York, USA, Third edition.

2: M. Taniguchi, J. S. Lindsay, *Photochem. and Photobio.*, **2018**, *94*, 290-327.

3: J. Zhang, R. E. Campell, A. Y. Ting, R. Y. Tsien, *Nat. Revs.*, **2002**, *3*, 906-918.

4: T. Terai, T. Nagano, *Curr. Opin. Chem. Bio.*, **2008**, *12*, 515-521.

5: J. Chan, S. C. Dodani, C. J. Chang, *Nat. Chem.*, **2012**, *4*, 973-984.

6: H. A. Goldwin, J. M. Berg, *J. Am. Chem. Soc.*, **1996**, *118*, 6514-6515.

7: W. Lu, X. Qin, S. Liu, G. Chang, Y. Zhang, Y. Luo, A. M. Asiri, A. O. Al-Yaoubi, X. Sun, *Anal. Chem.*, **2012**, *84*, 5351-5357.

8: Y. Yang, Q. Zhao, W. Feng, F. Li, *Chem. Revs.*, **2013**, *113*, 192-270.

9: S. R. Mikkelson, E. Cotón, *Bianalytical Chemistry*, **2004**, John Wiley & Sons, Inc.,

10: B. C. Dickinson, C. J. Chang, *Nat. Chem. Bio.*, **2005**, *8*, 504-511.

11: T. Rasheed, C. Li, M. Bilal, C. Yu, H. M. N. Iqbal, *Sci. Total Environ.*, **2018**, 640-641, 174-193.

12: H. Dobrev, *Photodermatol. Photoimmunol. Photomed.*, **2010**, *26*, 285-289.

13: C. E. S. Hoogstins, Q. R. J. G. Tummers, K. N. Gaarenstroom, C. D. de Kroon, J. B. M. Z. Trimbos, T. Bossee, V. T. H. B. M. Smit, J. Vuyk, C. J. H. van de Velde, A. F. Cohen, P. S. Low, J. Burggraaf, A. L. Vahrmeijer, *Clin. Cancer Res.*, **2016**, *12*, 2929-2938.

14: J. Wu, W. Liu, J. Ge, H. Zhang, P. Wang, *Chem. Soc. Rev.*, **2011**, *40*, 3483-3495.

15: A. Kaur, Z. Lim, K. Yang, E. J. Evans, *Comprehensive Supramolecular Chemistry II*, **2017**, *8*, 295-317.

16: V. S. Lin, A. R. Lippert and C. J. Chang, *Hydrogen Sulfide in Redox Biology*, Pt A, **2015**, *554*, 63-80.

17: V. S. Lin and C. J. Chang, *Curr. Opin. Chem. Biol.*, **2012**, *16*, 595-601.

18: T. D. James, K. R. S. Sandanayake, S. Shinkai, *Angew. Chem. Int. Ed. Engl.*, **1996**, *35*, 1910-1922.

19: T.D. James, K. R. S. Sandanayake, R. Iguchi, S. Shinkai, *J. Am. Chem. Soc.*, **1995**, *117*, 8932-8987.

20: V. Ramamurthy, K. S. Schanze, *Organic and Inorganic Photochemistry*, **1998**, Marcel Dekker.

21: G. Wang, J. Qin, L. Fan, C. Li, Z. Yang, *J. Photochem. Photobiol.*, **2016**, *314*, 29-34.

22: A. Margineanu, J. J. Chan, D. J. Kelly, S. C. Warren, D. Flatters, S. Kumar, M. Katan, C. W. Dunsby, P. W. French, *Sci. Rep.*, **2016**, *6*, 21816.

23: J. Mu, F. Liu, M. S. Rajab, M. Shi, S. Li, C. Goh, L. Lu, Q. Xu, B. Liu, L. G. Ng, B. Xing, *Angew. Chem. Int. Ed.*, **2014**, *53*, 14357-14362

24: J. F. Callan, A. P. de Silva and D. C. Magri, *Tetrahedron*, **2005**, *61*, 8551-8588.

25: S. Sahana, G. Mishra, S. Sivakumar, P. K. Bharadwaj, *J. Photochem. & Photobiol.*, **2018**, *351*, 231-239.

26: X. Yang, L. He, K. Xu, Y. Yang, W. Lin, *New J. Chem.*, **2018**, *42*, 12361-12364.

27: A. C. Sedgwick, L. Wu, H. Han, S. D. Bull, X. He, T. D. James, J. L. Sessler, B. Z. Tang, H. Tian, J. Yoon, *Chem. Soc. Revs.*, **2018**, *47*, 8842-8880.

28: M. An, B. Kim, H. Seo, A. Helal, H. Kim, *Spectrochim. Acta. A*, **2016**, *169*, 87-94.

29: R. Hu, J. Feng, D. Hu, S. Wang, S. Li, Y. Li, G. Yang, *Angew. Chem. Int. Ed. Eng.*, **2010**, *49*, 4915-4918.

30: A. Kaur, Z. L. Yang, E. J. New, *Comprehensive Supramolecular Chemistry II*, **2015**, *8*, 295-317.

31: P. Zatta, D. Drago, S. Bolognin, S. L. Sensi, *Trends Pharmacol. Sci.*, **2009**, *30*, 346-355.

32: A. R. Khan, F. R. Awan, *J. Diabetes Metab. Disord.*, **2014**, 13: 16

33: L. Fouani, S. V. Menezes, M. Paulson, D. R. Richardson, *Pharma. Res.*, **2017**, *115*, 275-287.

34: Z. Zhou, M. Yang, H. Yang, K. Huang, F. Li, T. Yi, C. Huang, *Chem. Commun.*, **2008**, *29*, 3387-3389.

35: V. Tharmaraj, K. Pitchumani, *Anal. Chim. Acta*, **2012**, *751*, 171-175.

36: J. H. Petretski, M. M. Kanashiro, F. R. Rodrigues, E. W. Alves, O. L. Machado, T. L. Kipins, *Biochem. Biophys. Res. Comms.*, **2000**, *276*, 29-34.

37: T. Weinberg, *Am. J. Clin. Path.*, **1958**, *29*, 54-60.

38: K. Mumtaz, Z. Azam, S. Hamid, S. Abid, S. Memon, H. A. Shah, W. Jafri, *Heptol Int.*, **2009**, *3*, 563-570.

39: Y. Zhou, J. Won, J. Y. Lee, J. Yoon, *Chem. Commun.*, **1997**, *47*, 1997-1999.

40: X. Zhou, Y. Yip, W. Chan, A. W. M. Lee, *Bleinstein J. Org. Chem.*, **2011**, *7*, 75-81.

41: J. A. Kellum, *Critical Care*, **2000**, *4*, 6-14.

42: J. Han, K. Burgess, *Chem. Rev.*, **2010**, *110*, 2709-2728.

43: P. Swietach, R. D. Vaughan-Jones, A. L. Harris, A. Hulikova, *Phil. Trans. R. Soc B*, **2014**, *369*, 20130099

44: N. J. Blacklock, J. P. Beavis, *Brit. J. Urol.*, **1974**, *46*, 537-542.

45: S. Charier, O. Ruel, J. Baudin, D. Alcor, J. Allemande, A. Meglio, L. Jullien, *Angew. Chem. Int. Ed.*, **2004**, *43*, 4785-4788.

46: S. D. Meo, T. T. Reed, P. Vendetti, V. M. Victor, *Oxid. Med. Cell Longev.*, **2016**,

1245049, 44.

47: A. Bachi, I. Dalle-Donne and A. Scaloni, *Chem, Rev.*, **2013**, *113*, 596-698.

48: Y. X. Zhang, Y. Z. Du, W. D. Le, K. K. Wang, N. Kieffer and J. Zhang, *Antioxd. Redox Signal.*, **2011**, *15*, 2867-2908.

49: G. Filomeni, D. D. Zio, F. Cecconi, *Cell Death Diff.*, **2014**, *22*, 377-388.

50: S. Manoharan, G. J. Guillemin, R. S. Abiramasundari, M. M. Essa, M. Akbar, M. D. Akbar, *Oxid. Med. Cell. Longev.*, **2016**, 2016: 8590578.

51: G. Y. Liou, P. Storz, *Free Radical Res.*, **2010**, *44*, 479-496.

52: H. Kaneto, N. Katakami, M. Matsuhisa, T. Matsuoka, *Mediators of Inflammation*, **2010**, *453892*, 11.

53: F. He, L. Zuo, *Int. J. Mol. Sci.*, **2015**, *16*, 27770-27780.

56: F. L. Muller, M. S. Lustgarten, Y. Jang, A. Richardson, H. V. Remmen, *Free Radic. Biol. Med.*, **2007**, *43*, 477-503.

57: H. R. Warner, *Free Radic. Bio. Med.*, **1994**, *17*, 249-258.

58: P. G. Winyard, D. A. Willougby, *Methods in Molecular Biology*, **2003**, *225*, Humana Press Inc. Totowa, NJ.

59: J. J. Hu, N. Wong, S. Ye, X. Chen, M. Lu, A. Q. Zhao, Y. Guo, A. C. Ma, A. Leung, J. Shen, D. Yang, *J. Am. Chem. Soc.*, **2015**, *137*, 6837-6843.

60: K. Kundo, S. F. Knight, N. Willet, S. Lee, W. R. Taylor, N. Murthy, *Angew. Chem. Int. Ed.*, **2009**, *48*, 299-303.

61: J. Fan, H. Mu, H. Zhu, J. Du, N. Jiang, J. Wang, X. Peng, *Ind. Eng. Chem. Res.*, **2015**, *36*, 8842-8846.

62: M. Lucas, M. C. Rodriguez, J. M. Gata, M. D. Zayas, F. Solano, G. Izquierdo, *Neurochemistry Int.*, **2003**, *42*, 67-71.

63: S. Olszowski, P. Mak, E. Olszowska, J. Marcinkiewicz, *Acta BioChim. Pol.*, **2003**, *50*, 471-479.

64: Z. Sun, F. Liu, Y. Chen, P. K. H. Tang, D. Yang, *Org. Lett.*, **2008**, *10*, 2171-2174.

65: A. Strzepa, K. A. Pritchard, B. N. Dittel, *Cell. Immunol.*, **2017**, *317*, 1-8.

66: J. V. Hunt, R. T. Dean, S. P. Wolff, *Biochem. J.*, **1988**, *256*, 205-212.

67: H. Sies, Eur. *J. Biochem.*, **1993**, *215*, 213-219.

68: N. B. Yapici, S. Jockusch, A. Moscatelli, S. R. Mandalapu, Y. Itagaki, D. K. Bates, S. Wiseman, K. M. Gibson, N. J. Turrow, L. Bi, *Org. Lett.*, **2012**, *14*, 50-53.

69: S. Charier, O. Ruel, J. Baudin, D. Alcor, J. Allemand, A. Meglio, L. Jullien, *Angew. Chem.*, **2004**, *116*, 4889-4892.

70: J. R. Kanofsky, *Chem. Biol. Intrac.*, **1989**, *70*, 1-28.

71: E. Skovsen, J. W. Snyder, J. D. C. Lambert, P. R. Ogilby, *J. Phys. Chem. B*, **2005**,

109, 8570-8573.

72: A. M. Elvis, J. S. Ekta, *J. Nat. Sci. Bio. Med.*, **2011**, *2*, 66-70.

73: V. Bocci, Oxygen-Ozone Therapy, **2002**, *Springer Science + Business Media.*

74: B. M. Babior, C. Takeuchi, J. Ruedi, A. Gutierrez, P. Wentworth, *Proc. Natl Acad. Sci. U.S.A*, **2003**, *100*, 3031-3034.

75: L. Yu, Y. Li, H. Yu, K. Zhang, X. Wang, X. Chen, J. Yue, T. Huo, H. Ge, K. A. Alarmy, H. M. Marwani, S. Wang, *Sens. Act. B: Chem.*, **2018**, *266*, 717-723.

76: K. Xu, S. Sun, J. Li, L. Li, M. Qiang, B. Tang, *Chem. Commun.*, **2014**, *48*, 648-686.

77: M. Rosseli, P. J. Keller, R. Dubey, *Hum. Reprod.*, **1998**, *4*, 3-24.

78: V. W. T. Liu, P. L. Hang, *Cardi. Res.*, **2008**, *77*, 19-29.

79: H. Zhang, J. Chen, X. Guo, H. Wang, H. Zhang, *Anal. Chem.*, **2014**, *86*, 3115-3123.

80: H. Kojima, N. Nakatsubo, K. Kikuchi, S. Kawahara, Y. Kirino, H. Nagoshi, Y. Hirata, T. Nagano, *Anal. Chem.*, **1998**, *70*, 2446-2453.

81: B. Halliwell, M. V Clement, L. H. Long, *FEBS Letts.*, **2000**, *486*, 10-13.

82: N. G. N. Milton, *Drugs Aging*, **2004**, *21*, 81-100.

83: C. Wittmann, P. Chockley, S. K. Singh, L. Pase, G. J. Lieschke, C. Grabher, *Adnv. Hematol.,* **2009**, *2012*, 541471, 6.

84: M. P. Lisanti, U.E. Martinez-Outschoom, Z. Lin, S. Pavlides, D. Whitaker-Menezes, R. G. Petsell, A. Howell, F. Sotgia, *Cell Cycle*, **2011**, *10*, 2440-2449.

85: J. Chan, S. C. Dodani and C. J. Chang, *Nat. Chem.*, **2012**, *4*, 973-984.

86: C. Chung, D. Srikun, C. S. Lim, C. J. Chang and B. R. Cho, *Chem.Commun.*, **2011**, *47*, 9618-9620.

87: A. R. Lippert, G. C. V. De Bittner and C. J. Chang, *Accs. Chem. Res.*, **2011**, *44*, 793-804.

88: E. W. Miller, A. E. Albers, A. Pralle, E. Y. Isacoff and C. J. Chang, *J. Am. Chem. Soc.*, **2005**,*127*, 16652-16659.

89: A. E. Albers, V. S. Okreglak and C. J. Chang, *J. Am. Chem. Soc.*, **2006**, *128*, 9640-9641.

90: K. Zamojc, M. Zdrowowocz, D. Jacewicz, D. Wyrzykowski, L. Chmurzynski, *Crit. Rev. Anal. Chem.*, **2016**, *46*, 3, 171-200.

91: K. H. Xu, B. Tang, H. Huang, G. W. Yang, Z. Z. Chen, P. Li and L. G. An, *Chem. Commun.,* **2005**, *0*, 5974-5976.

92: M. Onoda, H. Tokuyama, S. Uchiyama, K. Mawatari, T. Santa, K. Kaneko, K. Imai and K. Nakagomi, *Chem. Commun.*, **2005**, *54*, 1848-1850.

93: C. A. Bunton, *Nature*, **1949**, *163*, 444.

94: Y. Liao, K. Li, M. Wu, T. Wu, X. Yu, *Org. Biomol. Chem.*, **2014**, *12*, 3004-3008.

95: Z. Zhuang, Q. Yang, Z. Zhang, Q. Zhang, G. Zhang, F. Zhan, *J. Photochem. Photobio. A: Chem.*, **2017**, *344*, 8-14.

96: B. Halliwell, Free Radicals and other reactive species in Disease, ***2001***, *Nature Publishing Group*.

97: K. Lin, J. Xue, M. Nomen, B. Spur, P. Wong, *J. Bio. Chem.*, **1995**, *270*, 16487-16490.

98: M. Trujillo, L. Folkes, S. Bartesaghi, B. Kalyanaraman, P. Wardman, R. Radi, *Free Rad. Biol. & Med.*, **2005**, *39*, 279-288.

99: R. Radi, *J. Biol. Chem.*, **2013**, *288*, 26464-26472.

100: D. Yang, H. Wang, Z. Sun, N. Chung, J. Shen, *J. Am. Chem. Soc.*, **2006**, *128*, 6004-6005.

101: S. Palanisamy, P. Wu, S. Wu, Y. Chen, S. Tzou, C. Wang, C. Chen, Y. Wang, *Biosens. Bioelec.*, **2017**, *91*, 849-856.

102: J. Zhang, Y. Li, J. Zhou, W. Guo, *Sensors & Actuators*, **2016**, *237*, 67-74.

103: H. Zhang, J. Li, Y. Sun, Y. Huo, Y. Li, W. Liu, Z. Wu, N. Zhu, W. Guo, *Chem. Commun.*, **2015**, *51*, 2721-2724.

104: X. Sun, Q. Xu, G. Kim, S. E. Flower, J. P. Lowe, J. Yoon, J. S. Fossey, X. Qian, S. D. Bull, T. D. James, *Chem. Sci.*, **2014**, *5*, 3368-3373.

105: S. Erbas-Cakmak, S. Kolemen, A. C. Sedgwick, T. Gunnlaugsson, T. D. James, J. Yoon, E. U. Akkaya, *Chem. Soc. Rev.*, **2018**, *47*, 2228-2248.

106: L. Yun, S. Wang, K. Huang, Z. Liu, F. Gao, W. Zeng, *Tetrahedron*, **2015**, *71*, 4679-4706.

107: H. komatsu, T. Miki, D. Citterio, T. Kubota, Y. Shindo, Y. Kitamura, K. Oka, K. Suzuki, *J. Am. Chem. Soc.*, **2005**, *127*, 10798-10799.

108: A. L. Drexler, J. E. Pietri, N. Pakpour, E. Hauk, B. Wang, E. K. K. Glennon, M. Georgis, M. A. Riehle, S. Luckhart, *PLOS Pathog.*, **2014**, *6*, e1004231.

109: M. Tiwari, S. K. Chaube, *Biores. Open Access*, **2017**, *6.1*, 110-122.

110: P. A. Jansson, *J. Int. Med.*, **2007**, *262,* 173-183.

111: J. L. Kolanowski, F. Liu, E. J. New, *Chem. Soc. Rev.*, **2018**, *47*, 195-208.

112: A. P. de Silva, *Chem. Asian J.*, **2011**, *6*, 750-766.

113: S. Sreejith, A. Ajayaghosh, *Indian J. Chem.*, **2012**, *51A*, 47-56.

114: J. Andreasson, U. Pischel, *Chem. Soc. Rev.*, **2015**, *44*, 1053-1069.

115: T. Miyamoto, S. Razavi, R. DeRose, T. Inoue, *ACS Synth. Biol.*, **2013**, *2*, 72-82.

116: L. Yuan, Y. Xie, B. Chen, S. Zhu, *J. Am. Chem. Soc.*, **2012**, *134*, 1305-1315.

117: C. Dai, X. Liu, X. Du, Y. Zhang, Q. Song, *ACS Sens.*, **2016**, *7*, 888-895.

2.0 Coumarin Based Probes

In this chapter a brief overview of the coumarin unit shall be given, with its use in sensor systems being exemplified and discussed. The remainder of this chapter will describe a range of coumarin-based probes that were produced during my research programme, including a justification of the development of each probe, their synthesis and analysis.

2.1 Introduction

Coumarins are a broad class of compounds containing a benzopyrone structure comprised of a fused arene and pyrone ring with a carbonyl group present at the 2-position of the pyrone (**Figure 55**).[1]

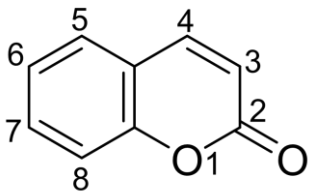

32

Figure 55 – The structure of coumarin **32**.

Found in many plant species, coumarin was first isolated in 1820 by the German Chemist A. Vögel from Tonka beans (*Dipteryx odorata*) and then synthesized by the English chemist William Henry Perkin in 1868.[1]

Since then, coumarin based compounds have found uses in many different areas, including as appetite suppressors,[2] as drugs for the treatment of lymphedema,[3] and their fluorescent properties are exploited to prepare OLED emitters.[4] Coumarins exhibit high sensitivity towards the polarity and viscosity of their local environment,[5] and they have been widely exploited for the development of fluorescent probes for sensing applications.[6]

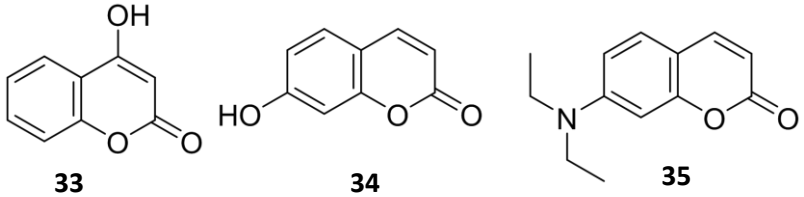

33 **34** **35**

Figure 56 – Structure of three coumarin derivatives, 4-hydroxycoumarin (**33**), umbelliferone (**34**) and 7-diethylaminocoumarin (**35**).

Many derivatives of coumarin have been reported as components of fluorescence probes (**Figure 56**), including 4-hydroxycoumarin **33**, 7-hydroxycoumarin **34** (umbelliferone), 7-diethyl-aminocoumarin **35** and benzocoumarin.[6] The synthesis of these coumarins and their derivatives can be achieved using several named reactions, including the Perkin synthesis,[7] the Kostanecki acylation[8] and the Pechmann condensation reactions (**Figure 57**).[9] The Pechmann condensation reaction involves condensation of a phenol and carboxylic acid (or ester) with a β-carbonyl ester in an acidic environment. The reaction proceeds *via* transesterification of the ester with the phenol, followed by intramolecular Friedel-Crafts acylation and dehydration to form the new pyrone ring system of the coumarin skeleton. The presence of additional functional groups on the coumarin skeleton can be used to increase its fluorescence, with the addition of heteroatoms increasing the ability to access ICT type fluorescence pathways.

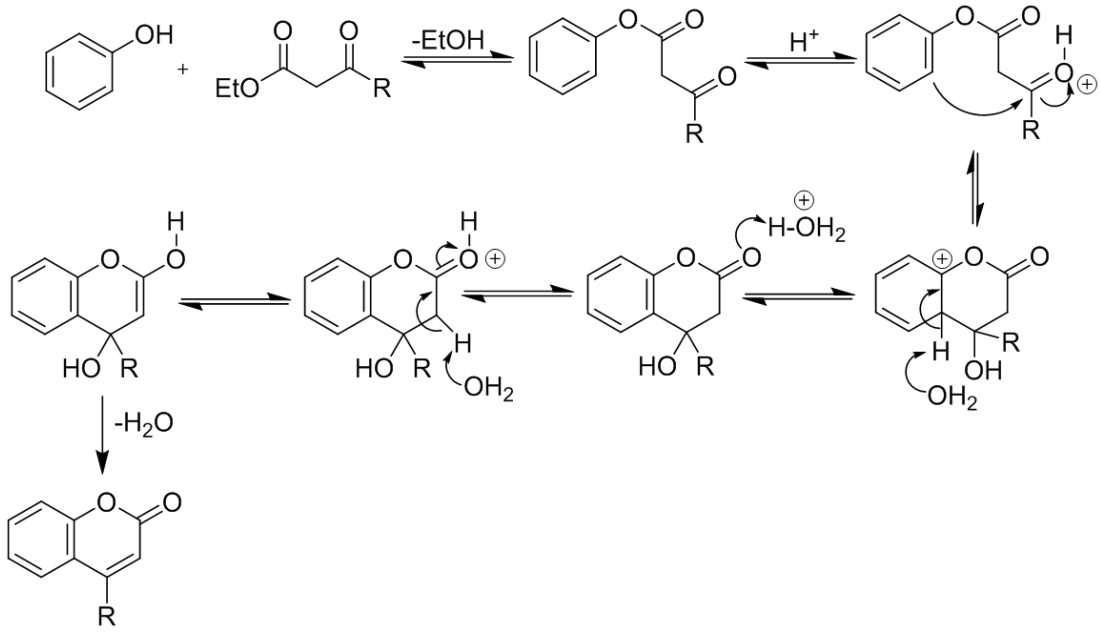

Scheme 57 – Reaction mechanism of the Pechmann condensation between phenol and a β-keto ester.

Mondal *et al.* have used a coumarin core structure containing diethylamino and trifluoroacetyl acetonate groups to synthesize a probe (**36**, **Figure 58**) for the ratiometric detection of hydrazine (N_2H_4).[10] Selectivity for N_2H_4 occurs through selective hydrazinolysis of the carbonyl of the trifluoroacetyl acetonate, which triggers a subsequent reaction cascade to produce a cyclized fluorescent pyrazole compound (**37**). This enables this probe to be used for the ratiometric detection and quantification of N_2H_4.

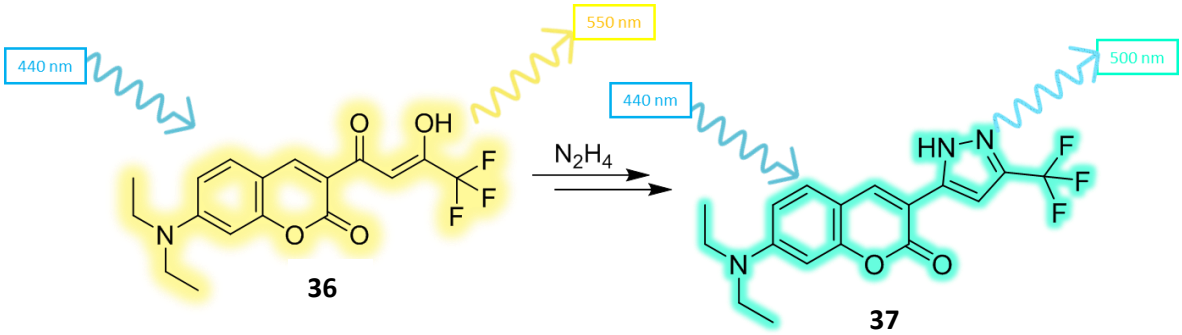

Figure 58 – The probe **36** reacts with N_2H_4 to create **37** which affords a ratiometric response.

Wang *et al.* developed an Fe^{2+} probe based on a non-fluorescent coumarin core structure attached to a 2-phenol moiety through an imino linker (**38**, **Figure 59**).[11] The reactivity of the sensor is triggered by an Fe^{2+} mediated cyclization/aromatisation reaction which affords a fluorescent benzoxazole fragment. This probe was found to be highly selective for Fe^{2+} enabling it to be used for imaging Fe^{2+} in cell studies.

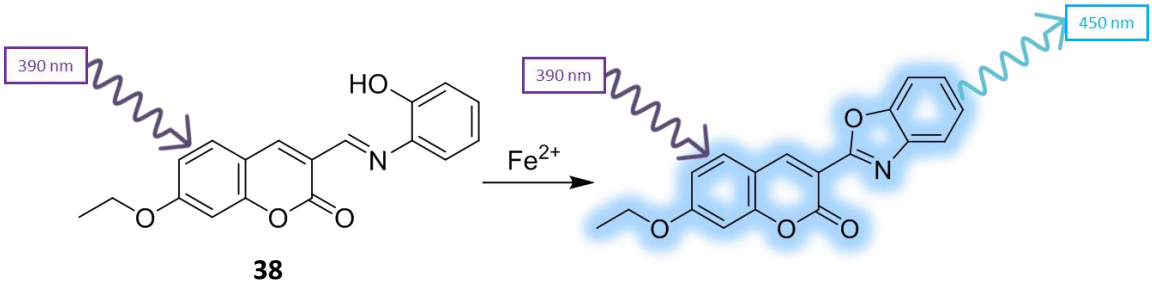

Figure 59 – Probe **38** reacts with Fe^{2+} to give a fluorescent response.

2.2 A Coumarin Based Probe for the Detection of $ONOO^-$ AND Hcys / Cys in Cells

2.2.1 Literature Precedent

$ONOO^-$ is a potent RNS that is largely deleterious in biological systems, where it can damage DNA, proteins and lipids when its concentration is elevated (**Section 1.5.4**).[12-14] As discussed in the introduction, 4-methylphenylboronic acid pinacol ester (Bpin) has previously been shown to be a reactive unit for peroxynitrite in numerous fluorescent probes.[15]

Homocysteine (Hcys) is a homologue of the amino acid cysteine (Cys). It is a non-coded (non-proteogenic) amino acid that is formed from de-methylation of the terminal C_ε methyl group of methionine.[16] One of the main uses of Hcys is as a substrate for the formation of Cys in cells, *via* an enzymatic pathway that employs vitamin B_6 as a cofactor.[17] High levels of Hcys (>15 µmol/ L) result in a medical condition called hyperhomocysteinemia[18] which has been linked to many different illnesses, including cardiovascular disease,[19] Alzheimer's disease,[20] bone fractures[21] and kidney disease.[22]

There are difficulties that arise when sensing Hcys over other amino acids. With the structural similarities between Hcys, Cys and Glutathione (GSH, **Section 2.5.1**) presenting difficulties in designing probes for their selective detection.[23] Receptor groups that are designed to react with the thiol unit of Hcys are also prone to reaction with Cys and GSH. This is not always a problem, as for some applications the levels of off-target species are in such low concentration that they only make a negligible contribution to the overall fluorescence of the system.[24]

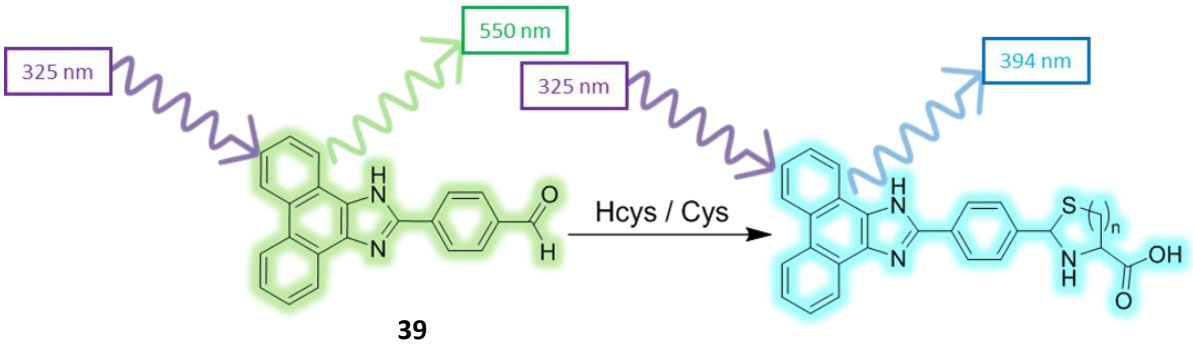

Figure 60 – Tan's Hcys / Cys probe **39** that produces fluorescence through formation of thiazolidine or thiazinane fragments.

Tan *et al*. developed a Hcys/ Cys probe using a simple ICT based system **39** containing a phenanthroimidazole moiety (electron donator) appended to an aldehyde group (electron acceptor) (**Figure 60**).[25] The aldehyde group is used to target the reactivity of the thiol group of Hcys and Cys to form thiazolidine and thiazine ring systems, respectively. This binding and cyclisation caused a significant blue shift (125 nm) in the emission of the fluorophore upon excitation.

Methods for the specific detection of Hcys over other intracellular thiols have been discovered and utilised in some probes. An example from Yoon *et al.*, who designed a simple "turn-on" fluorescent probe **40** based on a pyrene structure appended to an aldehyde and ester side-chain (**Figure 61**).[26] Exposure of the probe to Hcys and Cys analytes results in the aldehyde being attacked to afford either a 6-membered thiazinane, or 5-membered thiazolidine ring system, respectively. However, only the 6-membered thiazinane ring system generated from the Hcys is fluorescent, which is proposed to be a result of an increase in the efficiency of ICT and PET based pyrene singlet excited state quenching by this ring system. This sensor was successfully used for the detection of Hcys in mammalian cells and is an excellent example of how a good design can be used to overcome selectivity challenges in detection.

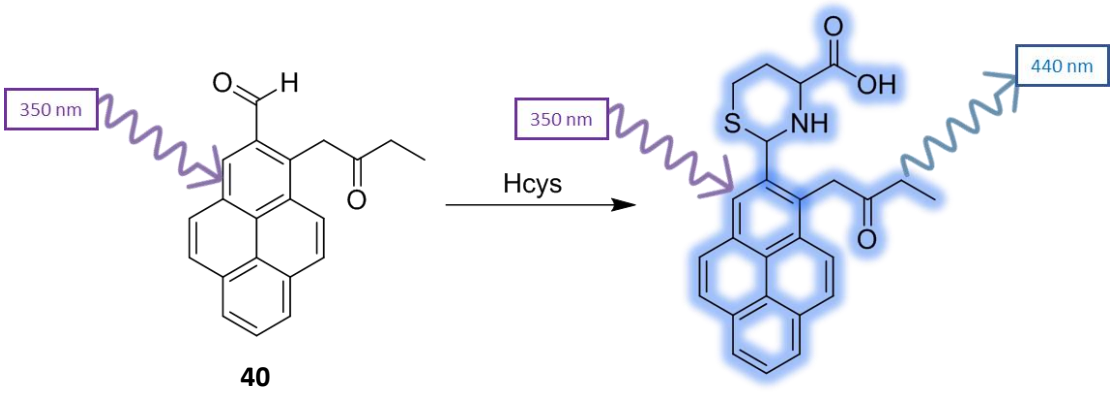

Figure 61 – Probe **40** reacts with Hcys to elicit a selective fluorescent response.

Hong *et al.* developed a simple coumarin based fluorescent probe for the detection of Hcys and Cys in water (**Figure 62**).[27] Reaction of its aldehyde functionality with Cys or Hcys results in formation of a heterocyclic ring, with the nitrogen atom of the ring system acting

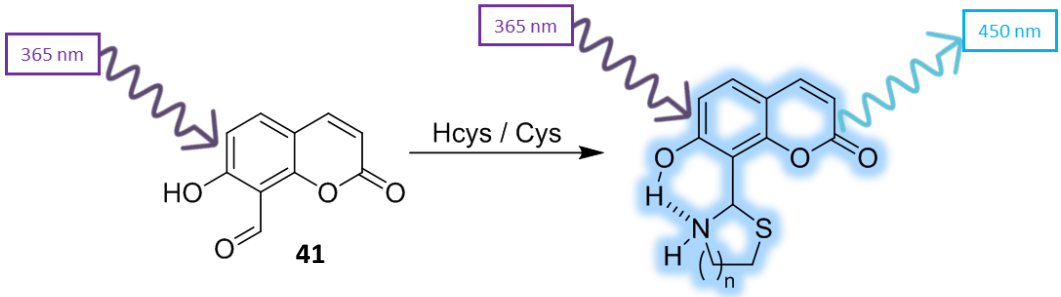

Figure 62 – Hcys / Cys reacting with Hong's simple coumarin probe **41**.

as a HB acceptor for the phenolic hydrogen atom, which disables its PET quenching properties to turn on fluorescence. Even though there was no initial intention to achieve selectivity of Hcys over Cys, there was a significantly higher fluorescence response when Hcys was added to the sensor relative to Cys. This is thought to be due to the increased stability of the six-membered ring that is formed from reaction of Hcys, relative to the five-membered ring formed from reaction of the probe with Cys.

2.2.2 Design of Probe **42**

It was decided to develop a dual analyte sensor for $ONOO^-$ and Hcys / Cys by adding extra sensing functionality to Hong's simple coumarin probe **41**. The design of new probe **42** would employ an aldehyde functionality that reacts with the thiol functionality of the Hcys/ Cys analyte and a 4-methylphenylboronic acid pinacol ester fragment to react with $ONOO^-$ (**Figure 63**).

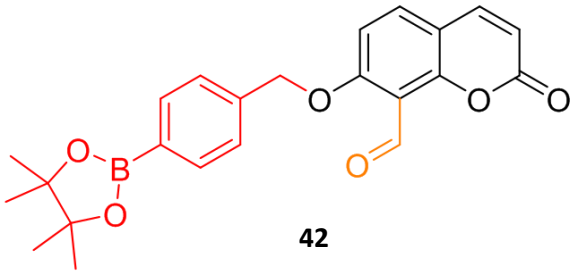

42

Figure 63 – Design of a new dual 'AND' probe **42** for the simultaneous detection of $ONOO^-$ and Hcys/Cys.

2.2.3 Synthesis of Probe **42**

The synthesis of the new probe commenced with the acetylation of the phenol group of umbelliferone **34** with pyridine and acetic anhydride which proceeded in near quantitative yield (98 %) to give **43**. The next step employed a Duff reaction (hexamethylenetetramine aromatic formylation) which introduced an aldehyde group onto the phenyl ring, with concomitant cleavage of the acetyl group of the coumarin in 69 % yield, producing **41**. This formylated phenol was then reacted with 4-bromomethylphenylboronic acid pinacol ester and K_2CO_3 in DMF, to yield the final product **42** in 51 % yield (**Scheme 1**).

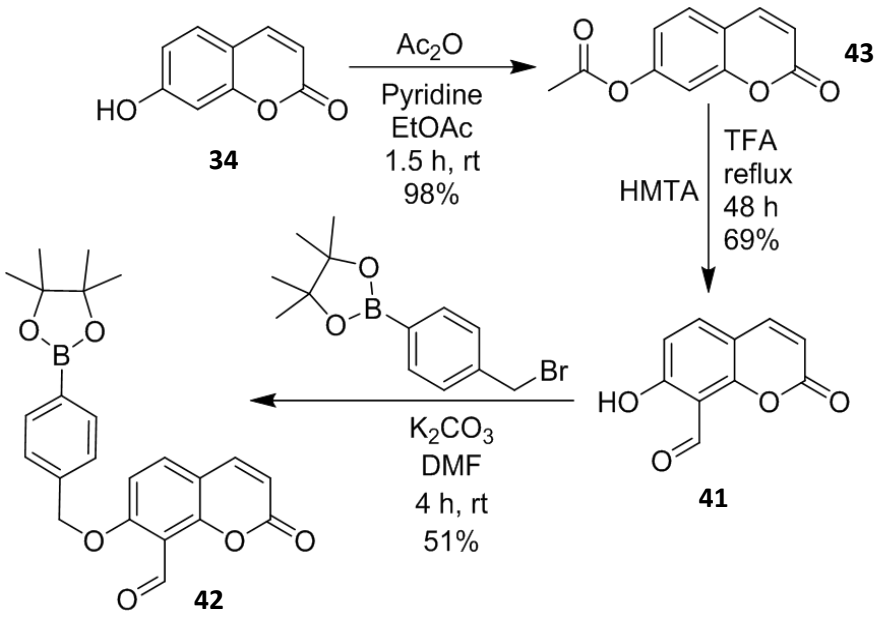

Scheme 1 – Synthesis of a dual AND probe **42** for $ONOO^-$ and Hcys / Cys probe.

2.2.4 Fluorescent Analysis of **42**

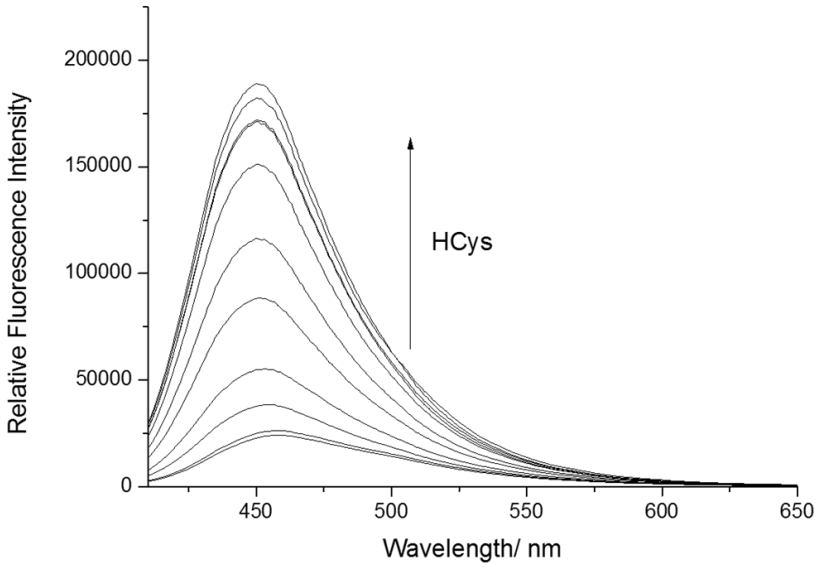

Figure 64 – Fluorescence of **41** (10 µM) produced from sequential addition of Hcys (5-500 µM) in buffer (PBS pH 7.4) after a 40 min incubation period. λex = 353 nm (bandwidth 15).

Initial fluorescence studies on probe **42** were then carried out to determine its ability to react with Hcys/ Cys and $ONOO^-$. Firstly, the assay system described by Hong *et al.* for their coumarin probe **41** for Hcys was repeated to confirm that carrying out the assay in phosphate-buffered saline (PBS) pH 7.4 buffer would give satisfactory results. Changing the buffer system did not result in a significant change in the behaviour of the probe **41** (**Figure 64**), with a large increase in fluorescence intensity being observed when in the presence of Hcys.

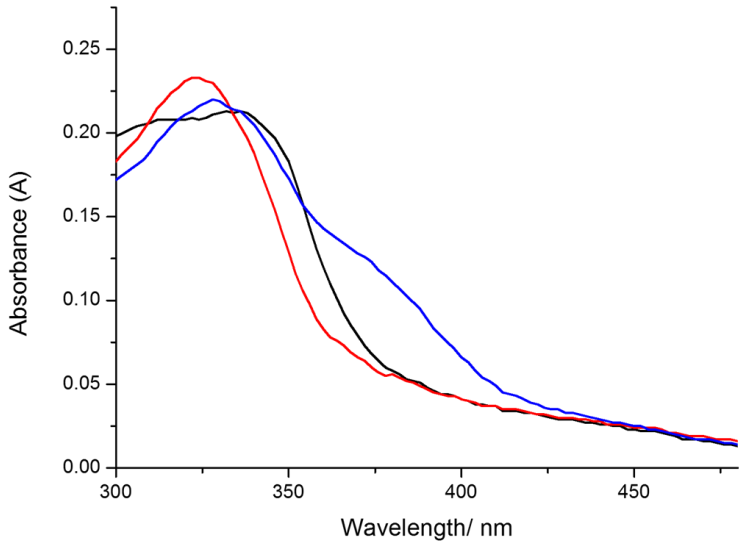

Figure 65 – UV-Vis spectra of: (a) **42** (30 µM) – black; (b) **42** (30 µM) and Hcys (3 mM) – red; (c) **42** (30 µM) and Hcys (3 mM) and $ONOO^-$ (60 µM) – blue. In PBS buffer (pH 7.4), 40 min incubation after Hcys addition.

I next measured the UV absorption of the probe **42** in the presence of Hcys (3 mM) and **42** with both Hcys (3mM) and $ONOO^-$ (60 µM) (**Figure 65**). These results showed that the UV absorption maxima of the probe shifted upon sequential addition of each analyte, which is caused by reaction of the aldehyde and boronic ester functionalities of the coumarin probe, respectively. Importantly, addition of both analytes resulted in a bathochromic shift in the absorbance (340 → 370 nm) when compared to the UV spectra of an un-activated, or partially activated probe.

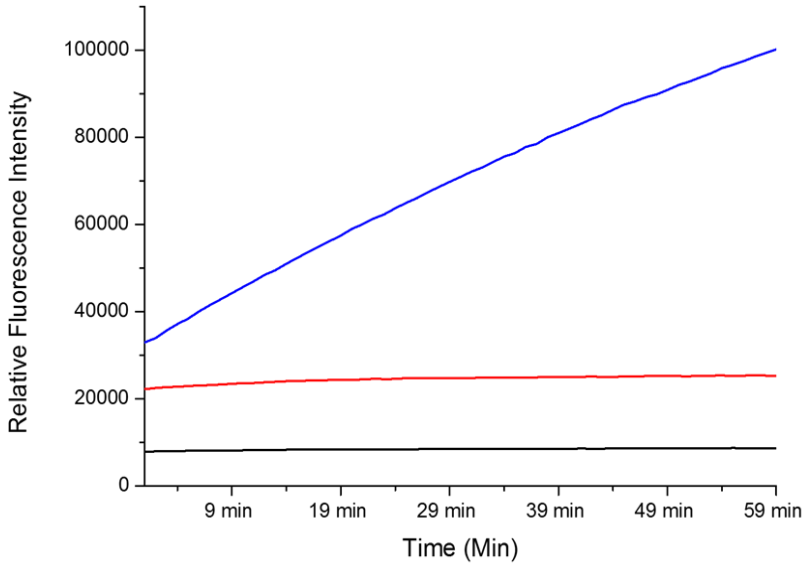

Figure 66 – Fluorescence intensity changes of **42** over time: (a) **42** (15 µM) – black line; (b) **42** (15 µM) with addition of $ONOO^-$ (18 µM) – red line; (c) **42** (15 µM) with addition of Hcys (1 mM) and $ONOO^-$ (18 µM) – blue line. In PBS buffer (pH 7.4) λex = 371 (bandwidth 20 nm)/ λem = 448 (bandwidth 100 nm).

I was aware of the need to allow sufficient time for Hcys to react with the aldehyde functionality of the probe, since the rate of the Hcys cyclisation reaction is much slower than the corresponding reaction of the boronate ester fragment with $ONOO^-$. Therefore, I carried out a study to measure the fluorescent response of the probe towards Hcys over time, which revealed that the thiazolidine ring forming reaction took around 60 minutes to proceed to full completion (**Figure 66**). Given these results, an incubation time for **42** with Hcys 40 min was used in all subsequent assays, before spectroscopic analysis was then carried out.

The new probe **42** was then subject to titration tests to confirm that both analytes were required for full fluorescence of the probe. When Hcys (1 mM) was added to **42**, there was a slight turn on to the fluorescence of the probe, which is likely to be due to the formation

of the thiazoline fragment on the aldehyde of **42**. As expected, subsequent addition of $ONOO^-$ (2-24 µM) resulted in a dose dependent increase in the fluorescence response (**Figure 67**, **Figure 68**), which is consistent with the cleavage of the Bpin unit, resulting in dual activation.

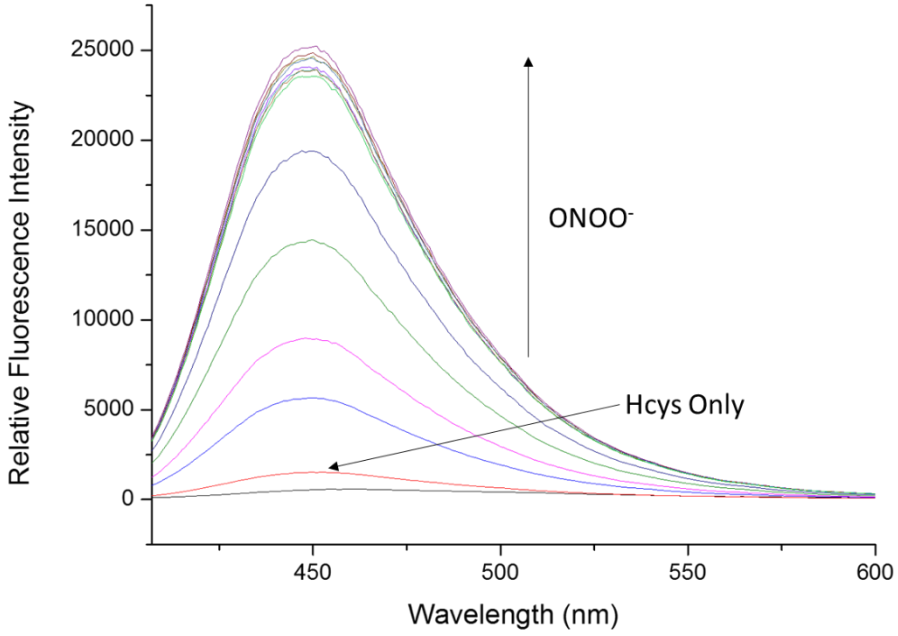

Figure 67 – Fluorescence spectra of **42** (15 µM) and Hcys (1 mM), 40 min incubation then sequential addition of $ONOO^-$ (2-24 µM) in buffer (PBS pH 7.4). λex = 371 nm (bandwidth 20 nm).

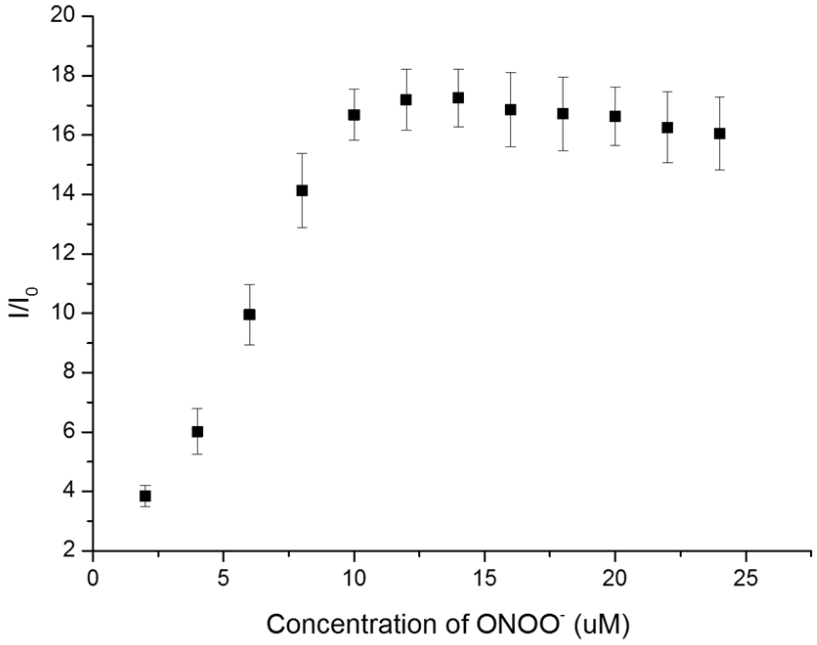

Figure 68 – Fluorescence intensity (I/I_0) of **42** (15 µM) and Hcys (1 mM), 40 min incubation then sequential addition of $ONOO^-$ (2-24 µM) in buffer (PBS pH 7.4). λex = 371 nm (bandwidth 20 nm) / λ_{em} = 448 nm.

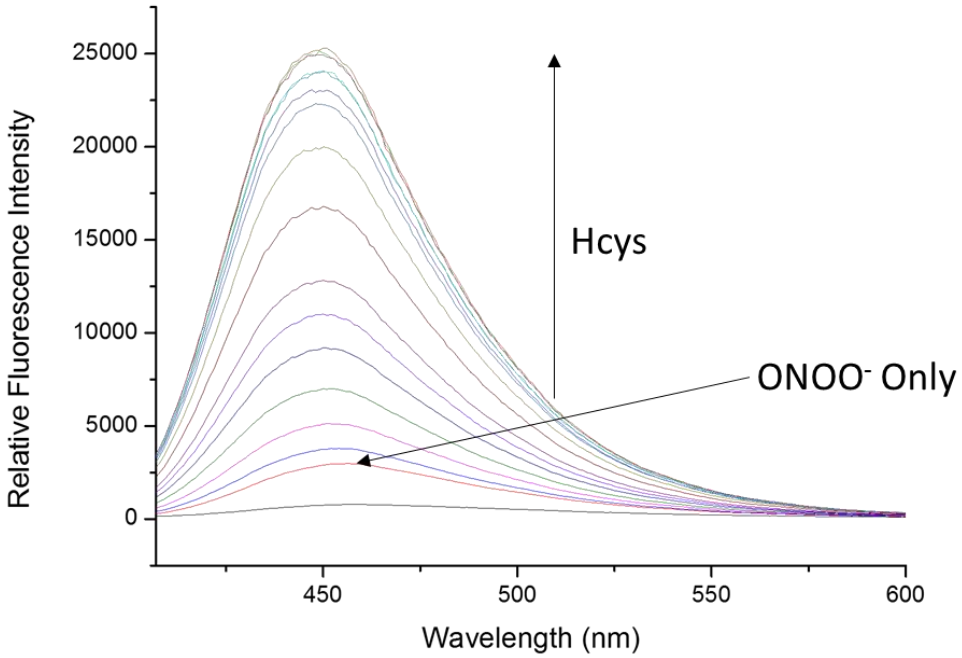

Figure 69 – Fluorescence spectra of **42** (15 µM) and $ONOO^-$ (16 µM) then sequential addition of Hcys (0.1-5.5 mM). In buffer (PBS pH 7.4) after 40 min. λex = 371 nm (bandwidth 20 nm).

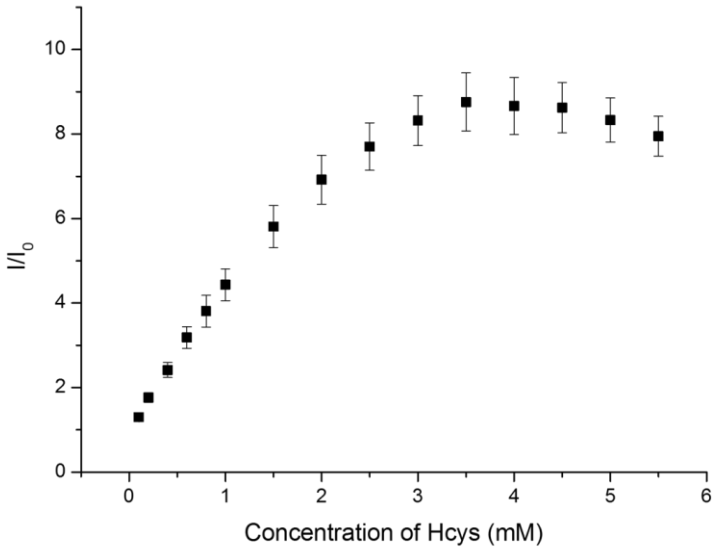

Figure 70 – Fluorescence intensity (I/I_0) of **42** (15 µM) and $ONOO^-$ (16 µM) then sequential addition of Hcys (0.1-5.5 mM) with 40 min incubation. In buffer (PBS pH 7.4). λex = 371 nm (bandwidth 20 nm) / λ_{em} = 448 nm.

The opposite order of analyte addition was then carried out, with addition of $ONOO^-$ (16 µM) also leading to a small increase in the level of fluorescence, which was thought to be due to partial activation of the probe upon Bpin cleavage. As expected, addition of Hcys (0.1-5.5 mM) then caused an increase in the level of fluorescence of **42**, until an upper limit was achieved, then a slight decrease in the level of fluorescence, possibly due to an artificially high level of analyte (**Figure 69**, **Figure 70**).

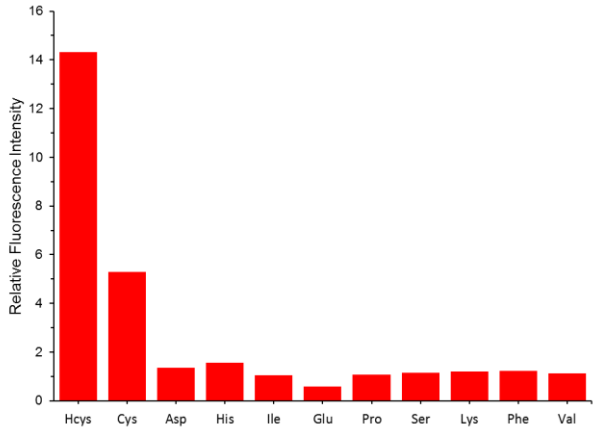

Figure 71 – Fluorescence intensity of **42** (15 µM) after addition of $ONOO^-$ (16 µM) and various amino acids (2.5 mM) in PBS buffer (pH 7.4) after 40 mins. λ_{ex} = 371 nm (bandwidth 20 nm)/ λ_{em} = 448 nm.

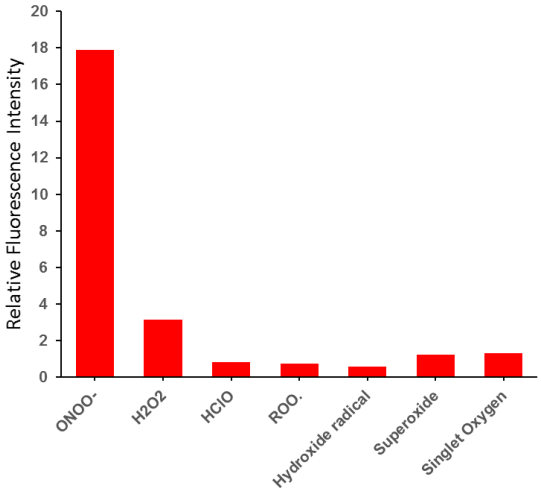

Figure 72 – Fluorescence intensity of **42** (15 µM) after addition of Hcys (1 mM) and a 40 min incubation, followed by addition of $ONOO^-$ (10 µM, 1 min incubation) and various ROS (100 µM, 30 min incubation). λ_{ex} = 371 nm (bandwidth 20 nm)/ λ_{em} = 448 nm.

These initial fluorescence experiments showed that **42** was capable of detecting both $ONOO^-$ and Hcys irrespective of the order of analyte addition, and only occurring when both analytes are present.

After these successful initial studies, off target interactions were analysed using two selectivity studies. I first screened the response of a range of common amino acids that could potentially react with the aldehyde functionality of the probe to afford an imine functionality. These results revealed that only Hcys produced a significant turn on of fluorescence in the presence of $OONO^-$. Cys also produced a slight turn on, as expected due to its structural similarity with Hcys (**Figure 71**). A selection of ROS species was then investigated to determine if they exhibited any competing reactivity towards the Bpin

group of the probe (**Figure 72**). In the ROS selectivity, $ONOO^-$ was found to cause the highest fluorescence response by a significant amount, with other off target reactive oxygen analytes not eliciting a substantial fluorescence increase, even at a far greater concentration.

These results were positive and showed that **42** had good selectivity towards both groups of potential off target analytes. Consequently, it was then decided to send **42** to Professor Xiao-Peng He at East China University of Science and Technology (ECUST) for cellular studies. Unfortunately, it was discovered that **42** had poor cellular solubility and did not respond in the way that I expected, forming insoluble aggregates in cellular systems.

2.2.5 Conclusion and Future Work

The adaption of Hong *et al.*'s simple coumarin Cys / Hcys probe through the incorporation of a Bpin group has produced the dual analyte probe **42**. **42** has shown to be sensitive to both $ONOO^-$ "AND" Cys / Hcys in an "AND" molecular logic gate (**table 2**). **42** has good selectivity to other potential thiol triggers. Unfortunately, **42** was not suitable for cellular studies as it forms insoluble aggregates. Future changes to the structure of the probe could include the addition of groups that increase the solubility of the probe (e.g. a PEG group), or the introduction of different triggering groups to add sensitivity to other target analytes.

$ONOO^-$	Hcys / Cys	Output
0	0	0
1	0	0
0	1	0
1	1	1

Table 2 – Truth table of input / output for **42**.

2.3 A Dual Hcys AND Nitroreductase Probe **46**

2.3.1 Literature Precedent

Nitroreductases (NTRs) are a group of enzymes that are responsible for the reduction of nitro containing aromatic metabolites and xenobiotics in cells based on reduction of a nitro ($-NO_2$) group to its corresponding amine.[28] This is achieved through the use of reducing cofactors, such as flavin mononucleotide (FMN), flavin adenine dinucleotide (FAD), nicotinamide adenine dinucleotide (NADH) or nicotinamide adenine dinucleotide phosphate (NADPH).[29] In the body, these enzymes play a critical role in the bioremediation of toxic nitro-containing compound that are often produced from bacterial metabolism.

In solid tumours there is often an insufficient supply of oxygen to cells creating hypoxic conditions. One of the effects of hypoxia is to dysregulate the natural reduction-oxidation (redox) cycle which can result in overexpression of certain proteins, including NTRs.[30] In solid tumours the amount of NTRs produced is directly related to the level of hypoxia in the cell, a fact that can be exploited for the development of NTR fluorescent probes to detect and monitor hypoxic tissues in tumours.

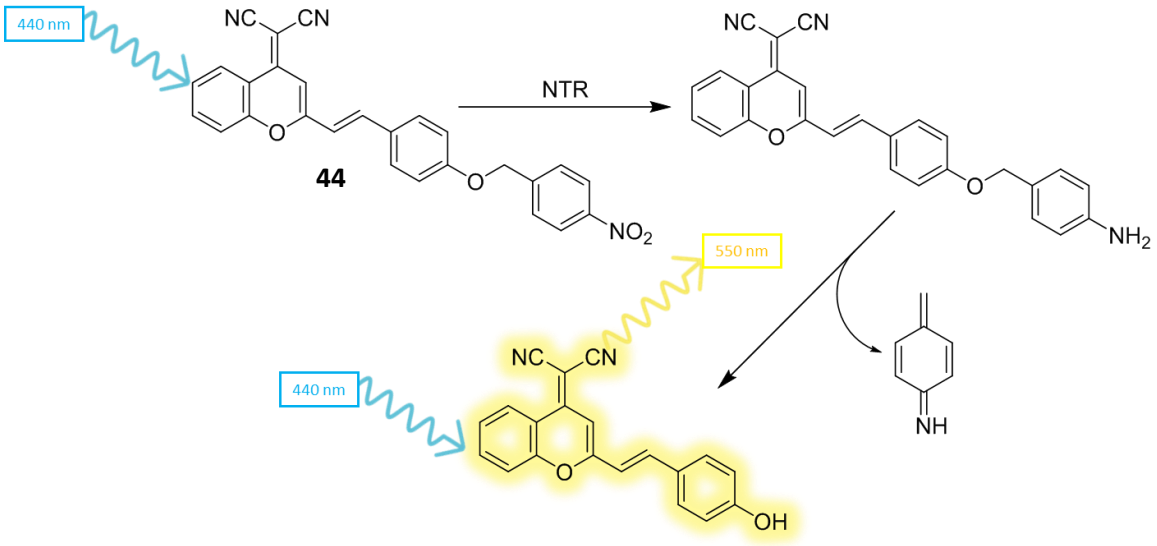

Figure 73 – Reduction of a nitro group on **44** by an NTR results in cleavage, to afford a fluorescent signal.

Zhang *et al.* have reported an ICT based probe containing a 4-nitrobenzyl moiety bound to a dicyanomethylene-4H-pyran (DCM) fluorophore that is a substrate for reductive

activation by NTR (**Figure 73**).[30] Once its nitro group is reduced to an amine group, then an auto-elimination reaction occurs to produce 4-methylenecyclohexa-2,5-dien-1-imine, CO_2 and the active DCM fluorophore. This probe could be used to monitor the levels of endogenous NTRs and the presence of hypoxic conditions in cells. They subsequently developed a longer wavelength fluorescent NTR probe (**45**) using a cyanine fluorophore and a reactive 4-nitrophenol unit (**Figure 74**).

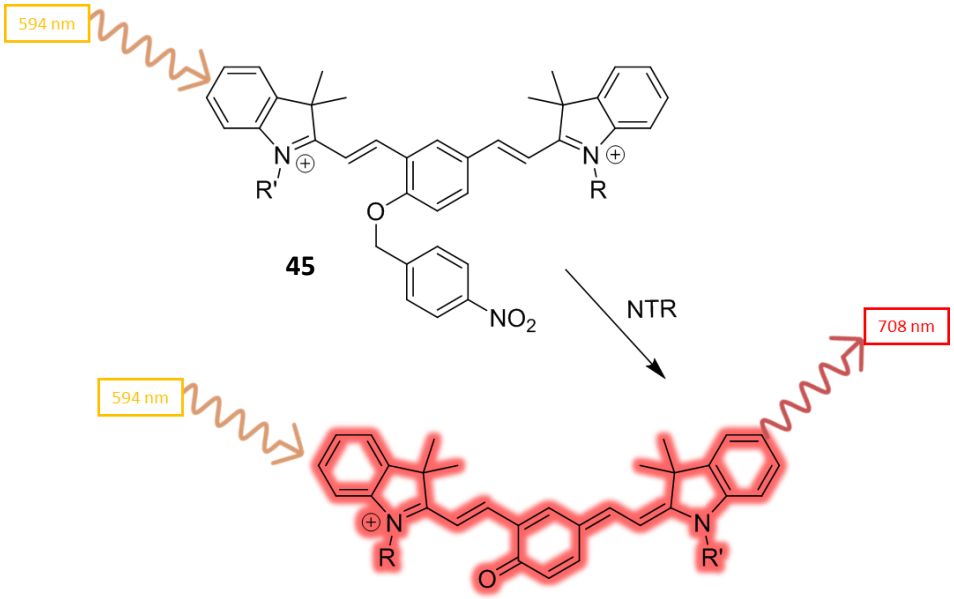

Figure 74 – The turning on of probe **45** *via* NTR.

Hcys is an intracellular thiol that has several deleterious effects at perturbed levels (**Section 2.3.1**). In addition to these effects, it has also been observed to be a risk factor in the development of cancer, through mechanisms including folate deficiency and aberrant DNA methylation. Levels of Hcys, therefore, can be used as a method for the monitoring of cancer cells. Additionally, levels of Hcys also decrease with the death of cancer cells, unlike other metabolites used for the monitoring of the disease, possibly yielding a more comprehensive method of tracking the efficacy of a treatment.

Developing a sensor capable of detecting two cancer associated biological targets is a highly desirable prospect and could be possible by targeting NTRs and Hcys.

2.3.2 Design of Probe **46**

Given the precedent, it was decided to develop a new probe **46** as an AND sensor for monitoring the concentration of Hcys and NTR by appending an NTR sensitive 4-nitrophenyl group to the 7-hydroxy position of the Hcys sensitive coumarin compound, **41** (**Figure 75**).

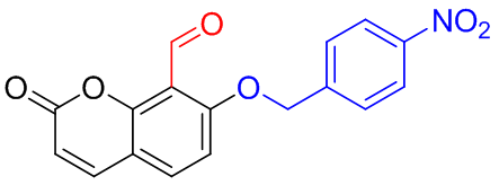

46

Figure 75 – Structure of probe **46**, with the thiol reactive aldehyde (red) and NTR reactive nitro group (blue).

2.3.3 Synthesis of Probe **46**

The aldehyde **41** was prepared as an intermediate in previous synthesis of probe **42** (**Section 2.2.3**), was used as a substrate for reaction with 4-nitrobenzylbromide and K_2CO_3 in DMF, which afforded the desired probe **46** in 49% yield.

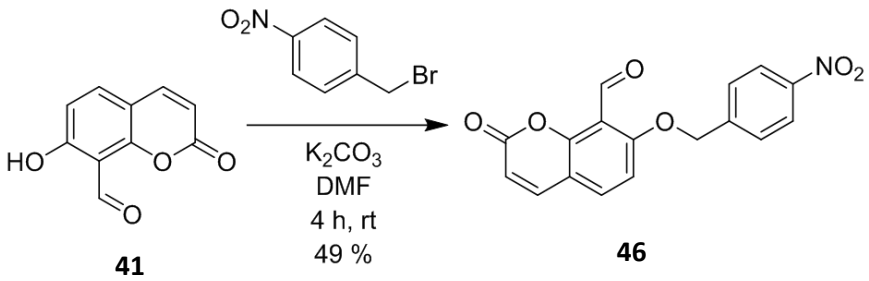

41 **46**

Scheme 2 – The Synthesis of probe **46**.

2.3.4 Fluorescent Analysis of Probe **46**

The probe was then reacted with an NTR enzyme (in collaboration with Dr Robert Elmes, from Maynooth University), with analysis of cleavage products carried out using HPLC-

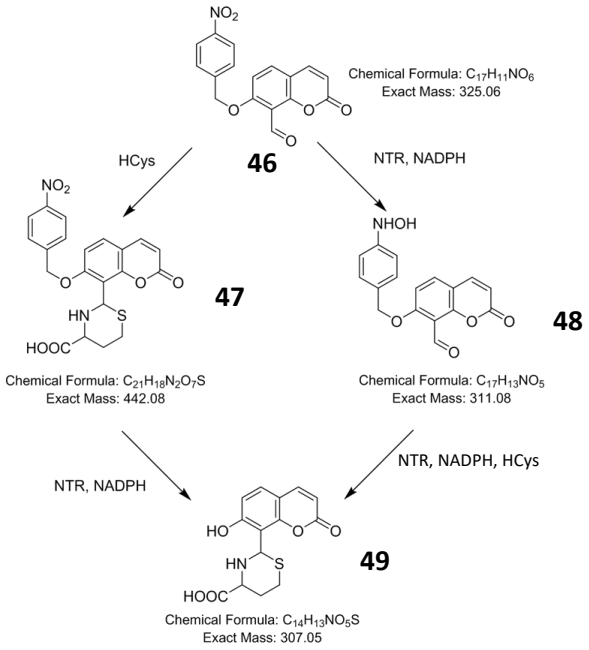

Figure 76 – Reaction pathway of **46** with NTR + NADPH and Hcys, with intermediate structures **47** & **48** and finally **49** confirmed by HPLC-MS analysis.

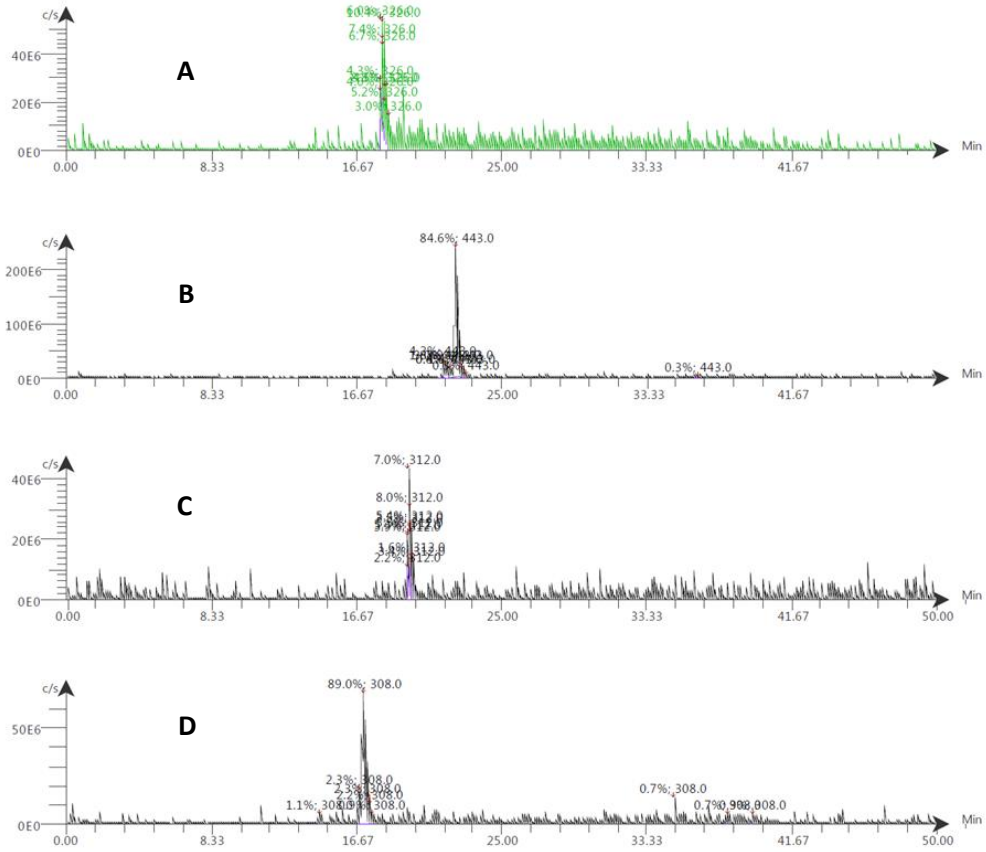

Figure 77 – HPLC-MS of a) **46** b) **47** (thiazolidine formed) c) **48** (hydroxylamine intermediate) d) **49**.

MS analysis. HPLC-MS confirmed the reaction pathway between **46**, Hcys and NTR in the presence of cofactor NADPH) gave a correct mass ion for a product whose nitrobenzyl group had been reductively cleaved by the NTR which contained a thiazoline ring system formed from reaction with Hcys (**Figure 76**, **Figure 77**).

Initial treatment with Hcys first afforded a nitro-thiazoline intermediate **47** (M_R = 442.08) which on exposure to NTR was reduced to its corresponding thiazoline phenol **49** (M_R = 307.05). Alternatively, treatment of probe **46** with the NTR initially gave a hydroxylamine intermediate **48** (M_R = 311.08), that was further reduced on addition Hcys to give the thiazoline phenol product **49**.

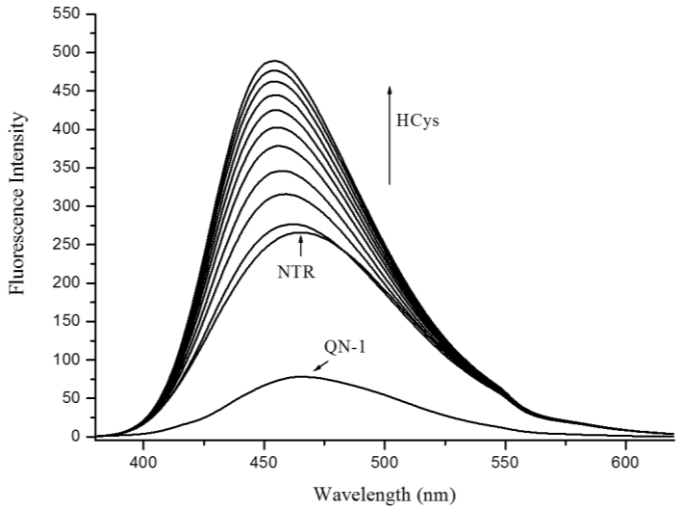

Figure 78 – Fluorescence spectra of **46** (15 µM) with initial addition of 400 µM NADPH and 4 µL/mL NTR with 60-min incubation, followed by Hcys (2 mM) from 0-90 min. In PBS buffer (pH 7.4), slit widths ex = 5 nm and em = 5 nm.

Fluorescence analysis was then undertaken. **46**, referred to as **QN-1** in these figures (15 µM) showed little initial response, however addition of NTR + NADPH resulted in a significant increase in fluorescence intensity (~4 fold). Hcys (2 mM) was then added and the response of the probe measured over 90 minutes, which resulted in a gradual increase in fluorescence (2 fold) caused by cleavage of the 4-nitrobenzyl group from the sensor and formation of the thiazolidine ring (**Figure 78**).

The probe **46** was then subjected to incubation with Hcys (2 mM) for 60 minutes, which resulted in a small increase in fluorescence, which was smaller than the increase when NTR + NADPH was added to **46**. This was thought to be due to the greater effect of the free phenol on the mechanism of fluorescence, when compared to formation of the thiazolidine ring. Addition of NTR (4 µL/ mL) and NADPH (400 µM) to the solution of **46** + Hcys (2 mM) resulted in a sharp increase in fluorescent intensity followed by a further

gradual increase in fluorescence over a 90-minute period (~2 fold over initial level) (**Figure 79**).

These two analyses showed that there was a significant fluorescence response of **46** when exposed to both NTR (+NADPH) and Hcys, relative to the presence of just one analyte, meaning that is it an effective "AND" MLG.

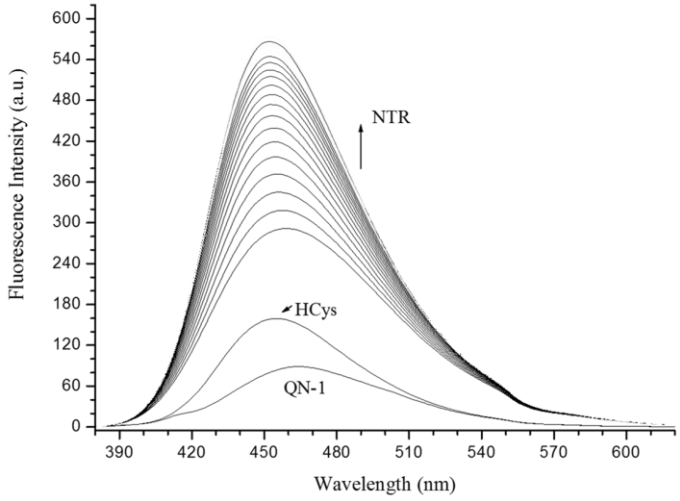

Figure 79 – Fluorescence spectra of **46** (15 µM) with initial addition of Hcys (2 mM) with 60-minute incubation followed by 400 µM NADPH and 4 µL/mL NTR from 0-90 min. In PBS buffer (pH 7.4), slit widths ex = 5 nm and em = 5 nm.

Studies that were undertaken next, involved incubation with one of the analytes followed by titrations with different concentrations of the other analyte. Firstly, **46** (15 µM) was incubated with NADPH (400 µM) and NTR (4 µL/ mL) for 90 minutes, before Hcys (0.5 mM, 1 mM, 2 mM, 4 mM) was added and the fluorescence monitored for another 110 min (**Figure 80**). The colours in these graphs are used to distinguish between closely spaced lines and represent different time points. This resulted in the fluorescence initially increasing after NTR (+NAPDH) addition to a relatively stable value after 90 minutes. Addition of Hcys then resulted in a dose dependent increase in the response of the probe, with the highest response found from addition of 4 mM Hcys after 210 min, which gave a maximum response of ~2 fold relative to NTR (+NAPDH) and ~3 fold relative to no analyte (**Figure 81**).

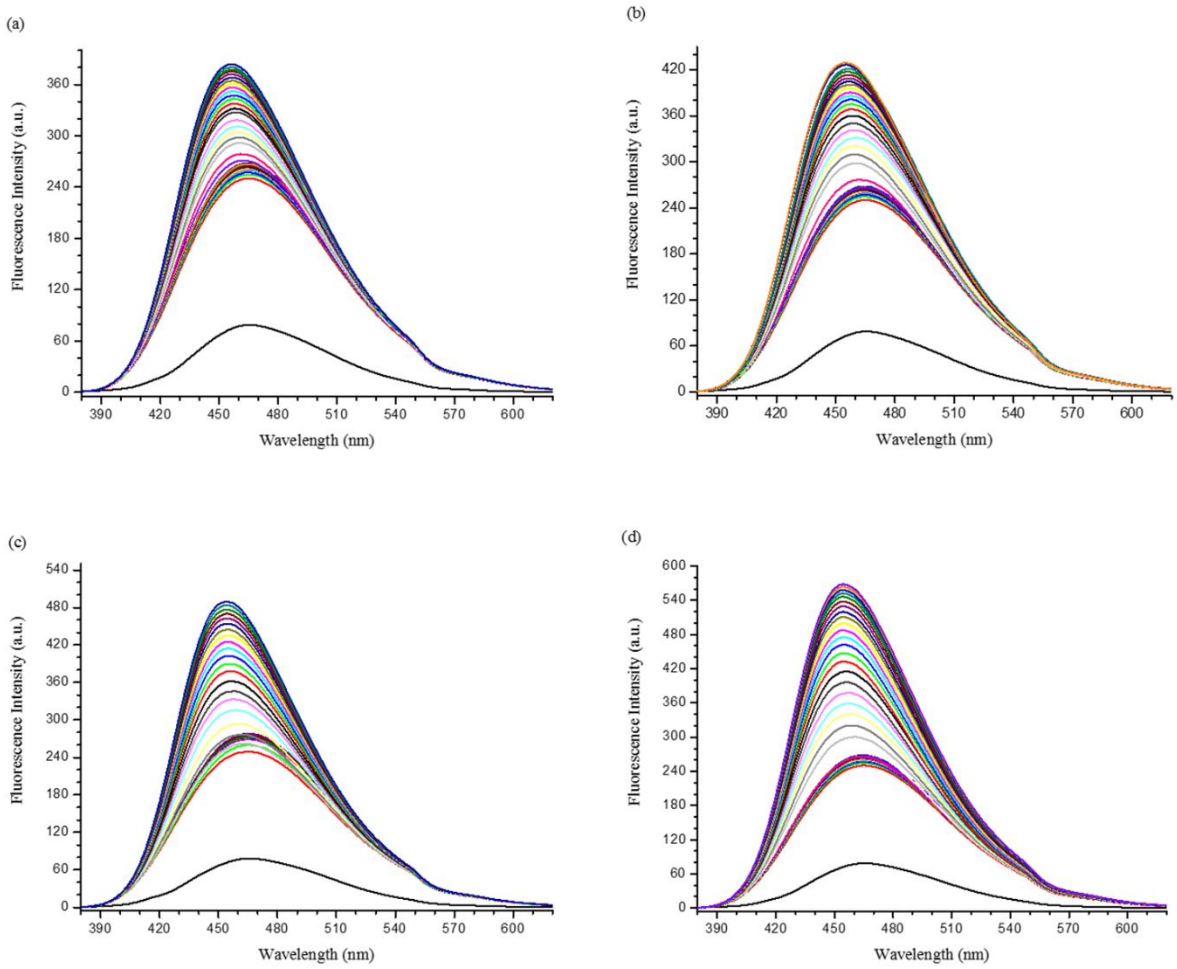

Figure 80 – Fluorescence spectra of **46** (15 µM) produced by initial addition of 400 µM NADPH and 4 µL/mL NTR incubation for 90 min, followed by addition of a) 0.5 mM, b) 1 mM, c) 3 mM, d) 4 mM Hcys, respectively. Reactions then monitored for a further 120 min. All assays carried out in PBS buffer (pH 7.4, 1% DMSO, slit widths ex = 5 nm and em = 5 nm.

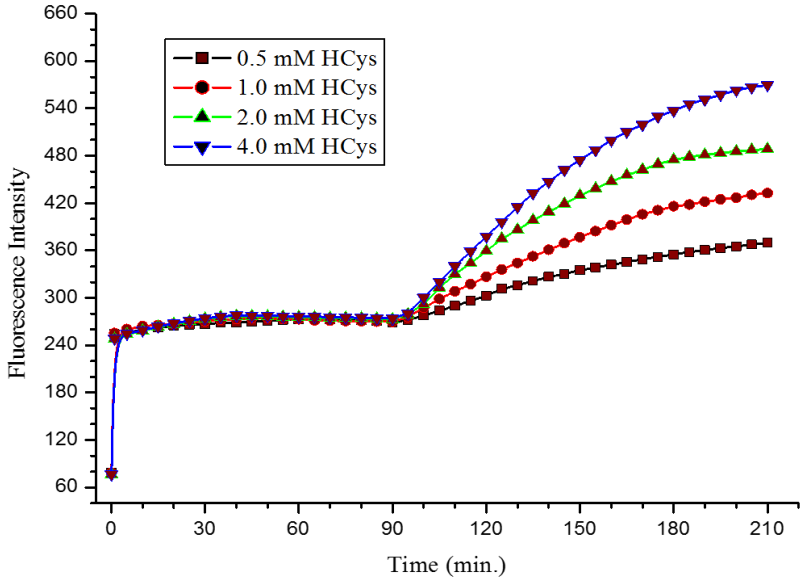

Figure 81 – Fluorescence intensity at 453 nm vs. time. **46** (15 µM) with initial addition of 400 µM NADPH and 4 µL/mL NTR (0-90 min), followed by addition of a) 0.5 mM, b) 1 mM, c) 3 mM, d) 4 mM Hcys (90-210 min). All assays carried out in PBS buffer (pH 7.4, 1% DMSO, slit widths ex = 5 nm and em = 5 nm.

The use of different concentrations of NTR was then explored. **46** (15 µM) was incubated with NADPH (400 µM) and NTR (1 µL/mL, 2 µL/mL, 4 µL/mL, 10 µL/mL) and incubated for 90 minutes. Hcys (2 mM) was then added and the assay was further monitored for 120 minutes (**Figure 82**). The results showed that **46** responded to the initial addition of the NTR with a small increase in fluorescence. Larger doses of NTR (4 µL/ mL, 10 µL/mL) show similar levels of fluorescence suggesting that all of the probe in the test solution had reacted. Upon addition of Hcys, further increases in the level of fluorescence were observed in a dose dependent manner relative to the concentration of the initial amount of NTR added (**Figure 83**).

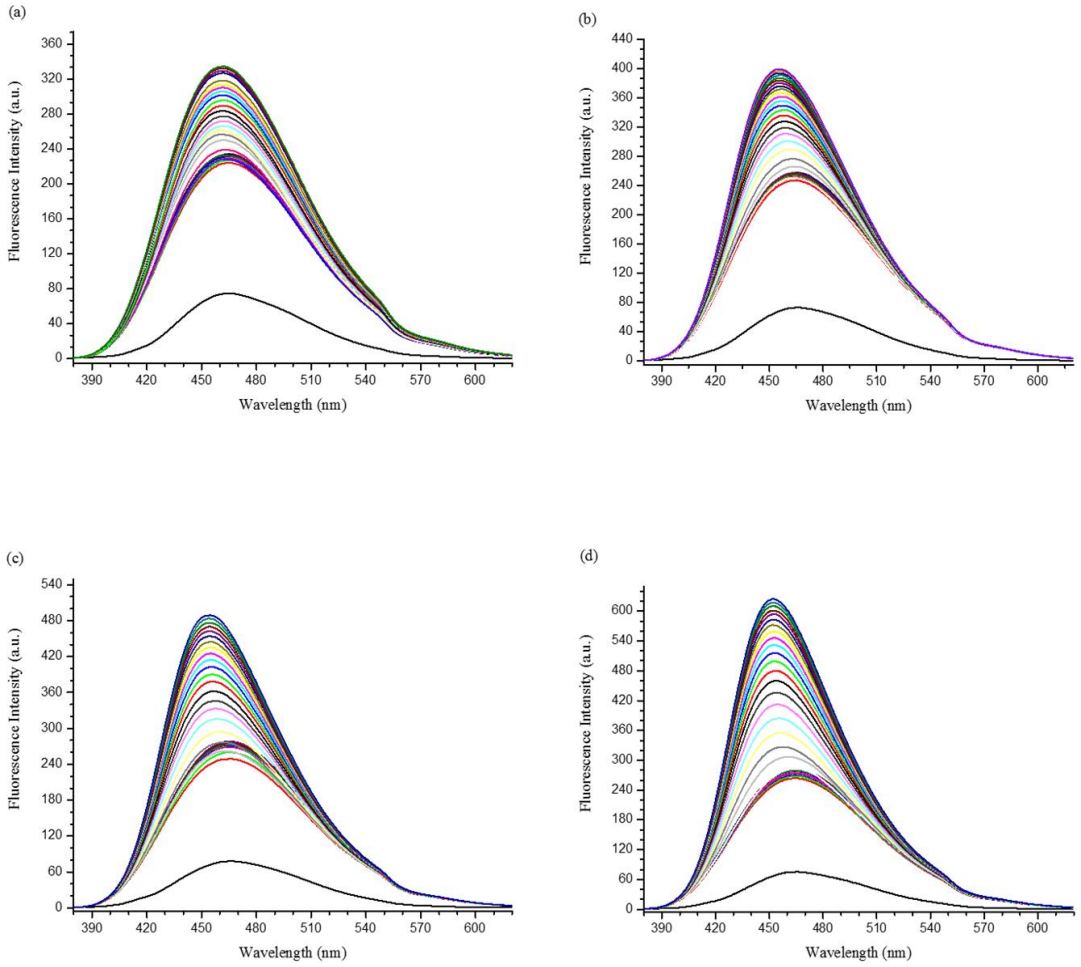

Figure 82 – Fluorescence spectra of **46** (15 µM) with initial addition of 400 µM NADPH and a) 1 µL/mL b) 2 µL/mL c) 4 µL/mL d) 10 µL/mL NTR followed by incubation for 90 min, followed by addition of 2 mM Hcys and the assay monitored for a further 120 min. All assays carried out in PBS buffer (pH 7.4, 1% DMSO, slit widths ex = 5 nm and em = 5 nm.

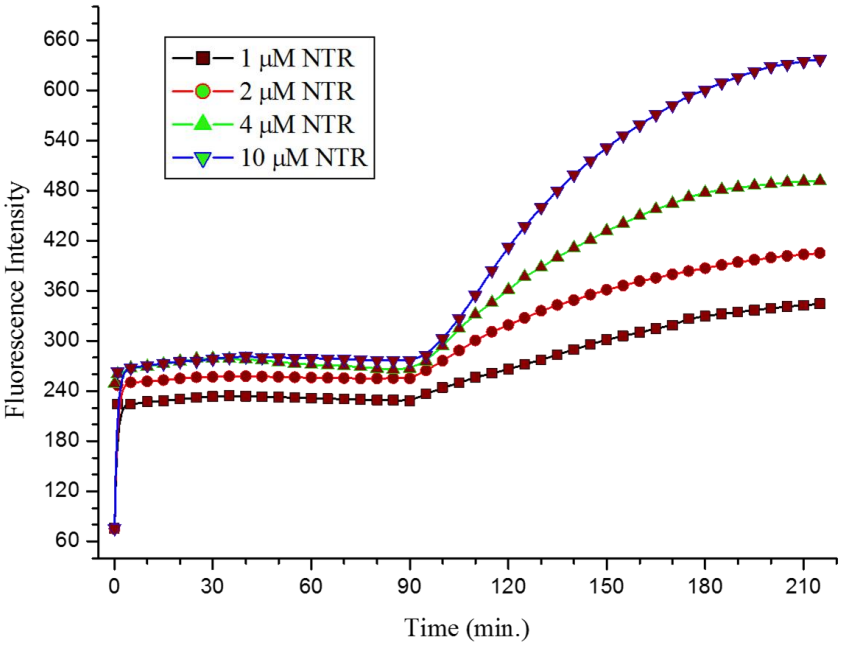

Figure 83 – Fluorescence intensity at 453 nm vs. time. **46** (15 µM) after initial addition of 400 µM NADPH and a) 1 µL/mL b) 2 µL/mL c) 4 µL/mL d) 10 µL/mL NTR (0-90 min), respectively, followed by addition of 2 mM Hcys (90-210 min). All assays carried out in PBS buffer (pH 7.4, 1% DMSO), slit widths ex = 5 nm and em = 5 nm.

The effect of increasing the concentration of Hcys used in the assay was then explored for constant NTR value. Probe **46** (15 µM) was incubated with Hcys (0.5 mM, 1 mM, 2 mM, 4 mM) for 90 min, followed by addition of NADPH (400 µM) and NTR (4 µL/mL) and incubation for another 120 min (**Figure 84**). Upon initial addition of Hcys, there was a small, gradual increase in the levels of fluorescence, indicative of the formation of a thiazolidine ring from reaction of the aldehyde group and Hcys. This gradual increase in fluorescence levelled off after 80 min, which is likely to be due to saturation of the probe with Hcys. Addition of NADPH and different concentrations of NTR caused a further dose dependent increase in the fluorescence intensity level, relative to the concentration of the initial Hcys addition (**Figure 85**).

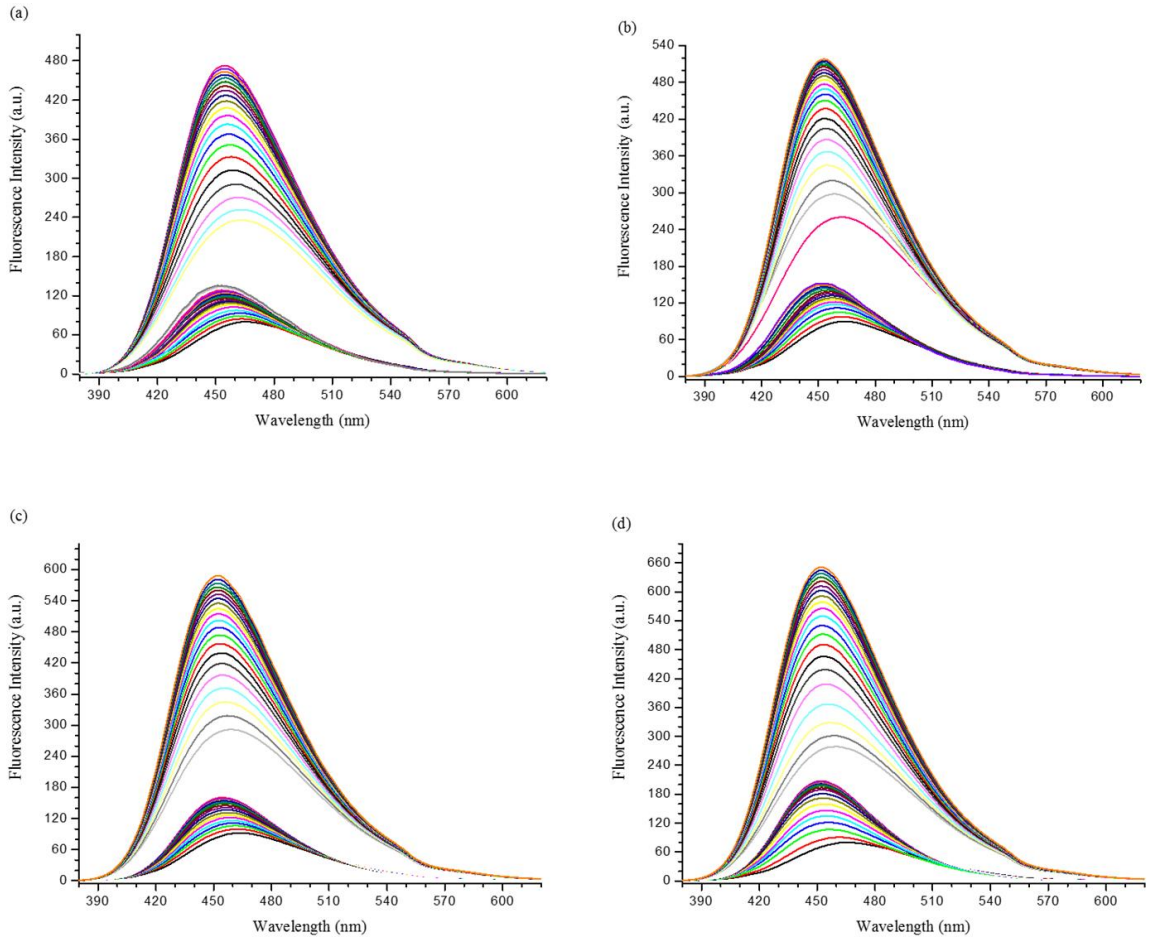

Figure 84 – Fluorescence spectra of **46** (15 µM) after initial addition a) 0.5 mm, b) 1 mM, c) 2 mM, d) 4mM of Hcys, respectively. Assays incubated for 90 min followed by addition of 400 µM NADPH and 4 µL/mL NTR followed by incubation for a further 120 min. All incubations carried out in PBS buffer (pH 7.4, 1% DMSO), slit widths ex = 5 nm and em = 5 nm.

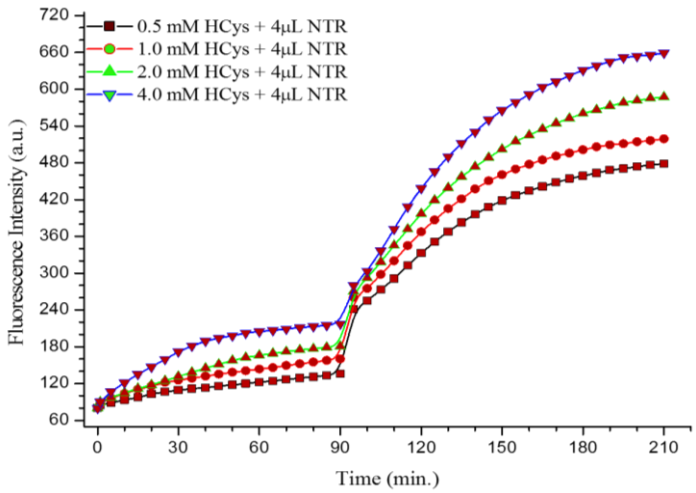

Figure 85 – Fluorescence intensity at 453 nm vs. time. **46** (15 µM) with initial addition a) 0.5 mm, b) 1 mM, c) 2 mM, d) 4mM (0-90 min) Hcys respectively, followed by addition of 400 µM NADPH and 4 µL/mL NTR (90-120 min), slit widths ex = 5 nm and em = 5 nm.

Incubation with a fixed concentration of Hcys and varying concentrations of NTR were then studied. **46** (15 µM) was initially mixed with Hcys (2 mM) and incubated for 90 min, with 400 µM NADH and NTR ((a) 1.0 µL/mL, (b) 2.0 µL/mL, (c) 4.0 µL/mL, (d) 10.0 µL/mL) then added (**Figure 86**). Addition of Hcys to each aliquot of **46** caused an equal response from the sensor, involving a small uniform increase in its fluorescence response. Addition of various concentrations of the NTR (+NADPH) resulted in a further fluorescence response, with higher concentrations of NTR giving a larger response (**Figure 87**).

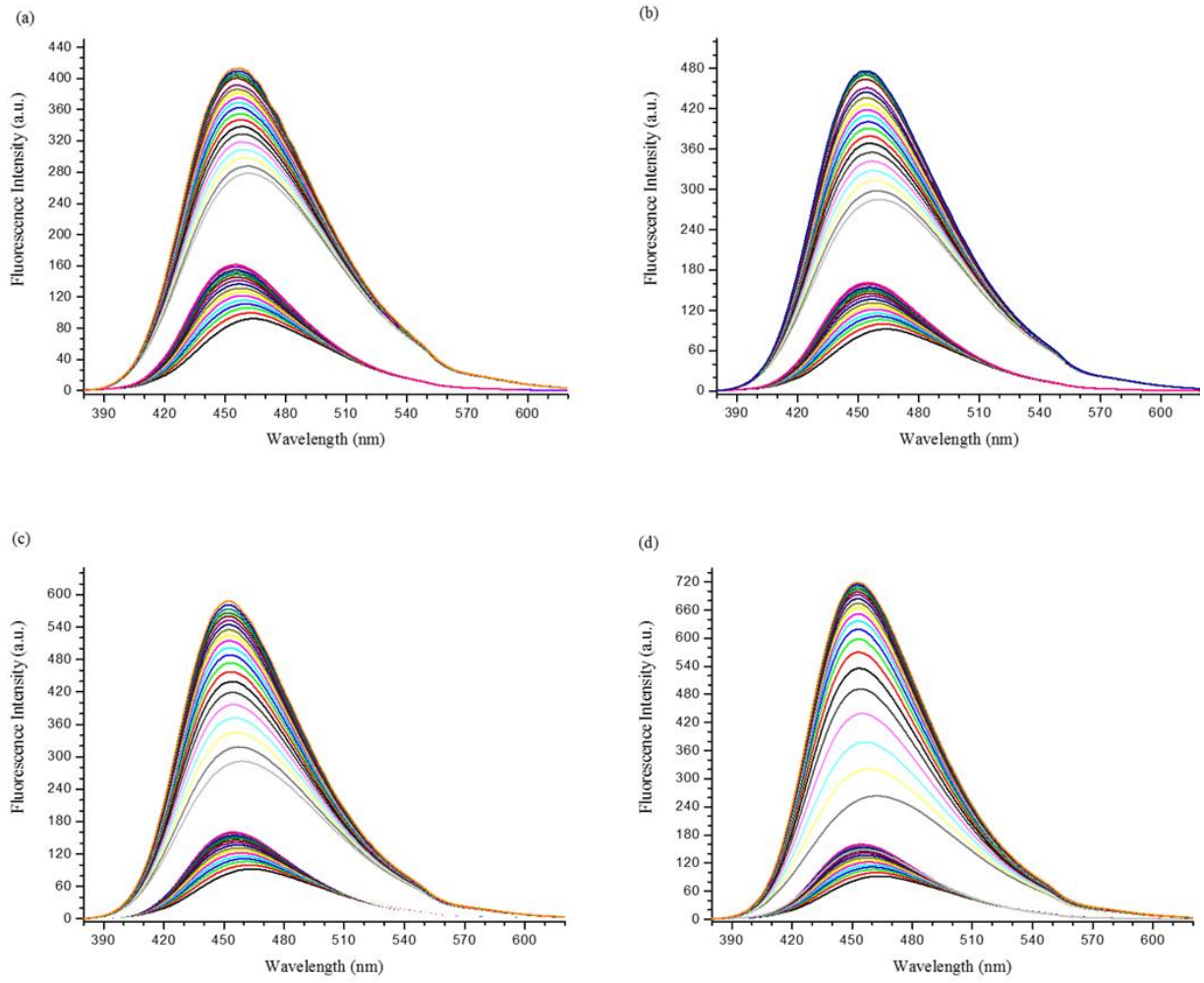

Figure 86 – Fluorescence spectra of **46** (15 µM) after initial addition of Hcys 2 mM and incubation for 90 minutes, followed by addition of 400 µM NADPH and a) 1 µL/mL b) 2 µL/mL c) 4 µL/mL d) 10 µL/mL NTR respectively. Assay then incubated for a further 120 minutes. All assays carried out in PBS buffer (pH 7.4, 1% DMSO), slit widths ex = 5 nm and em = 5 nm.

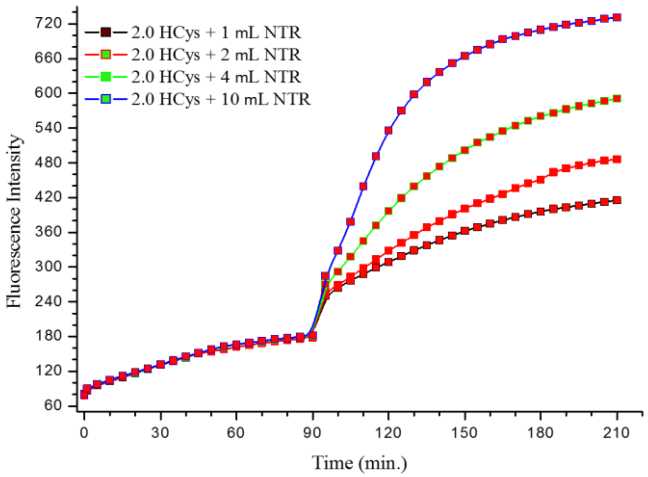

Figure 87 – Fluorescence intensity at 453 nm vs. time. **46** (15 µM) after initial addition of Hcys 2 mM (0-90 min), followed by addition of 400 µM NADPH and 1 µL/mL, 2 µL/mL, 4 µL/mL, 10 µL/mL NTR (90-120 min), slit widths ex = 5 nm and em = 5 nm.

These fluorescence results show that **46** is an effective probe for the detection of both NTR and Hcys in solution-based assays, with an increase in the fluorescence of the probe (~10 fold) when exposed to higher concentrations of these analytes. This sensor has been sent to collaborators in South Korea for cellular studies to determine whether **46** can detect the presence of Hcys and NTR *in vivo*.

2.3.5 Conclusion and Future Work

In conclusion, I have modified Hong *et al.*'s probe **41** to develop a dual analyte coumarin based probe **46** for the fluorescent detection of NTR "AND" Hcys/Cys. Solution analysis of **46** showed that although addition of a single analyte caused a measurable response, the presence of both target analytes caused a much greater response. I am currently awaiting the results of cellular assays from our collaborators in South Korea.

$ONOO^-$	NTR	Output
0	**0**	**0**
0	**1**	**0**
1	**0**	**0**
1	**1**	**1**

Table 3 – Truth table of **46** inputs and output.

2.4 Triple Analyte Probe for Sensing $ONOO^-$, Glutamate AND Zinc

2.4.1 Literature Precedent

Glutamate (Glu) is used as a neurotransmitter in vertebrate nervous systems to transmit signals between each cell and Glu is used in over 90% of the synapses in the human brain.[31] Therefore, healthy levels of Glu are essential in the development and function of brain tissue.

An overabundance of Glu has been associated with multiple neurological disorders / diseases, including multiple sclerosis,[32,33] Alzheimer's disease,[34] Parkinson's disease,[35] stroke[36] and Lou Gehrig's disease.[37] Additionally, problems in pathways used to produce Glu have been linked to other mental health disorders such as autism,[38] schizophrenia[39] and clinical depression.[40]

Many methods have been developed to detect this important chemical signalling molecule, including capillary electrophoresis,[41] micro-electrochemistry[42] and mass spectrometry-based techniques.[43] However, these techniques suffer from drawbacks like low throughput and poor spatial resolution. Fluorescence based techniques have been developed to combat these problems, with probes designed to afford a high level of spatial resolution for rapid application and fast response times.

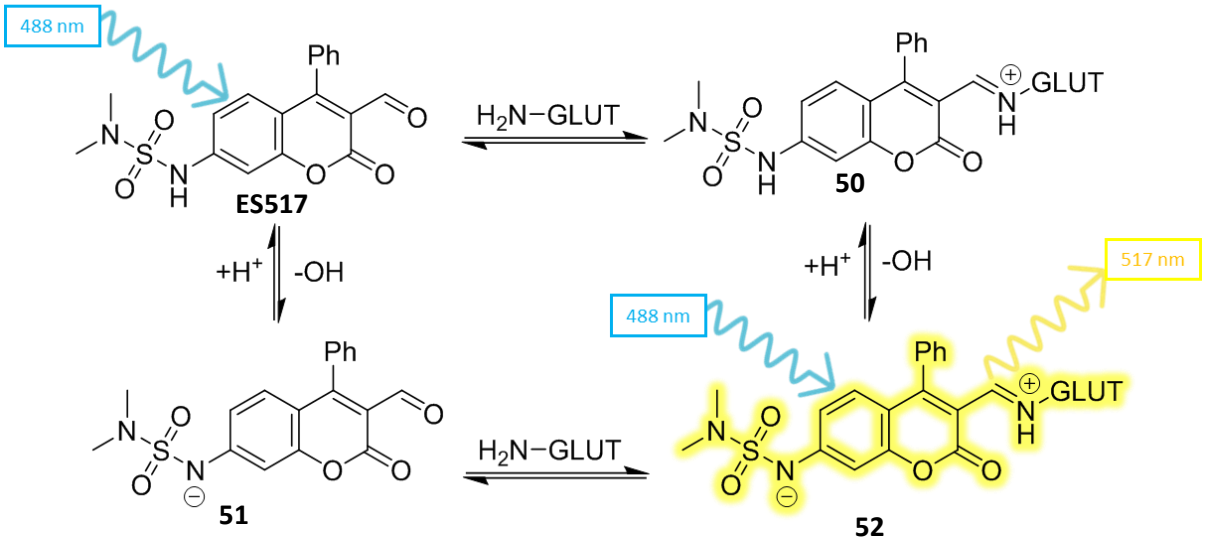

Figure 88 – Reaction of **ES517** with Glut at basic pH.

An example of a fluorescence probe for the detection of Glu in biological systems was reported by Tsien *et al.* who harnessed FRET interactions between a cyan (CFP) dye and yellow fluorescent protein (YFP) that occurs when glutamate binds to the protein through inotropic glutamate receptors.[44] Tsien's sensor was successfully used for the detection of glutamate release, spill-over and reuptake by monitoring the fluorescence. The pitfalls of this technique are that genetic manipulation is required to prepare the sensor, which generally exhibits low reversibility for Glu binding and a relatively low change in fluorescence intensity.

To combat these problems, Glass *et al.* developed a small molecule dual-analyte AND fluorescent sensor (**ES517**) for visualising release of Glu, which was comprised of a coumarin scaffold appended to an aldehyde at its 3-position and an electron poor sulfonamide at its 7-position (**Figure 88**).[45] The method used to detect the Glu involves the reaction of the aldehyde of the sensor with the amine group of the Glu to form a positively charged imminium ion **50** inside the vesicle that cannot pass across the vesicular membrane. Release of the contents of the vesicle exposes the probe to the neuronal connection, whose pH of 7.4 is significantly higher than inside the vesicle (~pH 5). This results in deprotonation of the sulfonamide (**51**). After both events have occurred **52**, a bathochromic shift in the fluorescent absorbance of the probe at 488 nm. A twelve-fold fluorescence increase was observed on exposure of the probe to Glu, with a relatively low binding affinity for Glu, meaning that the probe has the ability to reversibly detect Glu outside the vesicle.

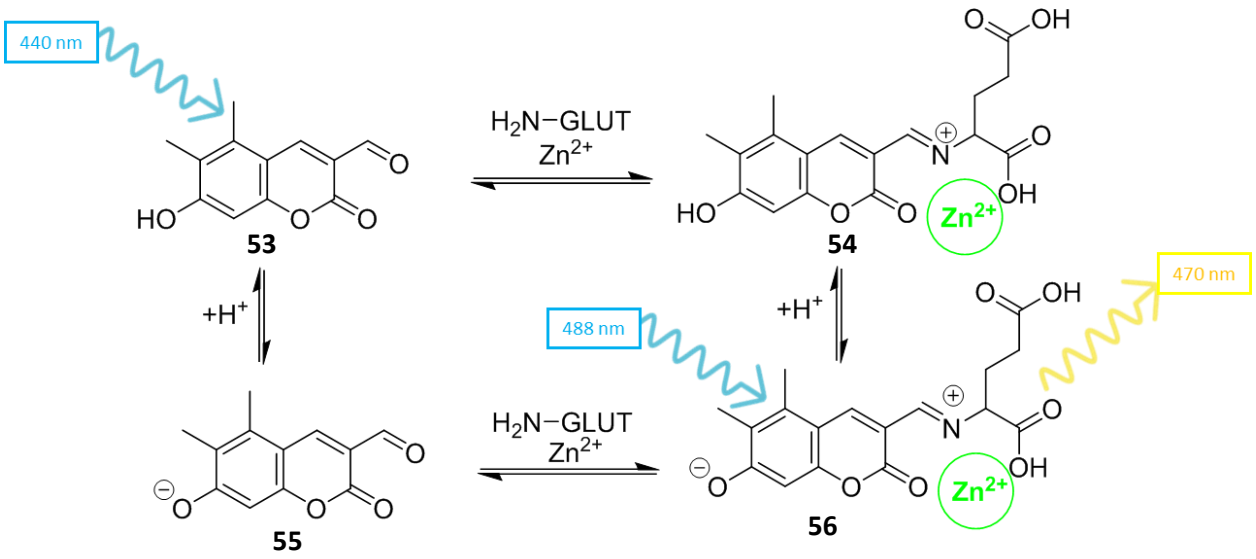

Figure 89 – Reaction pathway for **53** with Glut and Zn^{2+}.

Further to this development, Glass *et al.* developed a three-input AND logic gate sensor **53** (**Figure 89**) to study a specific subset of glutamatergic neurons in the forebrain.[46] Probe **53** was based on the structure of **ES517**, containing an additional binding unit for Zn^{2+} ions. Formation of an imminium ion with Glu creates a multipoint binding pocket between the lactone fragment of the coumarin and the carboxylate of the Glu whose functional groups can coordinate Zn^{2+} (**54**). The binding of Zn^{2+} causes a blue shift in the absorbance which was hypothesized to be formation of an imine group, which is normally protonated as its iminium species at physiological pH. A slight increase in fluorescence arises from rigidification of the sensor structure on binding of the Zn^{2+}. The third trigger point in the sensor is the phenol group at the 7-position of the coumarin ring which is deprotonated when exposed physiological pH (~7.4) (**55**) allowing the probe to fluoresce upon excitation at 440 nm in **56**.

2.4.2 Design of Probe **57**

There are strong links to the overproduction of $ONOO^-$ and numerous neurological disorders (**Section 1.5.4**), with dysregulation in signalling pathways arising from either overproduction or underproduction of signalling molecules. Therefore, access to a probe that could simultaneously detect Glu, Zn^{2+} and $ONOO^-$ might reveal interesting information on the progression of these diseases. Consequently, I saw an exciting opportunity to add $ONOO^-$ sensitivity to the Glu and Zn^{2+} probe through attachment of a 4-methyl-phenylboronic acid pinacol ester group the phenol group at the 7-position of the coumarin to make probe **57** (**Figure 90**).

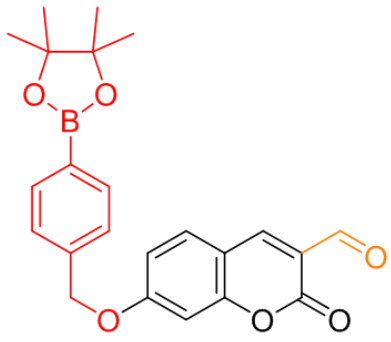

57

Figure 90 – Probe **57** containing a $ONOO^-$ reactive phenyl-Bpin unit (red) and a Glu reactive aldehyde, which can bind Zn^{2+} ions (orange).

2.4.3 Synthesis of Probe **57**

The synthesis of **57** differed from those used for previous coumarin probes as it required a protocol based on preparation of the coumarin backbone, as compared to derivatising commerically available umbelliferone (**Scheme 3**).

Firstly, 2,4-dihydroxybenzaldehyde **58** was used as a substrate for a Perkin synthesis by refluxing with sodium propionate, propionic anhydride and pyridine for six hours which gave the desired 3-(bromomethyl)-2-oxo-2H-chromen-7-yl propionate product (**59**) in 30 % yield. **59** was then brominated under classical free radical conditions *via* treatment with N-Bromosuccinimide (NBS) and 2,2′-azobis(2-methylpropionitrile) (AIBN) in MeCN for three hours to give the desired mono-brominated product **60** in 48 % yield. Refluxing **60** in acetic anhydride (Ac_2O) with sodium acetate (NaOAc) then gave the di-acetylated product

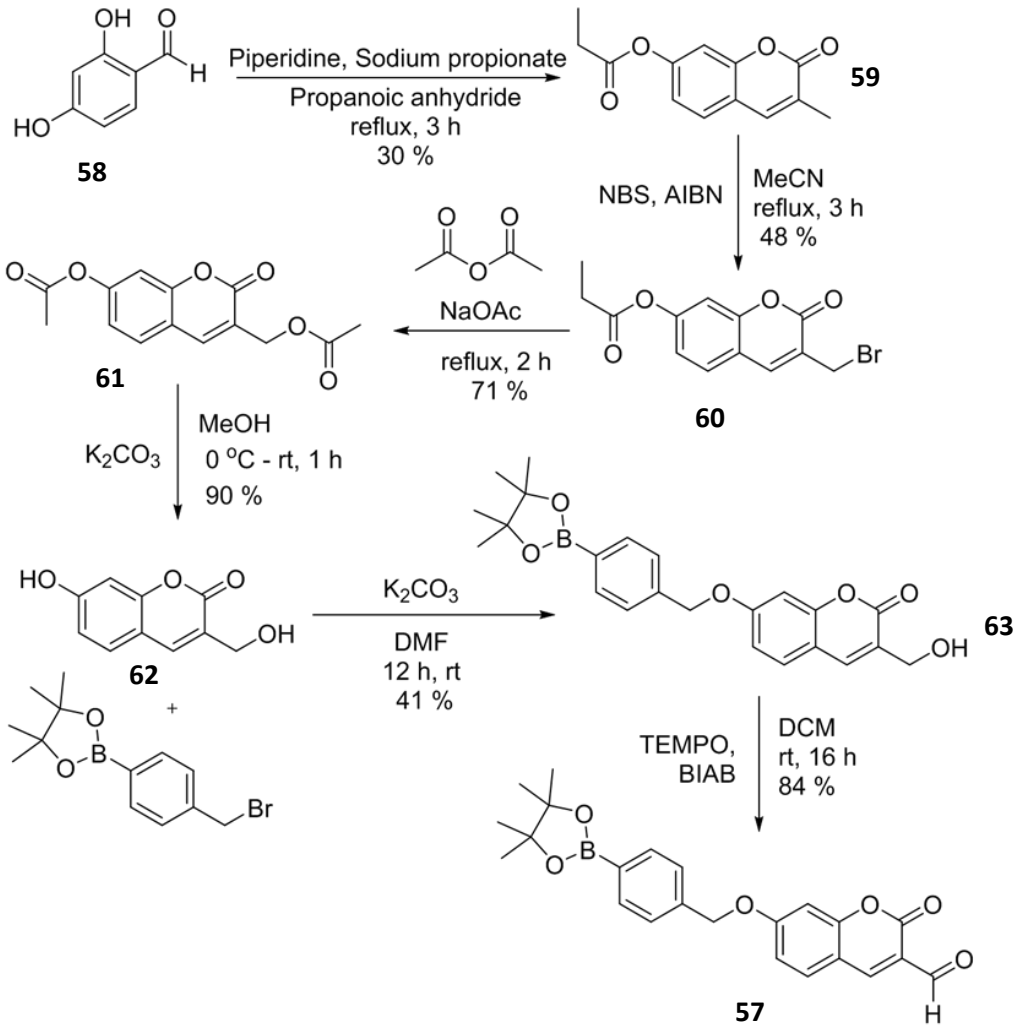

Scheme 3 – Synthesis of probe **57**.

61 in 71% yield. Cleavage of both acetyl groups was achieved through treatment of **61** with K_2CO_3 in MeOH at 0°C followed by warming to RT to afford diol **62** in 90% yield. 4-Bromomethylphenylboronic acid pinacol ester was then attached to the coumarin skeleton *via* treatment with K_2CO_3 in DMF for twelve hours at RT, which gave product **63** in 41% yield.

The final step of the synthesis involved treatment of **63** with (2,2,6,6-tetramethylpiperidin-1-yl)oxyl or (2,2,6,6-tetramethylpiperidin-1-yl)oxidanyl (TEMPO) and [acetyloxy(phenyl)-λ_3-iodanyl] acetate (BIAB) in dichloromethane ($CHCl_3$) at rt overnight, which resulted in oxidation of the primary alcohol to yield the final aldehyde product **57** in 84% yield.

2.4.4 Fluorescence Analysis of Sensor **57**

In solution fluorescence analyses of **57** in the presence of various analytes was then carried out (**Figure 90**). The concentrations used were determined from previous work carried out on Glu sensors by Glass *et al.*[46] and experience with detecting $ONOO^-$ with other probes. Various concentrations of Glu and Zn^{2+} were added to pre-incubated mixtures of **57** and

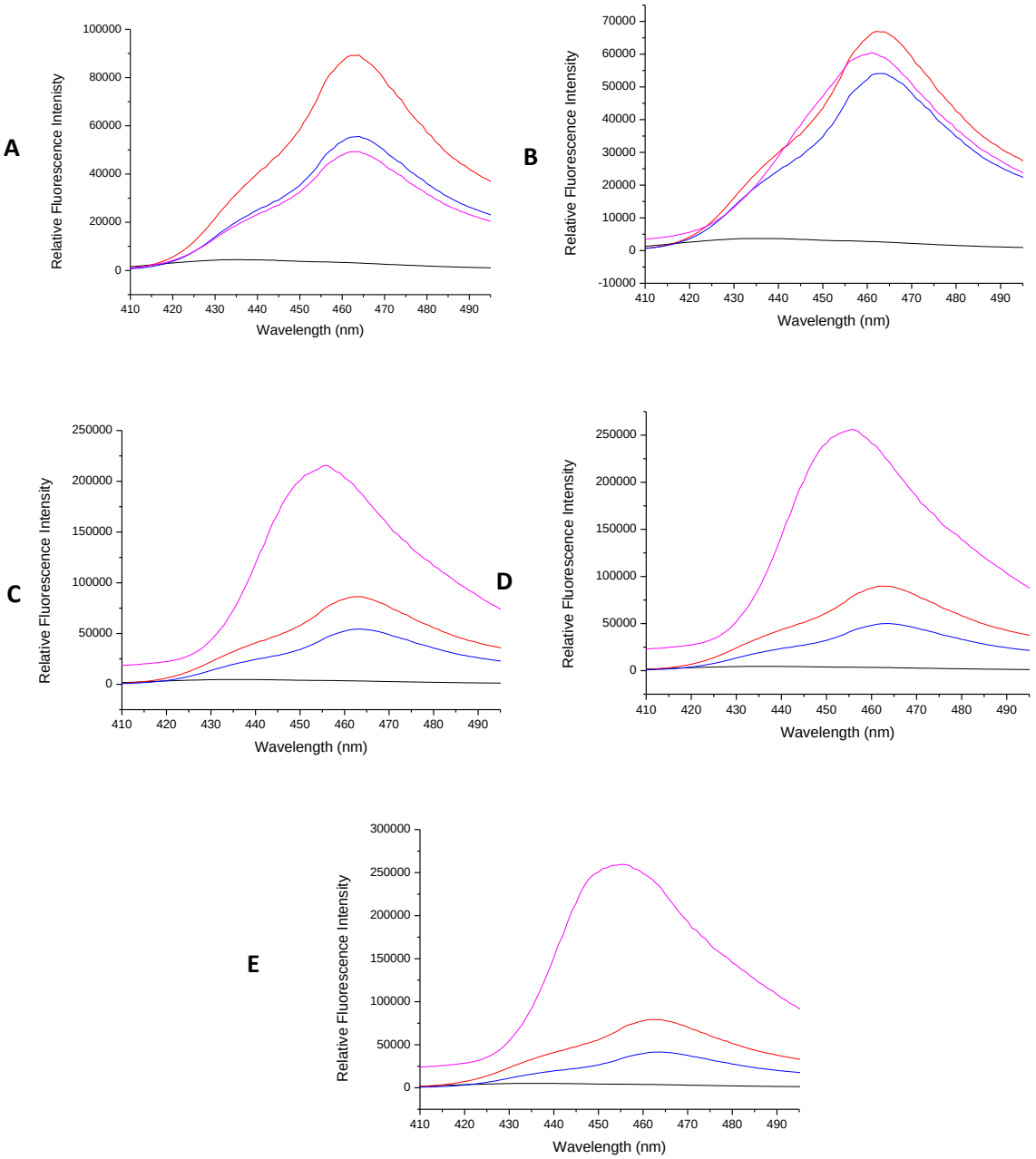

Figure 90 – Fluorescence spectra of **57** (10 µM) + Glu ((a) 100 mM, (b) 200 mM, (c) 300 mM, (d) 400 mM, (e) 500 mM) with Zn^{2+} ((a) 5 mM, (b) 10 mM, (c) 20 mM, (d) 30 mM, (e) 40 mM), respectively. Assays carried out in PBS buffer (pH 7.4). Black line – negative control, blue line – **57**, red line – **57** + Glu, pink line – **57** + Glu + Zn^{2+}, λ_{ex} = 380 nm (bandwidth

$ONOO^-$, whose concentrations were held at fixed values consistent with levels determined in previous experiments on other sensors.

The concentration of Glu was varied from 100 mM to 500 mM and Zn^{2+} concentrations varied from 5 mM to 40 mM based on amounts used by Glass *et al.* for comparable assays used for the development of ES517 and **57**. Therefore, **57** (10 µM) was mixed with $ONOO^-$ (150 µM) before being exposed to Glu (100 mM, 200 mM, 300 mM, 400 mM, 500 mM) and incubated for 40 minutes. $Zn(OAc)_2$ (Zn^{2+} precursor) was then added followed by incubation for a further 15 minutes.

These experiments enabled me to establish the conditions required to characterise the behaviour of **57**, with low concentrations of Glu and Zn^{2+} (**Figure 90**, **A** & **B**) resulting in the probe **57** not responding in the expected manner. At the lowest concentrations (**Figure 90**, **A**) initial addition of the $ONOO^-$ caused a large increase in fluorescence, relative to addition of the other analytes. The response to larger concentrations of Glu and Zn^{2+} (**Figure 90**, **C**, **D** & **E**) of **57** was much more in line with expectation, as the largest increase was in the presence of all three analytes. The best results are gained from the two most concentrated runs (**Figure 90**, **D**, **E**). The lower of these two concentration levels (Glu 400 mM and Zn^{2+} 30 mM) were then chosen for further analysis of **57**, because these values were more representative of the physiological concentrations at synapses in neuronal systems.

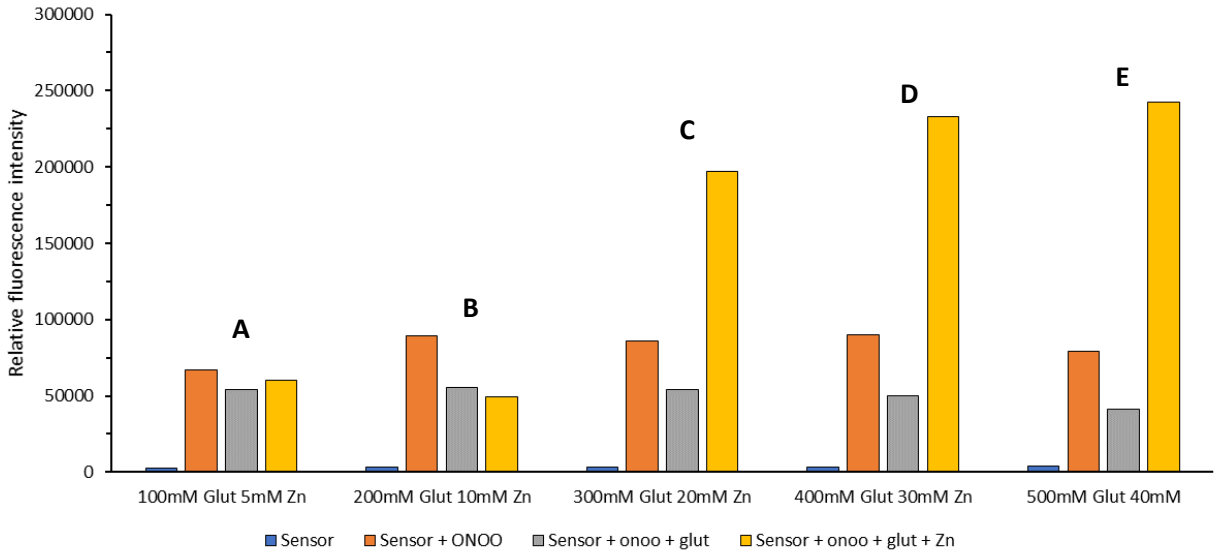

Figure 91 – Comparison of the levels of fluorescence at 462 nm for probe **57** and different concentrations of Glut and Zn^{2+}, λ_{ex} = 380 nm (bandwidth 10 nm).

The results from the concentration screen are best summarised in a column chart (**Figure 91**). This clearly shows an increase in fluorescence signal when all three analytes are present at relatively high concentrations, relative to the lack of fluorescence when the concentrations of Glu and Zn^{2+} were too low.

Taking these conditions into consideration, I next completed a titration of **57** (10 µM) that had been preincubated with Glu (300 mM) and Zn^{2+} (30 mM) against different concentrations of $ONOO^-$ (5-200 µM). Preincubation of **57**, Glu and Zn^{2+} formed a complex that was fluorescent at 417 nm upon excitation at 380 nm. Upon addition of $ONOO^-$ this peak decreased, in conjunction with the appearance of a bathochromically shifted peak at 455 nm (**Figure 91**). This demonstrated a ratiometric response of the **57**-Glu-Zn^{2+} complex towards $ONOO^-$, caused by an increase in the concentration of the deprotected coumarin-Glu-Zn^{2+} complex (**Figure 92**). Although there was an overall decrease in fluorescence intensity, this relationship is potentially very useful for determining the presence of $ONOO^-$, either inside the vesicle or once it has been released, much the same as **53** (**Figure 93**).

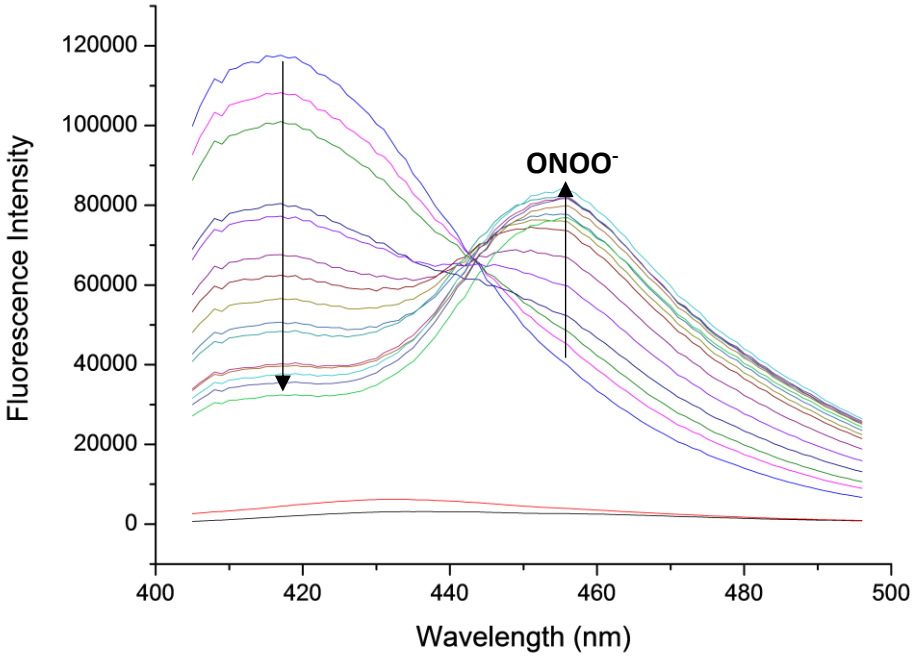

Figure 92 – Titration of **57** (10 µM) pre-incubated with Glu (300 mM) and Zn^{2+} (30 mM) against $ONOO^-$ (5-220 µM). Assays carried out in PBS buffer (pH 7.4), λ_{ex} = 380 nm (bandwidth 10 nm).

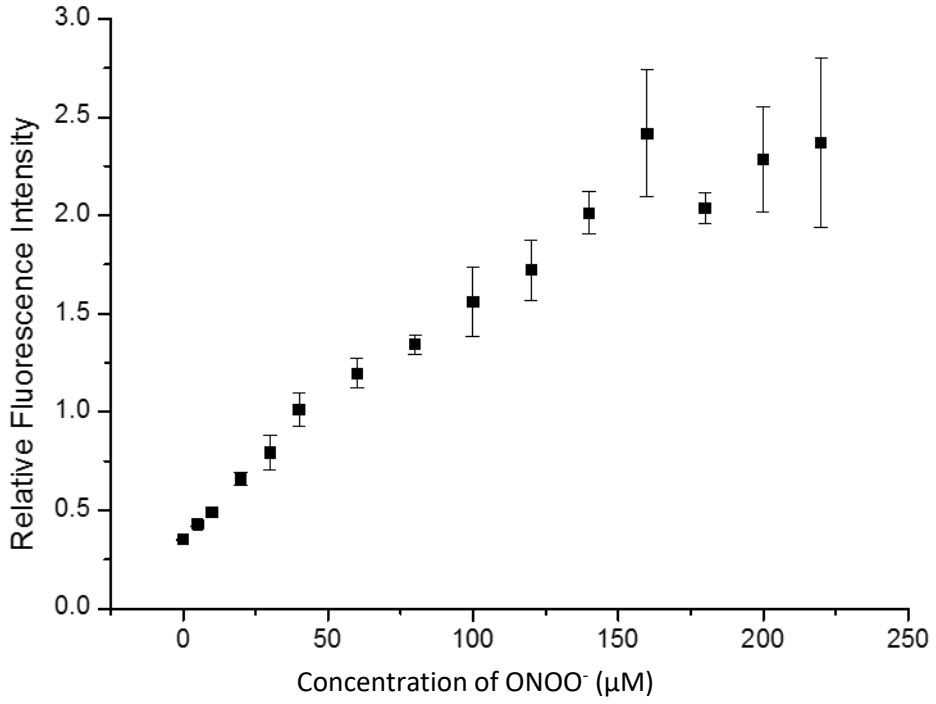

Figure 93 – Ratiometric curve (417 nm / 455 nm) of **57** (10 μM) pre-incubated with Glu (300 mM) and Zn^{2+} (30 mM) against $ONOO^-$ (5-220 μM) in PBS buffer (pH 7.4), λ_{ex} = 380 nm (bandwidth 10 nm).

I next sought to test the selectivity of **57** for $ONOO^-$, with previous work by Glass *et al*. was sufficient evidence that the probe design was likely to be selective for the other two analytes. Therefore, **57** (10 μM) was incubated with Glu (300 mM) and Zn^{2+} (30 mM) and then exposed to a selection of different ROS to test the selectivity of the phenyl boronic acid pinacol ester unit for $ONOO^-$ mediated cleavage (**Figure 94**). Pre-incubation of the sensor with Glu and Zn^{2+} gave a **57**-Glu-Zn^{2+} complex with a constant fluorescence level at 417 nm. However, addition of the various ROS changed the fluorescence in unforeseen ways. All ROS except $ONOO^-$ caused an increase in the level of the fluorescence level of the **57**-Glu-Zn^{2+} complex, which may be due to perturbation of complexation between Zn^{2+} and the Glu moiety. $ONOO^-$ on the other hand, causes a dramatic decrease in the fluorescence of the **57**-Glu-Zn^{2+} complex at 417 nm, accompanied by the appearance of a significant new peak at a longer wavelength of 455 nm, which is representative of cleavage of the phenyl boronic acid pinacol ester.

The selectivity of probe **57** is more clearly observed in the column chart (**Figure 95**), which compares the intensity of the change of fluorescence at the two peaks in the presence of different ROS species, which clearly shows that **57** has selectivity for $ONOO^-$.

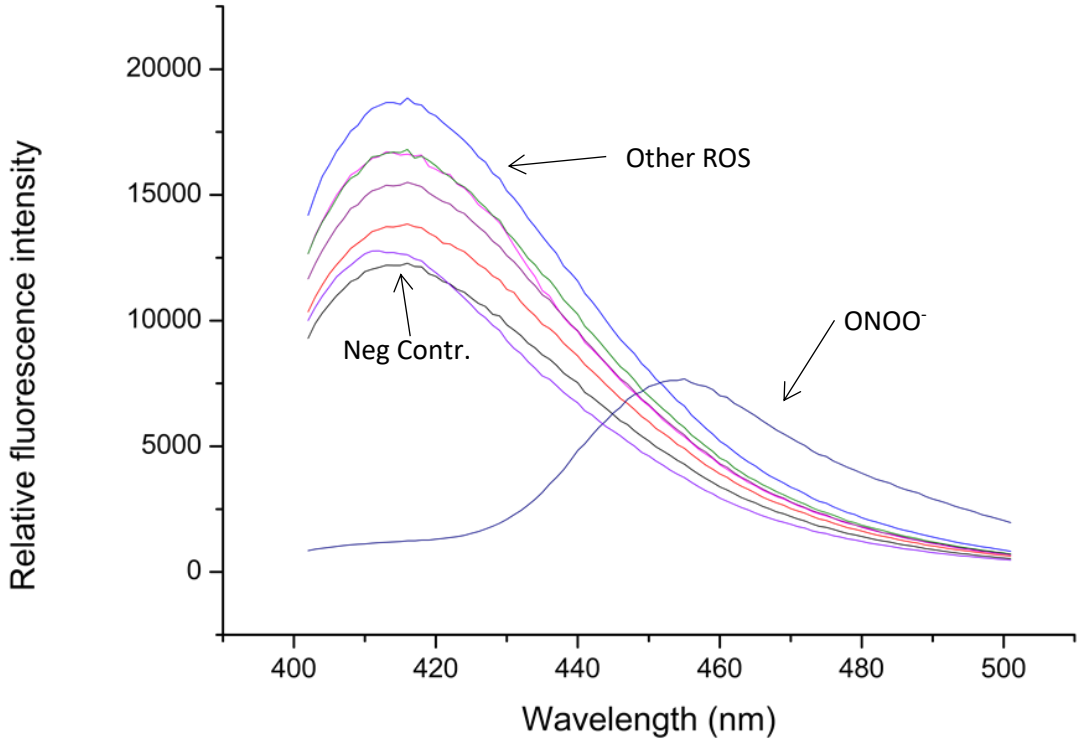

Figure 94 – Fluorescence spectra of **57** (10 µM) incubated with Glu (400 mM) and Zn^{2+} (30 mM) before addition of various ROS species (100 µM). All assays carried out in PBS buffer (pH 7.4), λ_{ex} = 380 nm (bandwidth 10 nm).

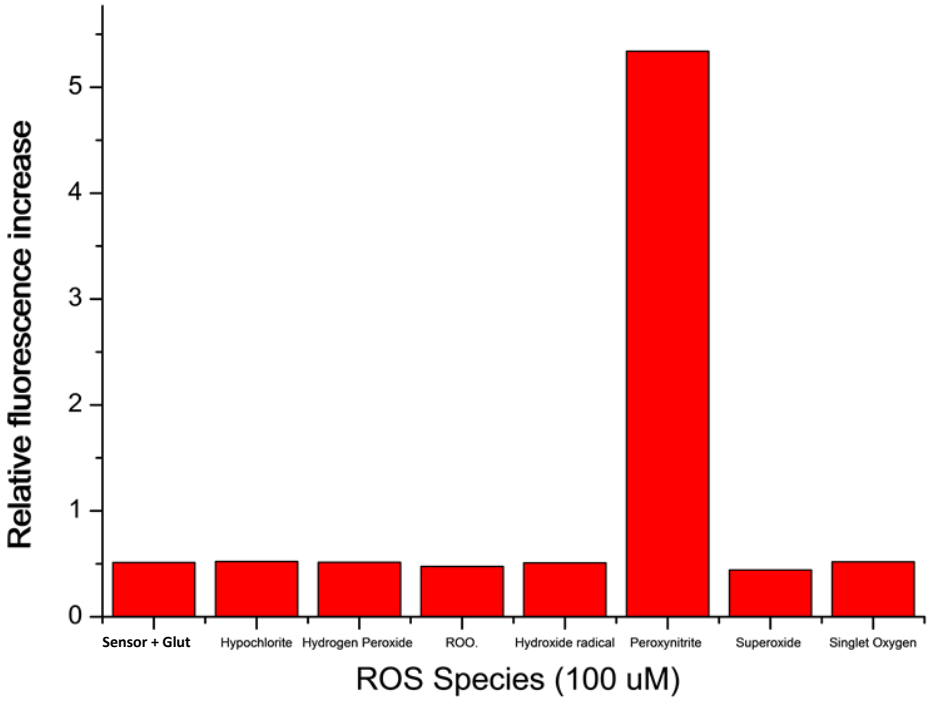

Figure 95 – Fluorescence intensity of **57** at 455 nm/ 417 nm (10 µM) when incubated with Glu (400 mM) and Zn^{2+} (30 mM) test against various ROS species (100 µM). All assays in PBS buffer (pH 7.4), λ_{ex} = 380 nm (bandwidth 10 nm).

2.4.5 Conclusion and Future Work

A modification of Glass *et al.*'s probe **53** has resulted in the production of a triple analyte logic gate **57**. In solution analysis of **57** shows that it responds to the presence of Glu, Zn^{2+}, giving a peak at 417 nm, then exposure to $ONOO^-$ causes the cleavage of the Bpin unit and a bathochromic shift in the fluorescence to form an emission at 455 nm, confirming it can be used as a three-input MLG (**table 4**).

This is a positive proof of concept and justifies further investigation of this probe, which could include more in-solution assays to gain a deeper analysis of the unusual selectivity profile of this probe for other ROS. Alternatively, cleavage of **57** by $ONOO^-$ can afford a phenol group whose pK_a value is in the right range to enable monitoring of pH after the cleavage of the Bpin group. This could potentially expand the use of **57**, to make it an MLG that reacts once with $ONOO^-$ and reversibly with Glu, Zn^{2+} whose fluorescent response is also dependent on pH levels.

$ONOO^-$	Glut	Zinc	Output
0	0	0	0
0	0	1	0
0	1	0	0
1	0	0	0
1	0	1	0
1	1	0	0
0	1	1	0
1	1	1	1

Table 4 – Truth table of **57** inputs and outputs.

2.5 Dual Analyte Sensor for $ONOO^-$ AND Hcys/Cys OR GSH

2.5.1 Literature Precedent

Glutathione (GSH) is a tripeptide of glutamate (Glu), cysteine (Cys) and glycine (Gly), which is a naturally occurring anti-oxidant that occurs in a wide range of living species (**Figure 96**).[47] GSH reduces other biological compounds by acting as an electron donor

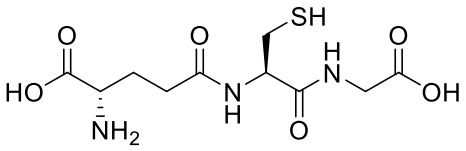

Figure 96 – Structure of GSH

which results in it being transformed into an oxidised dimer of itself (GSSG).[47] GSH is found in higher concentrations than either Cys or Hcys within the cell, with dysregulation of GSH levels implicated in the etiology and progress of several human diseases,[48] including cancer,[49] chronic inflammation,[50] neurodegenerative diseases[51] and metabolic disorders.[52] Given its importance, many fluorescent probes have been developed for the detection of GSH in living systems with a number of reactive pathways available for targeting GSH. Some of these approaches involve reaction of the thiol moiety on GSH with an aldehyde group to afford a fluorophore.[53,54] However, this approach is not

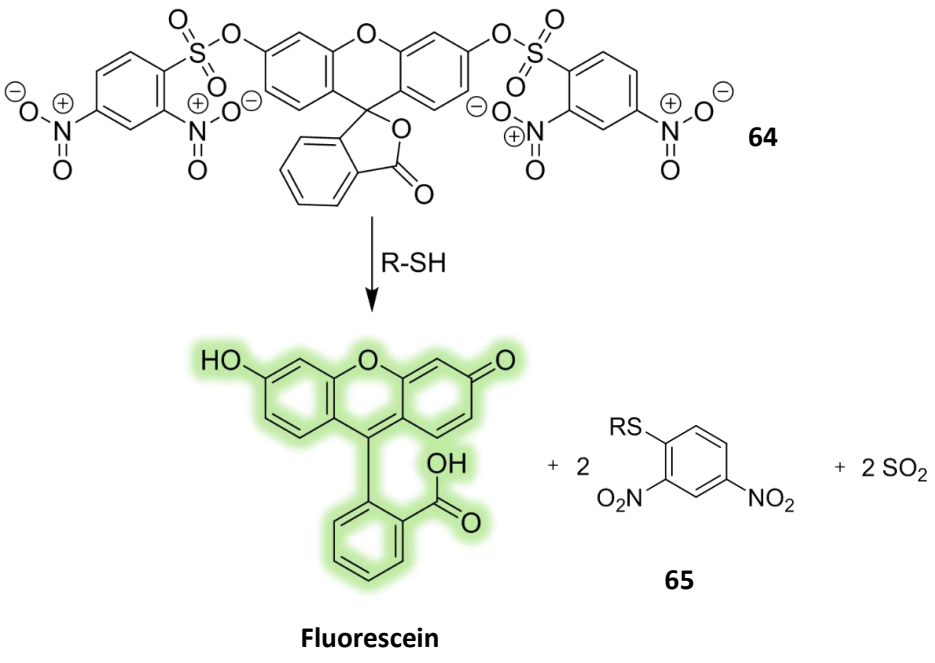

Figure 97 – Fluorescein based 2.4-DNBS probe **64** for detection of thiols.

generally selective for GSH, because the probe is able to react with other sulfur amino acids, such as Hcys and Cys (**Section 2.3.1**). For example, the 2,4-dinitrobenzene sulfonyl ester (2,4-DNBS) group, based on Ellman's reagent, is electron deficient and can be attacked by the thiol group of GSH *via* a nucleophilic aromatic substitution reaction.[55] Attaching this group to a fluorophore (**64**) as a masking unit, achieved by Itoh *et al.*, increases sensitivity towards GSH. Attack from GSH liberates a new aromatic-GSH group (**65**), sulfur dioxide (SO_2) and an active fluorophore. (**Figure 97**).[56]

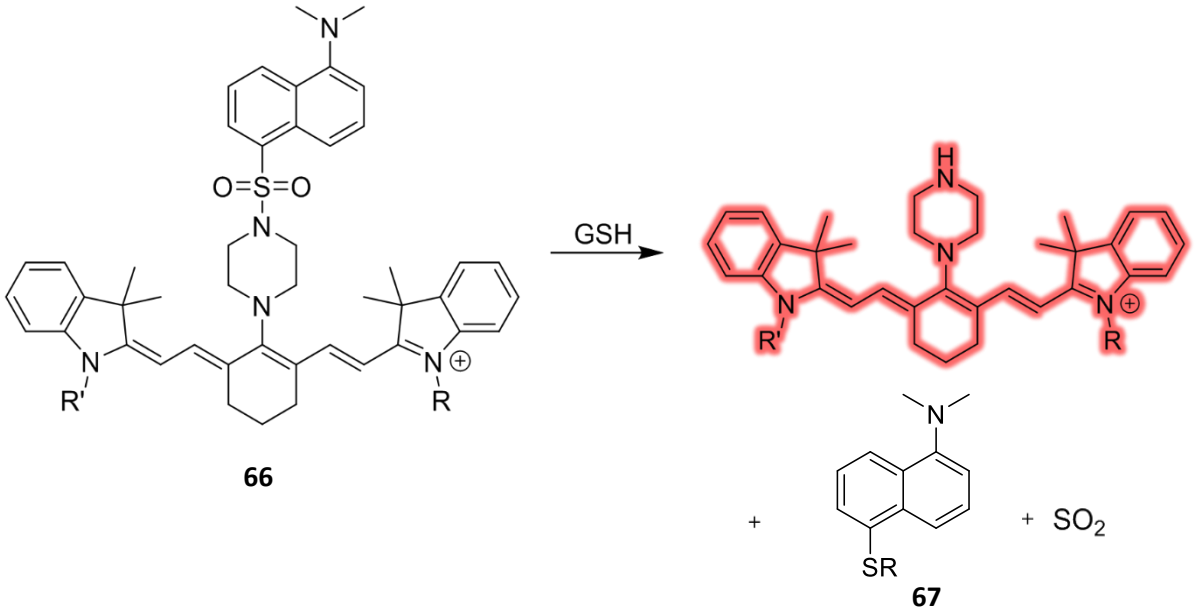

Figure 98 – Specific GSH cyanine probe **66** reacting with GSH and producing the fluorophore, aromatic GSH group **67** and sulfur dioxide.

More specific receptor groups have also been developed for the targeting of GSH over other biological thiols, including a 5-(dimethylamino) naphthalenesulfonamide unit that reacts with GSH selectively over Cys.[57] When incorporated into a probe (**66**), specificity is obtained *via* a mix of the preferred chair conformation of the piperazine linker unit and the equatorial position of the sulfonimide, as well as a weaker S-N bond, relative to other similar probes (**Figure 98**).

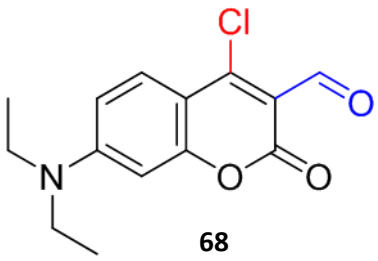

Figure 99 – GSH specific probe **68** with the aldehyde functionality (blue) and chloro group (red).

Yin *et al.* have developed a colorimetric and ratiometric chlorinated coumarinyl aldehyde probe that can be used to differentiate GSH from Hcys and Cys (**Figure 99**, **68**).[58] S_NAr displacement of the chloro group of **68** by GSH (**71**) is followed by macrocyclization *via* iminium formation from condensation of its primary amino and aldehyde groups (**72**). The selectivity of the probe towards GSH, over other thiols, occurs as the thioene intermediates of Hcys and Cys undergo S-N rearrangement (**69)** to afford their corresponding amino-coumarins (**70**). Further reaction of the thiol with the aldehyde functionality is disfavoured because it results in an unstable macrocyclic hemi-thioacetal product. The different species that are formed from reaction of the probe with Hcys/ Cys or GSH have different absorption / emission properties relative that enable the different thiol analytes to be distinguished. The Hcys/ Cys reaction product causes a blue-shifted absorbance relative to the probe; however, GSH has the opposite effect. The absorbance of the probe is shifted to longer wavelengths. The fluorescent output of Hcys/ Cys-Coumarin analogues was maximal for excitation at 385 nm, whilst fluorescence for the GSH-coumarin product was maximal for excitation at 476 nm.

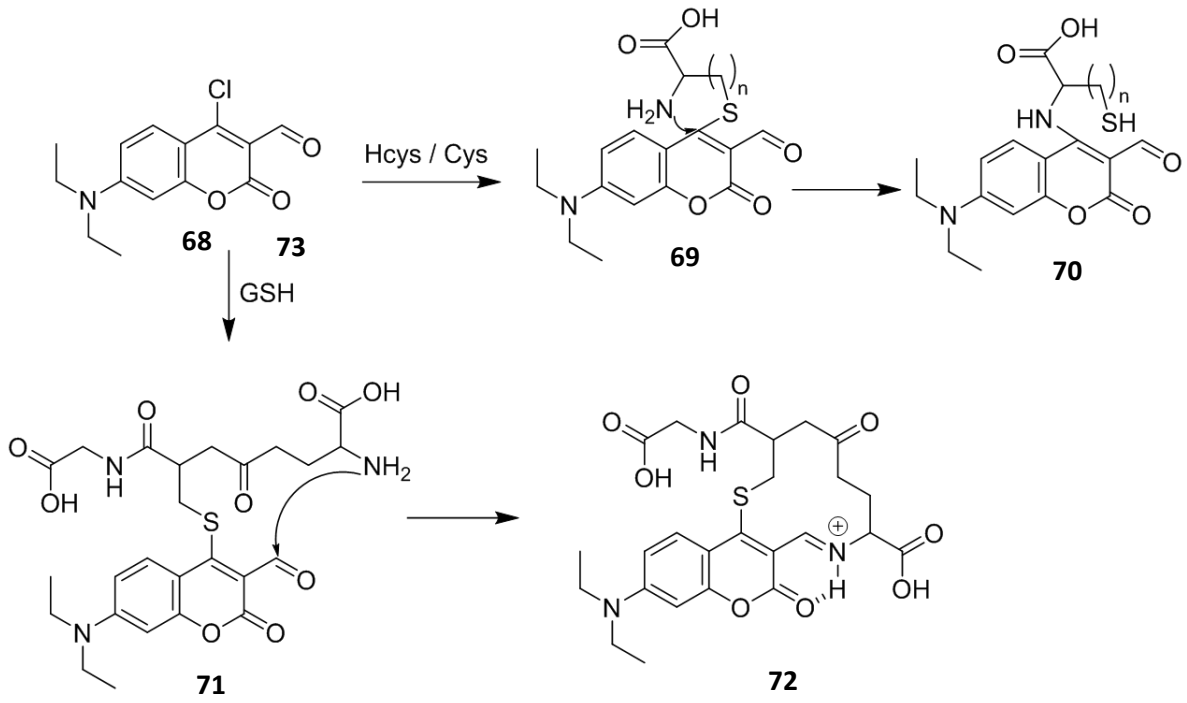

Figure 100 – The reaction pathway of **68** towards GSH and Hcys / Cys. GSH is not able to form the amino-coumarin, like the smaller thiols and instead forms the stabilized iminium cation.

2.5.2 Design of Probes **73** and **74**

Figure 101 – Structure of **73** containing a 7-hydroxy group (pink), chloro group (green), aldehyde group (blue) and **74** containing a phenyl-Bpin group (red), chloro group (green), aldehyde group (blue).

The structure of Yin's probe (**68**) was modified to replace its diethylamino group with a phenol group to produce **73**. This phenol group would then be appended to a 4-methylphenylboronic acid pinacol ester to convey $ONOO^-$ sensitivity, producing probe **74**. It was hoped that this new sensor would then function as a dual activated probe for sensing $ONOO^-$ AND GSH OR Hcys / Cys probe.

2.5.3 Synthesis of **73** and **74**

The proposed synthesis of **73** and **74** started with synthesis of the core 4,7-dihydroxy-2H-chromen-2-one (**77**) through Pechmann condensation of malonic acid (**75**) and resorcinol (**76**) in the presence of $ZnCl_2$ and $POCl_3$. This reaction required quite a wasteful work-up

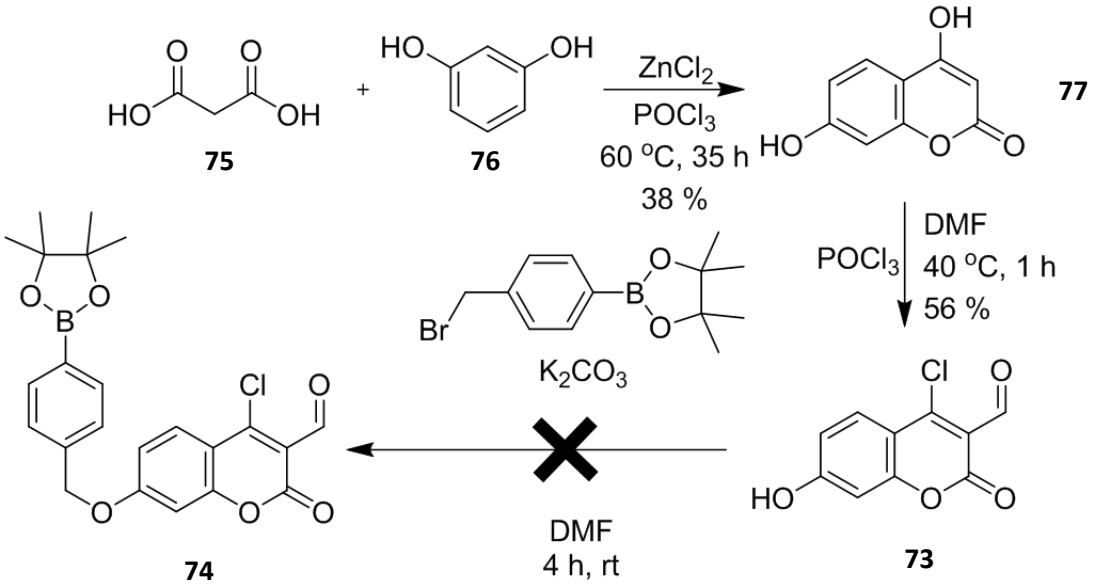

Scheme 4 – Synthetic route to **73** and the failed synthesis of **74**.

that was responsible for the poor 38% yield. A Vilsmeier Haack reaction with **77** and $POCl_3$ gave **73** in a moderate 56% yield. The last step of the synthesis involved attempted alkylation of the phenol unit with 4-bromomethylphenylboronic acid pinacol ester, which proved unsuccessful, primarily due to the insolubility of **73** in common organic solvents. Several methods were carried out to encourage the reaction to proceed, including addition of KI to the reaction (the Finkelstein method), warming the reaction and using different solvents and bases – all to no avail.

2.5.4 Fluorescence Analysis of **73**

Although I was unsuccessful in preparing the full dual activated probe **74**, it was decided to explore the fluorescent properties of the new parent probe **73**, to see how its performance compared with Yin's original probe.

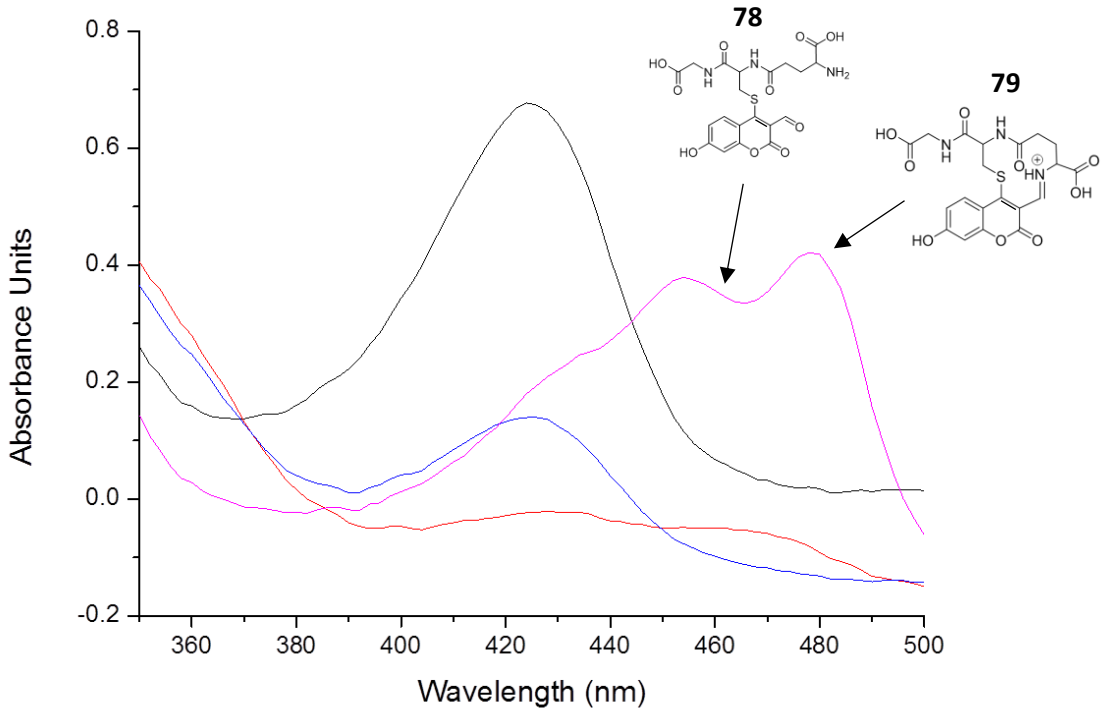

Figure 102 – UV-Vis absorption spectrum of **73** (20 µM) – blue line, **73** (20 µM) + Cys (200 µM) – orange line, **73** (20 µM) + Hcys (200 µM) – grey, **73** (20 µM) + GSH (200 µM) – pink. Intermediate **78** and iminium ion **79** both shown on the graph.

Firstly, the UV-vis absorbance of **73** (20 µM) was observed in the presence of GSH (200 µM), Cys (200 µM) and Hcys (200 µM) (**Figure 102**). **73** alone showed a large absorption at 420 nm. Addition of Cys (200 µM) [or Hcys (200 µM)] resulted in a significant drop in this absorption and a slight increase in absorption at lower wavelengths (240-370 nm).

Addition of GSH (200 µM) resulted in a decrease in absorbance at 420 nm, in conjunction with the appearance of two new bathochromically shifted peaks. These two peaks are most probably due to the intermediate (**78**) and the final iminium ion (**79**) being produced. This allows for detection of the two different analytes at different wavelengths, much like **68**. Exposing **73** (20 µM) to all three analytes (Cys, Hcys and GSH, 200 µM) and exciting the probe at the lower excitation of 360 nm revealed that that **73** was capable of distinguishing small thiols (Hcys / Cys) from GSH (**Figure 103**). Furthermore, the **68**-GSH adduct gave a significant increase in the relative fluorescence when **73** was excited at the longer

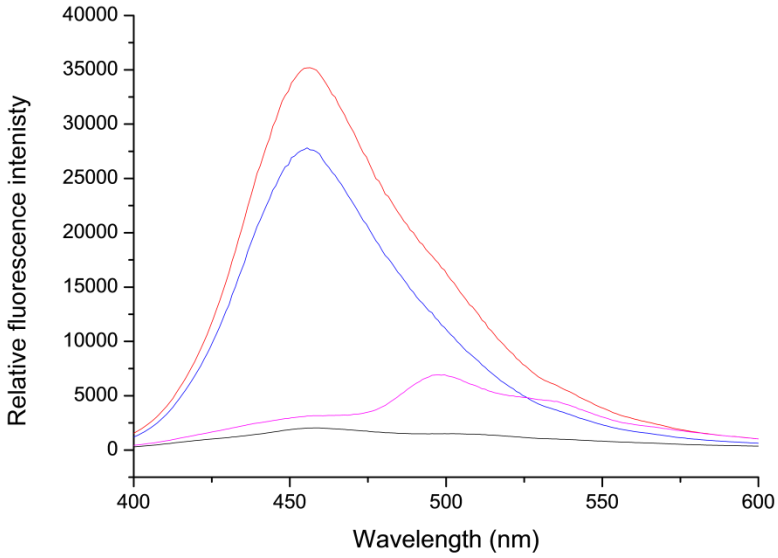

Figure 103 – Fluorescence spectra of **73** (20 µM) – grey and **73** (20 µM) with Cys (200 µM) – red, Hcys (200 µM) – blue, GSH (200 µM) - pink. All assays carried out In PBS buffer (pH 7.4) λ_{EX} 360 nm (bandwidth 10 nm).

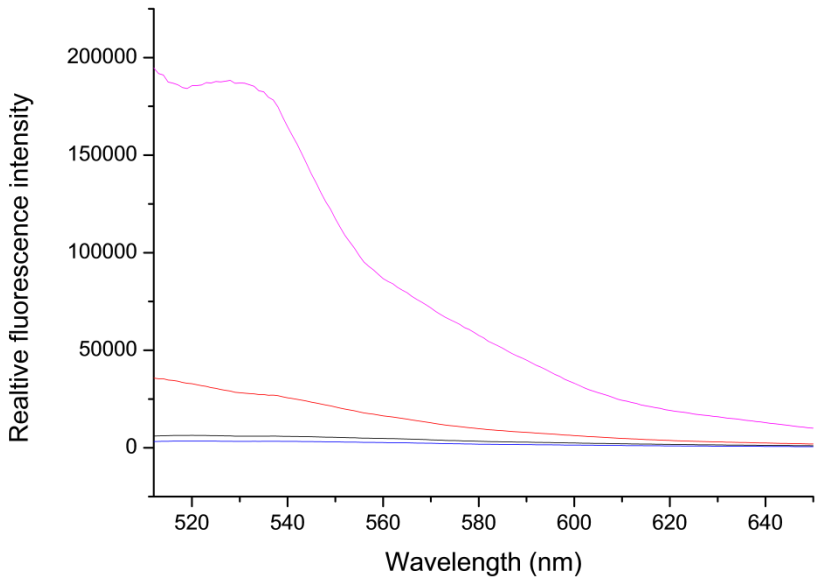

Figure 104 – Fluorescence spectra of **73** (20 µM) – grey and **73** (20 µM) with GSH (200 µM) – pink, Hcys (200 µM) – grey, Cys (200 µM) – orange. All assays carried out in PBS buffer (pH 7.4) λ_{EX} 460 nm (bandwidth 10 nm).

wavelength of 460 nm (**Figure 104**). Further selectivity studies and pH studies on this sensor are currently being carried out by another member of our research group to fully analyse the potential of the probe.

2.5.5 Conclusion and Future Work

A new coumarin based probe **73** has been developed from Yin *et al.*'s probe **68**. **73** can be used in solution for the differentiation of small cellular thiols (Hcys & Cys) and GSH *via* the excitation at different wavelengths. **74** was designed to retain the ability to differentiate between thiols, but with added sensitivity to $ONOO^-$ to make it a dual analyte MLG. However, solubility issues hindered the synthesis.

Further investigation into **73** and its behaviour with different analytes is being investigated, with the aim of its application in cells. Attempts are ongoing to successfully synthesise **74** and test its function as an MLG, as well as attaching new reactive groups to add sensitivity to more target analytes.

2.6 Chapter Conclusion

In this chapter a number of new, coumarin based probes have been developed for the detection of multiple analytes. **42** was observed to have a good fluorescence response to both $ONOO^-$ and thiols in solution. However, cellular investigation showed that the probe was not soluble in physiological conditions.

46 is a new probe that gives a large fluorescence response upon being exposed to NTR and Hcys in solution. It is currently being tested in cellular analysis by collaborators.

Probe **57** is a three-input MLG that responds to glutamate, zinc and $ONOO^-$. More in solution investigations are required to fully understand the behaviour of this probe. Also, selectivity studies for each of the analytes need to be conducted. Also, once exposed to $ONOO^-$ **57** could also potentially used as a pH indicator. After these have been completed, cell studies could be initiated.

Finally, **74**, an $ONOO^-$ "AND" GSH / Hcys probe was designed, but the final step was not achieved in the timeframe available. The precursor **73**, however, was tested for behaviour

as it was also a novel compound. This showed that the design was capable of differentiating between GSH and the smaller thiols (Hcys and Cys). Attempts are being made to successfully synthesise the final compound and fully analyse the probe.

2.7 Chapter References

1: H. Martial, P. Poumale, R. Hamm, Y. Zang, Y. Shiono, V. Kuete, *Med. Plant Res. In Africa*, **2013**, 261-300.
2: K. P. Link, *Circulation*, **1959**, *19*, 97-107.
3: C. Badger, K. Seers, N. Preston, P. Mortimer, *Cochrane Database Syst. Rev.*, **2009**, *2009*, 1-5.
4: M. Lee, C. Yen, W. Yang, H. Chen, C. Liao, C. Tsia, C. H. Chen, *Org. Lett.*, **2004**, *6*, 1241-1244.
5: B. D. Wagner, *Molecules*, **2009**, *14*, 210-237.
6: Y. Jung, J. Jung, Y. Huh, D. Kim, *J. Anal. Meth. Chem.*, **2018**, *2018*, 1-11.
7: W. H. Perkin, *J. Chem. Soc.*, **1868**, *21*, 53-63.
8: A. Gaspar, M. J. Matos, J. Garrido, E. Uriarte, F. Borges, *Chem. Rev.*, **2014**, *114*, 4960-4992.
9: H. V. Pechman, *Berichte*, **1884**, *17*, 929-936.
10: S. Goswami, S. Das, K. Aich, D. Sarkar, T. K. Mondal, *Tet. Lett.*, **2014**, *55*, 2695-2699.
11: L. Long, N. Wang, Y. Han, X. Yuan, S. Cao, A. Gong, K. Wang, *Analyst*, **2018**, *143*, 2555-2562.
12: B. Halliwell, *Free Radicals and other reactive species in Disease*, **2001**, Nature Publishing Group.
13: K. Lin, J. Xue, M. Nomen, B. Spur, P. Wong, *J. Bio. Chem.*, **1995**, *270*, 16487-16490.
14: M. Trujillo, L. Folkes, S. Bartesaghi, B. Kalyanaraman, P. Wardman, R. Radi, *Free Rad. Biol. & Med.*, **2005**, *39*, 279-288.
15: S. Palanisamy, P. Wu, S. Wu, Y. Chen, S. Tzou, C. Wang, C. Chen, Y. Wang, *Biosens. Bioelec.*, **2017**, *91*, 849-856.
16: J. D. Finkelstein, J. J. Martin, *Int. J. Bio. & Cell Bio.*, **2000**, *32*, 385-389.
17: M. Cattaneo, *Int. J. Lab. Res.*, **1997**, *27*, 139-144.
18: B. A. Maron, J. Loscalzo, *Annu. Rev. Med.*, **2009**, *60*, 39-54.
19: P. Ganguly, S. F. Alam, *Nutr. J.*, **2015**, *14*, 1-10.
20: M. S. Morris, *Lancet*, **2003**, *2*, 425-428.
21: V. Fratoni, M. L. Brandi, *Nutrients*, **2015**, *7*, 2176-2192.

22: G. Cianciolo, A. De Pascalis, L. Di Lullo, C. Ronco, C. Zannini, G. La Manna, *Cardiorenal Med.*, **2017**, *7*, 255-266.

23: W. Wang, O. Rusin, X. Xu, K. K. Kim, J. O. Escobedo, S. O. Fakayode, K. A. Fletcher, M. Lowry, C. M. Schowalter, C. M. Lawrence, F. R. Fronczek, I. M. Warner, R. M. Strongin, *J. Am. Chem. Soc.*, **2005**, *127*, 15949-15958.

24: L. Long, L. Zhou, L. Wang, S. Meng, A. Gong, F. Du, C. Zhang, *Org. & Biomol. Chem.*, **2013**, *11*, 8214-8220.

25: W. Lin, L. Long, L. Yuan, Z. Cao, B. Chen, W. Tan, *Org. Lett.*, **2008**, *10*, 5577-5580.

26: H/ Y. Lee, Y. P. Choi, S. Kim, T. Yoon, Z. Guo, S. Lee, K. M. K. Swamy, G. Kim, J. Y. Lee, I. Shin, J. Yoon, *Chem. Commun.*, **2014**, *50*, 6067-6769.

27: K. Lee, T. Kim, J. H. Lee, H. Kim, J. Hong, *Chem. Commun.*, **2008**, *0*, 6173-6175.

28: I. M. de Oliveira, D. Bonatto, J. A. P. Henriques, *Tech. Educ. Topics in App. Microbiol. And Microbial Biotech.*, **2010**, *0*, 1008-1019.

29: B. D. Palmer, P. V. Zijl, W. A. Denny, W. R. Wilson, *J. Med. Chem.*, **1991**, *38*, 1229-1241.

30: D. Yang, H. Y. Tian, M. Li, Y. Zhou, J. F. Zhang, *Sci. Rep.*, **2017**, *7*, 9174.

31: B. S. Meldrum, *J. Nut.*, **2000**, *130*, 1007-1015.

32: R. Srinivasan, N. Sailasuta, R. Hurd, S. Nelson, D. Pelletier, *Brain*, **2005**, *128*, 1016-1025.

33: M. Frigo, M. G. Cogo, M. L. Fusco, M. Gardinetti, B. Frigeni, *Curr. Med. Chem.*, **2012**, *19*, 1295-1299.

34: R. Wang, P. H. Reddy, *J. Alzheimers Dis.*, **2017**, *57*, 1041-1048.

35: K. W. Lange, J. Kornhuber, P. Riedierer, *Neurosci. Biobehav. Rev.*, **1997**, *21*, 393-400.

36: S. Cheng, Y. Zhao, J. Li, X. Chen, R. Wang, J. Zeng, *Psychoneuroendocrinology*, **2014**, *47*, 126-135.

37: S. Zarei, K. Carr, L. Reily, K. Diaz, O. Guerra, P. F. Altamirano, W. Pagani, D. Lodin, G. Orozco, A. Chinea, *Surgical Neur. Int.*, **2015**, *6*, 171.

38: D. C. Rojas, *J. Neural. Transm.*, **2014**, *121*, 891-905.

39: O. Howes, R. McCutcheon, J. Stone, *J. Psychopharmacol.*, **2015**, *29*, 97-115.

40: G. Sanacora, G. Treccani, M. Popoli, *Neuropharmacology*, **2012**, *62*, 63-77.

41: M. W. Lada, T. W. Vickroy, R. T. Kennedy, *Anal. Chem.*, **1997**, *69*, 4560-4565.

42: M. Jamal, S. Chakrabarty, M. A. Yousuf, A. Khosla, K. M. Razeeb, *Microsystem Tech.*, **2018**, *24*, 4193-4206.

43: K. Buck, P. Voehringer, B. Ferger, *J. Neurosci. Meth.*, **2009**, *182*, 78-84.

44: S. A. Hires, Y. Zhu, R. Y. Tsien, *Proc. Nat. Acad. Sci. USA*, **2008**, *105*, 4411-4416.

45: J. L. Klockow, K. S. Hettie, T. E. Glass, *ACS Chem. Neurosci.*, **2013**, *4*, 1334-1338.

46: K. S. Hettie, J. L. Klockow, T. E. Glass, *J. Am. Chem. Soc.*, **2014**, *136*, 4877-4880.

47: A. Pompella, A. Visvikis, A. Paolicchi, V. D. Tata, A. F. Casini, *Biochem. Pharma.*, **2003**, *66*, 1499-1503.

48: N. Ballatori, S. M. Krance, S. Notenboom, S. Shi, K. Tieu, C. L. Hammond, *Biol. Chem.*, **2009**, *390*, 191-214.

49: A. Bansal, M. C. Simon, *J. Cell Biol.*, **2018**, *217*, 2291-2298.

50: M. L. Steele, S. Fuller, A. E. Maczurek, C. Kerstaitis, L. Ooi, G. Munch, *Cell. Mol. Neurobiol.*, **2013**, *33*, 19-30.

51: C. Cecchi, S. Latorraca, S. Sorbi, T. Iantomasi, F. Favili, M. T. Vincenzini, G. Liguri, *Neurosci. Lett.*, **1999**, *275*, 152-154.

52: V. Rani, G. Deep, R. K. Singh, K. Palle, U. C. S. Yadav, *Life Sciences*, **2015**, *148*, 183-193.

53: J. Li, Y. Kwon, K. S. Chung, C. S. Lim, D. Lee, Y. Yue, J. Yoon, G. Kim, S. Nam, Y. W. Chung, H. M. Kim, C. Yin, J. Ryu, J. Yoon, *Theranostics*, **2018**, *8*, 1411-1420.

54: H. Peng, W. Chen, Y. Cheng, L. Hakuna, R. Strongin, B. Wang, *Sensors*, **2012**, *12*, 15907-15946.

55: H. Maeda, H. Matsuno, M. Ushida, K. Katayama, K. Saeki, N. Itoh, *Angew. Chem. Int. Ed.*, **2005**, *44*, 2922-2925.

56: A. Shibata, K. Furukawa, H. Abe, S. Tsuneda, Y. Ito, *Bioorg. Med. Chem. Lett*., **2008**, *18*, 2246-2249.

57: J. Yin, Y. Kwon, D. Kim, D. Lee, G. Kim, Y. Hu, J. Ryu, J. Yoon, *J. Am. Chem. Soc.*, **2014**, *136*, 5351-5358.

58: C. Xu, H. Li, B. Yin, *Biosens. Bioelec.*, **2015**, *72*, 275-281.

3.0 Fluorescein Based Probes

In this chapter a brief overview of fluorescein and its use in fluorescent sensors shall be given. Then, a number of new probes that have been developed as a part of my research programme will be discussed. This will include literature precedent, probe design, analysis and a conclusion of their efficacy.

A number of these probes (**Section 3.2**, **Section 3.4** and **Section 3.5**) were developed and analysed as an equally contributed cooperation between myself and Dr Adam Sedgwick, a former member of the James group at Bath University.

3.1 Introduction

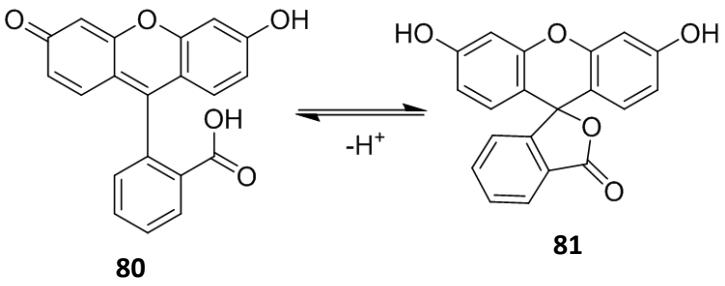

80 **81**

Figure 105 – Dynamic interconversion between acid **80** and lactone **81** forms of Fluorescein.

Fluorescein is one of the most widely used fluorescent compounds that have been used extensively for the synthesis of fluorescent probes.[1-5] It has an easily modifiable structure, high quantum yield and is non-toxic. The structure of fluorescein incorporates a benzoic acid moiety and a xanthene group (**Figure 105**), with the benzoic acid group potentially acting as a PET quencher of its xanthene fragment.[6]

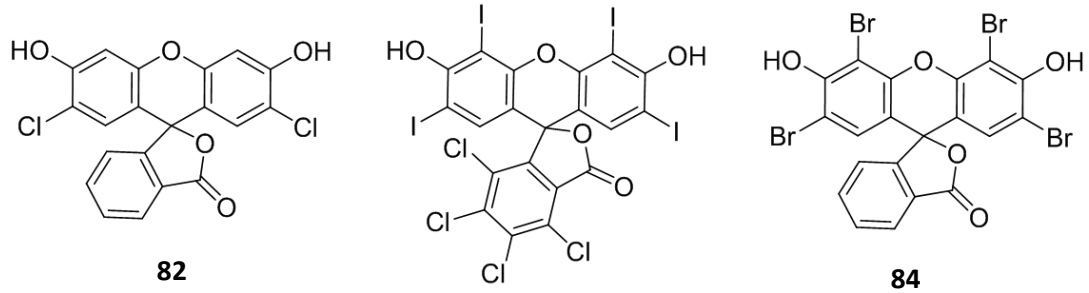

82 **83** **84**

Figure 106 – Structures of DCF **82**, Rose Bengal **83** and Eosin **84**.

A variety of different fluorescein-based compounds have been produced to fully exploit fluorescein as a good fluorophore, including derivatives that incorporate halide variants like dichlorofluorescein (DCF, **82**),[7] rose Bengal (**83**)[8] eosin (**84**, **Figure 106**)[9], metal binding derivatives like Calcein,[10] and other structural variants such as 6-carboxyfluorescein,[11] fluorescein isothiocyanate (FITC)[12] and merbromin.[13]

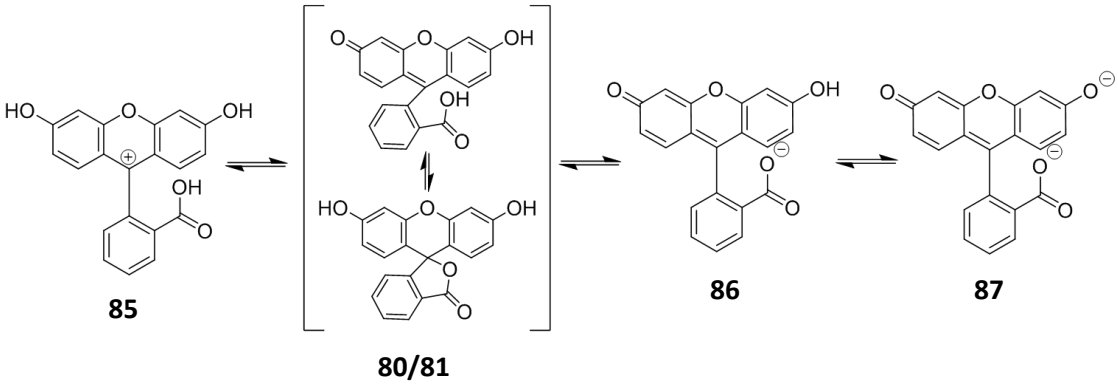

Figure 107 – Ionic forms of fluorescein.

Fluorescein does not need to be modified to be used as a pH probe (**Figure 107**). At extremely low pH, it can exist as a cation **85**. Otherwise, the lactone form **80** (pKa ~ 2.2) predominates in low pH environments. As the pH increases then the neutral form **81** is produced (pKa ~ 4.4), followed by the ring opened form **86** (pKa ~ 6.7) and finally the dianionic form **87** (pKa~ 9). This means that an increase in pH results in a dramatic increase in fluoresceence.[14]

Adolf von Baeyer first synthesised fluorescein in 1871.[15] Reaction of phthalic anhydride and resorcinol in the presence of a zinc chloride catalyst produces fluorescein through a Friedel-Crafts type mechanism. Later developments resulted in methanesulfonic acid being used as a Brønsted acid catalyst under milder conditions, with a reasonable mechanism for its formation shown in **Figure 108**.[16]

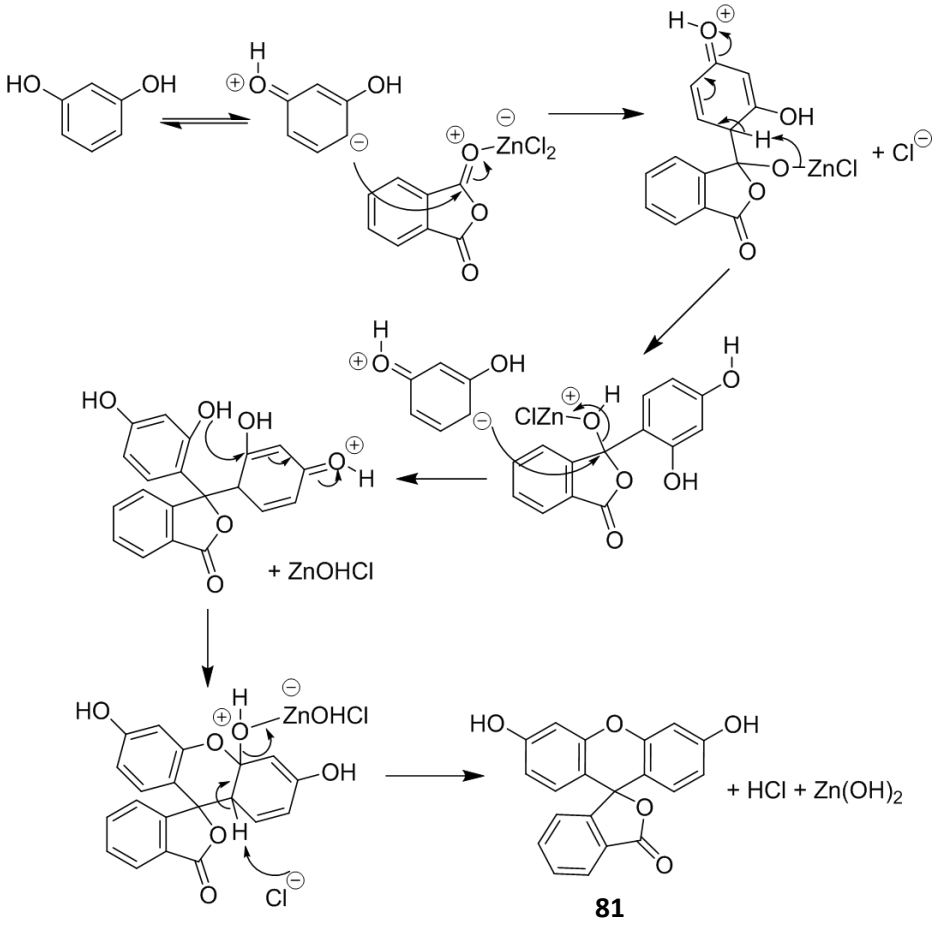

Figure 108 – Mechanism for formation of fluorescein.

Methods to add functionality and sensitivity to fluorescein include blocking the electron donating ability of the oxygen atoms on the xanthene ring, which prevents ICT in the xanthene fragment, which results in fluorescent quenching. Other methods include attaching binding groups to different aromatic positions on either the xanthene or benzoic acid fragments, which can be used to modulate the PET characteristics of the compound. Several fluorescein probes for specific biological targets have been developed (See **Section**

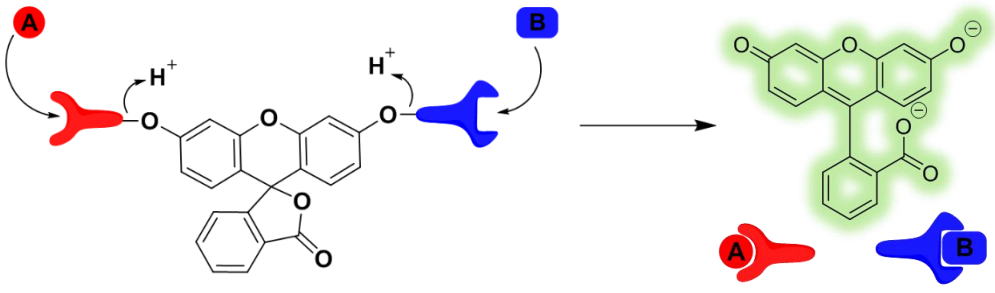

Figure 109 – Multi-analyte cleavage of a masked fluorescein probe to afford a fluorescent response.

1.5), including the $^{\cdot}O_2$ probe HKSOX-1 (**Figure 27**)[17] and the NO probe containing a *o*-phenylenediamine reactive group (**Figure 39**).[18]

Modification of the phenols on the xanthene ring commonly occurs *via* deprotonation of the phenol group with the resultant phenolate anion reacting with an electrophile to afford a masked fluorophore (**Figure 109**). Subsequent reaction of these analytes with the masked phenol units then release a fluorescent unit which enables fluorescein to be potentially used as a core scaffold for multi-analyte detection (**Section 1.6**).

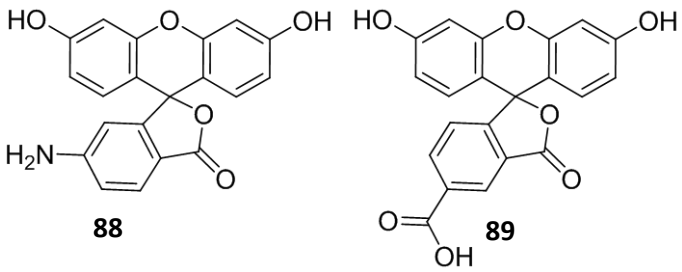

Figure 110 – Structures of 5-aminofluorescein **88** and 6-carboxyfluorescein **89**.

Other positions of the core fluorescein can be modified *via* pre-functionalisation of sub-units prior to assembly of its heterocyclic core, with this approach having been used to produce amino-[19] and carboxy- derivatives (**Figure 110**),[11] as well as variants with extended aromatic systems.[20] Therefore, the versatility of the synthetic methodology available for the synthesis of fluorescein-based probes allows a wide variety of reactive functional groups to be attached to the central fluorophore that can be used to detect a large number of reactive analytes.

3.2 Dual Analyte Probe for Detection of $ONOO^-$ and Fluoride

3.2.1 Literature Precedent

$ONOO^-$, as discussed previously (**Section 1.5.4**) is an ROS/ RNS that can be damaging in biological systems. It can be generated or observed at elevated levels in numerous human diseases. Fluoride (F^-) is a highly reactive anion that is not used or produced in mammals, however, it can be introduced into biological systems through environmental exposure.[21] Fluoride anions are inherently toxic, with high levels known to cause damage to the brain,[22] teeth,[23] kidneys[24] and thyroid.[25] Several probes exist for the individual detection of $ONOO^-$ (**Section 1.5.3.7**) and F^- individually,[26-28] however, no dual analyte probes existed for the simultaneous detection of both species in the same sample.

3.2.2 Design of Probe **90**

It was decided to synthesise a fluorescein-based probe **90** for the dual detection of $ONOO^-$ and F^-, using two reactive groups bound to each of the xanthene phenols (**Figure 111**). Sensitivity to $ONOO^-$ would arise from cleavage of a Bpin unit with sensitivity for F^- coming from cleavage of a tert-butyl di-methyl silyl (OTBDMS) group. Simultaneous cleavage of both units produces an active fluorescein probe leading to a 'turn-on' response.

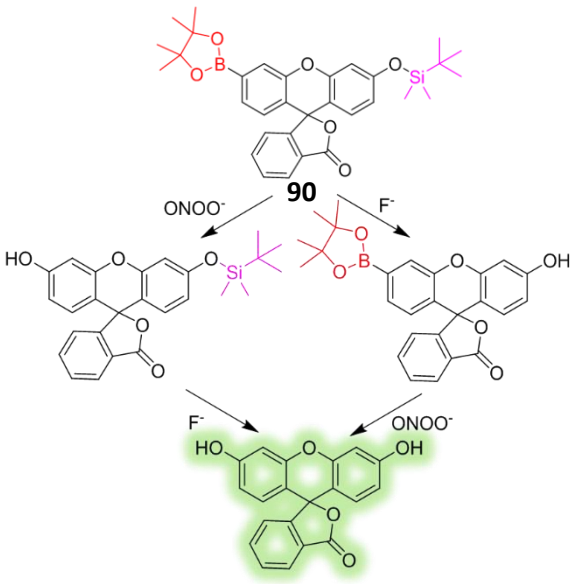

Figure 111 – Dual analyte probe **90** for the detection of $ONOO^-$ using a Bpin group (red) and F^- using a tert-butyl di-methyl silyl ether group (pink).

3.2.3 Synthesis of Probe **90**

One of the phenol groups of fluorescein **81** was first reacted with *N*-phenyl bis(trifluoromethanesulfonamide) and DIPEA to afford mono triflate **91** in 46 % yield. This mono-triflate was then subjected to Pd^0 catalysed Suzuki-Miyaura coupling conditions resulting in boronate ester **92** in 25% yield. Finally, protection of the phenol group of **92** was achieved *via* reaction of tert-butyl di-methylsilyl chloride (TBDMS-Cl) and K_2CO_3 to afford the desired probe **90** in 67% yield.

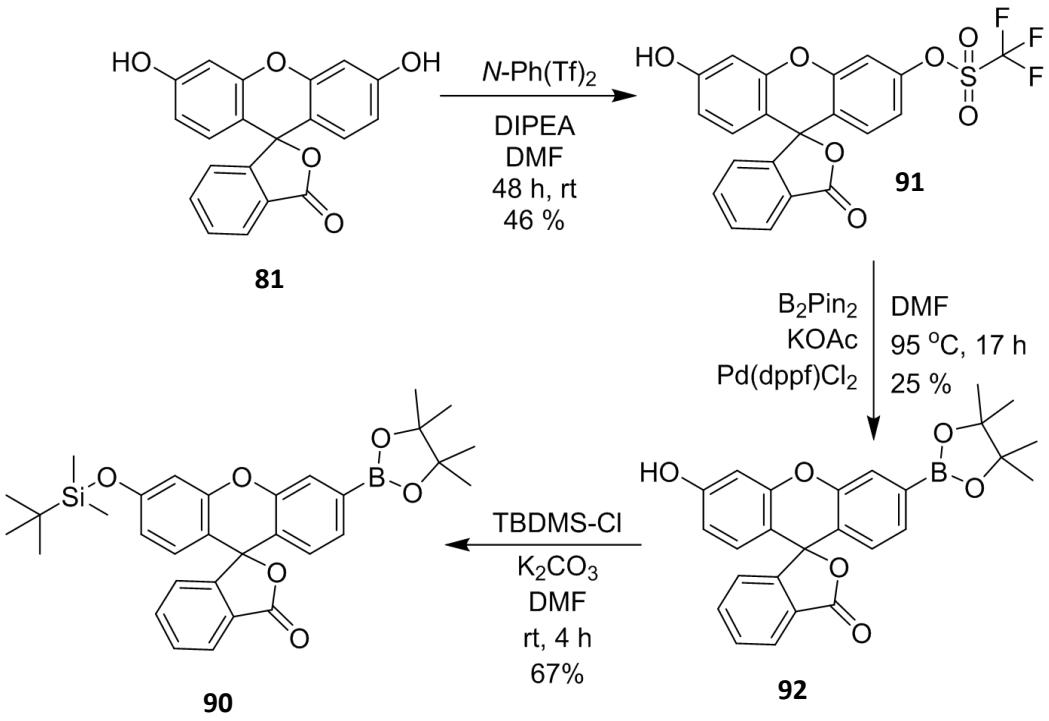

Scheme 5 – Synthesis of dual probe **90**.

3.2.4 Fluorescent Analysis of Probe **90**

Initial studies on the performance of **90**, revealed that this sensor fluoresced when dissolved in water, but not when dissolved in tetrahydrofuran (THF) (**Figure 112**). This unexpected observation was thought to be have been caused by the TBDMS group being too labile in aqueous systems, resulting in its hydrolysis and partial fluorescence of the sensor when no analyte was present. Therefore, this probe was deemed not to be useful as a sensor in aqueous and biological systems; however, it could potentially be used to detect $ONOO^-$ and F^- in organic solvents.

A B

Figure 112 – Sensor **90** dissolved in THF (A) and water (B).

ON/ OFF tests were conducted with the individual analytes using a prepared solution of $ONOO^-$ and tetrabutylammonium fluoride (TBAF, a standard stabilised alternative for F^-). A small increase in fluorescence was observed on addition of 2 mM TBAF to 0.5 µM solution of the probe in THF, which was assigned to the TBDMS group being cleaved to liberate the first phenol of the xanthene fragment. Subsequent additions of $ONOO^-$ (1-600 µM) resulted in oxidation of the boronic acid pinacol ester fragment to generate the fully deprotected fluorescein unit (**Figure 113**). This second cleavage event resulted in a 66-fold increase in the fluorescence intensity of the compound at 525 nm which enabled a linear relationship with the peroxynitrite concentration to be extrapolated (**Figure 114**). Changing the order of addition of each analyte, initial addition of $ONOO^-$ (500 µM) to the sensor first, resulted in a small increase in the baseline fluorescence. Pleasingly, subsequent addition of TBAF (2 mM) once again resulted in a large increase in

fluorescence of 57-fold, thus demonstrating the ability of the sensor for the dual detection of fluoride and peroxynitrite anions (**Figure 115**).

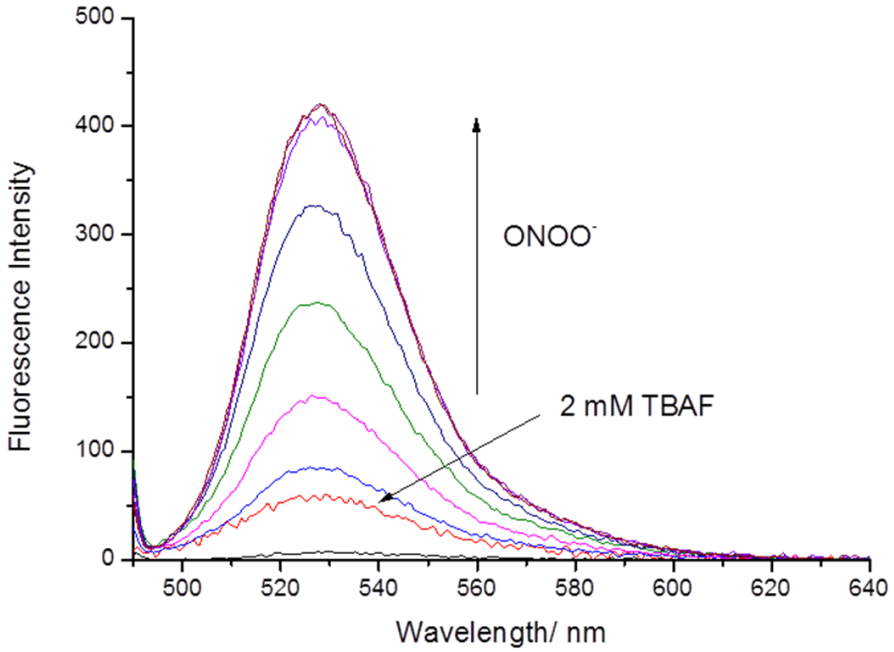

Figure 113 – Fluorescent spectra of sensor **90** (0.5 μM): (a) Sensor (black); (b) Sensor and TBAF (2 mM) (red); (c) Sensor and TBAF (2 mM) plus increasing amounts of ONOO- (0 – 600 μM). λ_{EX} = 480 nm (bandwidth 10 nm).

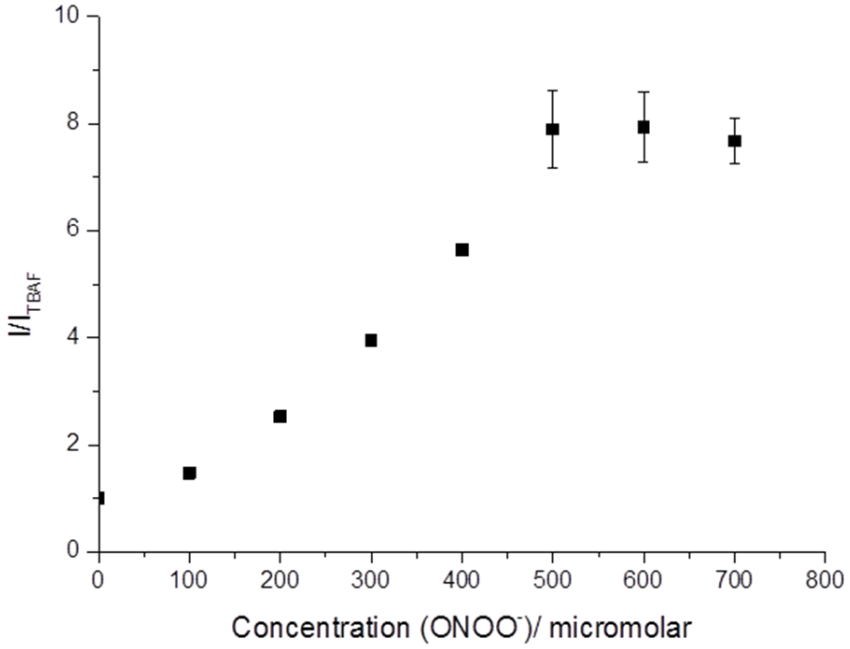

Figure 114 – Fluorescent intensity changes (I/I_0) of sensor **90** (0.5 μM) with addition of TBAF (2 mM) first and then addition of ONOO- (0 – 600 μM) in solution of THF. λ_{EX} = 480 nm (bandwidth 10 nm) and λem = 525 nm.

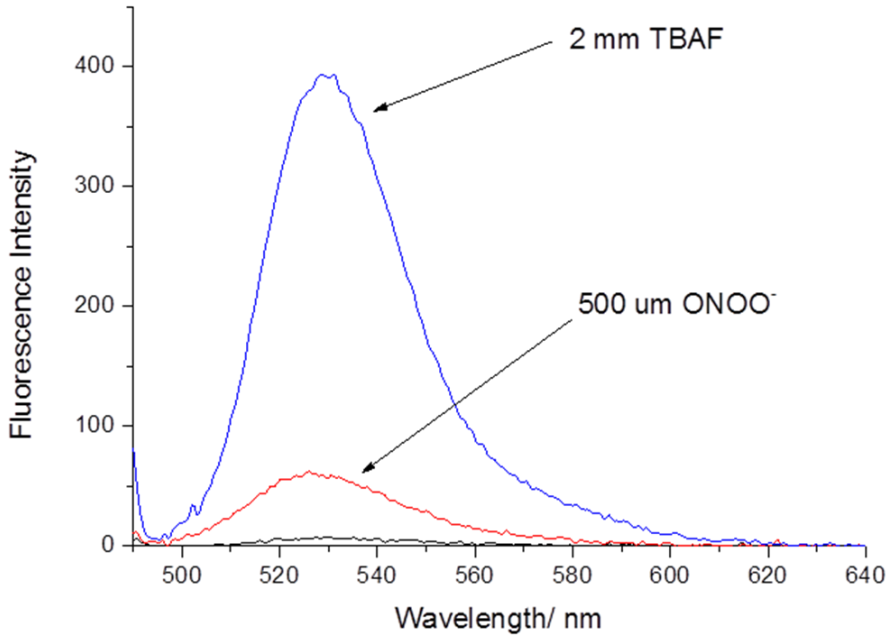

Figure 115 – Fluorescent spectra of sensor **90** (0.5 µM): (a) **90** (black); (b) **90** and $ONOO^-$ (500 µM) (red); (c) **90** and $ONOO^-$ (500 µM) and TBAF (2 mM) (blue). λ_{EX} = 480 nm (bandwidth 10 nm)

These analyses clearly revealed that **90** could be used as a dual sensing probe for the detection fluoride and peroxynitrite anions in organic solvent.

3.2.5 Conclusion and Future Work

Probe **90** was designed to be an $ONOO^-$ "AND" F^- probe that used the reactivity of the analytes to cleave receptor groups and yield and active fluorescein fluorophore. However, it was observed to be fluorescent in aqueous systems and had to be tested in an organic solvent. In THF **90** was observed to react only in the presence of both of the target analytes. A dose dependent increase in the fluorescence was observed after the incubation of the probe with TBAF and subsequent addition of $ONOO^-$.

However, due to the lack of applicability of the probe in biological systems, further analysis was halted. Modification of the probe to have a slightly less reactive F^- sensitive group could produce a usable probe; work into the development of such a probe is being undertaken in the group, including investigation into the cause of the fluorescence and possible AIE.

3.3 Fluorescein Hydrazone Based Probes for $ONOO^-$

3.3.1 Literature Precedent and Design

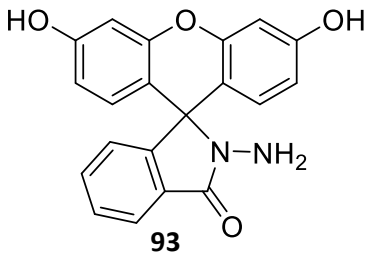

Figure 116 – Fluorescein hydrazone **93**.

Fluorescein-hydrazone **93** is a structural variant of fluorescein containing a hydrazine (NH_2-NH_2) group in place of the lactone oxygen group of fluorescein. This compound has sensitivity to copper (Cu) and structural variants have been shown to exhibit sensitivity towards chemical species, such as Hg^{2+} and HClO.[29-31] This type of hydrazide motif has also been used to develop several $ONOO^-$ probes.[32,33]

For example, Feng *et al.* developed a rhodamine like non-fluorescent spiro probe **94** which is oxidized by $ONOO^-$ to afford a fluorescent compound **95** with a large increase in fluorescence response.[33] Several other probes of this type have been developed to detect $ONOO^-$, however, the simplest form of the fluorescein-hydrazone (**93**) had only been tested against HClO and not against the more biologically relevant $ONOO^-$. Consequently, we decided to synthesize **93** and test it for reactivity towards $ONOO^-$, with the aim of further modifying its structure to introduce new sensing functionality as required.

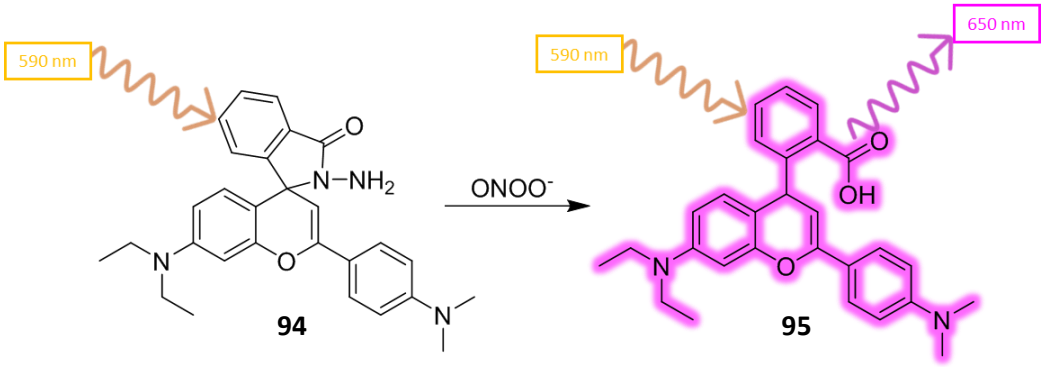

Figure 117 – Probe **94** reacting to form the fluorescent compound **95**.

3.3.2 Synthesis of Probe **93**

The synthesis of **93** was achieved by refluxing fluorescein **81** and hydrazine hydrate ($NH_2NH_2•H_2O$) in MeOH for twelve hours which gave the desired sensor in 93% yield.

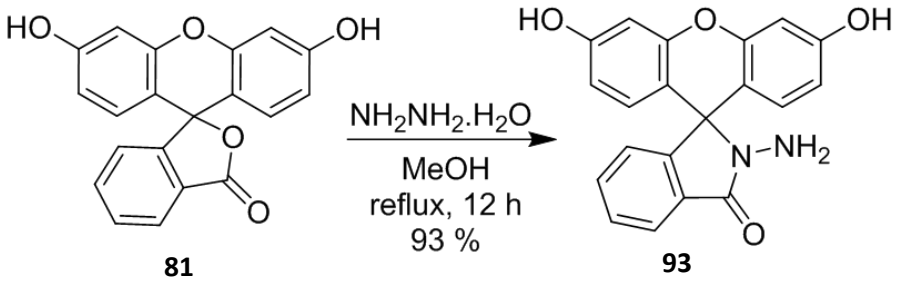

Scheme 6 – The synthesis of **93**.

3.3.3 Fluorescent analysis of sensor **93**

Initial studies into the fluorescent properties of **93** were determined by exposing it to known concentrations of $ONOO^-$ and HClO to compare their reactivities. **93** (10 µM) was dissolved in PBS buffer (pH 7.2) and exposed to increasing concentrations of $ONOO^-$ and HClO. These studies showed that **93** was reactive to both species but showed a significantly higher reactivity to $ONOO^-$ (**Figure 118**, **Figure 119**) over HClO (**Figure 120**, **Figure 121**), exhibiting a relative increase in intensity of ~560 fold compared to ~20 fold, respectively. Interestingly, the fluorescence maxima observed when **93** was reacted with $ONOO^-$ occurred at a slightly lower wavelength relative to when **93** was reacted with HClO. This indicates that a different structurally related product may be produced from each analyte, however further study into this phenomenon was not conducted. The reactivity differences between the two analytes can be attributed to the much higher nucleophilicity of $ONOO^-$ relative to $HClO/ClO^-$, which can be maximised by measuring the response of the sensor directly after addition of each analyte.

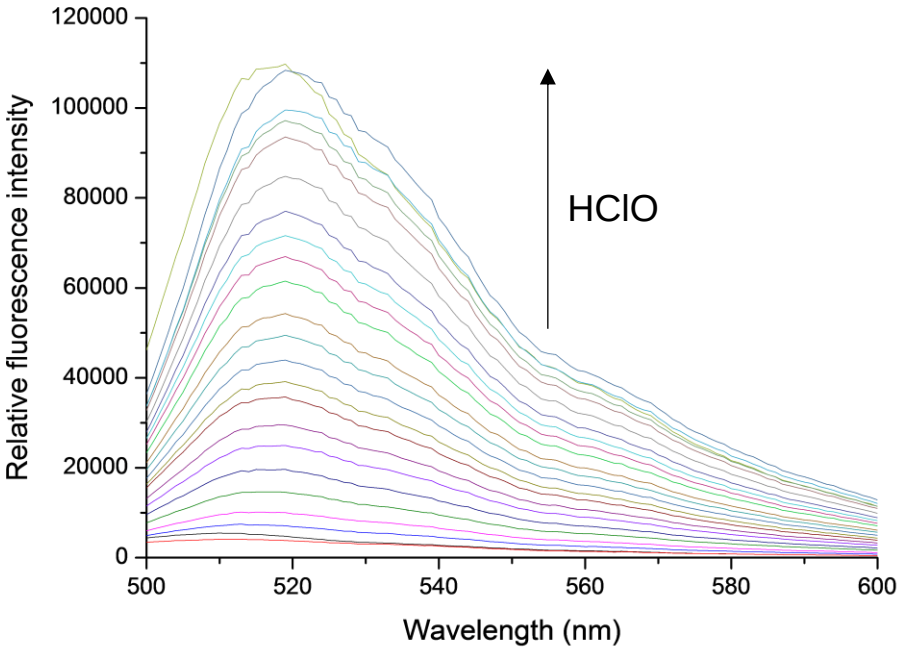

Figure 118 – Fluorescence spectra of **93** (10 μM) upon addition of HClO (0-400 μM) in PBS buffer (pH 7.4), λ_{ex} = 480 nm (bandwidth 10 nm).

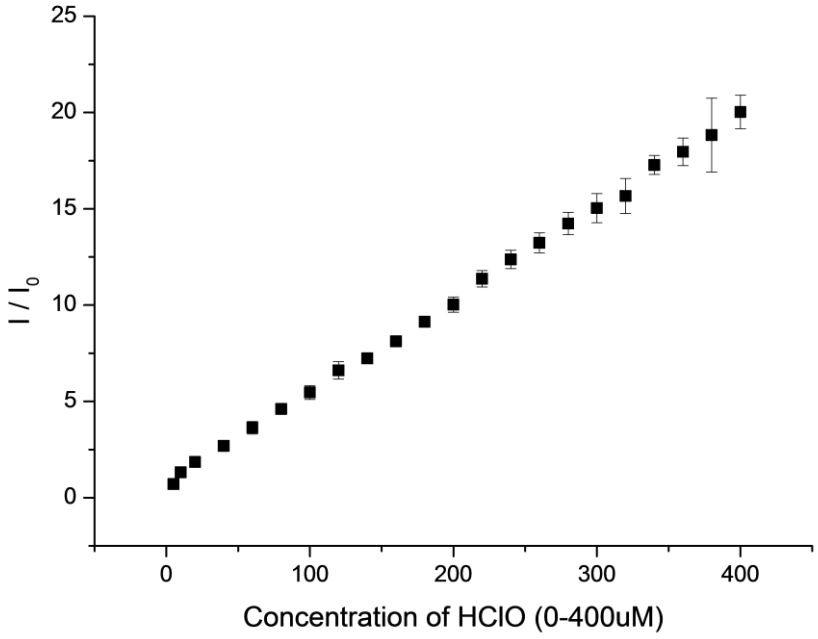

Figure 119 – Fluorescence intensity changes (I/I_{ONOO^-}) for **93** (10 μM) upon addition of HClO (0-400 μM) in PBS buffer (pH 7.4), λ_{ex} = 480 nm (bandwidth 10 nm), λ_{em} = 519 nm.

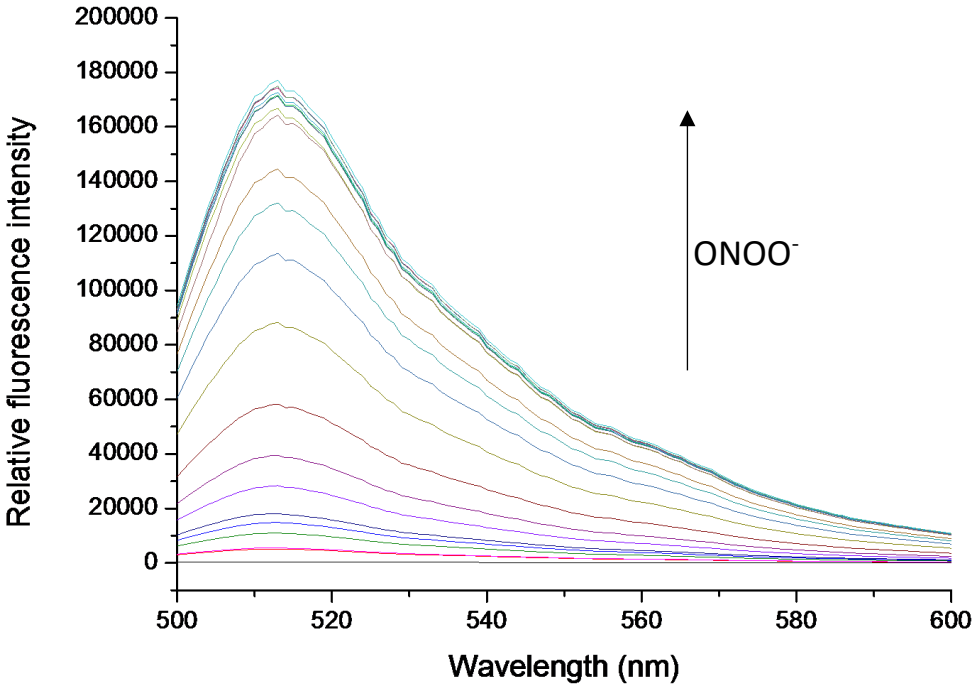

Figure 120 – Fluorescence spectra of **93** (10 μM) with addition of $ONOO^-$ (0-400 μM) in PBS buffer (pH 7.4), λ_{ex} = 480 nm (bandwidth 10 nm)

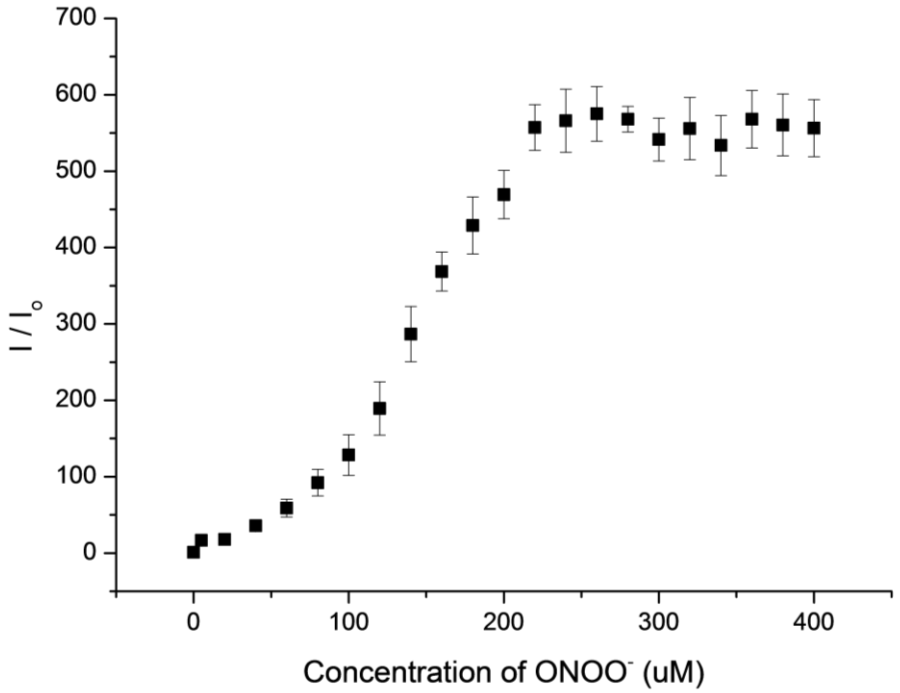

Figure 121 – Fluorescence intensity changes (I/I_{ONOO^-}) for **93** (10 μM) upon addition of HClO (0-400 μM) in PBS buffer (pH 7.4), λ_{ex} = 480 nm (bandwidth 10 nm), λ_{em} = 519 nm.

Next a selectivity study was carried out to test the reactivity of **93** against several other ROS/ RNS (**Figure 122** & **Figure 123**). This revealed that other ROS/ RNS species had a much lower response than either $ONOO^-$ or HClO, showing the selectivity of hydrazine reactive group.

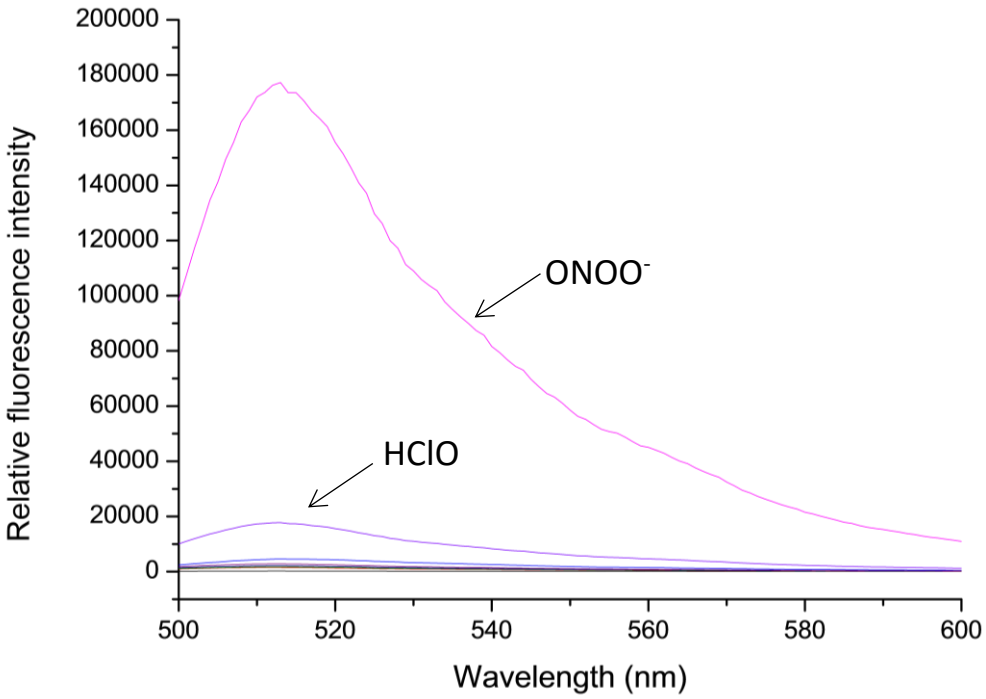

Figure 122 – Fluorescence spectra of **93** (10 µM) upon addition of $ONOO^-$ (500 µM), HClO (500 µM) and other ROS species (H_2O_2, •OH, O_2^- and $^1O_2$. In PBS buffer (pH 7.4), λ_{ex} = 480 nm (bandwidth 10 nm).

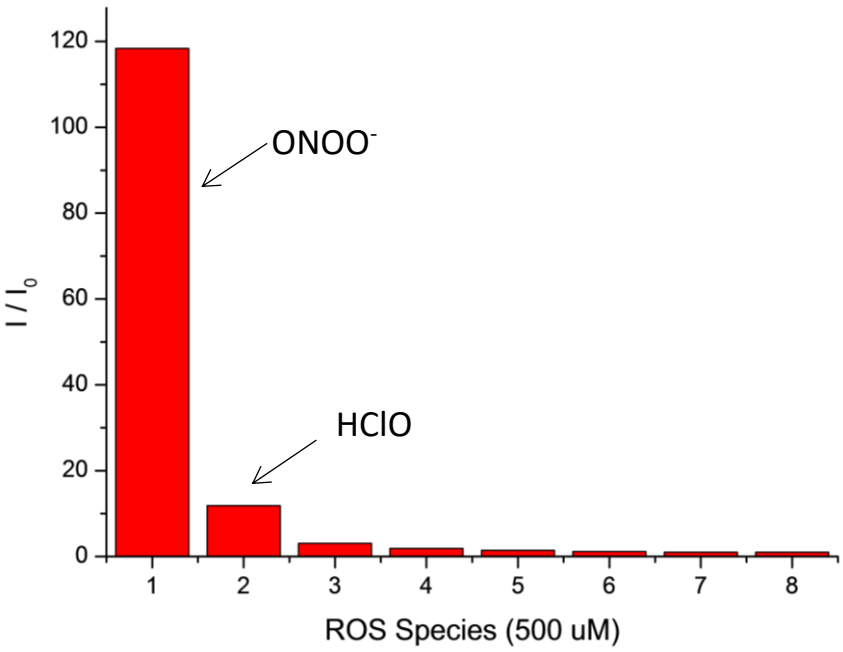

Figure 123 – Column chart for the selectivity of **93** (10 µM) against 1) RO•, 2) HClO, 3) H_2O_2, 4) $ONOO^-$, 5) •OH, 6) O_2^-, 7) $^1O_2$ (500 µM) and incubated for 30 mins. In PBS buffer (pH 7.4), λ_{ex} = 480 nm (bandwidth 10 nm), λ_{em} = 513 nm.

3.3.4 Additional Design and Synthesis of **96**

Having demonstrated that the hydrazine sensor **93** could be used to detect $ONOO^-$ and HClO, it was decided to carry out structural modifications to see if selectivity would change and whether we could add further sensitivity and develop an MLG for multi-analyte detection. This was achieved by reacting **93** with benzaldehyde in EtOH to form the hydrazinyl imine **96** in a good 89% yield (**Scheme 7**).

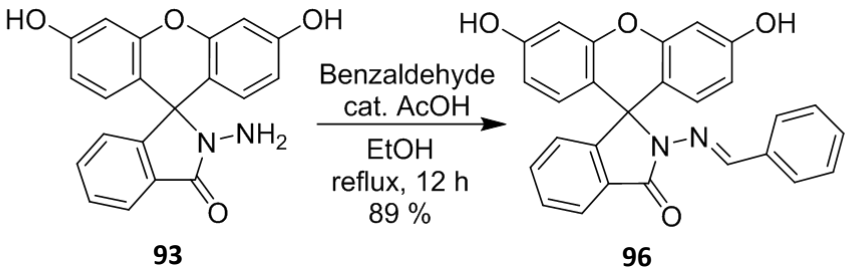

93 **96**

Scheme 7 – Synthesis of **96**

3.3.5 Fluorescence Analysis of **96**

The reactivity of imine sensor **96** towards $ONOO^-$ and HClO was then determined. **96** (10 µM) was monitored in the presence of increasing concentrations of $ONOO^-$ (**Figure 124** & **Figure 125**) and HClO (**Figure 126** & **Figure 127**) (0-220 µM), respectively. This

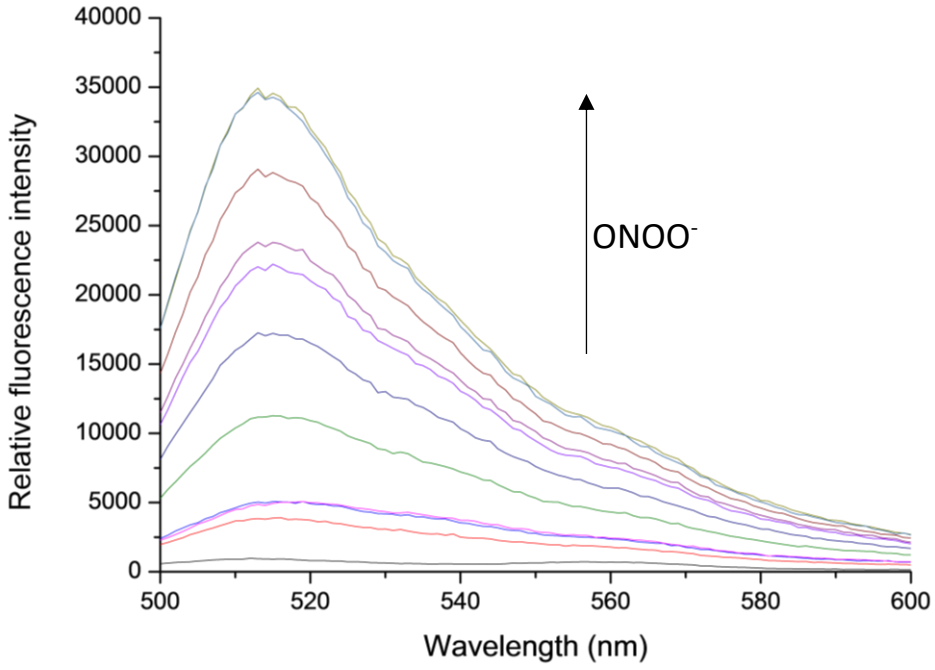

Figure 124 – Fluorescence spectra of **96** (10 µM) upon addition of $ONOO^-$ (0-220 µM) in PBS buffer (pH 7.4), λ_{ex} = 480 nm (bandwidth 10 nm).

revealed that **96** was also sensitive to both of these analytes, although it exhibited a lower fluorescent response towards ROS species than the parent hydrazine sensor **93**. **96** only had a ~40-fold increase in fluorescence towards $ONOO^-$, and a ~2-fold increase in fluorescence for HClO. This decrease in fluorescence intensity relative to **93** could be attributed to the intrinsically lower reactivity of the probe, due to the presence of its alkylated hydrazine group.

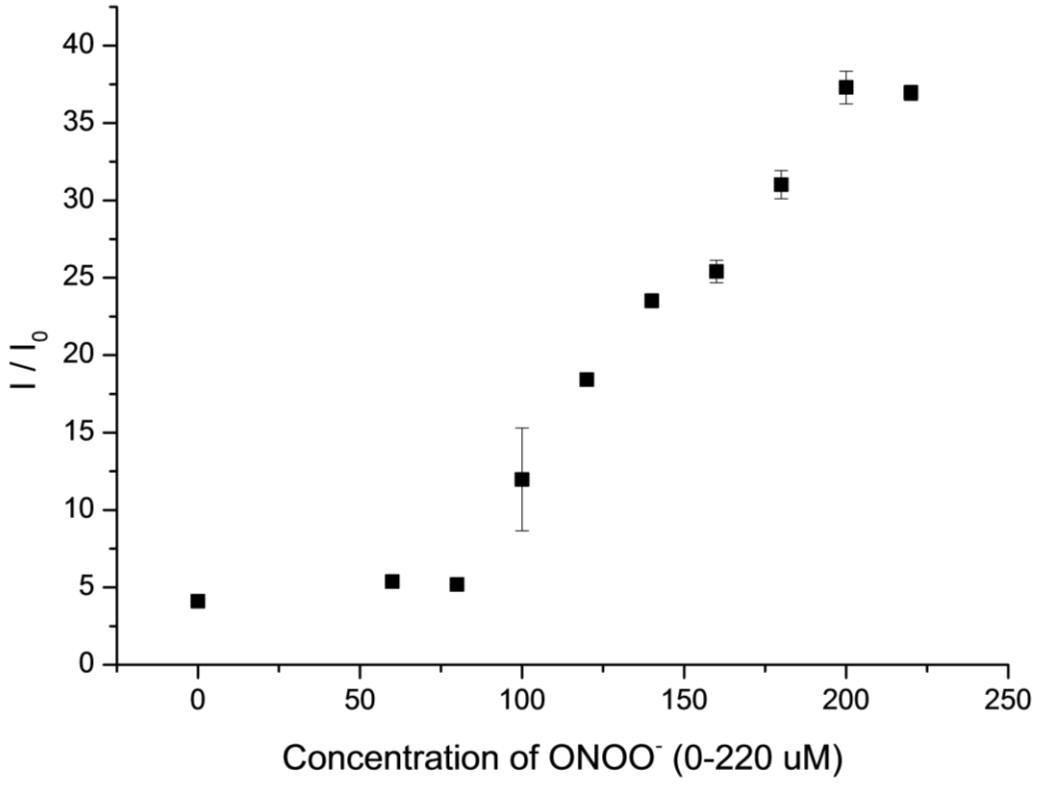

Figure 125 – Fluorescence intensity changes (I/I_{ONOO^-}) for **96** (10 µM) upon addition of $ONOO^-$ (0-220 µM) in PBS buffer (pH 7.4), λ_{ex} = 480 nm (bandwidth 10 nm), λ_{em} = 513 nm.

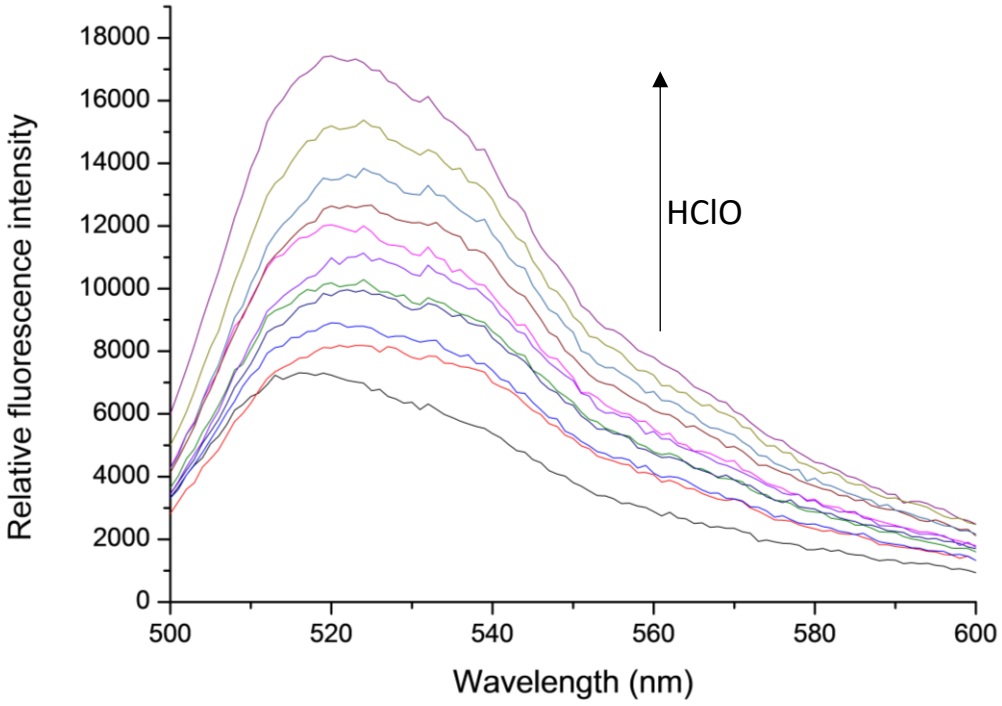

Figure 126 – Fluorescence spectra of **96** (10 μM) upon addition of HClO (0-220 μM) in PBS buffer (pH 7.4), λ_{ex} = 480 nm (bandwidth 10 nm).

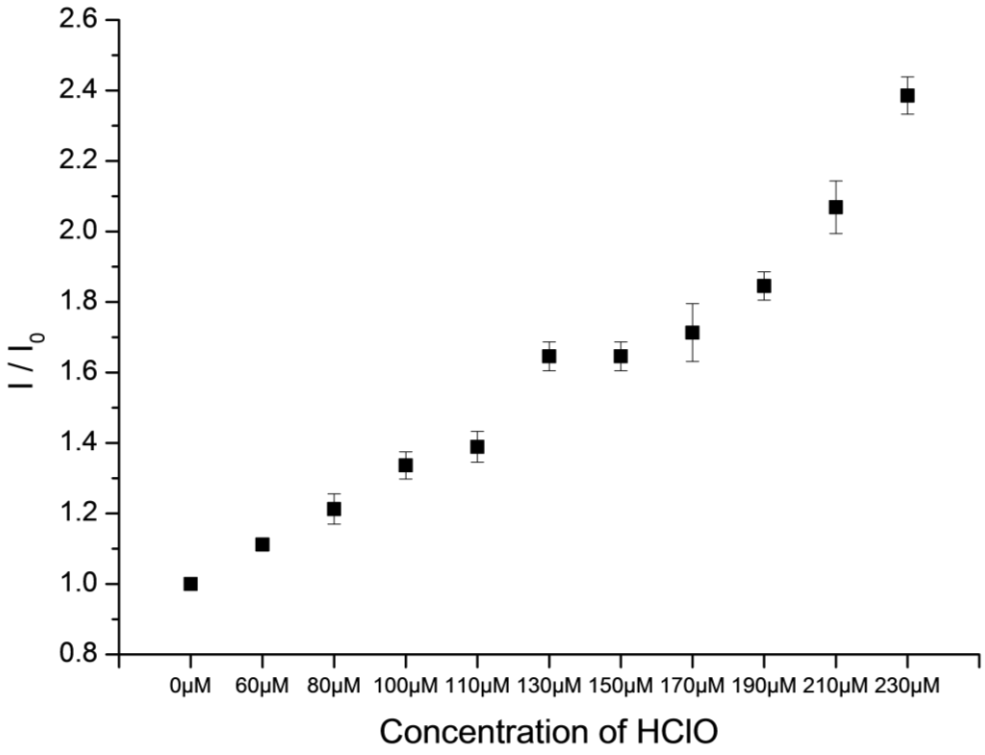

Figure 127 – Fluorescence intensity changes (I/I_{ONOO^-}) for **96** (10 μM) upon addition of HClO (0-220 μM) in PBS buffer (pH 7.4), λ_{ex} = 480 nm (bandwidth 10 nm), λ_{em} = 519 nm.

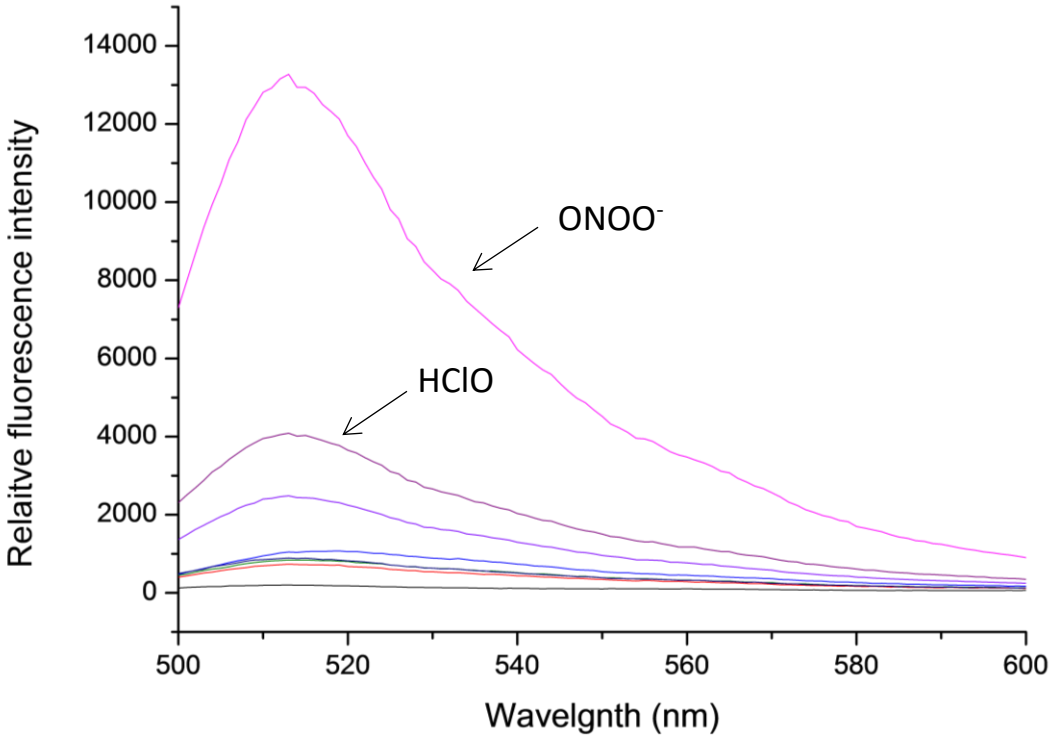

Figure 128 – Fluorescence spectra of **96** (10 µM) with addition of $ONOO^-$ (500 µM), HClO (500 µM) and other ROS species (500 µM). in PBS buffer (pH 7.4), λ_{ex} = 480 nm (bandwidth 10 nm).

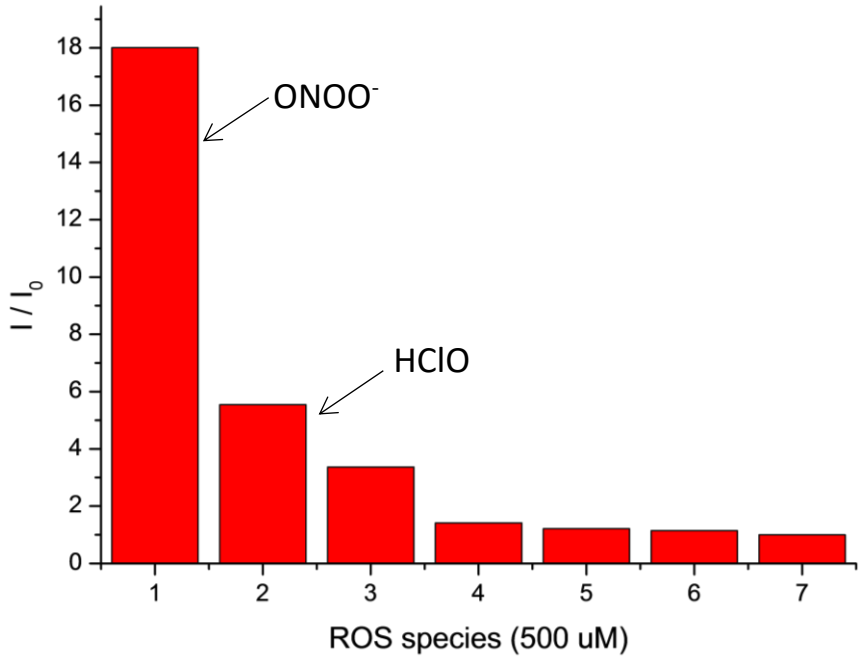

Figure 129 – Column chart for the relative selectivity of **96** (10 µM) against 1) RO•, 2) HClO, 3) H_2O_2, 4) $ONOO^-$, 5) •OH, 6) O_2^-, 7) $^1O_2$ (500 µM) and incubated for 30 mins. In PBS buffer (pH 7.4), λ_{ex} = 480 nm (bandwidth 10 nm), λ_{em} = 513 nm.

Selectivity studies were then conducted on **96** to test its selectivity to ROS/ RNS species. **96** (10 µM) was incubated with other ROS/ RNS species (500 µM) (**Figure 128**). These results confirmed that the benzyl appended **96** had a lower selectivity for $ONOO^-$ relative to other ROS species when compared to the original **93**. Selectivity can be more easily visualised in a column chart (**Figure 129**), showing the lower specificity relative to **93**, more easily and a higher level of fluorescence from the other ROS/ RNS.

3.3.6 Conclusion and future work

In this section, we have used the fluorescein hydrazine **93** to selectively detect $ONOO^-$ over other ROS/ RNS species, including HClO. In an attempt to potentially expand the use of this probe, a phenyl group was bound to the primary amine functionality to yield **96**. Fluorescence studies showed that although the same overall reactivity profile was retained, a lower fluorescence response was observed, with a lower selectivity for $ONOO^-$. Ideally, we would see an increase in each of these factors, selectivity and sensitivity, for the second iteration of a probe. However, the potential for adding secondary functionality on this probe, might compensate for the loss in each of these.

Work into the hydrazine functionality is ongoing, with the aim of developing an "AND" MLG for the dual detection of $ONOO^-$ and a second analyte, with the potential of adding a third reactive group for a triple analyte "AND" logic gate.

3.4 Dual $ONOO^-$ and Nitroreductase probe

3.4.1 Literature Precedent and Design of Probe **97**

$ONOO^-$, as discussed previously (**Section 1.5.4**), is an RNS that can be damaging in cellular environments and is found in numerous human diseases and so there is an urgent need to develop a sensitive probe to image it in cell systems.

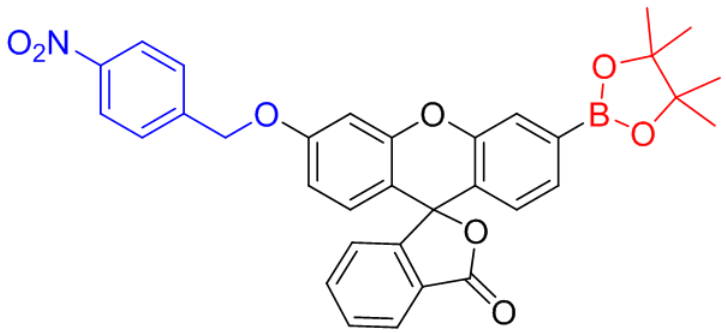

97

Figure 130 – Structure of **97**, with its B-pin group shown in red and its 4-nitrophenyl group shown in blue.

Nitroreductases (NTRs) are overexpressed in tumours, whose expression levels can be used to monitor the hypoxic state of their cells (**Section 2.4.1**), with several agents having been developed for their imaging.[34,35]

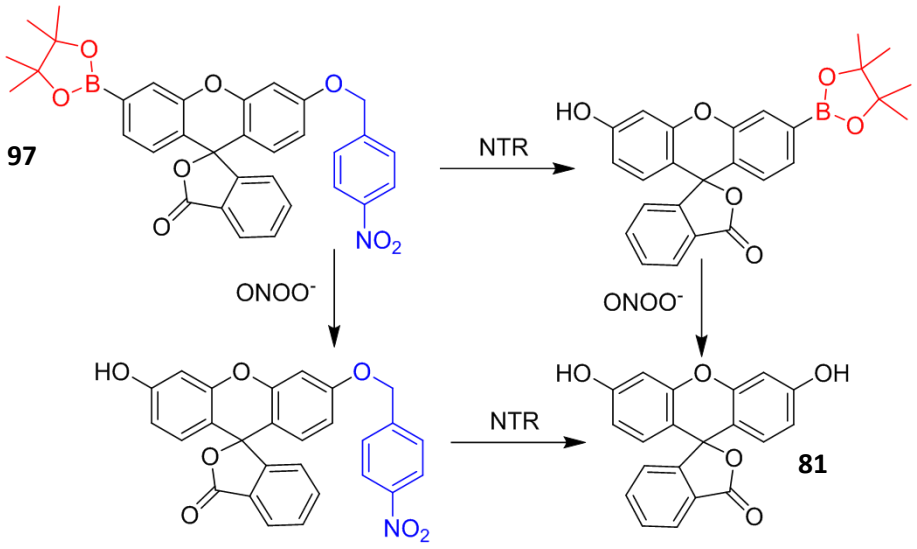

Figure 131 – Reaction of probe **97** with both analytes to yield fluorescein.

Similar to the design used for our previous fluorescein-based sensor (**Section 3.4**), we wanted to employ a dual analyte fluorophore design based on attaching $ONOO^-$ and NTR

sensitive receptor groups to a fluorescein core (**Figure 130**). This would be achieved by attaching a Bpin group to one of the xanthinic oxygen atoms and a 4-nitrophenyl group to its other aryl fragment. This should result in a dual analyte "AND" MLG for the detection of NTR and $ONOO^-$ with good solubility and photophysical properties (**Figure 131**).

3.4.2 Synthesis of Probe **97**

The synthesis of the new dual NTR and $ONOO^-$ probe **97** followed the synthesis of probe **90** (**Section 3.3.2**) until the last step, with 4-nitrobenzyl bromide used as an electrophile in place of 2,4-dinitrobenzylsulfonly chloride. Therefore, the Bpin compound **92** was coupled with 4-nitrobenzyl bromide and K_2CO_3 in acetonitrile (MeCN) at 0 °C to afford the desired final compound **97** in 68% yield (**Scheme 8**).

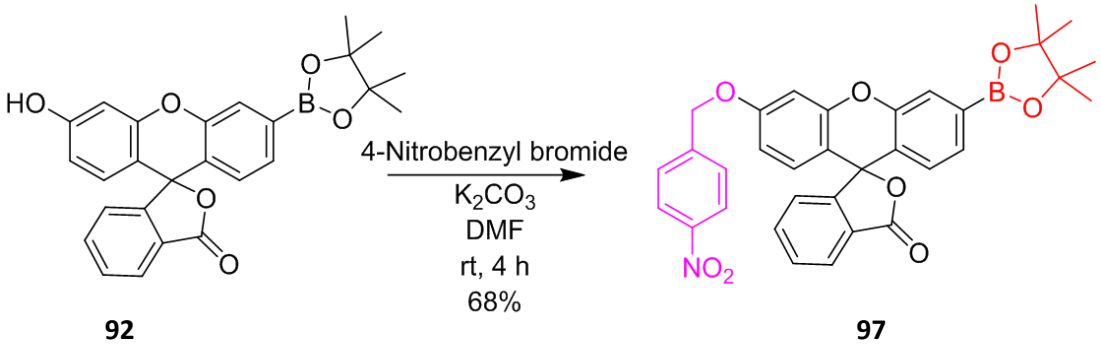

92 **97**

Scheme 8 – Synthesis of dual NTR and $ONOO^-$ probe **97**

3.4.3 Fluorescent properties of probe **97**

The successful synthesis and characterisation of **97** allowed for initial fluorescence analysis of the probe to be undertaken. Singh *et al. previously* developed a dual analyte hypoxia and NO fluorescent probe which employed sodium dithionite ($Na_2S_2O_4$) (**Section 2.4**) as a surrogate reducing agent for NTR to reduce the nitro group to its corresponding amino group.[36] Hence, it was decided to use $Na_2S_2O_4$ as a trigger to reduce the nitro group (instead of NTR + NADPH) of the probe in the presence of $ONOO^-$, before sending it to our collaborators for full studies using NTR and NADPH as a reducing mixture.

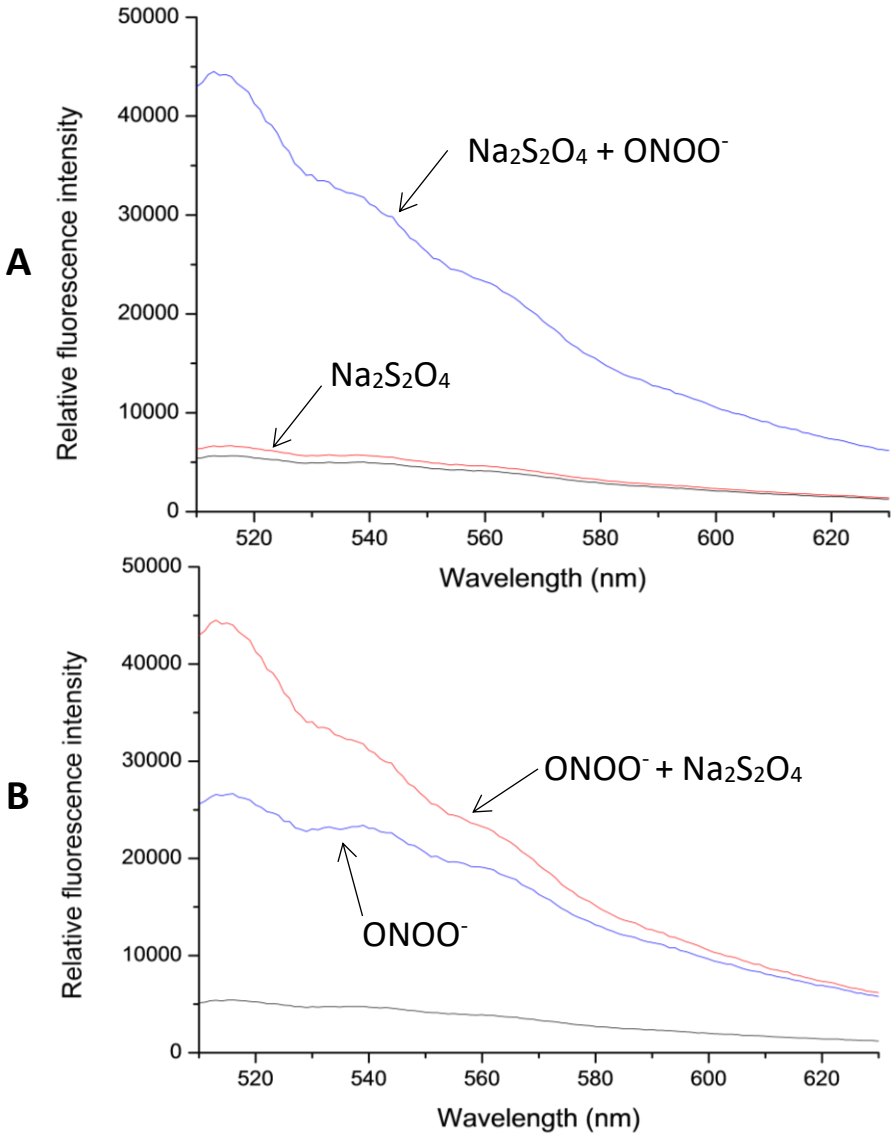

Figure 132 – Fluorescence spectra of **97** (10 µM) with A) $Na_2S_2O_4$ (200 µM) 20-minute incubation – orange; $Na_2S_2O_4$ (200 µM) + $ONOO^-$ (20 µM) – blue. B) $ONOO^-$ (20 µM) – blue; $ONOO^-$ (20 µM) + $Na_2S_2O_4$ (200 µM) 20-min incubation – orange. Buffer PBS (pH 7.4), λ_{EX} 485 nm (bandwidth 10 nm).

97 (10 µM) was exposed first to $Na_2S_2O_4$ (100 µM) followed by $ONOO^-$ (20 µM) and in the reverse order of this. Measurements were taken immediately after the addition of $ONOO^-$ and 20-minute incubation with the $Na_2S_2O_4$ was allowed for the reduction of the nitro-group.

In the first experiment $Na_2S_2O_4$ was first added, which only resulted in a small increase in fluorescence (**Figure 132**, **A**). Subsequent addition of $ONOO^-$ resulted in a large increase in fluorescence, indicating that the probe was behaving as envisaged. However, upon reversal of the addition of the analytes (**Figure 132**, **B**) a large response was seen on initial addition of $ONOO^-$, with subsequent addition of $Na_2S_2O_4$ affording a further increase in fluorescence, but not as large as expected. These results were best visualized in the column charts, with **97** working as expected in the first experiment (**Figure 133**, **A**) with a negligible increase from addition of the first analyte ($Na_2S_2O_4$), followed by fluorescence 'turn-on' on addition of the second analyte ($ONOO^-$).

However, the second experiment (**Figure 133**, **B**), reveals a large increase (~5-fold) addition of the first analyte ($ONOO^-$) and a further increase (~3-fold) on addition of the second analyte ($Na_2S_2O_4$). This behaviour was not ideal as the turn-on behaviour of **97** is essentially lost in the presence of $ONOO^-$, regardless of whether $Na_2S_2O_4$ is present. Nevertheless, this probe has been sent to Dr Robert Elmes (Maynooth University) to determine its fluorescent response using NTR (and NADPH cofactor) as a reducing agent for its nitro group in assay and cellular systems.

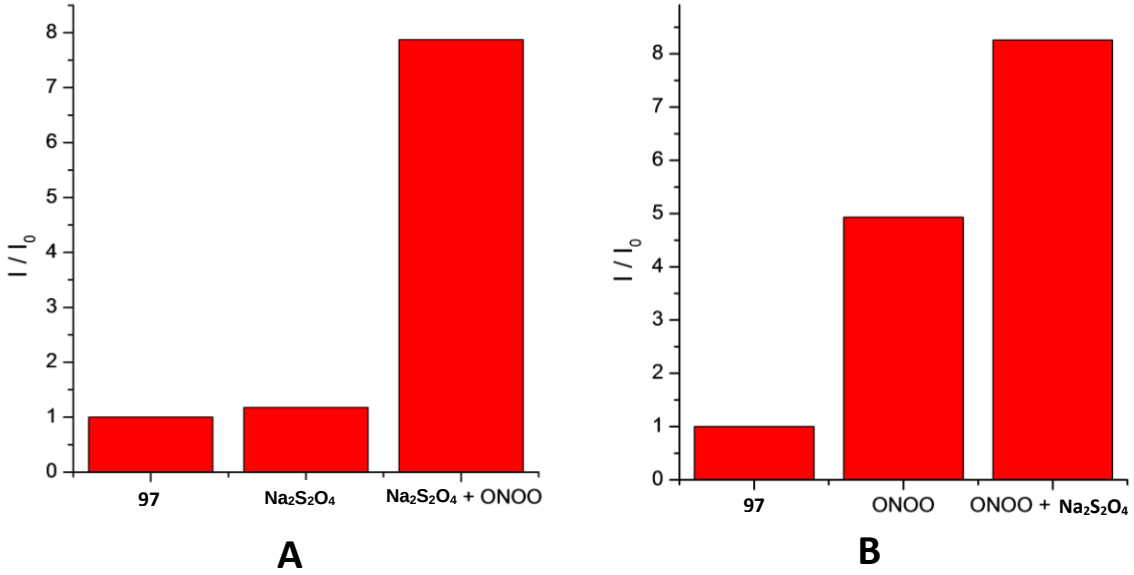

Figure 133 – Column chart of the fluorescence intensities (I/I_0) of **97** (10 µM) with A) $Na_2S_2O_4$ (200 µM) 20-minute incubation, $Na_2S_2O_4$ (200 µM) + $ONOO^-$ (20 µM). B) $ONOO^-$ (20 µM), $ONOO^-$ (20 µM) + $Na_2S_2O_4$ (200 µM) 20-minute incubation. Buffer PBS (pH 7.4), λ_{EX} 485 nm (bandwidth 10 nm), λ_{EX} 516 nm.

3.5 Dual analyte probe for Glutathione and $ONOO^-$

3.5.1 Literature precedent

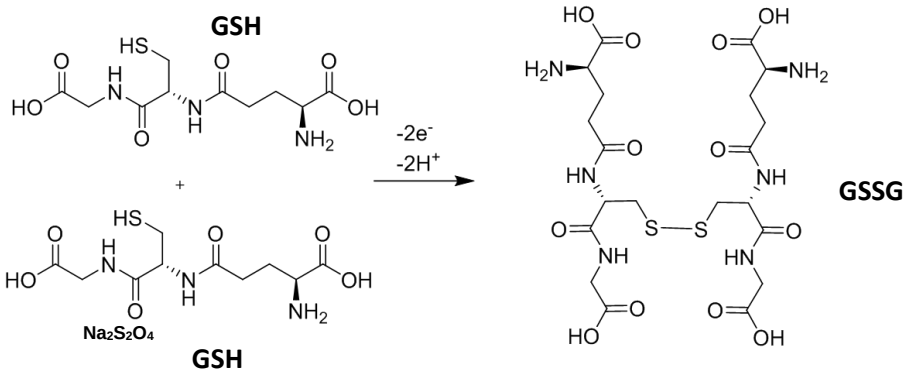

Figure 134 – GSH oxidised to GSSG.

Glutathione (GSH) is a tripeptide that occurs as a naturally occurring anti-oxidant at relatively high concentrations in a wide range of organisms, introduced earlier (**Section 2.5.1**).

GSH acts as an electron donor to reduce other potentially toxic biological compounds that may be formed within the cell (**Figure 134**), which results in GSH being oxidised glutathione disulphide (GSSG). Dysregulation of GSH levels in the body have been implicated in the etiology / progression of several human diseases, as such a number of probes have been developed for its detection, with varying levels of selectivity being achieved. These have been discussed previously (**Section 2.5.1**).

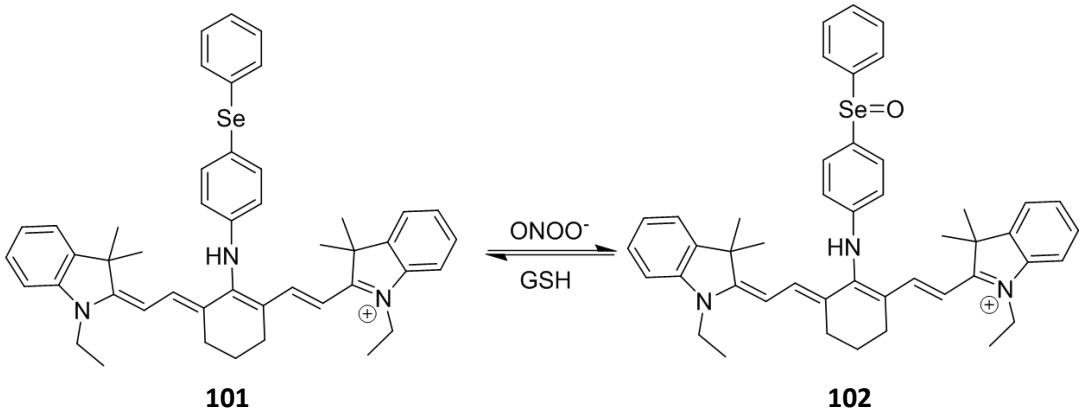

Figure 135 – Diagram of Se based OFF-ON-OFF probe **101** reacting with $ONOO^-$ to form **102** and GSH to react it back.

The harmful effects of $ONOO^-$ have been discussed in detail previously (**Section 1.5.3.7**), with GSH offering some protection against its oxidising effects in cellular systems. The balance between $ONOO^-$ and GSH can become unequal in diseased states, so a sensor that could be used to reveal the relationship that exists between them could afford a valuable insight into important mechanisms that underpin different disease states.

Only a few fluorescent probes exist that enable the detection of both species, with one example being developed by Han *et al.*, in an OFF-ON-OFF sensor that reversibly detects the presence of both species (**Figure 135**). Reaction with $ONOO^-$ first oxidises the selenium-based probe **101** to 'turn-on' its fluorescence in **102**, with GSH then serving to reducing the sensor to turn its fluorescence back off. This probe and others like it, allow for monitoring of the relative level of $ONOO^-$ and GHS over time, however, no AND probe that allowed the simultaneous quantification of both reactive species had been reported.

3.5.2 Design and Synthesis of Probe **103**

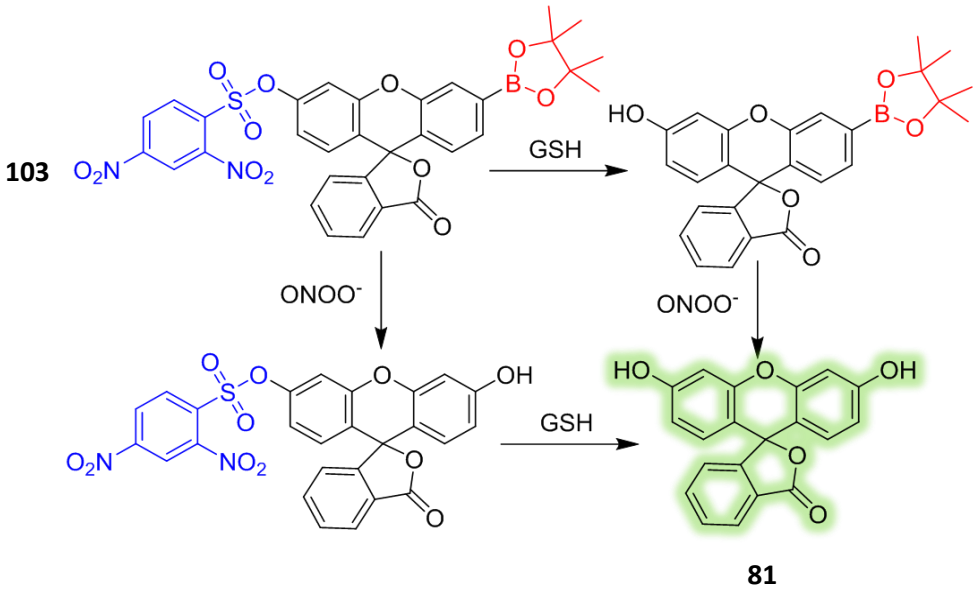

Figure 136 – Dual analyte probe **103** incorporating a boronic acid pinacol ester group (red) for the detection of $ONOO^-$ and a 2,4-dinitrobenzenesulfonyl group (blue) for detection of GSH.

We wished to develop a dual analyte sensor **103** based on a core fluorescein unit appended with a Bpin moiety as a reactive targeting group for $ONOO^-$ and 2,4-DNBS as a targeting group for GSH (**Figure 136**). The late stage Bpin intermediate **92** previously used to prepare the previous fluorescein sensor (see **Section 3.3**) was functionalised by treatment with 2,4-dinitrobenzenesulfonyl chloride in the presence of K_2CO_3 to produce the final probe **103** in 53 % yield.

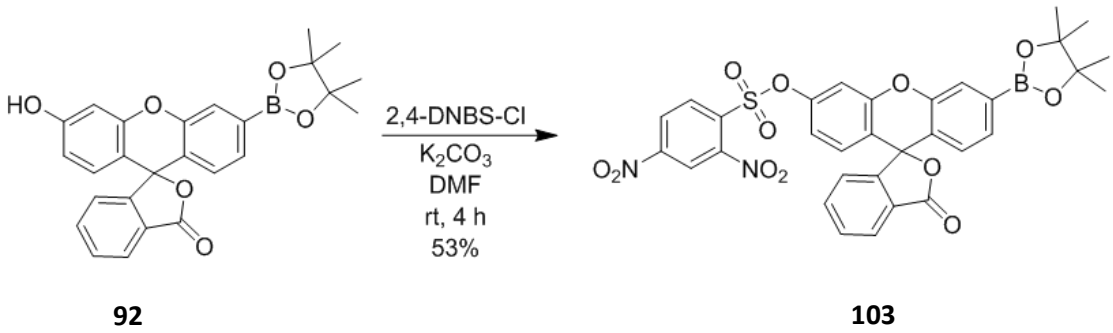

Scheme 9 – Synthesis of **103**.

3.5.3 Fluorescence Analysis of Probe **103**

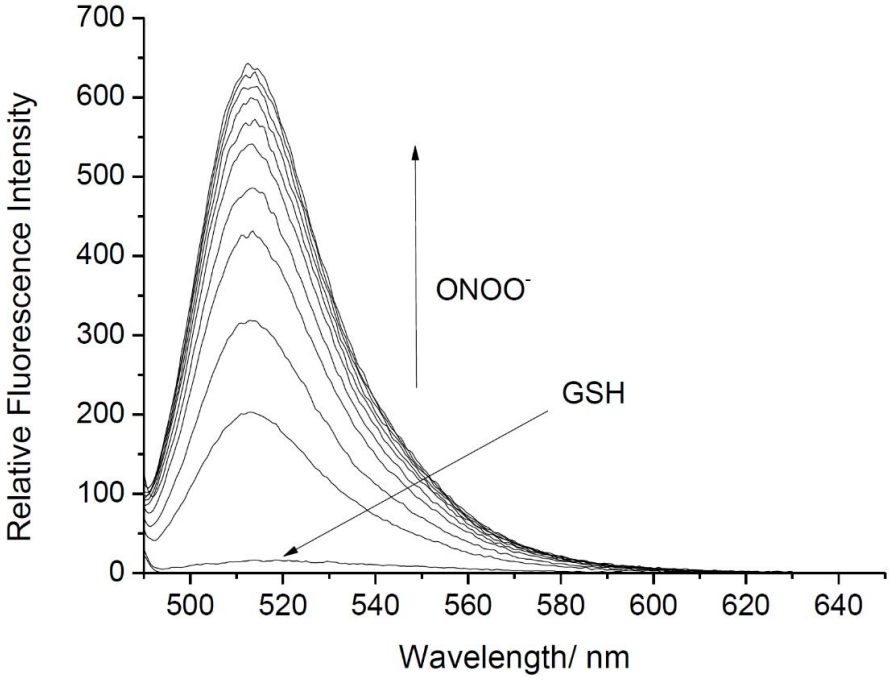

Figure 137 – Fluorescence spectra of **103** (0.5 µM) in the presence of GSH (200 µM) followed by subsequent addition of $ONOO^-$ (0-10 µM) in buffer (52 wt. % MeOH, pH 8.21 at 25 °C). Fluorescence intensities measured at λ_{ex} = 488 nm, slit widths ex = 5 nm and em= 2.5 nm.

The sensor **103** was dissolved in DMSO and diluted into a buffer solution (52 wt. % MeOH, pH 8.21 at 25 °C) which showed very negligible fluorescence. In the first test, GSH was added which caused a 10-fold increase in fluorescence, with subsequent addition of $ONOO^-$ resulting in cleavage of the B-pin group which triggered a further large (~650-fold) increase in fluorescence (**Figure 137** & **Figure 138**). These results confirmed that the 'turn on' of the probe **103** by both $ONOO^-$ and GSH was required for a large increase in fluorescence to occur. Reversal of the addition sequence of the analytes was then investigated, with the probe providing a negligible turn on when exposed to $ONOO^-$ and subsequent addition of GSH resulting in a ~700-fold increase in fluorescence (**Figure 139**). A linear relationship was observed between **103** incubated with the first analyte and the addition of the second analyte (**Figure 140**). A tailing off of the increases is seen at higher concentrations.

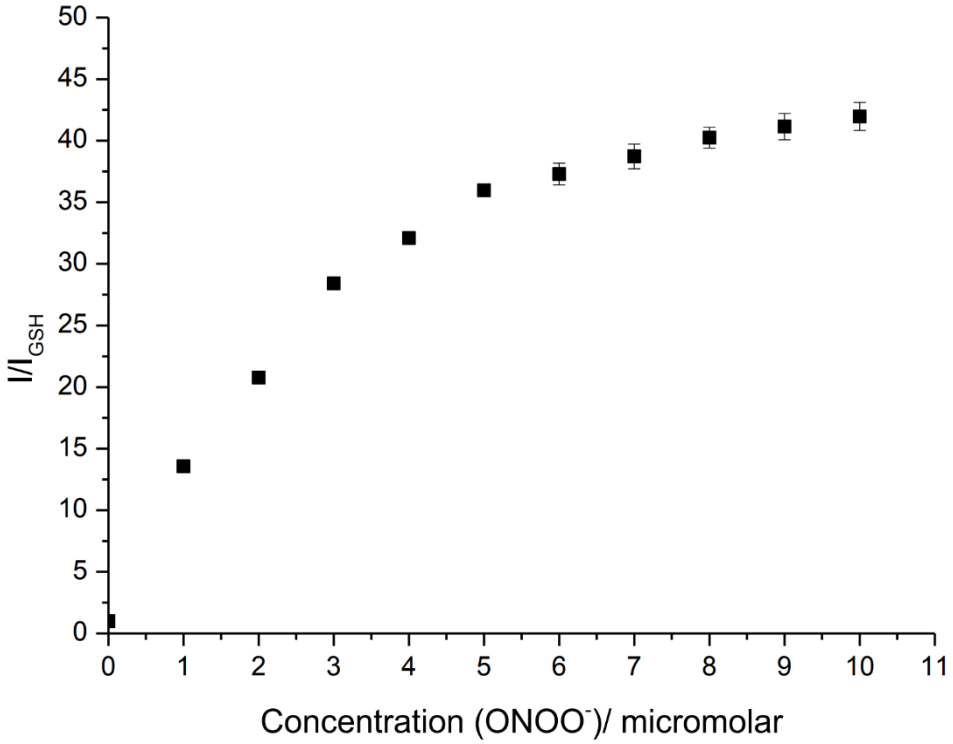

Figure 138 – Fluorescence intensity changes (I/I_{GSH}) for **103** (0.5 µM) with addition of GSH (200 µM) followed by the addition of $ONOO^-$ (0 - 10 µM), in buffer solution (52 wt. % MeOH, pH = 8.21 at 25 °C). Fluorescence intensities were measured with λ_{ex} = 488 nm/ λ_{em} = 512 nm, slit widths ex = 5 nm and em= 2.5 nm.

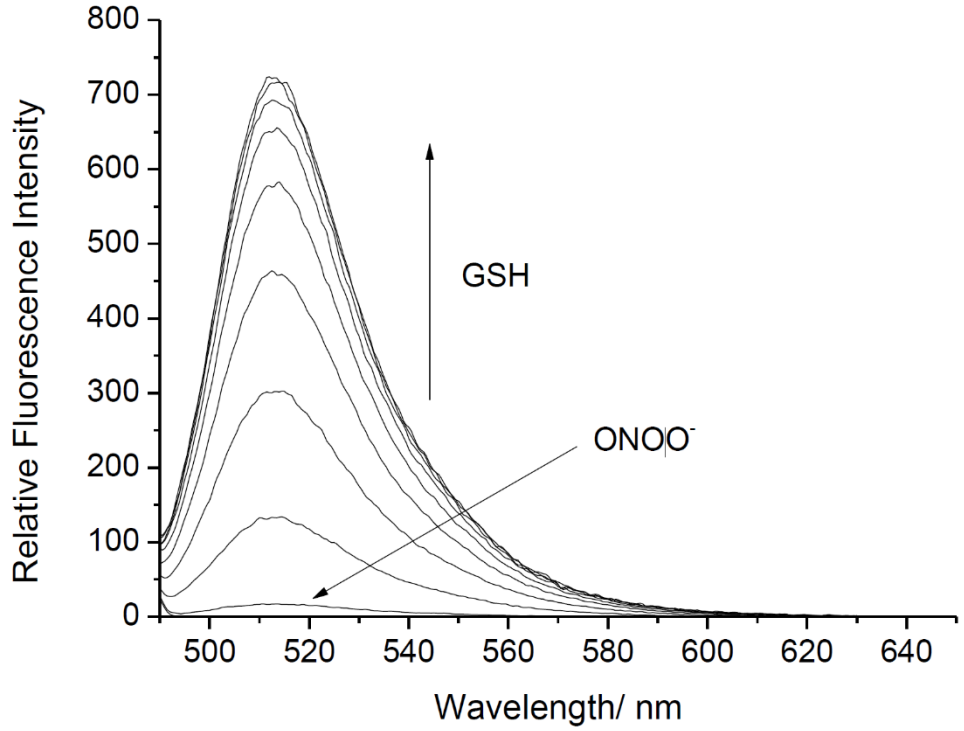

Figure 139 – Fluorescence spectra of **103** (0.5 µM) with addition of $ONOO^-$ (10 µM) then subsequent addition of GSH (0-80 µM) in buffer (52 wt. % MeOH, pH 8.21 at 25 °C). Fluorescence intensities were measured with λ_{ex} = 488 nm with, slit widths ex = 5 nm and em= 2.5 nm.

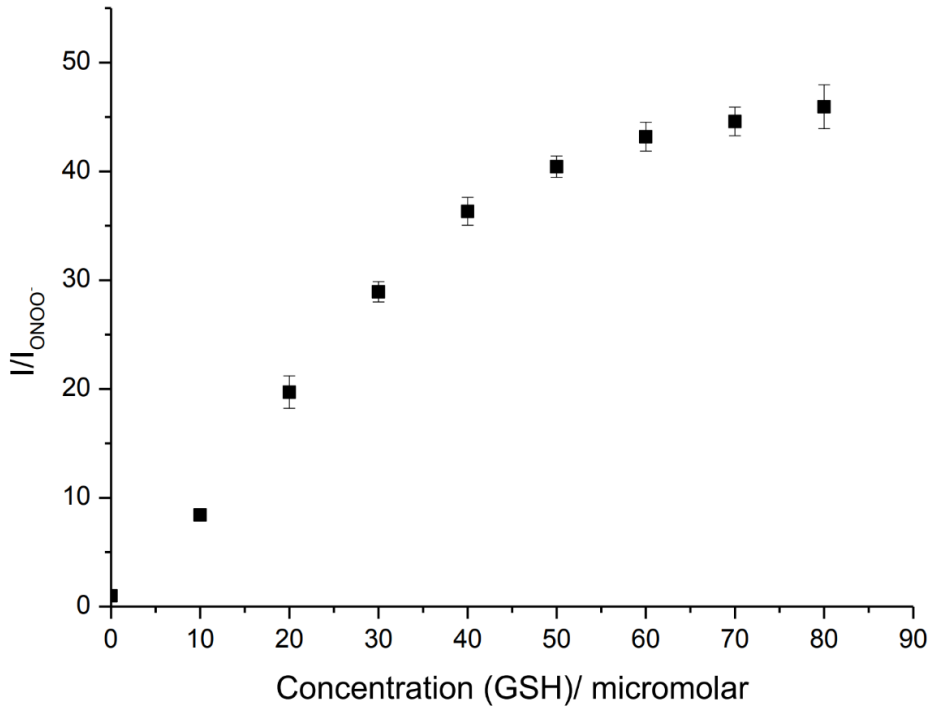

Figure 140 – Fluorescence intensity changes (I/I_{ONOO^-}) for **103** (0.5 µM) in the presence of $ONOO^-$ (10 µM) followed by addition of GSH (0 - 80 µM) in buffer solution (52 wt. % MeOH, pH = 8.21 at 25 °C). Fluorescence intensities measured at λ_{ex} = 488 nm/ λ_{em} = 512 nm, slit widths ex = 5 nm and em= 2.5 nm.

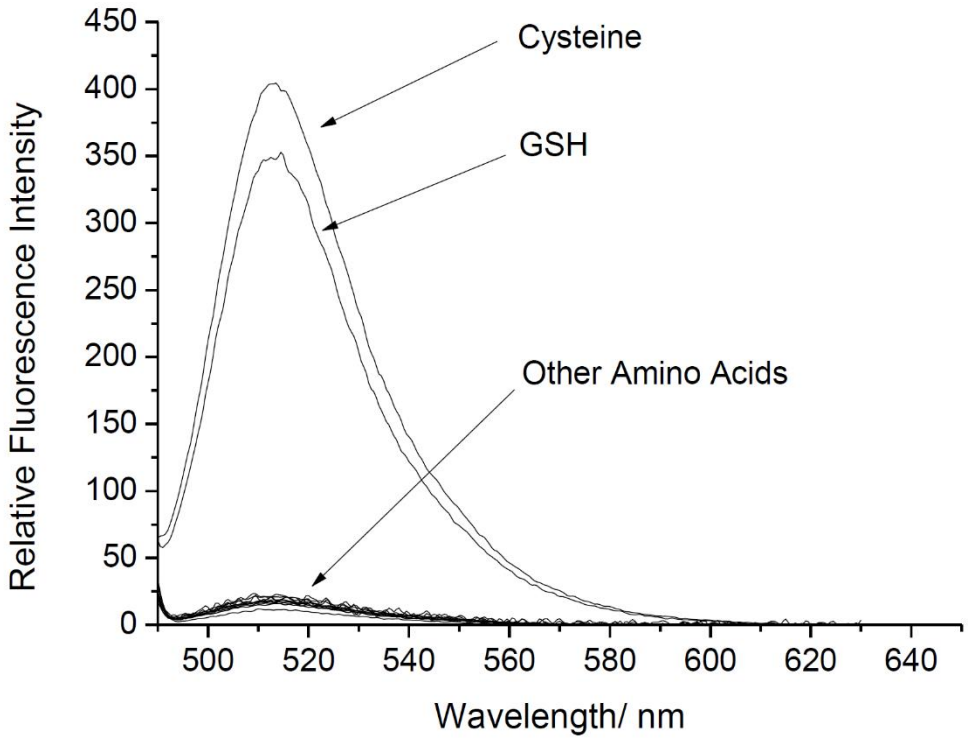

Figure 141 – Fluorescence spectra of **103** (0.5 µM) and $ONOO^-$ (10 µM) in the presence of GSH and other amino acids (100 µM) after 5 min incubation. Buffer solution (52 wt. % MeOH, pH = 8.21 at 25 °C). Fluorescence intensities measured at λ_{ex} = 488 nm/ λ_{em} = 512 nm, slit widths ex = 5 nm and em= 2.5 nm.

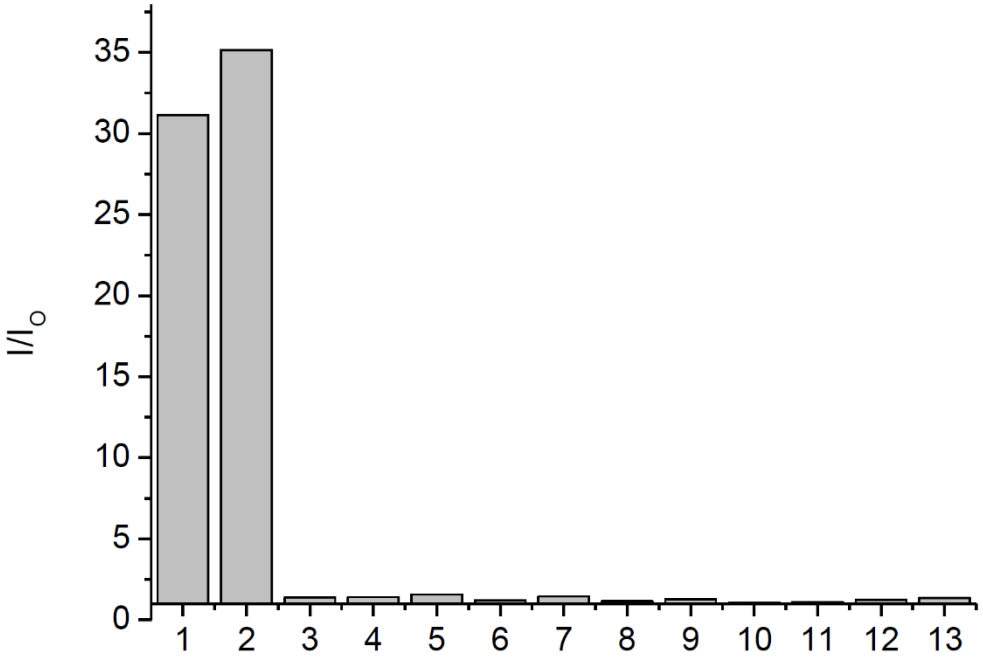

Figure 142 – Fluorescent response of **103** (0.5 µM) $ONOO^-$ (10 µM) in the presence of 100 µM amino acid solution (1- GSH, 2 – Cys, 3 – Met, 4 – Tryp, 5 – Ser, 6 – Lys, 7 – Leu, 8 – Glu, 9 – Val, 10 – Arg, 11 – His, 12 – Asp, 13 – Blank). Buffer solution (52 wt. % MeOH), pH = 8.21 at 25 °C. Fluorescence intensities measured at λ_{ex} = 488 nm/ λ_{em} = 512 nm, slit widths ex = 5 nm and em= 2.5 nm.

Since fluorescence studies had shown that the probe only gave a substantial response in the presence of both $ONOO^-$ and GSH analytes, the selectivity of the sensor over cysteine and other α-amino acids that are present in the cell were investigated. Cysteine gave a positive result, resulting in a similar increase in fluorescent response in the presence of $ONOO^-$ observed for GSH, with other amino acids resulting in a negligible increase in fluorescence (**Figure 141**). A column chart can visualise the results easily (**Figure 142**). However, the biological levels of GSH (1-10 mM) are far larger than that of Cys (30-200 µM) which would minimise the off-target activation of the probe.

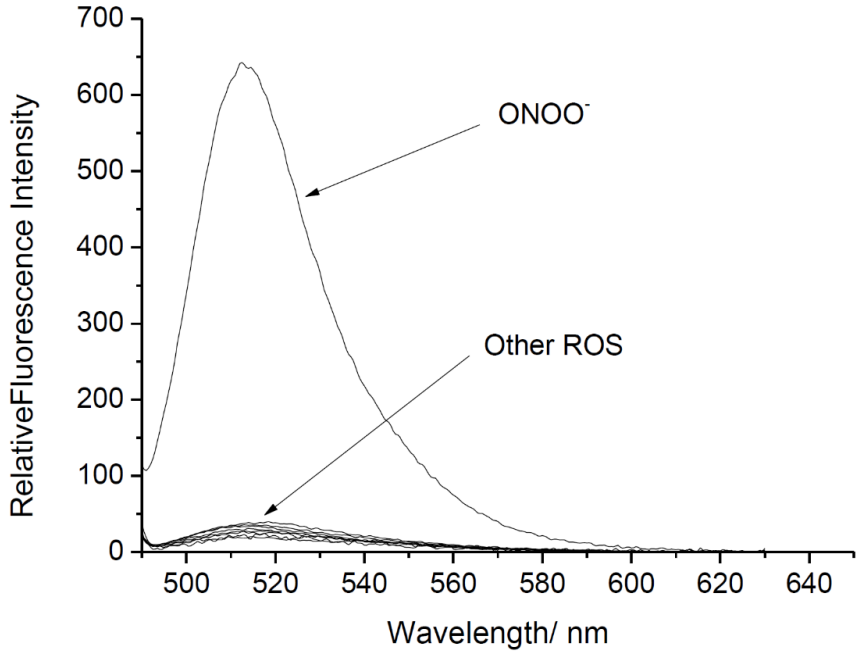

Figure 143 – Fluorescence spectra of **103** (0.5 μM) and GSH (200 μM) in the presence of $ONOO^-$ (10 μM) and other ROS / RNS (100 μM). Buffer solution (52 wt. % MeOH), pH = 8.21 at 25 °C. Fluorescence intensities measured at λ_{ex} = 488 nm/ λ_{em} = 512 nm, slit widths ex = 5 nm and em= 2.5 nm.

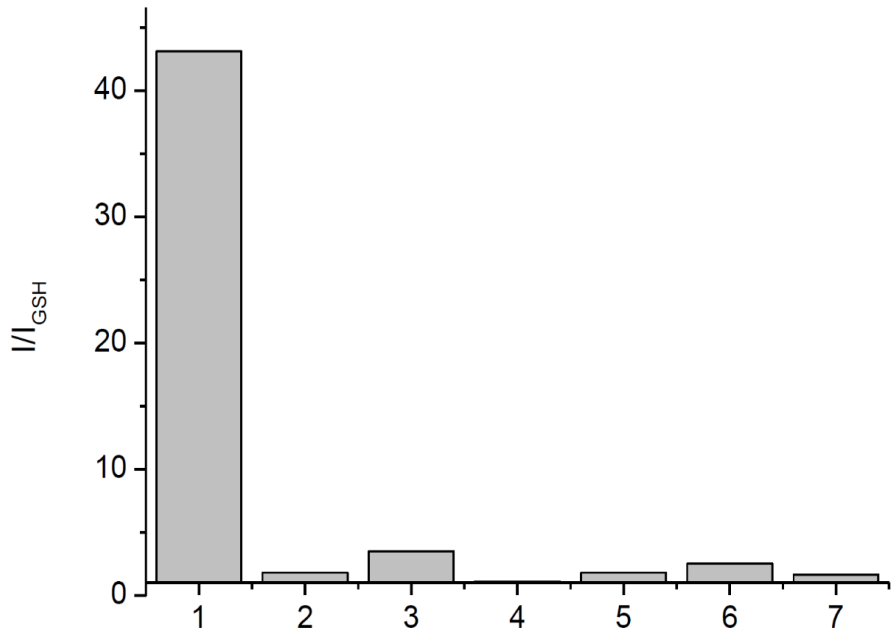

Figure 144 – Fluorescence spectra of **103** (0.5 μM) and GSH (200 μM) in the presence of $ONOO^-$ (10 μM) and other ROS / RNS species (100 μM): 1 – $ONOO^-$ (10 μM), 2 – H_2O_2, 3 – ClO^-, 4 – KO_2, 5 – $^1O_2$, 6 – $HO^\bullet$, 7 – $ROO^\bullet$. Buffer solution (52 wt. % MeOH), pH = 8.21 at 25 °C. Fluorescence intensities were measured with λ_{ex} = 488 nm/ λ_{em} = 512 nm, slit widths ex = 5 nm and em= 2.5 nm.

We then investigated the selectivity of the sensor **103** towards other ROS/ RNS (H_2O_2, ClO^-, KO_2, $^1O_2$, $HO^\bullet$, $ROO^\bullet$), which revealed that a 'turn-on' fluorescent response for this probe was only observed for $ONOO^-$ (**Figure 143**). Column chart of these results show this clearly (**Figure 144**).

Therefore, it was reasoned that this sensor should be capable of detecting GSH and peroxynitrite in levels in cellular systems with no interference from cysteine, or other biologically relevant ROS/RNS.

The "red-ox" cycle that both $ONOO^-$ and GSH have vital roles in, is perturbed in several diseases, including cancers (skin, kidney, breast), neurological diseases and ageing. A probe that could detect the levels of these analytes could possibly be used for an early diagnosis tool as well as a tool for the investigation between the two species.

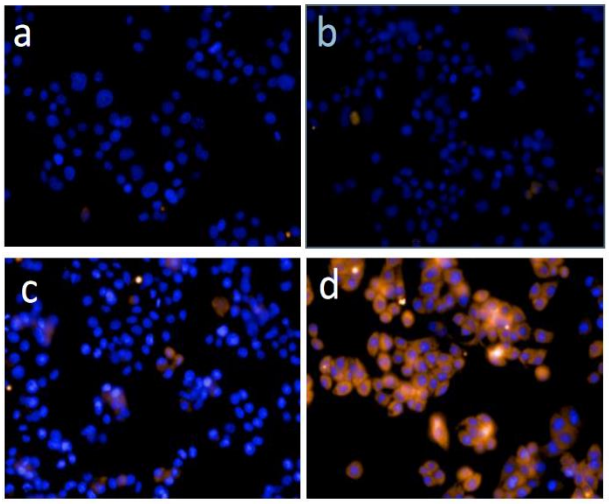

Figure 145 – a) Hep-G2 cells incubated with **103** (10 µM, 30 min). b) Cells incubated with **103** (10 µM, 30 min) and treated with GSH (0.3 mM, 30 min) and imaged. c) Cells treated with **103** (10 µM, 30 min) and 3-morpholinosydnonimine (SIN-1, a $ONOO^-$ donor, 0.5 mM, 30min). d) Cells treated with **103** (10 µM, 30 min), GSH (0.3 mM) and SIN-1 (0.5 mM, 30min). Fluorescence images were recorded using an Operetta high-content imaging system (Perkin Elmer, US) with an excitation wavelength of 460-490 nm and emission wavelength of 580-650 nm. Data was quantified and plotted using a Columbus analysis system (Perkin Elmer, US).

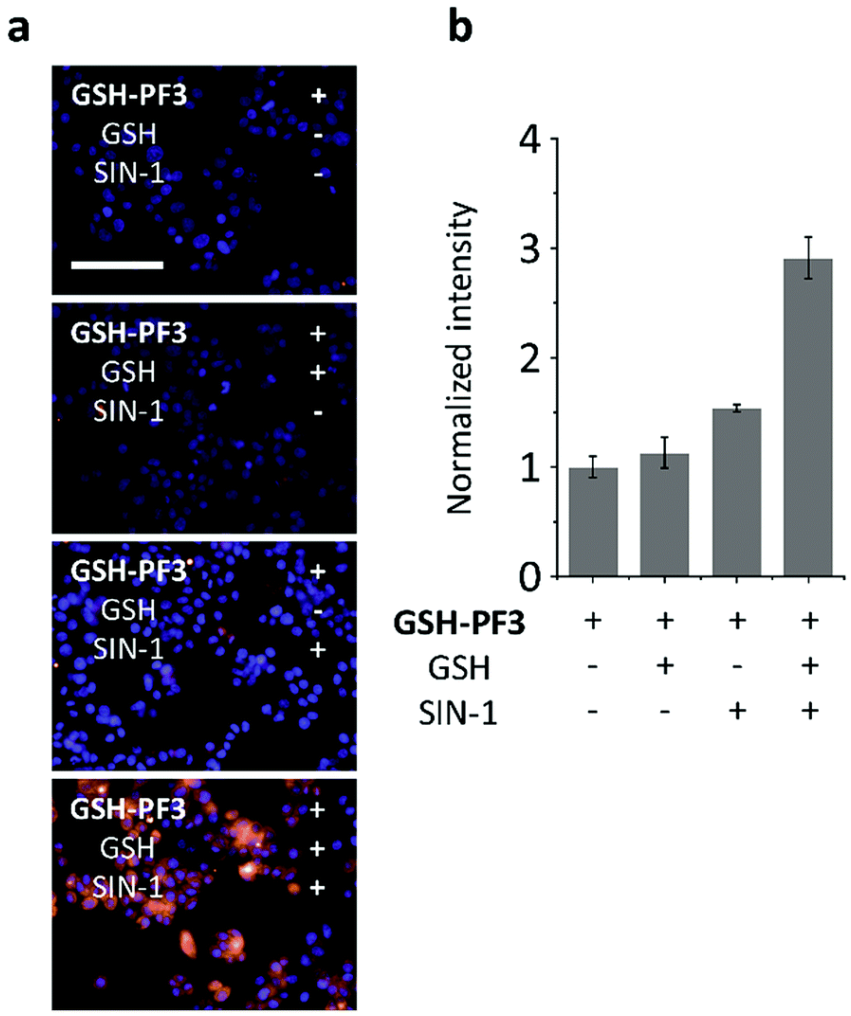

Figure 146 – a) Fluorescence imaging of RAW264.7 cells with **103** (10 µM, 30 min) with and without exogenously added GSH (50 µM) and/or SIN-1 (500 µM). Excitation channel = 460–490 nm, emission channel filtered = 530–590 nm. b) Bar chart of the normalized fluorescence intensity. Cell nuclei were stained with Hoechst 33342. Scale bar = 100 µm.

Following these successful fluorescence and selectivity tests and its possible use as a diagnostic tool, probe **103** was sent to the research group of Professor Xiao-Peng He at East China University of Science and Technology (ECUST) to test its ability to detect peroxynitrite and GSH in cellular systems. **103** was incubated with Hep-G2 cells where it was shown to exhibit good solubility in the buffer media as well as good membrane permeability (**Figure 145**, **a**). No fluorescence response was observed when the Hep-G2 cells were incubated with GSH (**Figure 145**, **b**), or when SIN-1 was used as an extracellular $ONOO^-$ donor (**Figure 145**, **c**). However, when cells that had been incubated with **103** were exposed to both GSH and $ONOO^-$ analytes, a clear and substantial turn on of fluorescence was observed. Similar results were also observed for a RAW264.7 cell line, with a near doubling in fluorescence intensity observed in the presence of both GSH and $ONOO^-$ (**Figure 146**).

The ability of probe **103** to react with GSH and $ONOO^-$ produced in-situ within the cell was then determined. Lipopolysaccharide (LPS) has previously been used to stimulate production of $ONOO^-$. It does this *via* its binding of CD14/TLR4/MD2 receptor and causing the production of many inflammatory cytokines, including NO and O^-_2 which can react to form $ONOO^-$. Caffeic acid (CA) has been used as a treatment for inflammation through its ability to induce intracellular production of GSH. When the HEP-G2 cells were incubated with **103** then no fluorescence was observed (**Figure 147**, **b**), with addition of LPS resulting in only a small amount of 'turn on' fluorescence of the cells (**Figure 147**, **c**).

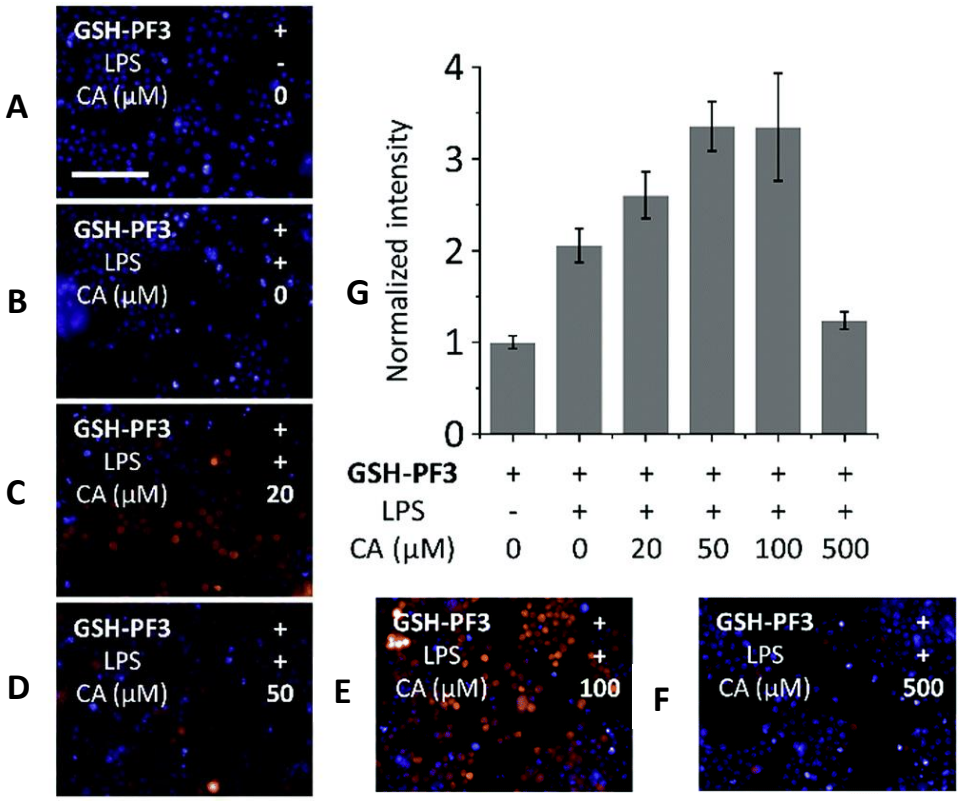

Figure 147 – Fluorescence imaging of RAW264.7 cells in the presence of a) **103** (10 μM, 30 min); b) **103** (10 μM, 30 min) and LPS (1 μg/ mL); c) **103** (10 μM, 30 min), LPS(1 μg/ mL) and 20 μM; d) **103** (10 μM, 30 min), LPS(1 μg/ mL) and 50 μM; e) **103** (10 μM, 30 min), LPS(1 μg/ mL) and 100 μM; f) **103** (10 μM, 30 min), LPS(1 μg/ mL) and 500 μM; g) Bar chart of the normalized intensity from the fluorescence intensity. Cell nuclei were stained with Hoechst 33342. Scale bar = 100 μm. Error bars represent SD.

However, subsequent addition of CA resulted in an increase in cellular fluorescence intensity (**Figure 147**, **d**), with the normalised fluorescence intensity values clearly demonstrating that this probe could be used to visualise cells containing elevated levels of $ONOO^-$ and GSH (**Figure 147**, **e**). As the concentration of CA increases from 0-100 µM, the level of GSH that is produced by the cells increases. Accordingly, the fluorescence of

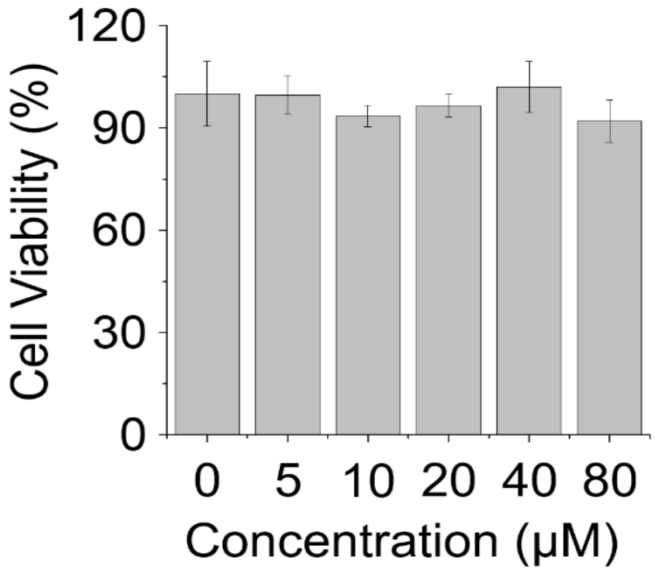

Figure 148 – Cell viability of RAW264.7 for increasing **103** concentrations.

the probe also increases, as more of the masking group is cleaved. At much higher levels of CA (500 µM) a quenching of the fluorescence is observed. This could be attributed to a large amount of GSH being produced, rapidly quenching the $ONOO^-$ that has been produced through LPS stimulation.

Cell proliferation assays were then carried out to determine the toxicity of this probe in cells (Figure 148), which clearly revealed that RAW264.7 cell division was viable in the presence of probe **103**. Cells were plated into 96 well plates with growth medium and left overnight. The cells were then seeded and treated with **103** of different concentrations for 24 h. Then a solution of MTS/PMS (20:1, Promega Corp) (10 µL per well) was added to each well containing 100 µL of growth medium. After being incubated at 37 °C under 5 % CO_2 for 2 h, absorbance of the solutions was measured at 490 nm using an M5 microplate reader (Molecular Device, USA). The optical density of the result in MTS assay was directly proportional to the number of viable cells.

3.5.4 Conclusion and future work

A new probe **103** has been designed and synthesized for the dual detection of GSH and $ONOO^-$ which contains reactive 2,4-DNBS and Bpin groups whose cleavage results in release of fluorescein as a fluorescent reporting unit. Fluorescent analysis showed only a small increase in the fluorescence when either GSH or $ONOO^-$ was present, with a clear and significant fluorescence occurring when both analytes were present. Cellular studies in human cancer cells showed that **103** could be used to simultaneously detect exogenous GSH and $ONOO^-$, as well as detect the presence of GSH and $ONOO^-$ that was generated in situ through the action of SIN-1 and CA. Further work is currently underway in the group to add targeting groups to the core structure of the probe that will enable it to be localised to specific organelles within the cell.

This successful development of a dual GSH "AND" $ONOO^-$ molecular probe has been published in *Chemical Science*.[38]

3.6 Chapter conclusion

A number of new fluorescein-based probes have been developed for the analysis of various analytes. **90** was an $ONOO^-$ and F^- probe that was not suitable for use in aqueous systems. However, in THF the probe showed that the dual detection of these two analytes was feasible. **93** is a hydrazone based $ONOO^-$ probe that was shown to detect both HClO and $ONOO^-$, with a modification of its hydrazine motif producing **96**, which showed much better selectivity to $ONOO^-$ over HClO. This probe has potential to be expanded through the addition of other functional units. **97** is an $ONOO^-$ and NTR probe that can detect various concentrations of these analytes in solution-based assays. Cellular studies are being undertaken with Dr Robert Elmes. **103** is a GSH and $ONOO^-$ probe that was very successful in the dual detection of these analytes. In solution assays showed that the probe has a very good response only when both analytes are present and that the probe is very selective to off target species. In addition, cell studies have shown that **103** can be used for the studying of the levels of both analytes in cellular environments and this had led to the publishing of a paper in a renowned journal.

3.7 Chapter references

1: Y. Urano, M. Kamiya, K. Kanda, T. Ueno, K. Hirose, T. Nagano, *J. Am. Chem. Soc.*, **2005**, *127*, 4888-4894.

2: S. C. Burdet G. K. Walkup, B. Spingler, R. Y. Tsien, S. J. Lippard, *J. Am. Chem. Soc.*, **2001**, *123*, 7831-7841.

3: X. Ma, C. Liu, Q. Shan, G. Wei, D. Wei, Y. Du, *Sens. Act. B*, **2013**, *188*, 1196-1200.

4: X. Jin, L. Hao, Y. Hu, M. She, Y. Shi, M. Obst, J. Li, Z. Shi, *Sens. Act. B*, **2013**, *186*, 56-60.

5: A. Minta, J. P. Y. Kao, R. Y. Tsien, *J. Biol. Chem.*, **1989**, *264*, 8171-8178.

6: T. Miura, Y. Urano, K. Tanaka, T. Nagano, K. Ohkubo, S. Fukuzumi, *J. Am. Chem. Soc.*, **2003**, *125*, 8666-8671.

7: K. L. Wolfe, R. H. Liu, *J. Agric. Food Chem.*, **2007**, *55*, 8896-8907.

8: W. Alexander, *ACSO 2010 Annual Meeting*, **2010**, *8*, 469-478.

9: J. P. Pooler, A. W. Girotti, *Photochem. Photobiol.*, **1986**, *44*, 495-499.

10: J. Uggeri, R. Gatti, S. Belletti, R. Scandroglio, R. Corradini, B. M. Rotoli, G. Orlandini, *Histochem. Cell Biol.*, **2004**, *122*, 499-505.

11: C. Parish, *Immun. Cell Biol.*, **1999**, *77*, 499-508.

12: T. H. The, T. E. Feltkamp, *Immunology*, **1970**, *18*, 865-873.

13: K. Gollnick, S. Held, *J. Photochem. Photobiol. B*, **1990**, *5*, 85-93.

14: R. Rathod, S. Bera, M. Singh, D. Mondal, *RSC Adv.*, **2016**, *6*, 34608-34615.

15: A. Baeyer, *Berichte*, **1871**, *4*, 555-558.

16: Y. Ueno, G. Jiao, K. Burgess, *Synthesis*, **2004**, *15*, 2591-2593.

17: J. J. Hu, N. Wong, S. Ye, X. Chen, M. Lu, A. Q. Zhao, Y. Guo, A. C. Ma, A. Leung, J. Shen, D. Yang, *J. Am. Chem. Soc.*, **2015**, *137*, 6837-6843.

18: H. Zhang, J. Chen, X. Guo, H. Wang, H. Zhang, *Anal. Chem.*, **2014**, *86*, 3115-3123.

19: N. O. Mchedlov-Petrossyan, T. A. Cheipesh, A. D. Roshal, A. O. Doroshenko, N. A. Vodolazkaya, *Meth. Appl. Fluoresc.*, **2016**, *4*, 034002.

20: Z. Fu, X. Han, Y. Shao, J. Fang, Z. Zhang, Y. Wang, Y. Peng, *Anal. Chem.*, **2016**, *89*, 1937-1944.

21: S. K. Jha, V. K. Mishra, D. K. Sharma, T. Damodaram, *Rev. Environ. Contam. Toxicol.*, **2011**, *211*, 121-142.

22: A. L. Choi, G. Sun, Y. Zhang, P. Grandjean, *Environ. Health Persp.*, **2012**, *120*, 1362-1369.

23: M. S. McDonagh, P. F. Whiting, P. M. Wilson, A. J. Sutton, I. Chestnut, J. Cooper, K. Misso, M. Bradley, E. Treasure, J. Kleijnen, *BMJ*, **2000**, *321*, 855-859.

24: H. Schiffl, *Nephrol. Dial. Transplant.*, **2008**, *23*, 411.

25: A. Strunecka, O. Strunecky, *J. Patocka, Physiol. Res.*, **2002**, *51*, 557-564.

26: B. Ke, W. Chen, N. Ni, Y. Cheng, C. Dai, H. Dinh, B. Wang, *Chem. Commun.*, **2013**, *49*, 2494-2497.

27: A. Roy, T. Saha, P. Talukdar, *Tett. Lett.*, **2015**, *35*, 4975-4979.

28: X. Chen, T. Leng, C. Wang, Y. Shen, W. Zhu, *Dyes and Pigments*, **2017**, *141*, 299-305.

29: X. Chen, H. Ma, *Anal. Chim, Acta.*, **2006**, *575*, 217-222.

30: K. Tripathi, A. Rai, A. K. Yadav, S. Srikrishna, N. Kumari, L. Mishra, *RSC Adv.*, **2017**, *7*, 2264-2272.

31: F. Huo, J. Zhang, Y. Yang, J. Chao, C. Yin, Y. Zhang, T. Chen, *Sens. Actu. B*, **2012**, *166*, 44-49.

32: G. Ambikapathi, S. Kumar, B. R. Lamani, S. K. Shivanna, H. B. Maregowda, A. Gupta, P. Malingappa, *J. Fluoresc.*, **2013**, *23*, 705-712.

33: X. Yang, X. Guo, Y. Zhao, *Talanta*, **2002**, *57*, 883-890.

34: I. M. de Oliveira, D. Bonatto, J. A. P. Henriques, *Tech. Educ. Topics in App. Microbiol. And Microbial Biotech.*, **2010**, *0*, 1008-1019.

35: D. Yang, H. Y. Tian, M. Li, Y. Zhou, J. F. Zhang, *Sci. Rep.*, **2017**, *7*, 9174.

36: S. Biswas, Y. Rajesh, S. Barman, M. Bera, A. Paul, M. Mandal, N. D. P. Singh, *Chem. Commun.*, **2018**, *54*, 7940-7943.

37: F. Yu, P. Li. G. Li. G. Zhou, T. Chu, K. Han, *J. Am. Chem. Soc.*, **2011**, *139*, 11030-11033.

38: A. C. Sedgwick, H. Han, J. E. Gardiner, S. D. Bull, X. He, T. D. James, *Chem. Sci.*, **2018**, *9*, 3672-3676.

4.0 TCF Based Probes

This chapter will briefly describe the TCF unit and how it has been harnessed as a tool in fluorescence sensing. Then a number of new probes based on the TCF unit for the detection of $ONOO^-$ and intracellular thiols will be designed, synthesised and analysed.

This work was completed with Dr Adam Sedgwick, a former member of the James research group at the University of Bath, with an equal contribution made by each party.

4.1 Introduction

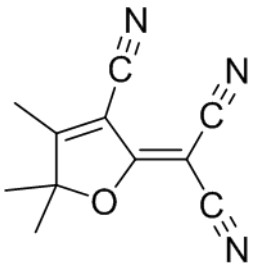

104

Figure 149 – Structure of TCF.

2-Dicyanomethylene-3-cyano-4,5,5-trimethyl-2,5-dihydrofuran (tricyanovinyldihydrofuran / TCF) was first synthesized in 2002 by Melikian *et al.* in 1995 for potential use as a cytostatic or pesticidal agent.[1] The di-methyl appended version of this molecule is dicyanomethylenedihydrofuran (DCDHF), but the acronym TCF has been used for this general class of molecule (**Figure 149**).

TCF is a highly functionalized furan ring with three highly electron withdrawing cyano (-C≡N) groups attached to one side of the furan ring. Due to the favourable electronics in this system it has been incorporated into many different non-linear optical materials (NLOs)[2-4] and a variety of push-pull ICT based probes for the detection of numerous analytes.[5-7] The long wavelength of TCF probe systems are beneficial for the imaging of living systems due to the propensity of longer wavelengths to penetrate deep into tissues and its ability to avoid auto-fluorescence.[8] The synthesis of the TCF unit **104** can be achieved *via* reaction of an α-hydroxy ketone (α-ketol) **106** and two equivalents of malonitrile **105** under basic conditions. The first step of this reaction was a condensation

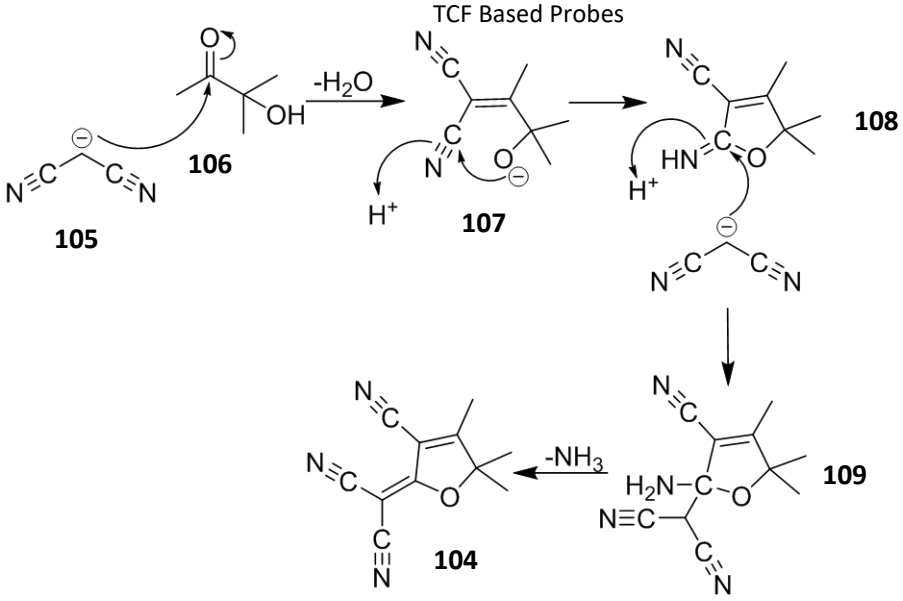

Scheme 150 – Synthesis of TCF **104** *via* an aldol reaction with and 2 eq. of malonitrile.

reaction between a malonitrile and aldehyde group with the resulting α-hydroxy group attacking a cyano group to form intermediate **107** and then iminolactone **108**. The iminolactone reacts with a second equivalent of malonitrile, producing ammonia and the tri-cyano containing TCF **104**, *via* the intermediate **109** (**Figure 150**).

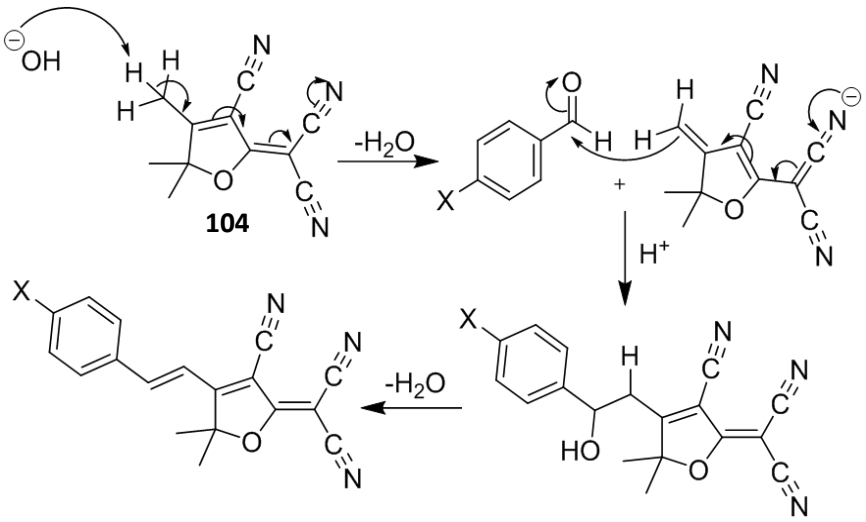

Figure 151 – Adol reaction of TCF **104** with an aromatic aldehyde.

The most popular method for the use of TCF for sensing applications includes connecting an electron donor moiety bound through a π-linker to the TCF unit. Upon reaction with an analyte the masking unit is cleaved and allows the ICT of the electron donor-π-acceptor behaviour of the sensor to turn on. These reaction units are normally formed through connection of TCF and an aromatic aldehyde to form a 4-substituted unsaturated dihydrofuran unit (**Figure 151**). Xu *et al.* harnessed this methodology to develop a

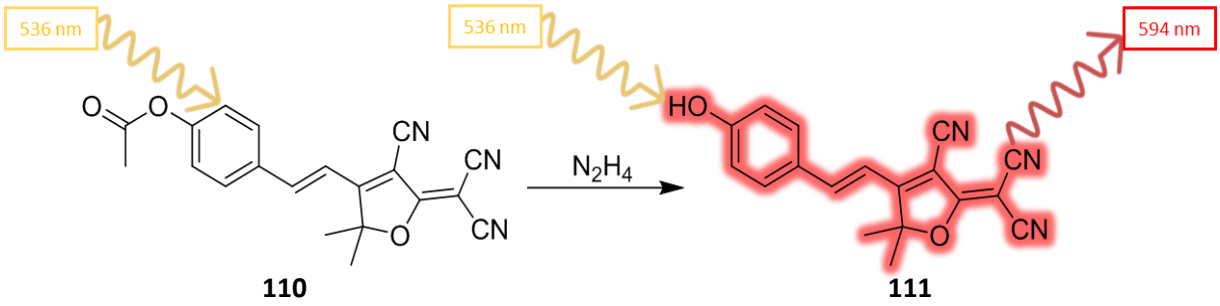

Scheme 152 – TCF probe **110** being activated by N_2H_4 into **111.**

hydrazine sensitive fluorescent probe (**Figure 152**).[9] The TCF base structure was reacted with 4-hydroxybenzaldehyde and subsequently masked with a hydrazine sensitive acetyl group, that blocks the ICT process from occurring. Upon exposure to hydrazine the acetyl group is cleaved and the resulting phenol group acts as an electron donating group that allows ICT and the sensor to turn on. This causes a bathochromic shift in both the absorbance and the emission spectra, which is associated with a dramatic increase in the fluorescence.

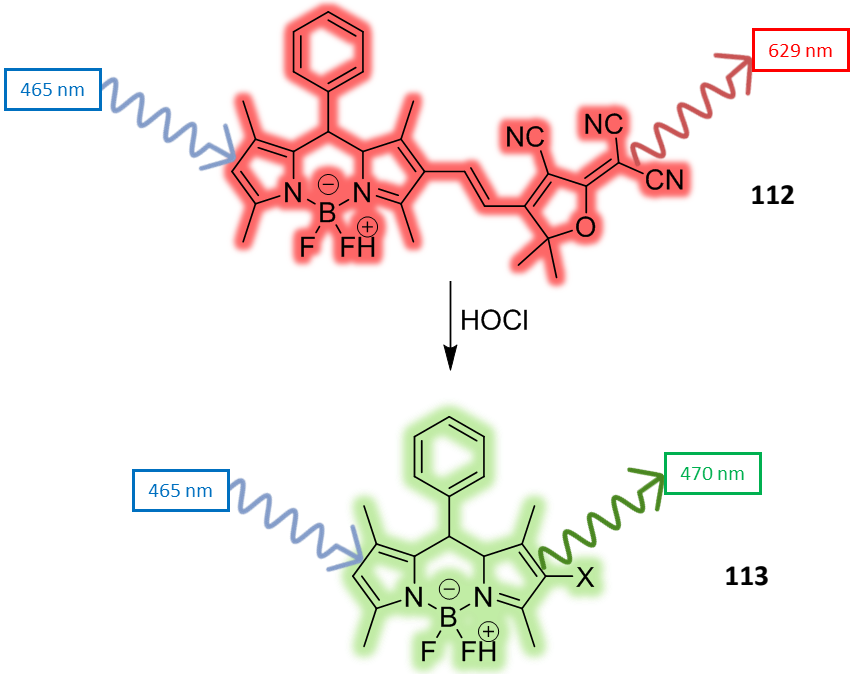

Scheme 153– Ratiometric dual-fluorophore probe for HClO **112**, and active fluorophore **113**.

Kim *et al.* used a BODIPY-TCF based probe for the detection of HClO (**Figure 153**).[10] The two fluorophores were connected through an alkene linker to create a highly

conjugated system which induces a bathochromic shift in the absorption and emission spectra of the BODIPY fragment. Upon exposure to HClO the alkene bond is oxidatively cleaved to disconnect the two systems, which causes a reversal of the shift in the absorption and emission spectra which results in a ratiometric response from the probe.

4.2 TCF based $ONOO^-$ probes

4.2.1 Design of Probes **114** and **115**

The need to develop sensitive probes for the detection of $ONOO^-$ has already been discussed in this thesis (**Section 1.3.5.7**). In this respect, the use of boronic acid pinacol ester units for the detection of $ONOO^-$ has been shown to be a proven and reliable trigger / masking unit. We postulated that there was an opportunity to produce a probe based on the TCF fluorophore **104** that was sensitive to $ONOO^-$, with the production of a TCF based long wavelength probe of particular use for the study of $ONOO^-$ in whole animal systems.

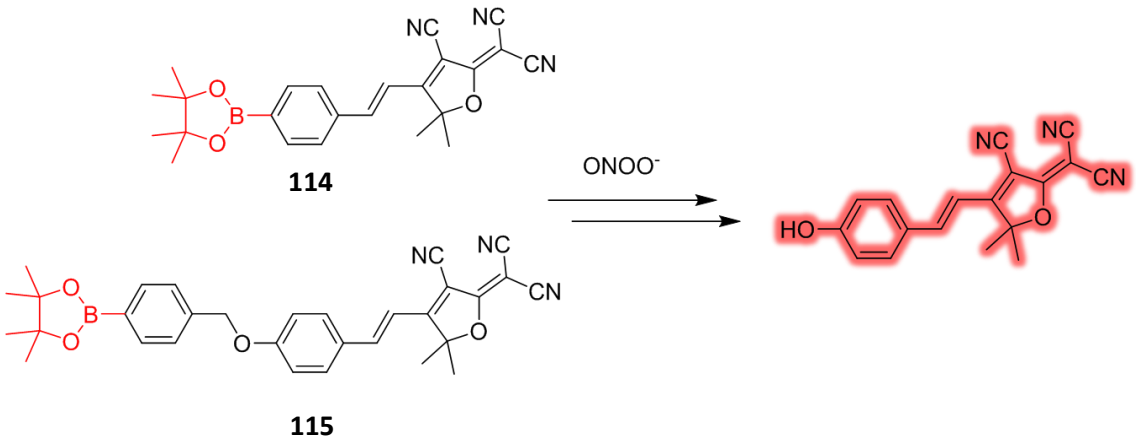

Figure 154 – Reaction of probes **114** and **115** in response to $ONOO^-$, resulting in the fluorescent TCF compound **111**.

We wanted to explore the use of two main methods for the attachment of B-pin groups to probes, either *via* the direct attachment of a phenyl B-pin group (**114**), or through the use of a self-eliminating 4-phenylboronic acid pinacol ester (**115**) which has previously been used as a ClO^- probe. These two groups would both make good masking moieties for electron donor units typically used for the construction of TCF based fluorophores (**Figure 154**).

4.2.2 Synthesis of Probes **114** and **115**

The synthesis of the two probes **114** and **115** commenced with the synthesis of the TCF unit which was achieved through reaction of 3-hydroxy-3-methyl-2-butanone **106**, malonitrile **105** and sodium ethanoate (NaOEt) in EtOH as solvent. The first probe (**114**) was then synthesized in one further step through coupling of 4-(4,4,5,5-tetramethyl-1,3,2-dioxaborolan-2-yl) benzaldehyde **116** with the TCF unit **104** using a base catalysed microwave assisted condensation reaction, in moderate yield. Alternatively, a coupling of 4-hydroxybenzaldehyde **117** and TCF, though the same microwave assisted, base catalysed reaction, gave the phenolic-TCF product **118** in good yield (75 %). This phenol was finally reacted using 4-bromomethylphenylboronic acid pinacol ester **119** and K_2CO_3 in DMF to give an O-alkylated TCF **115** in 47% yield (**Scheme 10**).

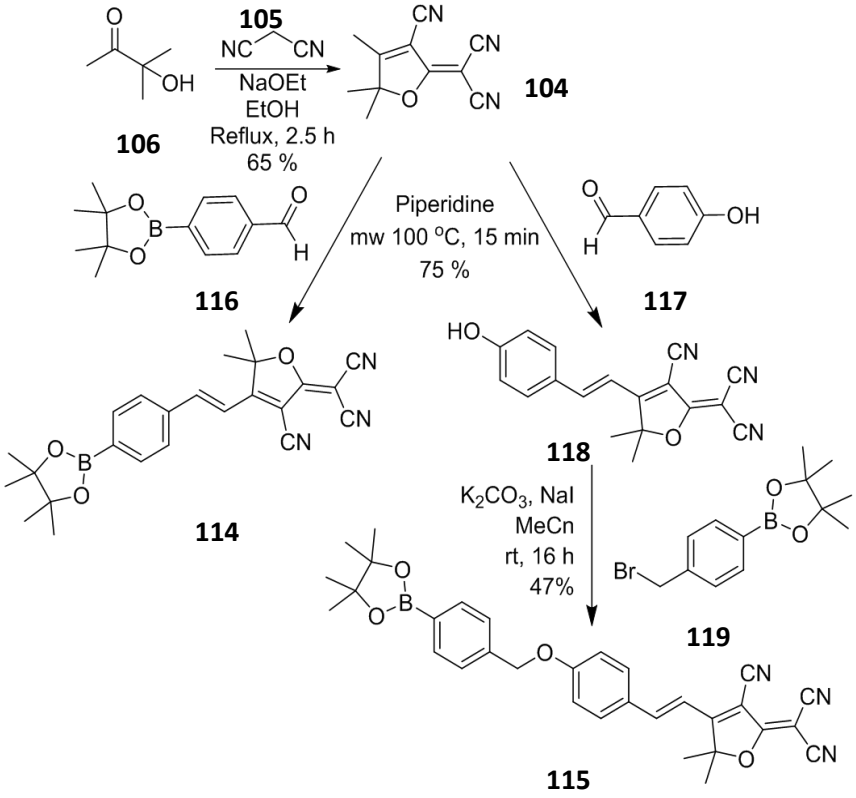

Scheme 10 – Synthesis of **114** and **115** *via* the TCF **104**.

4.2.3 Results and discussion

Both probes **114** and **115** were then subjected to initial fluorescence analysis. This included an exposure to $ONOO^-$ to test the probes UV-Vis and fluorescence response, including a titration of the probe against an increasing concentration of $ONOO^-$, as well as selectivity studies to establish any off-target interactions with other analytes and compare **115**'s reactivity toward ClO^- to $ONOO^-$.

4.2.3.1 Fluorescence Analysis of **114**

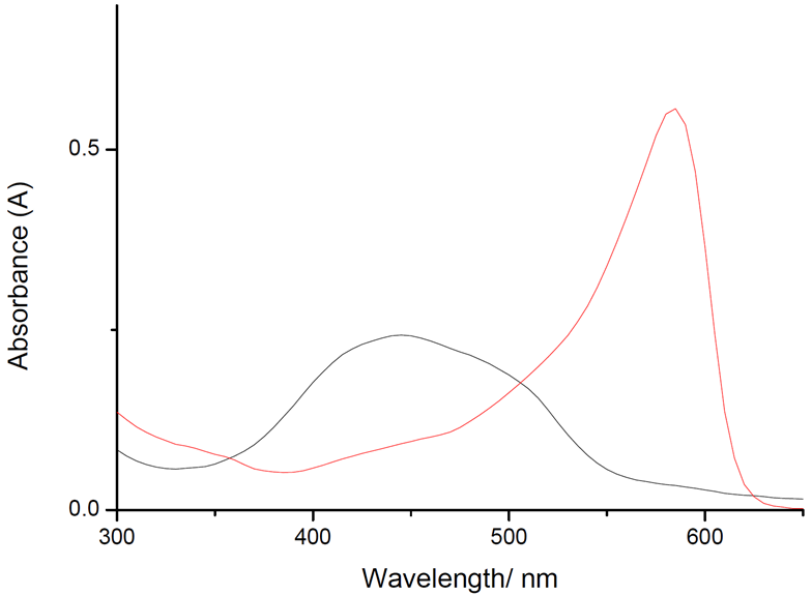

Figure 155 – UV-Vis spectrum of (i) **114** (10 µM) – BLACK and (ii) **114** (10 µM) + $ONOO^-$ (5 µM) – RED. Analysis carried out in PBS buffer (pH 8.0, 20 % DMSO).

114 (10 µM) was dissolved in PBS buffer (pH 8.0, 20 % DMSO) and its UV-Vis absorbance measured (**Figure 155**) which showed that there was a broad absorbance at 400-500nm. Upon exposure to $ONOO^-$ (5 µM) the peak absorption bathochromically shifted over 100 nm, which was attributed to the oxidative cleavage of the B-pin group and self-elimination of the resultant phenol to afford the activated donor-π-acceptor TCF fluorophore.

114 (10 µM) was then titrated against $ONOO^-$ (0-100 µM) with a dose dependent response

in the fluorescence of the probe being observed (**Figure 156**), with a maximum increase ~6-fold at 80 µM. A small decrease in the fluorescence is observed above 80 µM $ONOO^-$ (**Figure 157**) which could be attributed to the destruction of the TCF fluorophore by excess $ONOO^-$. Using this data, it was calculated that the limit of detection (LOD) was 5.6 µM $ONOO^-$.

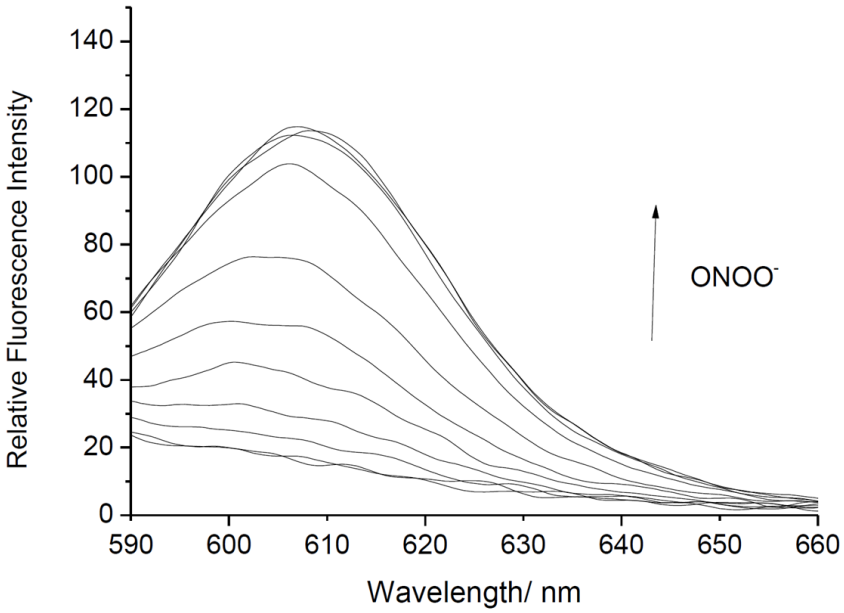

Figure 156 – Fluorescence spectra of **114** (10 µM) and $ONOO^-$ (0-100 µM). Carried out in PBS buffer (pH 8.0, 20 % DMSO), λ_{ex} = 560 nm, slit widths ex = 10 nm and em = 15 nm.

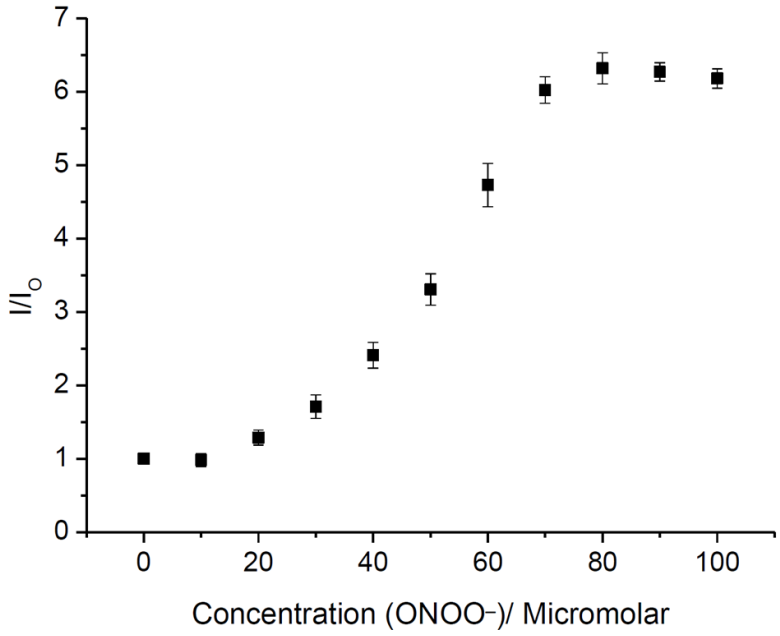

Figure 157 – Fluorescence intensity (I/I_0) of **114** (10 µM) and $ONOO^-$ (0-100 µM). Carried out in PBS buffer (pH 8.0, 20 % DMSO), λ_{ex} = 560 nm/ λ_{em} = 606 nm, slit widths ex = 10 nm and em = 15 nm.

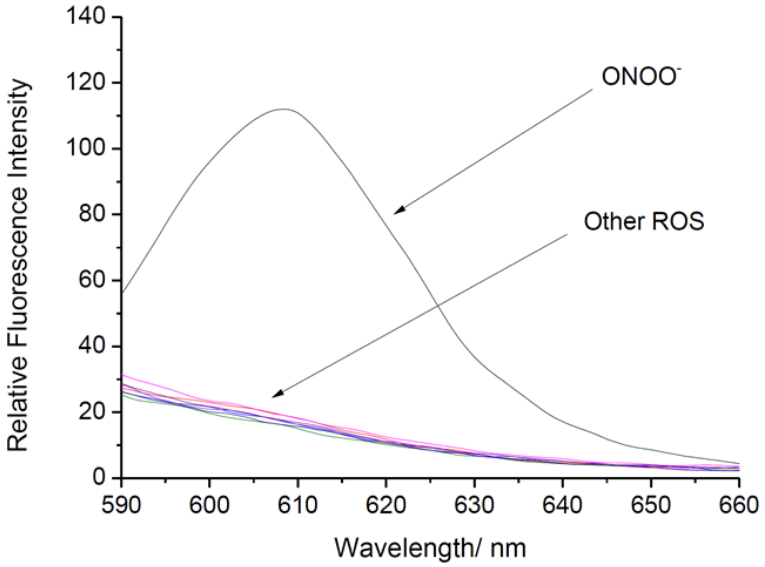

Figure 158 – Fluorescence spectra of **114** (10 µM), $ONOO^-$ (100 µM) and other ROS species (100 µM). Carried out in PBS buffer (pH 8.0, 20 % DMSO), λ_{ex} 560 nm, slit widths ex = 10 nm and em = 15 nm.

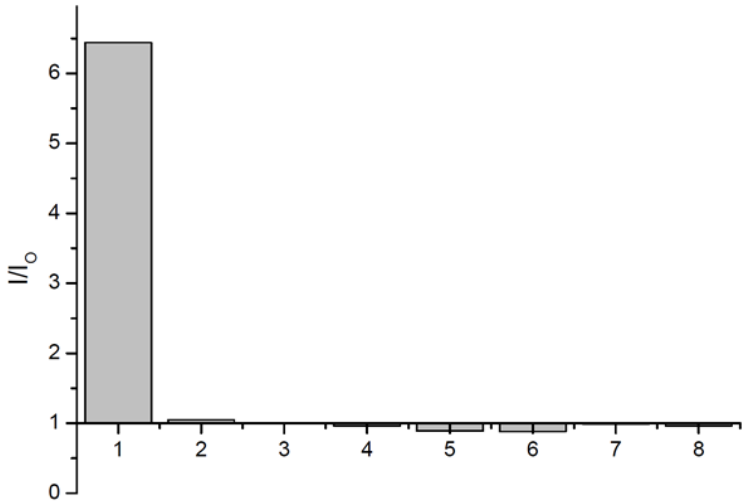

Figure 159 – Column chart for selectivity of **114** (10 µM) with 1) $ONOO^-$ (100 µM), 2) HClO (100 µM), 3) H_2O_2 (100 µM), 4) KO_2 (100 µM), 5) ROO• (100 µM), 6) $^-O_2$ (100 µM), 7) •OH (100 µM). Carried out in PBS buffer (pH 8.0, 20 % DMSO), λ_{ex} 560 nm / λ_{em} 606 nm, slit widths ex = 10 nm and em = 15 nm.

114 was then subjected to selectivity testing, involving its exposure to a selection of ROS species to determine how selective it was for $ONOO^-$ (**Figure 158**). **114** was shown to have very good selectivity over other ROS species, with a high specificity towards $ONOO^-$ which gave by-far the largest turn on (~6-fold) (**Figure 159**).

Following these initial assays that confirmed the ability of these probes to detect $ONOO^-$ in solution, they were sent to Professor Xiao-Peng He at ECUST University, China, to be

tested in cellular experiments. Unfortunately, **114** was seen to precipitate in these *in vitro* studies and so were not studied further. This was observed through the formation of precipitated agglomerations of sensor.

4.2.3.2 Fluorescence Analysis of **115**

115 was analysed in the same set of experiments as the previous probe **114**, with **115** having been previously used for the detection of ClO^-. Initially **115** was non-fluorescent,

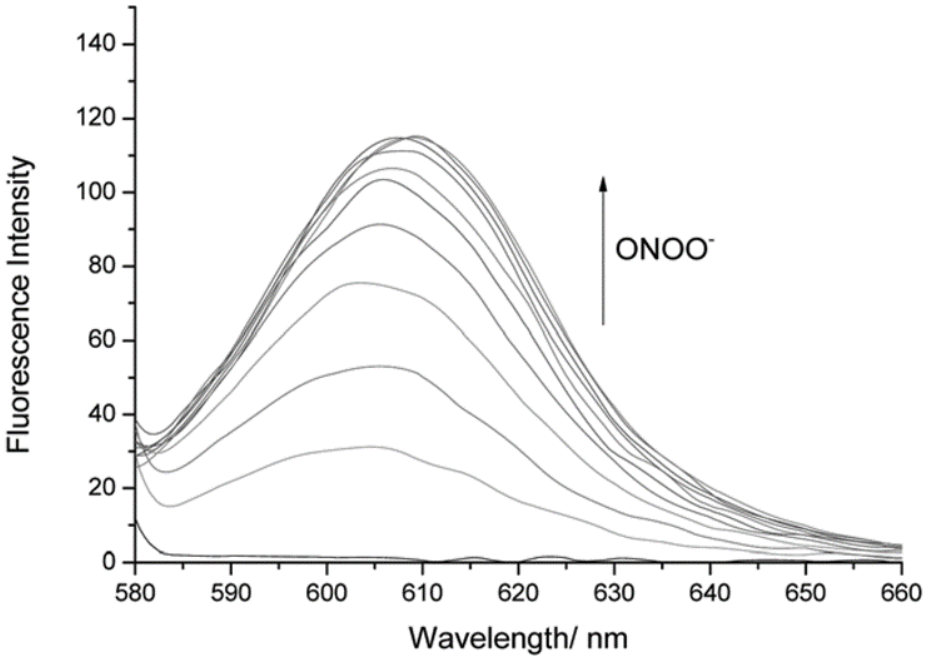

Figure 160 – Fluorescence spectra of **115** (10 µM) and $ONOO^-$ (0-10 µM). Carried out in PBS buffer (pH 8.0, 20 % DMSO), λ_{ex} = 560 nm, slit widths ex = 10 nm and em = 15 nm.

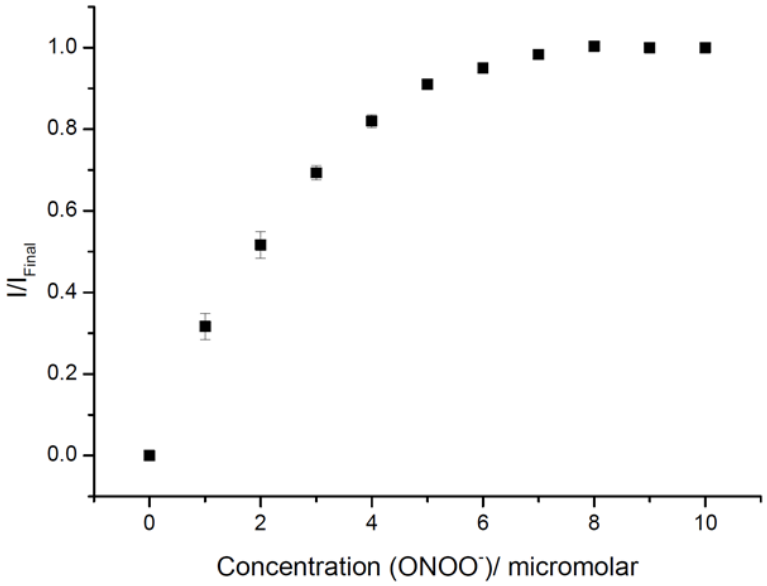

Figure 161 – Fluorescence intensity (I/IFinal) of **115** (10 µM) and $ONOO^-$ (0-10 µM). Carried out in PBS buffer (pH 8.0, 20 % DMSO), λ_{ex} = 560 nm/ λ_{em} = 606 nm, slit widths ex = 10 nm and em = 15 nm.

however, upon addition of $ONOO^-$ (0-10 µM) a fluorescence signal at 606 nm accompanied by a colour change from yellow to pink. Using this data, it was calculated that the LOD for **115** was 1.17 µM $ONOO^-$.

Selectivity studies with other ROS species were then undertaken. **115** is already known to react with both H_2O_2 and ClO^- to produce an unstable borate species that rapidly hydrolyses into a phenol and new boronic species. However, it was anticipated that the relative speeds of the reactions between $ONOO^-$, ClO^- and H_2O_2 would differ considerably, with $ONOO^-$ expected to be ~ $\times 10^3$ fold faster than ClO^- and ~ $\times 10^6$ fold faster than H_2O_2. Based on these facts, it was expected that ClO^- and H_2O_2 have the potential to react, but would not compete with $ONOO^-$.

To our surprise, the results of the selectivity study deviated from those predicted. Exposure to ONOO caused a rapid increase in fluorescence of **115**. H_2O_2 needed ~10-fold increase in the concentration and 30 mins for a significant response to be recorded, while the response of ClO^- was far less than expected (**Figure 162**). After some consideration, it was proposed that the high amount of DMSO in the buffer solution might be causing side reactivity issues with the ClO^- species, which has been previously observed for other sensors in the group.

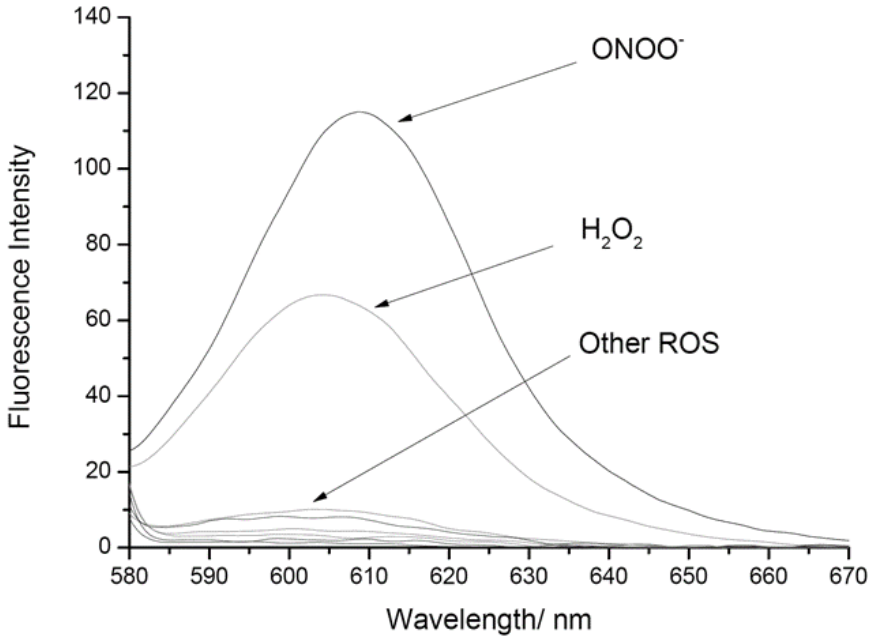

Figure 162 – Fluorescence spectra of **115** (10 µM) and $ONOO^-$ (10 µM, 1 min), ClO^- (100 µM, 30 min), H_2O_2 (100 µM, 30 min), ROO• (100 µM, 30 min), $^-O2$ (100 µM, 1 min), •OH (100 µM, 1 min). Analysis carried out in PBS buffer (pH 8.0, 20 % DMSO), λ_{ex} = 560 nm, slit widths ex = 10 nm and em = 15 nm.

Consequently, **115** was assayed in a different buffer solution (PBS pH 7.4) to determine its response to ClO^-. This showed a significantly higher response than was observed in the previous buffer containing DMSO and validated the previously recorded behaviour of probe **115** towards ClO^- (**Figure 163**). However, the response produced by $ONOO^-$ (10 µM, 1 min) was still significantly greater than for ClO^- (100 µM, 30 min) enabling it to be used for the detection of $ONOO^-$ selectively (**Figure 164**).

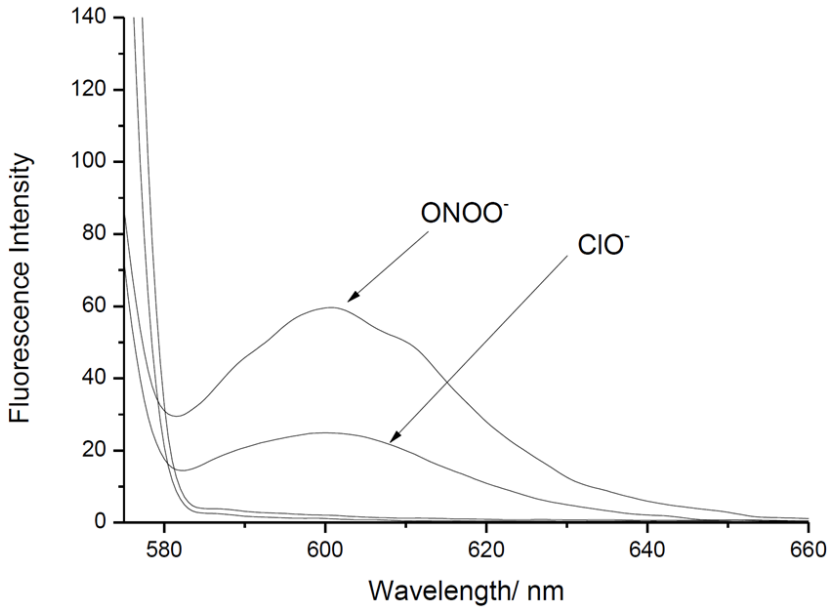

Figure 163 – Fluorescence spectra of **115** (10 µM) with addition of $ONOO^-$ (10 µM) and ClO^- (100 mM). Analysis carried out in PBS buffer (pH 7.4), λ_{ex} 560 nm, slit widths ex = 10 nm and em = 15 nm.

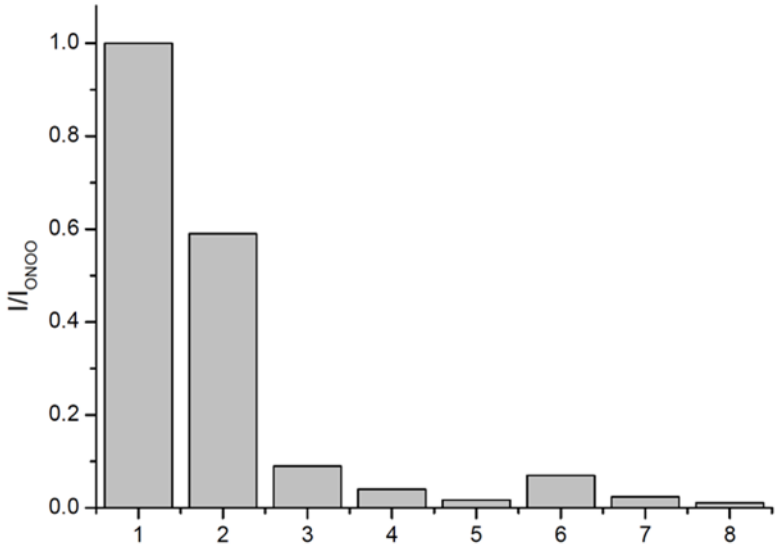

Figure 164 – Column chart for selectivity of **115** (10 µM) with 1) $ONOO^-$ (10 µM, 1 min), 2) H_2O_2 (100 µM, 30 min), 3) ClO^- (100 µM, 30 min), 4) KO_2 (100 µM, 30 min), 5) ROO• (100 µM, 30 min), 6) $^-O2$ (100 µM, 1 min), 7) •OH (100 µM, 1 min). Analysis carried out in PBS buffer (pH 8.0, 20 % DMSO), λ_{ex} 560 nm / λ_{em} 606 nm, slit widths ex = 10 nm and em = 15 nm.

115 was sent to Professor Xiao-Peng He for cellular analysis in the presence of exogenous and endogenous $ONOO^-$. **115** (10 µM) was incubated for 30 min in cell lines including Hep-G2: human hepatoma, HeLa: human cervical cancer, RAW 264.7: mouse macrophage and A549 cells: human lung cancer (**Figure 165**). **115** showed a clear "turn on" response when SIN-1 ($ONOO^-$ donor) was exogenously added to the cells. In addition, the presence of uric acid as a $ONOO^-$ scavenger, resulted in no "turn on" response of the probe when $ONOO^-$ was added.

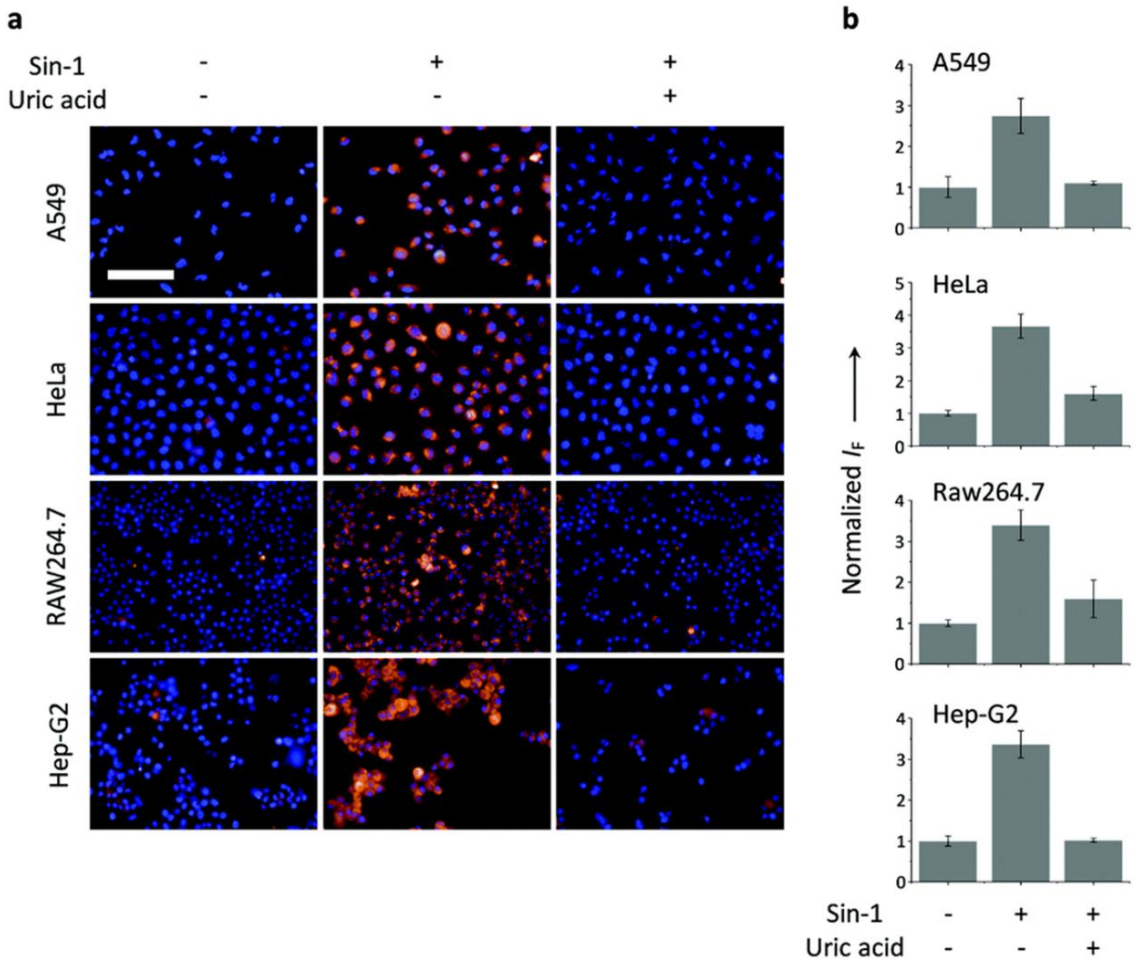

Figure 165 – a) Fluorescence imaging of different cell lines with **115** only, **115**+ SIN-1 and **115**+ SIN-1 + Uric acid. Scale bar = 100 µm b) Column charts of total level of fluorescence in each cell line. **115**λ_{ex} 560–580 nm and λ_{em} 580–650 nm. The cell nuclei were stained by Hoechst 33342.

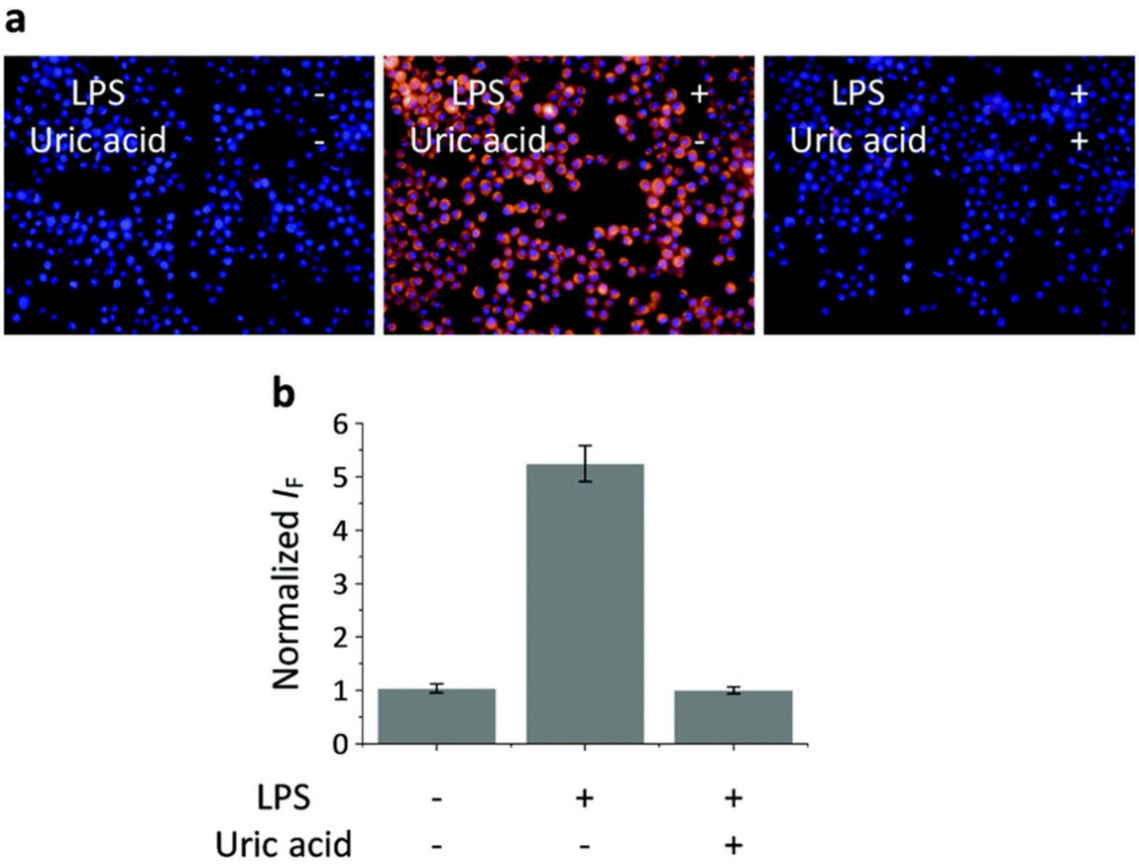

Figure 166 – a) Fluorescence imaging of RAW 264.7 with **115** (10 µM) only, **115** + LPS (1 µg/mL) and **115** + LPS + Uric acid (100 µM). Scale bar = 100 µm. b) Column chart of total level of fluorescence in RAW 264.7 cells. **115** λ_{ex} 560–580 nm and λ_{em} 580–650 nm. The Cell nuclei were stained using Hoechst 33342.

The ability of **115** to detect endogenous $ONOO^-$ was then tested with RAW 264.7 cells incubated with **115** (10 µM) for 30 minutes and rinsed with PBS (×3). The production of $ONOO^-$ was then stimulated in the cells *via* the addition of LPS, which caused a distinct "turn on" response in the fluorescence of the probe. Once again, addition of uric acid suppressed the fluorescent response, demonstrating the ability of **115** to detect the presence of $ONOO^-$ in cells both exogenously and endogenously. This can be seen in the large increase in fluorescence in the second image (**Figure 166**, **a**) relative to the first and the third images. The relative levels are more easily visualised in a column chart (**Figure 166**, **b**).

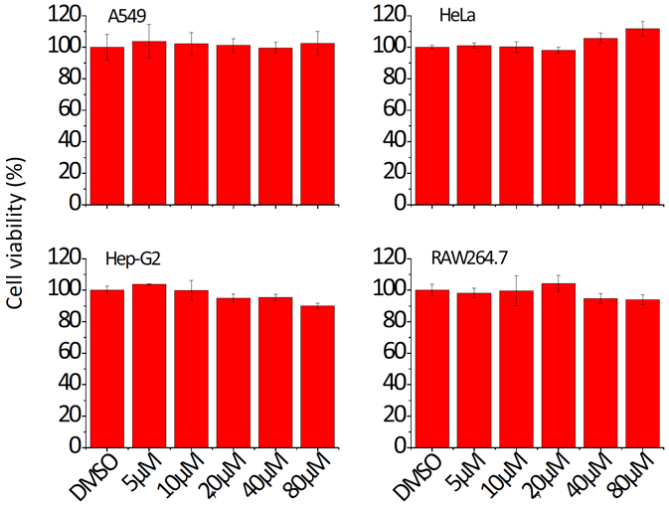

Figure 167– Column charts from the MTS cell viability study completed for **115** (10 μM) with different cell lines.

A cell proliferation assay was then conducted to ensure that the probe was not toxic to cells. **115** was incubated at a range of concentrations (5-80 μM) in the four cell lines used for the cellular testing, before being subjected to MTS cell proliferation assays. These results showed that **115** was non-toxic in these cell lines at concentrations far greater than required for imaging (**Figure 167**).

There is a large concentration of $O_2^{\bullet-}$ in mitochondria due to the electron transport pathway. $O_2^{\bullet-}$ can react with NO spontaneously to form $ONOO^-$, resulting in the

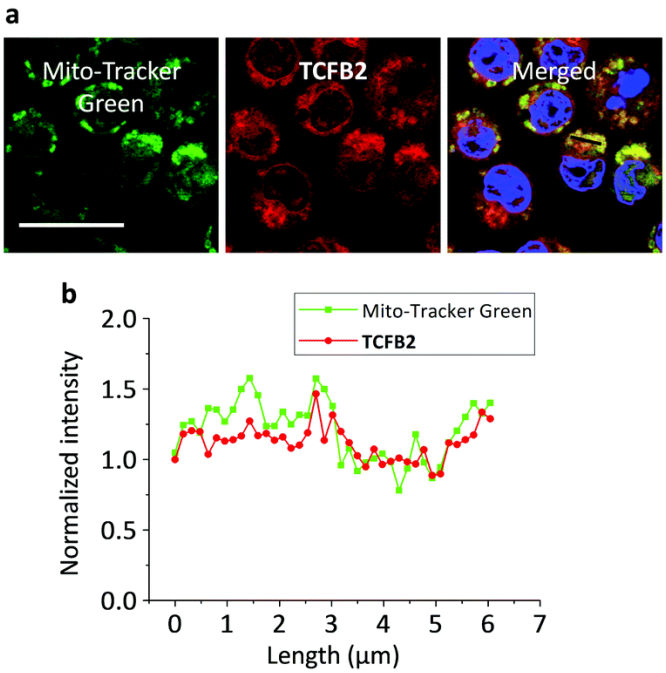

Figure 168 – a) Fluorescence images of RAW 264.7 cells images with Mito-tracker green (1 μM), **115** (10 μM) and a merge of the two images. Scale bar = 20 μM. Mito-tracker green λ_{ex} 489 nm, λ_{em} 506 nm. **115** λ_{ex} 579 nm, λ_{em} 603 nm. b) Fluorescence quantification of **115** and Mito-tracker green along a selected section of the merged images. Cell nuclei stained using Hoechst 33342.

observation that mitochondria are the main source of $ONOO^-$ in macrophages.

To further test **115**'s ability to detect $ONOO^-$ in cells, its sub-cellular localisation was compared against commercially available mitochondria tracking imaging agent (Mito-tracker green). **115** (10 µM) and Mito-tracker green (1 µM) were incubated in RAW 264.7 cells and then imaged (**Figure 168**, **a**). The results of this experiment showed a high correlation between the localisation of activated **115** and the Mito-tracker green within the substructure of cells, with a Pearson correlation coefficient (PCC, a measure of the strength of a linear relationship) of 0.84 (**Figure 168**, **b**). This indicates that **115** is activated more at the mitochondria than other parts of the cell. To further confirm this, an assay to test the co-localisation of **115** at the lysosome (**Figure 169**, **a**) was conducted whose PCC was found to be far lower (0.38) (**Figure 169**, **b**).

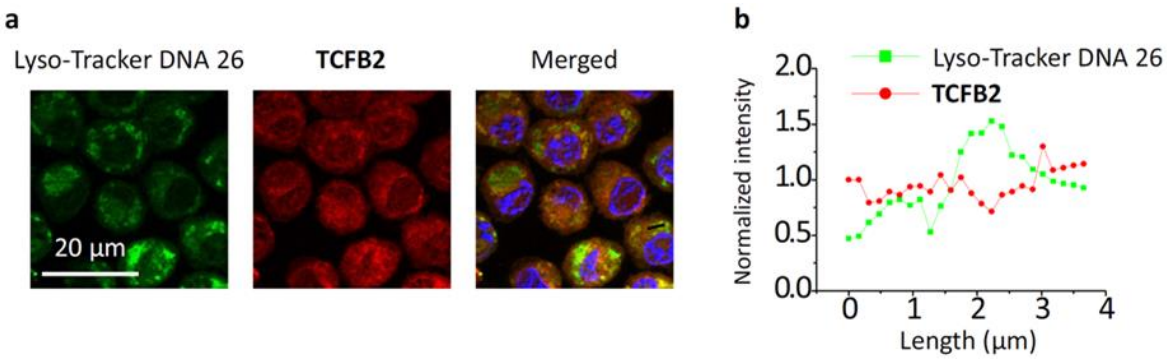

Figure 169 – a) Fluorescence images of RAW 264.7 cells images with **115** (10 µM) and Lyso-tracker DNA 26 (1 µM) a merge of the two images. Scale bar = 20 µM. **115** λ_{ex} 579 nm, λ_{em} 603 nm, Lyso-tracker DNS 26 λ_{ex} 489 nm, λ_{em} 506 nm. b) Fluorescence quantification of **115** and Lyso-tracker DNA 26 along a selected section of the merged images. The cell nuclei were stained by Hoechst 33342.

4.2.4 Conclusion

In conclusion, two long-wavelength TCF-based $ONOO^-$ probes **114** and **115** have been developed that show good selectivity and sensitivity for $ONOO^-$ in solution-based assays. **114**, however, showed poor solubility in cellular assays and was not further studied. **115** on the other hand showed good solubility in cells and was used for the detection of exogenous and endogenous $ONOO^-$ in four different cell lines. **115** was also found not to be toxic to these cell lines. A comparison with two commerically available fluorescent tracking agents found that **115** was most fluorescent in mitochondria, which corresponds with the higher concentration of $ONOO^-$ present in this organelle. This led to the publishing of a paper in the RSC journal "*Chemical Communications*".[12]

4.3 TCF based thiol probes

4.3.1 Probe design

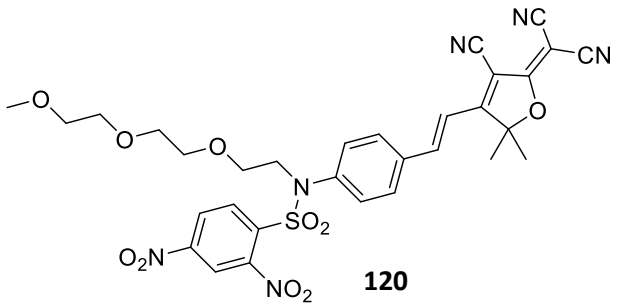

120

Figure 169 – Structure of **120.**

As explained previously (**Section 2.3.1** and **Section 2.5.1**) Hcys, Cys and GSH are all thiol containing metabolites that are produced in perturbed levels in several human diseases, with selective sensors for their detection and quantification required.

Hilderbrand *et al.* have previously developed a "turn-on" TCF probe for the detection of biological thiols using a reactive sulfonimide group (**120**, **Figure 169**) bound to a secondary amine appended with a small polyethyleneglycol (PEG) arm.[11] The function of the PEG group was to increase the solubility of the probe under physiological conditions, which was successful in detecting biological thiols in 3T3 cells.

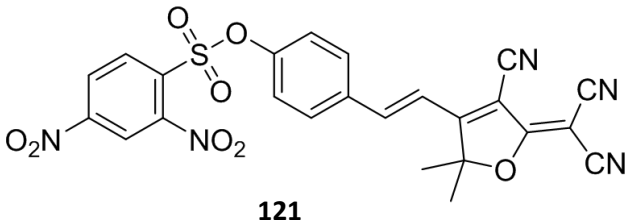

121

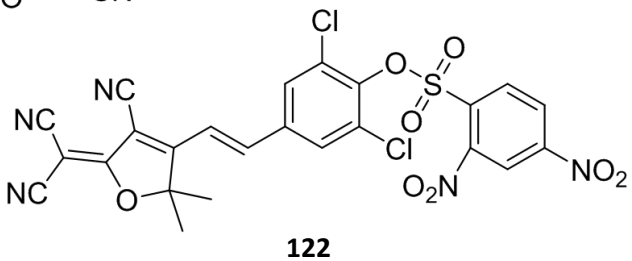

122

Figure 170 – Structure of **121** and **122**.

We believed that an analogous 2,4-DNBS-ester TCF probe would not require a PEG group to increase its solubility. Additionally, the synthesis of the analogous ester would be much more tractable. Two 2,4-DNBS-TCF ester based reactive probes were targeted for the detection of intracellular thiols (**121** and **122**, **Figure 170**) with the presence of two

chlorine atoms in one of the proposed probes (**122**) decreasing its reactivity towards analytes through increase of steric blocking effects from the two large chlorine atoms bound to the linking benzene moiety.

4.3.2 Synthesis of **121** and **122**

The synthesis of these two probes (**121** and **122**), commenced with an adol condensation reaction between 3-hydroxy-3-methyl-2-butanone, malonitrile and NaOEt in EtOH. The resultant TCF unit was then condensed with either 4-hydroxybenzaldehyde or 3,5-dichloro-4-hydroxybenzaldehyde *via* a microwave assisted reaction, to produce the two intermediates **118** and **124**, 72 % and 50 % respectively. Both **117** and **124** were then coupled with 2,4-DNBS-Cl *via* treatment with K_2CO_3 in MeCN to give the final products **121** and **122** in 45% and 72% respectively (**Scheme 11**).

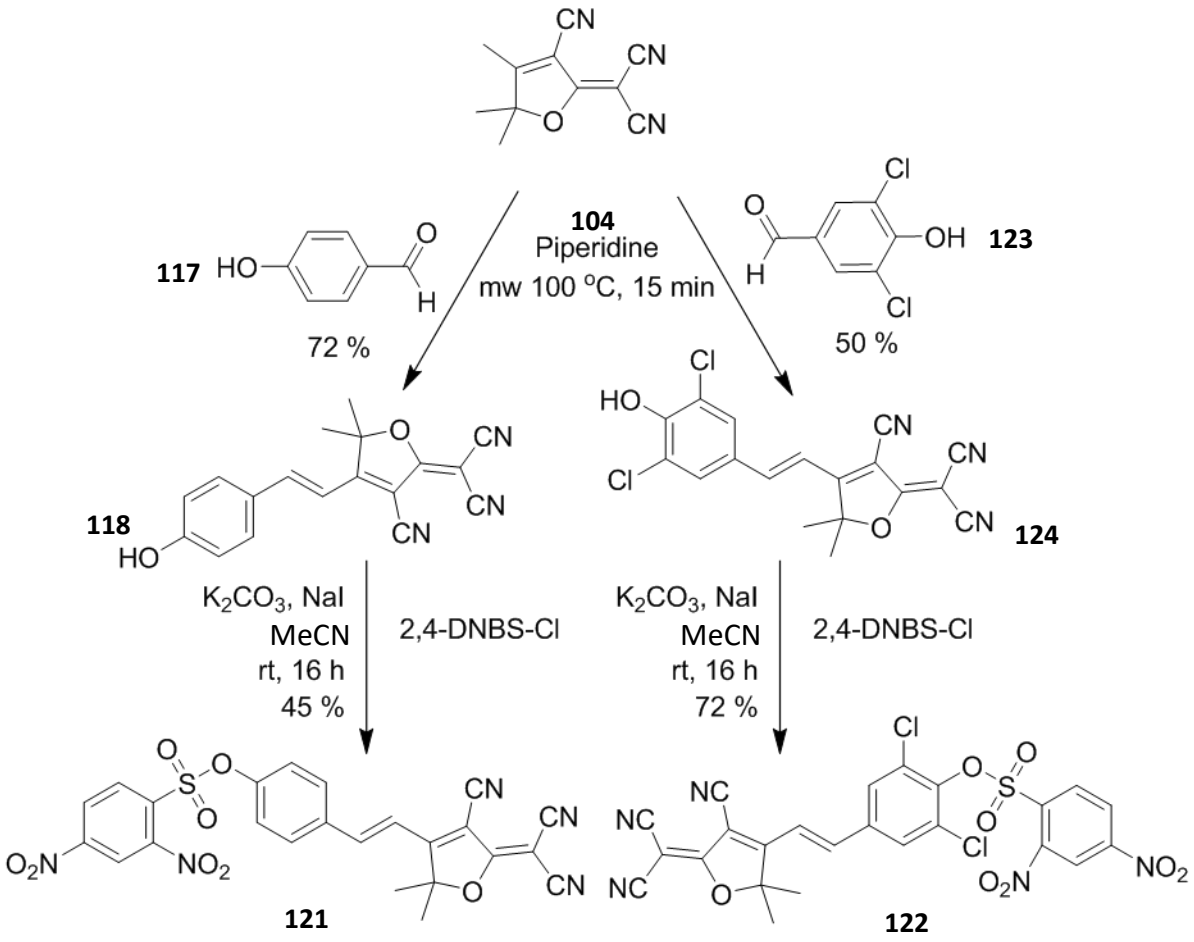

Scheme 11 – Synthesis of **121** and **122.**

4.3.3 Results and discussion

4.3.3.1 Fluorescent Analysis of **121**

121 was then analysed using in solution assays for its response towards GSH, as GSH is the most highly concentrated intracellular thiol. Firstly, **121** (5 µM) was exposed to an increasing concentration of GSH (0-500 µM) (**Figure 171**). This showed a "turn on" fluorescence response towards GSH at 25 µM, however, at higher concentrations (> 50 µM) there was a significant drop off in the intensity of the fluorescence (**Figure 172**). This

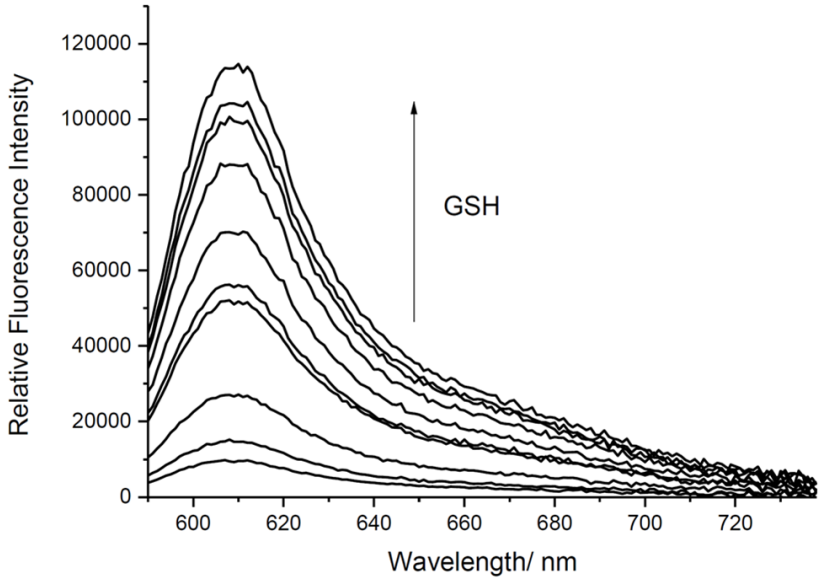

Figure 171 – Fluorescence spectra of **121** (5 µM) with addition of GSH (0-500 µM) after 15 min incubation. Conducted in PBS buffer (pH 8.0, 30 % DMSO), λ_{ex} 560 (bandwidth 15 nm).

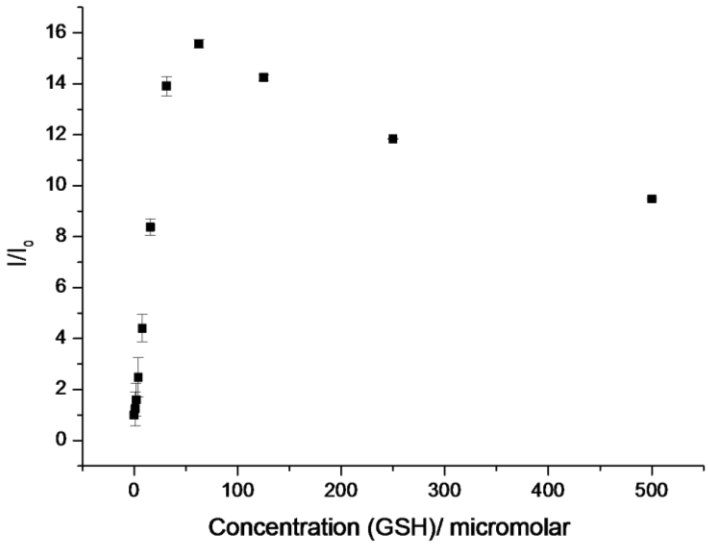

Figure 172 – Fluorescence intensity (I/I_0) of **121** (5 µM) and GSH (0-500 µM). Conducted in PBS buffer (pH 8.0, 20 % DMSO), λ_{ex} = 560 nm (bandwidth 15 nm) / λ_{em} = 610 nm (bandwidth 20 nm).

is hypothesized to be caused by side reactions between GSH and the probe, caused by the artificially high concentration of thiols used. Using this data, it was calculated that the LOD for **121** is 4.68 µM GSH. The selectivity of **121** was then tested against other thiol-containing compounds (Hcys / Cys) and a selection of amino acids. **121** reacted with both Cys and Hcys, as expected; Cys produced the largest response with Hcys and GSH slightly lower. Selectivity against non-sulfhydryl containing amino acids was very good (**Figure 173**, **Figure 174**).

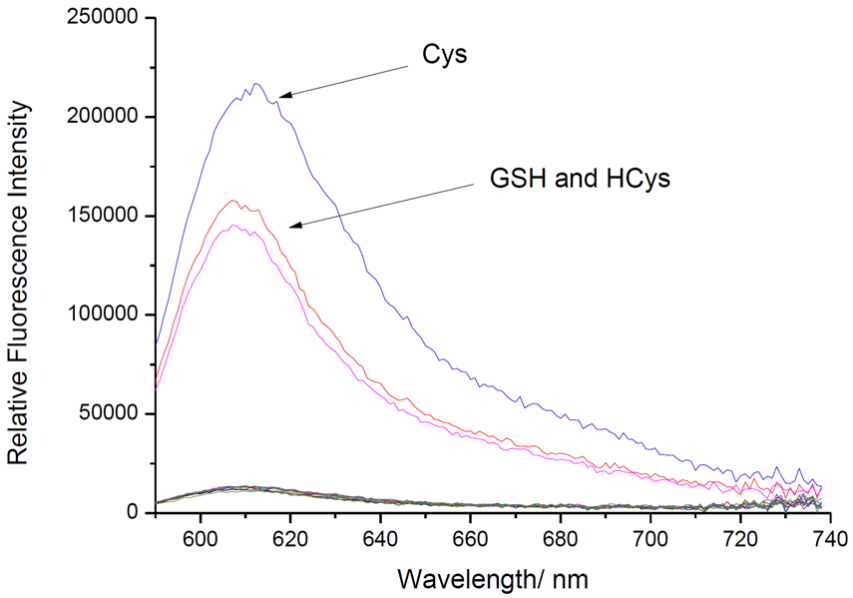

Figure 173 – Fluorescence spectra of **121** (5 µM) with addition of 100 µM GSH, Cys, Hcys and other amino acids after 15 min incubation. Carried out in PBS buffer (pH 8.0, 20 % DMSO), λ_{ex} 560 nm (bandwidth 15 nm).

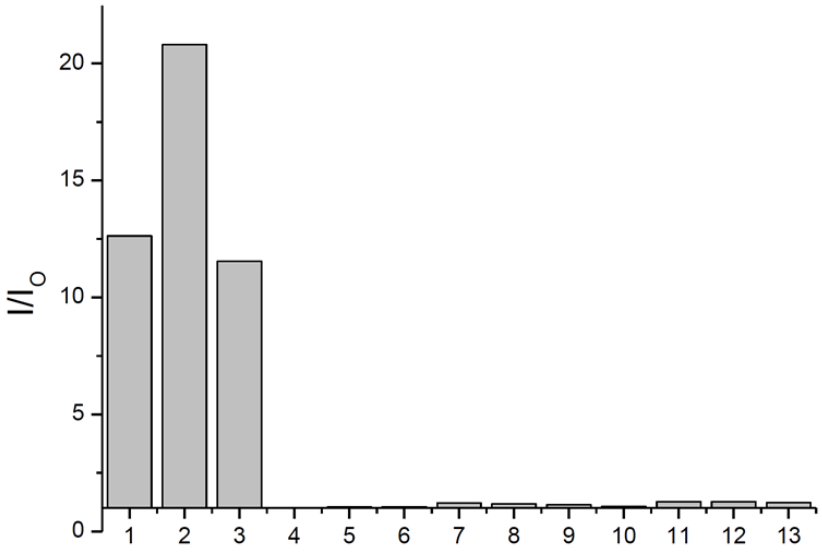

Figure 174 – Column chart for (I/I_0) of **121** (5 µM) with 100 µM 1) GSH, 2) Cys, 3) Hcys, 4) Negative control, 5) Pro, 6) Glut, 7) Ser, 8) Lys, 9) Arg, 10) Asp, 11) Phe, 12) Val, 13) Ile. Carried out in PBS buffer (pH 8.0, 20 % DMSO), λ_{ex} 560 nm (bandwidth 15 nm) / λ_{em} = 610 nm (bandwidth 20 nm).

The positive results for the analysis of **121** in solution-based assays led us to attempt to detect biological thiols in cell-based studies. **121** was sent to Professor Juyoung Yoon, Ewha Womans University, Seoul, Korea, for cellular assays to be carried out. Despite being sensitive towards GSH in the solution-based experiments, **121** only responded in an "turn on" manner when exposed to Cys exogenously in HeLa cells (**Figure 175**). Further to this, upon completion of cell viability experiments (**Figure 176**), it was found that **121** was toxic to the cells, breaking one of the fundamental requirements of fluorescence probes (**Section 1.3.2**), which ended the study into **121**.

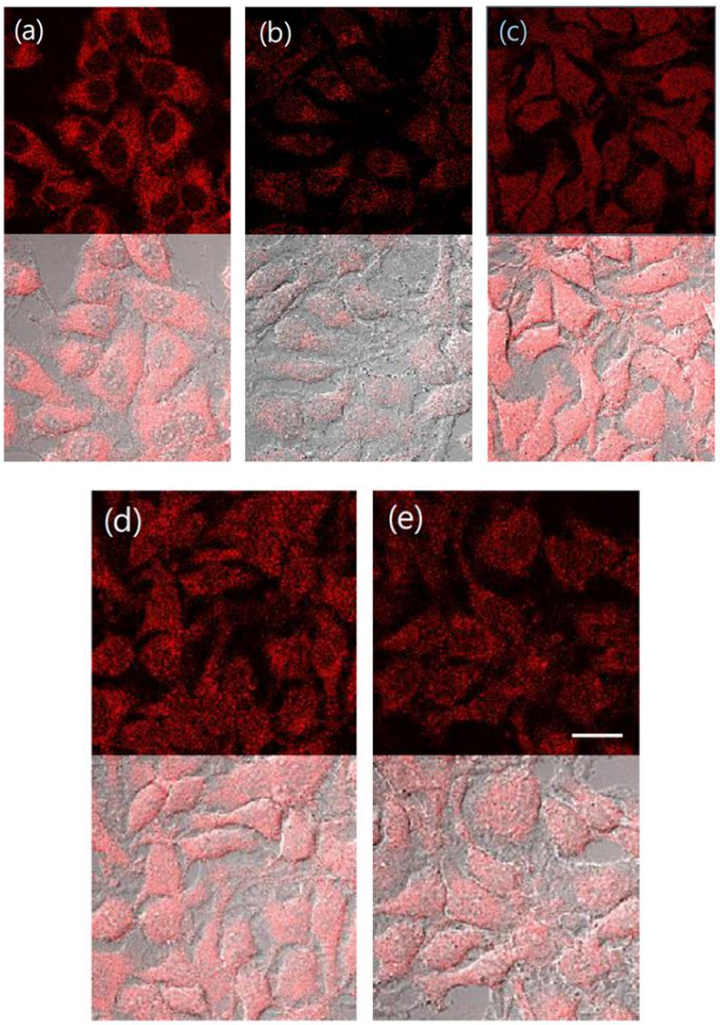

Figure 175 – Cell images of **121**. HeLa cells preincubated with 0.2 mM NMM for 20 min and washed with DPBS and incubated with 200 µM **121** for 20 min and acquired by confocal microscopy. a) **121**, b) NMM + **121**, c) NMM + Cys + **121**, d) NMM + Hcys + **121**, e) NMM + GSH-MEE + **121**. Top: fluorescence image (λ_{ex} 559 nm/ λ_{em} 575-676 nm). Bottom: merged image with DIC. Scale bar = 20 µm.

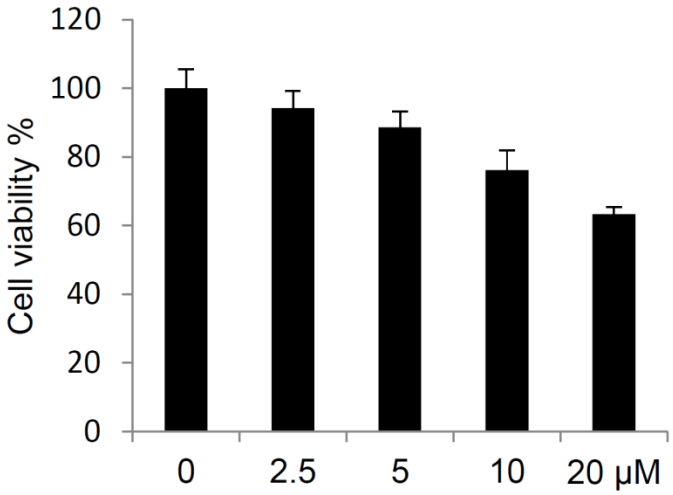

Figure 176 – Cell viability studies of **121**. Hela cells were incubated with varying concentrations of **121** for 24 h and assayed by MTT test. Results are a mean ± standard deviation of the three independent experiments.

4.3.3.2 Fluorescent Analysis of **122**

122 (5 μM) was exposed to increasing amounts of GSH (0-750 μM) with the predicted lower activity of **121** relative to **122** was evident from a larger concentration of GSH required to furnish a fluorescence response (**Figure 177**). Importantly, there was no decrease in the fluorescence intensity of **122** at the higher concentration of GSH used

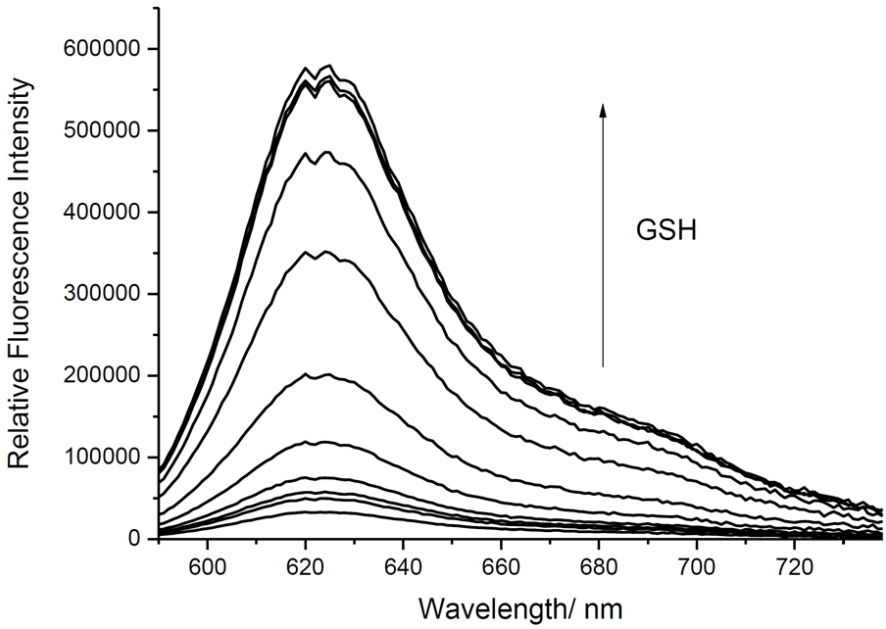

Figure 177 – Fluorescence spectra of **122** (5 μM) with addition of GSH (0-750 μM) and 15 min incubation. Carried out in PBS buffer (pH 8.0, 30 % DMSO), λ_{ex} 560 nm (bandwidth 15 nm).

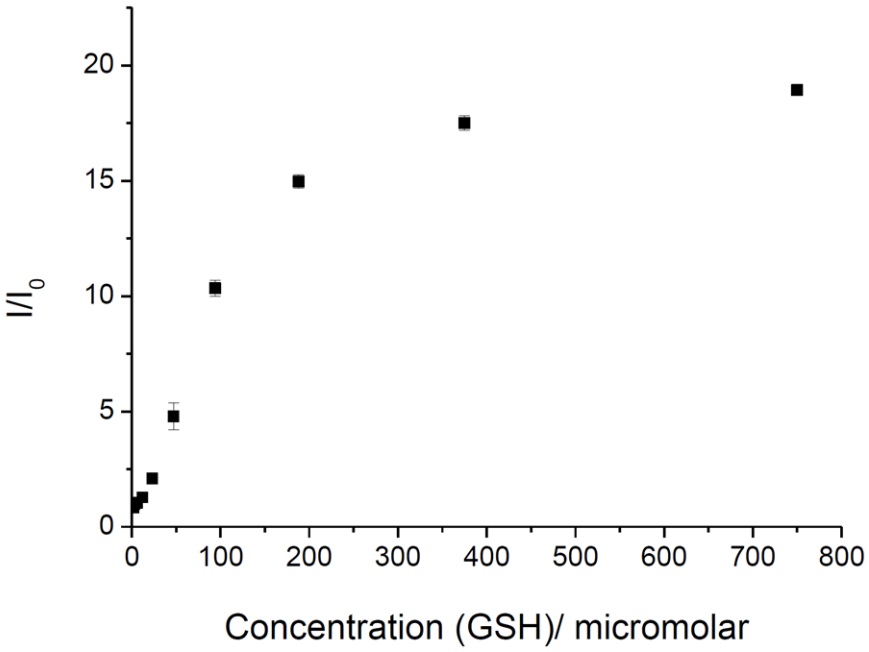

Figure 178 – Fluorescence intensity (I/I_0) of **122** (5 µM) and GSH (0-750 µM). Carried out in PBS buffer (pH 8.0, 20 % DMSO), λ_{ex} = 560 nm (bandwidth 15 nm) / λ_{em} = 610 nm (bandwidth 20 nm).

(**Figure 178**). This may be due to the lower reactivity of the resultant phenolate species of the probe due to the presence of the two appended chlorine atoms. From this data it was calculated that the LOD of **122** is 1.41 µM GSH.

The selectivity of **122** was then tested against the same selection of thiols and other amino acids previously used to test **122** (**Figure 179** & **Figure 180**). This revealed that **122** gave

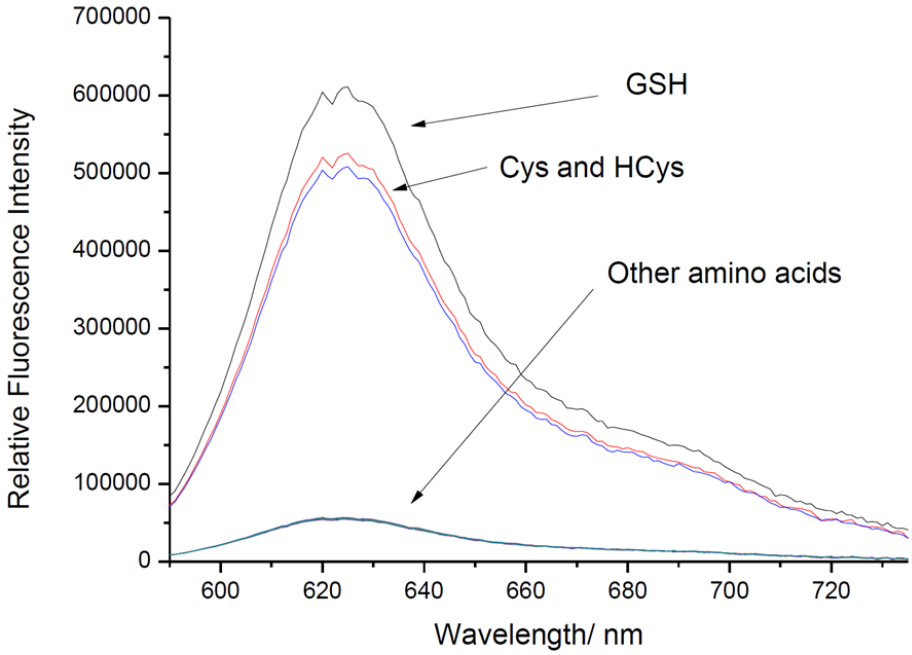

Figure 179 – Fluorescence spectra of **122** (5 µM) with addition of 100 µM GSH, Cys, Hcys and other amino acids after 15 min incubation. Carried out in PBS buffer (pH 8.0, 20 % DMSO), λ_{ex} 560 nm (bandwidth 15 nm).

positive results to GSH, Cys and Hcys, with negative results for all other amino acids that are commonly present in the cellular environment.

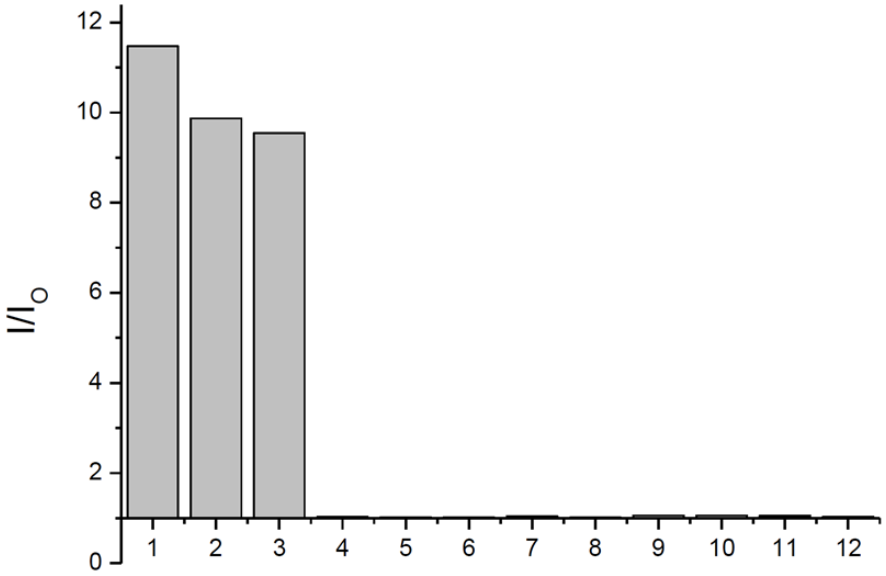

Figure 180 – Column chart for (I/I_0) of **122** (5 µM) with 100 µM 1) GSH, 2) Cys, 3) Hcys, 4) Negative control, 5) Pro, 6) Glut, 7) Ser, 8) Lys, 9) Arg, 10) Asp, 11) Phe, 12) Val, 13) Ile. Carried out in PBS buffer (pH 8.0, 20 % DMSO), λ_{ex} 560 nm (bandwidth 15 nm) / λ_{em} = 610 nm (bandwidth 20 nm).

The positive results from the in-solution assays gave enough evidence to justify testing **122** as a probe for biological thiols in cellular systems.

122 showed a significant signal when present in normal HeLa cells, without the presence endogenously and exogenous thiols (**Figure 181**, **a**). This is a result of the high concentration of intracellular endogenous thiols that are present in most cells. When the cells were pre-treated with the thiol reactive *N*-methylmaleimide (NMM) the resultant reduction in the amount of free thiol in cells, resulted in a lowering of the fluorescence signal observed (**Figure 181**, **b**). The addition of exogenous thiol (Cys, Hcys or GSH-Methyl ester, 200 µM) also caused a clear increase in fluorescence, demonstrating the ability of the probe to be used to detect the biologically relevant concentration levels of thiol in cells (**Figure 181**, **c**).

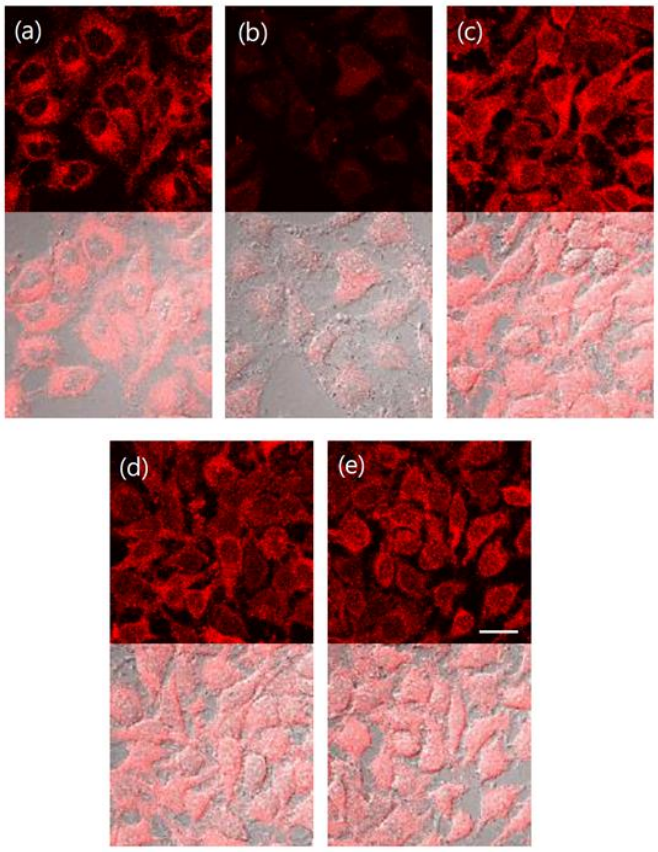

Figure 181 – Cell images of **122**. HeLa cells pre-incubated with 0.2 mM NMM for 20 min and washed with DPBS and incubated with 200 µM **122** for 20 min, with images then acquired by confocal microscopy. a) **122**, b) NMM + **122**, c) NMM + Cys + **122**, d) NMM + Hcys + **122**, e) NMM + GSH-MEE + **122**. Top: fluorescence image (λ_{ex} 559 nm/ λ_{em} 575-676 nm). Bottom: merged image with DIC. Scale bar = 20 µm.

These results were highly encouraging and showed that the probe could be used in cells, so the ability of **122** to detect endogenous thiols was then tested. HeLa cells were incubated with **122** and imaged (**Figure 182**). These cells were then exposed to H_2O_2 (500 µM) or Cisplatin (200 µM) to reduce the overall level of thiols in cells. This is achieved through the scavenging action of GSH when exposed to ROS species (H_2O_2). The nucleophilic thiol can also react with Cisplatin, replacing one of the chlorine atoms. In both cases, there was a marked reduction in the fluorescence level of the probe. Subsequent addition of *N*-Acetylcysteine (NAC, a GSH inducing drug) results in restoration of the fluorescence signal, thus demonstrating that **122** can detect endogenous changes in the levels of intracellular thiols in HeLa cells.

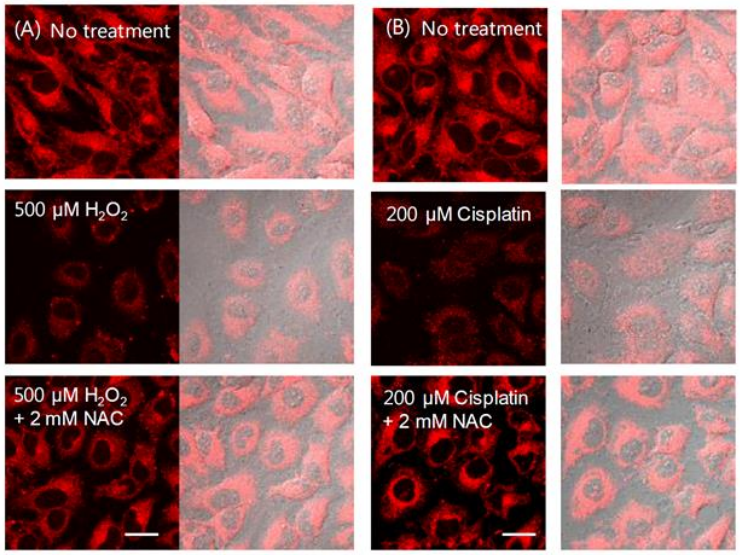

Figure 182 – Cell images of **122**. HeLa cells preincubated with 0.2 mM NMM for 20 min and washed with DPBS and incubated with 200 µM **122**for 20 min and images acquired by confocal microscopy. a) **122**, b) NMM + **122**, c) NMM + Cys + **122**, d) NMM + Hcys + **122**, e) NMM + GSH-MEE + **122**. Top: fluorescence image (λ_{ex} 559 nm/ λ_{em} 575-676 nm). Bottom: merged image with DIC. Scale bar = 20 µm.

Cell viability studies were then undertaken for **122 to** test its toxicity in cells (**Figure 183**). This showed that **122** was non-toxic to HeLa cells in the concentrations and duration tested.

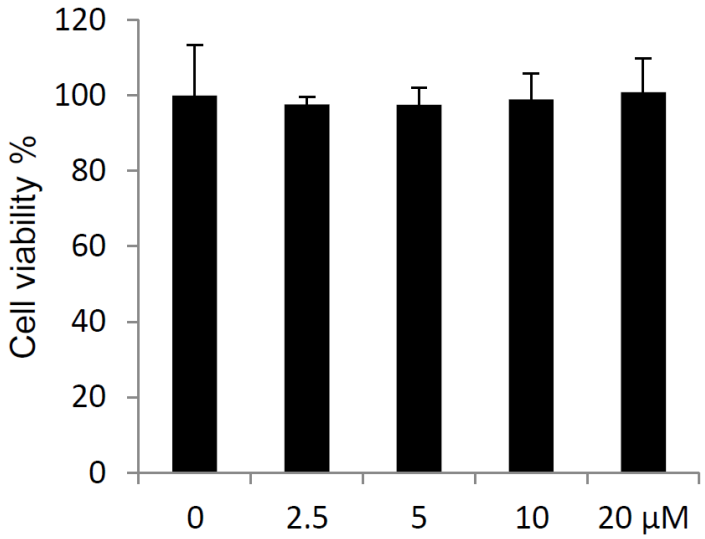

Figure 183 – Cell viability studies of **122**. Hela cells were incubated with varying concentrations of **122** for 24 h and assayed by MTT test. Results are a mean ± standard deviation of the three independent experiments.

4.3.4 Conclusion

In conclusion, two TCF-based thiol probes (**121** and **122**) have been designed, synthesized and analysed in solution and in cellular studies as sensors for biologically relevant thiols. **121** and **122** were both seen to be highly selective to the thiols in cellular systems. **121** was able to detect low concentrations of GSH but showed an unwanted drop in fluorescence intensity at higher concentrations. **122** on the other hand required a greater amount of GSH to turn on but showed no decrease in the level of signal at higher levels of GSH. In cell studies, **121** displayed poor solubility properties and was ultimately not useful for sensing thiols in cells. **122**, on the other hand, was soluble and could be used for fluorescent monitoring of exogenous and endogenous thiols in HeLa cells. This work has led to the publishing of an article in the RSC journal "*Chemical Communications*".[13]

4.4 Chapter conclusion

In this chapter, four new probes for the detection of both $ONOO^-$ and intracellular thiols have been designed, synthesised and analysed. **114** and **115** are two boronic acid pinacol ester functionalised TCF probes that are both highly sensitive to $ONOO^-$ in solution. **114** was not soluble in physiological conditions, but **115** showed favourable solubility and was used in cell studies. These cellular studies showed that **115** could be used to monitor $ONOO^-$ levels in four different cell lines, with endogenous and exogenous $ONOO^-$, and even monitor the levels of $ONOO^-$ within organelles of a cell.

121 and **122** are two new thiol reactive TCF based probes that are both sensitive and selective to intracellular thiols in solution. **121** was shown only to react to exogenous thiols in cellular experiments, and then was seen to be toxic to the cells. Alternatively, **122** was able to monitor the levels of endogenous and exogenous thiols in HeLa cells.

4.5 Chapter references

1: G. Melikian, F. P. Rouessac, C. Alexandre, *Synth. Commun.*, **1995**, *25*, 3045-3051.

2: A. Abbotto, L. Beverina, N. Manfredi, G. A. Pagani, G. Archetti, H. Kuball, C. Wittenburg, J. Heck, J. Holtmann, *Chem. Eur. J.*, **2009**, *15*, 6175-6185.

3: P. Gopalan, H. E. Katz, D. J. McGee, C. Erben, T. Zielinski, D. Bousquet, D. Muller, J. Grazul, Y. Olsson, *J. Am. Chem. Soc.*, **2004**, *126*, 1741-1747.

4: Y. Hao, Y. Zhang, K. Ruan, F. Meng, T. Li, J. Guan, L. Du, P. Qu, M. Xu, *Spectrochim. Acta A*, **2017**, *184*, 355-360.

5: L. Feng, Z. Liu, L. Xu, X. Lv, J. Ning, J. Hou, G. Ge, J. Cui, L. Yang, *Chem. Commun.*, **2014**, *50*, 14519-14522.

6: M. K. Lee, J. Williams, R. J. Tweig, J. Rao, W. E. Moener, *Chem. Sci.*, **2013**, *4*, 220-225.

7: X. Teng, M. Tian, J. Zhang, L. Tang, J. Xin, *Tett. Lett.*, **2018**, *59*, 2804-2808.

8: C. Staudinger, S. M. Borisov, *Methods Appl. Fluoresc.*, **2015**, *3*, 042005.

9: T. Yamada, I. Aoki, H. Miki, C. Yamada, *A. Omoto*, **2013**, *139*, 699-705.

10: J. Park, H. Kim, Y. Choi, Y. Kim, *Analyst*, **2013**, *138*, 3368-3371.

11: J. Bouffard, Y. Kim, T. M. Swager, R. Weissleder, S. A. Hilderbrand, *Org. Lett.*, **2008**, *10*, 37-40.

12: A. C. Sedgwick, H. Han, J. E. Gardiner, S. D. Bull, X. He, T. D. James, *Chem. Commun.*, **2017**, *53*, 12822-12825.

13: A. C. Sedgwick, J. E. Gardiner, G. Kim, M. Yevglevskis, M. D. Lloyd, T. A. Jenkins, S. D. Bull, J. Yoon, T. D. James, *Chem. Commun.*, **2018**, *54*, 4786-4789.

5.0 Conclusion and future work

A summation of fluorescence spectroscopy and the benefits of its use have been covered in the first chapter. Then, mechanisms of the common types of fluorescence are detailed, including ICT, PET and ESIPT. A number of analytes frequently targeted within the body are listed, and probes that have been developed to detect them are exemplified.

Over the proceeding chapters, a number of new fluorescent probes are designed, synthesised, analysed and discussed. These are split according to the main fluorescent core unit that was used in each. Coumarin (**Chapter 2**), fluorescein (**Chapter 3**) and TCF (**Chapter 4**) were the fluorophores that were used to build the new probes. In each of these chapters, a small introduction to the history of the fluorophore was given, along with their synthesis and examples of uses in previously developed probes.

In the second chapter, a number of coumarin-based fluorescent MLG probes were developed. Firstly, a Cys/Hcys "AND" $ONOO^-$ probe **42** was developed based on the work by Hong *et al.* This probe used a reactive Bpin unit and an aldehyde to produce a fluorescence response. It showed good sensitivity and selectivity in solution-based assays, but unfortunately is was shown to form insoluble aggregates in cell-based assays and was not suitable for desired purpose.

A second probe (**46**) was designed to detect NTR "AND" $ONOO^-$. This probe used a 4-nitro phenyl group and an aldehyde to as reactive groups to yield a fluorescence response. **46** has a good response in the presence of both NTR and Hcys, as seen in the solution-based assays. Further work on this probe, its selectivity and cellular studies are ongoing, with the aim of developing it to more selectively image hypoxic tissue.

57 was a three-input logic gate designed for the detection of $ONOO^-$, Glut and Zn^{2+}. It would achieve this by the cleavage of a Bpin unit, reaction of the probe with Glut and then coordination of this product with Zn^{2+}, causing a change in fluorescence. Initial solution-based studies show that **57** produces a sizable fluorescence response once exposed to all three of the analytes. Further work is needed to examine the selectivity of the probe and the potential use of **57** in cellular studies.

The last coumarin based probe **73** was intended to detect $ONOO^-$ "AND" GSH / Cys or Hcys. This probe would react with $ONOO^-$ and be able to distinguish between the smaller thiols (Cys and Hcys) and GSH. However, only the precursor **74** was synthesised due to

problems with solubility. However, initial results from **74** show that the compound has the ability to distinguish between the small thiols and GSH. Work on producing **73**, the $ONOO^-$ sensitive probe is ongoing. Once complete, studies into its reactivity, sensitivity and selectivity will be conducted.

Chapter three details fluorescein-based probes and starts with probe **90** that was developed for the dual detection of F^- and $ONOO^-$. -OTBDMS and Bpin groups were used as the reactive trigger units that would cleave upon exposure to the analytes and produce fluorescein, causing a fluorescence response. However, upon initial dilution of **90** into PBS buffer, fluorescence was observed. This was thought to be due to the high reactivity of the -OTBDMS group and its subsequent cleavage. Using **90** in THF for the analysis detection of F^- and $ONOO^-$ was more successful, with a dose dependent response observed to a pre-incubated solution of **90** and TBAF when titrated against $ONOO^-$. The lack of application of the sensor under physiological conditions caused the ceasing of investigations into the probe.

Two hydrazine-based probes were then investigated for sensitivity to $ONOO^-$. **93** is the simplest fluorescein-hydrazide which had previous sensitivity to Cu and HClO. **93** showed high sensitivity to $ONOO^-$ relative to other ROS/RNS, including HClO. A benzyl group was attached to the primary amine to form **96** and the fluorescence response was investigated. This was to determine if the fluorescein hydrazine group was suitable for further modification into an MLG and multi-analyte detection. However, a much lower fluorescent response was observed in addition to a lower selectivity to other ROS/RNS. Work in adding secondary functionality to **96** and producing an "AND" MLG is ongoing. **96** has many attachment points and could even be used to produce a triple input "AND" MLG.

A fluorescein based $ONOO^-$ "AND" NTR probe **97** was also described. This used the reactive 4-nitro phenyl group used in the previous probe **46**, as well as a Bpin unit. Initial investigations into the reactivity of **97** using Na_2SO_4 as reducing agent, in place of NTR, were unsuccessful. **97** has been sent to collaborators and we are awaiting the results from the analysis using NTR.

GSH and $ONOO^-$ were targeted in probe **103**, using 2,4-DNBS and Bpin reactive groups which cleave upon exposure, to yield fluorescein and a fluorescence response. This probe was seen to have an excellent response to the presence of both target analytes in solution-

based assays. Very high selectivity was also achieved, with very low off-target interactions being seen by other ROS/RNS or amino acids. Cell studies showed that the probe was also suitable for the detection of both these species *in vitro*. **103** was able to simultaneously detect exogenous GSH and $ONOO^-$ as well as GSH and $ONOO^-$ that was stimulated with SIN-1 and CA. Further work is being undertaken to attach directing groups to **103** so that the visualisation of specific organelles can be investigated. This work led to a publication in *"Chemical Science"*.

Two sets of TCF based probes were developed in the TCF chapter. The first two (**114** and **115**) are $ONOO^-$ probes that use the cleavage of a Bpin unit to yield an effective "push-pull" TCF fluorophore and a large fluorescent response. **114** was an effective in solution sensor for $ONOO^-$, being sensitive and selective against other ROS/RNS. However, it was found to be insoluble in cell-based experiments. **115** was also seen to be a highly sensitive and selective probe for the detection of $ONOO^-$ in solution.

Unlike **114**, however, **115** was found to be soluble under physiological conditions. It was used for the detection of endogenous and exogenous $ONOO^-$ in numerous cell lines and shown to activate in the area of the cell with high $ONOO^-$ concentration. **115** was also found not to be toxic *via* a cell viability assay. This work also led to a publication, in the RSC journal *"Chemical Communications"*.

Development of two thiol TCF based probes were documented next. **121** and **122** used the 2,4-DNBS group bound to TCF to furnish fluorescent responses when exposed to intracellular thiols. **121** was seen to have a good response to Cys, Hcys and GSH and soluble in cell studies, but it only responded to exogenously added GSH and was also found to be toxic to cells. **122** was structurally similar to **121**, with the addition of two chlorine atoms. This probe was slightly less sensitive to thiols in solution but was not toxic to cells. **122** was used to monitor the levels of exogenous and endogenous thiols in cellular experiments. This work was also proudly published in the RSC journal *"Chemical Communications".*

In conclusion, a variety of new probes for the detection of biologically relevant species have been detailed through the course of this thesis. These probes vary in their effectiveness with some being found unsuitable for cell studies, while others have been used to monitor exogenous and endogenous levels of target analytes. This work has led to the publishing of three articles in reputable scientific journals.

Further work on the development of a number of these probes could allow them to be used as tools for the investigation or early diagnosis of disease, as well as expand the development of MLG's and multi-analyte detection. New and expanded scopes and selectivities are being targeted in the lab, growing from work shown in this thesis and many more publications can be expected to result.

6.0 Experimental

6.1 General information

All reactions undertaken in this project were completed using standard laboratory conditions and good laboratory practice (GLP). Reactions were carried out in standard round bottom flasks (RBFs) unless otherwise stated and stirred with Teflon coated magnetic stir bars. Cooling was achieved either by ice bath (0 °C) or acetone and dry ice (-78 °C). Heating was carried out on a hot plate and a dry synth with a probe to ensure constant temperature. Büchi B-490 rotary evaporators and reduced pressure was used to remove solvents and an Edwards RV-12 was used to thoroughly dry compounds before analysis. Inert atmospheric conditions were created using an argon filled balloon attached to a sealed, argon flushed RBF. Utmost attempts were made to keep all reaction containing fluorophores hidden from ambient light using aluminium foil.

6.1.1Solvents and Reagents

All solvents and reagents were purchased from Sigma-Aldrich Company (Merk), Alfa Aesar, Fisher Scientific UK and Fluorochem. All solvents and reagents were reagent grade in purity and used without further purification. Anhydrous solvents dried on alumina columns by an Innovative Technology Inc. PS-400-7 solvent purification system and oven dried glassware was used where dry conditions were needed.

6.1.2 Thin Layer Chromatography (TLC)

TLC was performed using Merk aluminium backed Silica plates coated with a 0.2 mm layer of silica (60 Å) with a fluorescent indicator F254. Visualization of the TLC plates was achieved using ultraviolet light, where an aromatic moeity was present, or stained with potassium permanganate solution, ninhydrin solution, or iodine infused silica.

6.1.3 Silica Column Chromatography

Column chromatography was undertaken using Sigma-Aldrich 60 Å silica gel (35 – 75 μm). Conditions varied upon chemical mixture being purified and are stated for each of the compounds purified using this method.

6.1.4 ^{1}H Nuclear Magnetic Resonance (NMR) Spectra

Proton nuclear magnetic resonance spectroscopy (^{1}H NMR) was recorded at 500.06 MHz on an Agilent ProPulse NMR spectrometer an appropriate deuterated solvent purchased from either Sigma Aldrich or Alfa Aesar. Proton chemical shifts (δH) are quoted in parts per million (PPM) and are referenced to the residual solvent peak or an internal standard of tetramethylsilane. Coupling constants (J) are reported in Hertz and multiplicities using accepted abbreviations (singlet = s, doublet = d, triplet = t, quartet = q, quintet = quin, multiplet = m).

6.1.5 ^{13}C Nuclear Magnetic Resonance (NMR) Spectra

Carbon thirteen (^{13}C) nuclear magnetic resonance spectroscopy (^{13}C NMR) was recorded at 125.75 MHz on an Agilent ProPulse NMR spectrometer an appropriate deuterated solvent purchased from either Sigma Aldrich or Alfa Aesar. Carbon chemical shifts (δC) are quoted in parts per million (PPM) and are referenced to the residual solvent peak or an internal standard of tetramethylsilane. Coupling constants (J) are reported in Hertz.

6.1.6 Melting point

Capillary melting point determinations were carried out using Büchi 535 melting point apparatus and reported to the nearest degree Celsius.

6.1.7 Mass Spectrometry

High resolution mass spectroscopy (HRMS) results were typically acquired on an externally calibrated Bruker Daltonics micrOTOF time-of-flight mass spectrometer coupled to an electrospray source (ESI-TOF). Sodium formate solution was used as a standard for calibration. Samples were introduced using an autosampler system of an Agilent 1100 system. Bruker Daltonics software was used to process and analyse the data. The EPSRC National Mass Spectrometry Facility, Swansea University, was also used for MS analysis.

6.1.8 Fluorescence Measurements

Fluorescence Emission Measurements were performed on a BMG LABTECH CLARIO-star® high performance Microplate reader or a Perkin-Elmer Luminescence Spectrophotometer LS 50B/ LS 55 B utilising Starna Silica (quartz) cuvette with 10 mm path length, four faces polished. For the former, samples were loaded into a 96 well flat bottom 200 µL black polystyrene plate. Data were collected *via* the MARS software and exported in the format of Excel files for further data analysis. For the latter, data were collected *via* the Perkin-Elmer FL Winlab software package. All solvents used in fluorescence measurements were HPLC or fluorescence grade and the water was de-ionised. Further reprocessing of the data was carried in OriginPro 8.0 graph software.

6.1.9 pH Measurement

All pH measurements taken during fluorescence/absorption experiments were recorded on a Hanna Instruments HI 9321 Microprocessor pH meter which was routinely calibrated using Fisher Chemicals standard buffer solutions (pH 4.0 - phthalate, 7.0 - phosphate, and 10.0 - borate).

6.1.10 UV-Vis Measurement

UV-Vis Absorption measurements were performed on a Perkin-Elmer Lambda 20 Spectrophotometer, utilising Starna Silica (quartz) cuvette with 10 mm path lengths, two faces polished. Data was collected *via* the Perkin-Elmer UVWinlab software package. Further reprocessing of the data was carried in OriginPro 8.0 graph software. UV-Vis measurements were also obtained using a BMG LABTECH CLARIOstar® high

performance Microplate reader, using a transparent 96-well 200 µL plate. Data collected *via* the MARS software and exported into an excel format for analysis.

6.2 Synthesis of reactive oxygen species

6.2.1 Preparation of $^1O_2$

$^1O_2$ was generated by reacting H_2O_2 (1 mM) with NaClO (1 mM). The solution of H_2O_2 was added in one portion to the aqueous solution of NaClO and stir for 2 minutes, using the prepared solution immediately.

6.2.2 Preparation of ROO•

ROO• was generated from 2, 2'-azobis (2-amidinopropane) dihydrochloride (AAPH). AAPH is dissolved in di-ionised water and the solution is heated to 37 °C for 30 min to create a stock solution.

6.2.3 Preparation of $O_2^{\bullet-}$

$O_2^{\bullet-}$ was produced by dissolving KO_2 (1 eq.) and 18-crown-6 (2.5 eq.) in DMSO (5 mL). This produced a superoxide stock solution.

6.2.4 Preparation of HO•

The hydroxyl radical was generated using the Fenton reaction. Iron^{III} hypochlorite was added to a solution of H_2O_2 (10 eq., 37.0 wt. %). The solution changes colour to orange and is used immediately for analysis.

6.2.5 Preparation of $ONOO^-$

Peroxynitrite was produced by the reaction of a hydrogen peroxide with sodium nitrite and stabilised in a basic solution. To a cooled, stirred solution of NaOH (3 M, 0°C) was added KNO_2 (0.6 M), HCl (0.6 M) and H_2O_2 (0.7 M) simultaneously. The concentration of resultant yellow stock solution of peroxynitrite was determined by using an extinction coefficient of 1670 ±50 cm^{-1} M^{-1} at 302 nm in 0.5 M sodium hydroxide (aq.).

6.2.6 Preparation of $^{-}$OCl and H_2O_2

Concentrations of stock solutions of $^{-}$OCl were determined *via* UV/Vis analysis from the absorption at 292 nm using the extinction coefficient 350 cm^{-1} M^{-1}. H_2O_2 stock solution concentrations were calculated in the same manner using the absorption at 240 nm and an extinction coefficient of 43.6 cm^{-1} M^{-1}.

6.3 Synthesis

6.3.1 Synthesis for Coumarin probes

2-Oxo-2H-chromen-7-yl acetate (**43**):

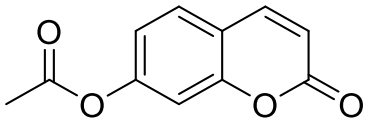

Umbelliferone (4 g, 22.2 mmol) was dissolved in EtOAc (100 mL) and stirred, while pyridine (2 mL, 24.6 mmol) was added. Acetic anhydride (8 mL, 82 mmol) was added slowly and the reaction mixture stirred for 90 minutes. After consumption of starting material, the reaction was poured into water (200 mL) and stirred for 30 minutes. The mixture was extracted with EtOAc (3×100 mL) and the organic layer was washed with 1 M aq HCl (100 mL), saturated aq. $NaHCO_3$ (100 mL) and brine (100 mL), dried over $MgSO_4$ and solvent removed *in vacuo* to yield 2-Oxo-2H-chromen-7-yl acetate (**43**) (4.44 g, 21.7 mmol, 98 % yield) with no further purification. M.p. 143-146 °C; ^{1}H NMR (500 MHz, $CDCl_3$) δ 7.68 (d, J = 9.6 Hz, 1H), 7.48 (d, J = 8.4 Hz, 1H), 7.11 (d, J = 2.2 Hz, 1H), 7.05 (dd, J = 8.4, 2.2 Hz, 1H), 6.39 (d, J = 9.6 Hz, 1H), 2.34 (s, 3H); ^{13}C NMR (100 MHz, $CDCl_3$) δ 168.6, 160.3, 154.7, 153.4, 142.8, 128.5, 118.3, 116.1, 110.4, 21.1; I.R (thinfilm) ν max (cm^{-1}): 1732.20 (C=O) 1619.69 (C=O); HRMS (TOF MS ASAP+): m/z calculated for $C_{11}H_9O_4$: requires 205.0495 for $[M+H]^+$, found 205.049.

7-Hydroxy-2-oxo-2H-chromene-8-carbaldehyde (**41**):

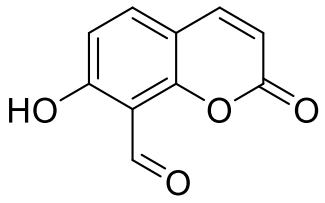

2-Oxo-2H-chromen-7-yl acetate (**43**) (1.5 g, 7.35 mmol) was dissolved in trifluoroacetic acid (10 mL) at 0 °C and hexamethylenetetramine (1.5 g, 10.7 mmol) was added. The mixture was heated to reflux overnight. The solvent was then removed *in vacuo* and the residue taken up in water (30 mL). This mixture was then heated to 60 °C for 30 min then cooled to RT. Upon cooling a yellow precipitate formed, that was collected *via* filtration to yield 7-Hydroxy-2-oxo-2H-chromene-8-carbaldehyde (**41**) (0.96 g, 5.05 mmol, 69%). M.p. 151-152 °C; ^{1}H NMR (500 MHz, DMSOd$_6$) δ 10.40 (s, 1H), 7.99 (d, J = 9.6 Hz, 1H), 7.84 (d, J = 8.7 Hz, 1H), 6.93 (d, J = 8.7 Hz, 1H), 6.34 (d, J = 9.6 Hz, 1H); ^{13}C NMR (126 MHz, DMSOd$_6$) δ 191.22, 164.33, 159.51, 156.09, 144.91, 136.65, 114.35, 112.98, 111.57, 109.62; I.R (thinfilm) ν max (cm^{-1}): 3076.23(OH), 1726.43 (C=O), 1597.58 (C=O); HRMS (TOF MS ASAP-): m/z calculated for $C_{10}H_5O_4^-$: requires 189.0254 for [M-H]$^-$, found 189.0249.

2-Oxo-7-((4-(4,4,5,5-tetramethyl-1,3,2-dioxaborolan-2-yl)benzyl)oxy)-2H-chromene-8-carbaldehyde (**42**):

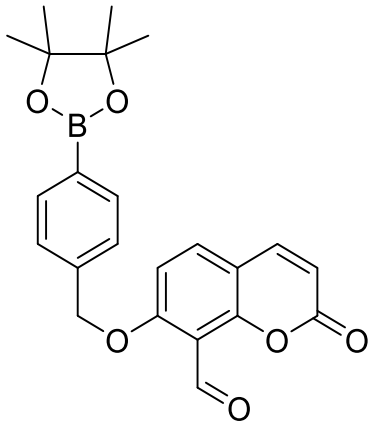

7-Hydroxy-2-oxo-2H-chromene-8-carbaldehyde (**41**) (100 mg, 1.05 mmol) was dissolved in DMF (5 mL) and K_2CO_3 (215 mg, 3.15 mmol) was added while stirring. 2-(4-(bromomethyl)phenyl)-4,4,5,5-tetramethyl-1,3,2-dioxaborolane (343 mg, 1.157 mmol) was then added and the reaction was stirred for four hours at RT. When complete, the reaction was poured into water (50 mL) and stirred for 10 minutes. The mixture was filtered to yield a yellow solid. This solid was purified by column chromatography MeOH: DCM (5: 95) to yield pure 2-oxo-7-((4-(4,4,5,5-tetramethyl-1,3,2-dioxaborolan-2-yl)benzyl)oxy)-2H-chromene-8-carbaldehyde (**42**) (217 mg, 0.53 mmol, 51%). M.p. 212-216 °C; ^{1}H NMR (500 MHz, $CDCl_3$) δ 10.70 (s, 1H), 7.83 (d, J = 8.0 Hz, 2H), 7.61 (d, J = 9.6 Hz, 1H), 7.55 (d, J = 8.8 Hz, 1H), 7.44 (d, J = 7.9 Hz, 2H), 6.93 (d, J = 8.8 Hz, 1H), 6.31 (d, J = 9.6 Hz, 1H), 5.31 (s, 2H), 1.34 (s, 12H); ^{13}C NMR (126 MHz, $CDCl_3$) δ 186.66, 162.24, 159.39, 155.78, 142.87, 138.23, 135.22, 133.81, 126.04, 114.22, 113.28, 112.80, 109.60, 83.91, 71.13, 53.40, 24.84. M.P. 212-216 °C; I.R (thinfilm) ν max (cm^{-1}): 1720.03 (C=O), 1690.84 (C=O); HRMS (TOF MS ASAP+): m/z calculated for $C_{23}H_{23}BNaO_6$: requires 429.1484 for $[M+Na]^+$, found 429.1454.

7-((4-Nitrobenzyl)oxy)-2-oxo-2H-chromene-8-carbaldehyde (**46**):

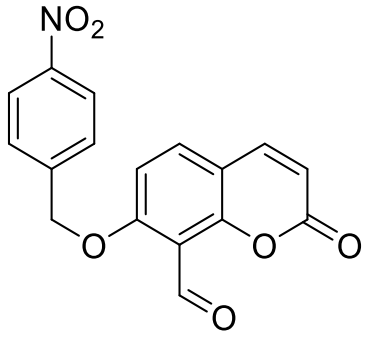

7-Hydroxy-2-oxo-2H-chromene-8-carbaldehyde (**41**) (100 mg, 1.05 mmol) was dissolved in DMF (5 mL) and K_2CO_3 (215 mg, 3.15 mmol) was added while stirring. 4-nitrobenzylbromide (249 mg, 1.157 mmol) was then added and the reaction was stirred for four hours at RT. When complete, the reaction was poured into water (50 mL) and stirred for 10 minutes. The mixture was filtered to yield a yellow solid. This solid was recrystallised in MeOH/ DCM to yield pure 2-oxo-7-((4-(4,4,5,5-tetramethyl-1,3,2-dioxaborolan-2-yl)benzyl)oxy)-2H-chromene-8-carbaldehyde (**46**) (161 mg, 49%). M.p. 238-241 °C; ^{1}H NMR (500 MHz, DMSOd_6) δ 10.55 (s, 1H), 8.27 (d, J = 8.8 Hz, 2H), 8.03 (d, J = 9.6 Hz, 1H), 7.96 (d, J = 8.8 Hz, 1H), 7.80 (d, J = 8.8 Hz, 2H), 7.29 (d, J = 8.9 Hz, 1H), 6.4 (d. J = 9.6 Hz, 1H), 5.53 (s, 2H); 13C NMR (126 MHz, DMSOd_6) δ 187.18, 162.01, 159.61, 155.05, 147.58, 144.61, 144.28, 135.59, 128.46, 124.12, 114.01, 113.42, 112.76, 110.51, 69.85; M.P. 238-241 °C; I.R (thinfilm) ν max (cm^{-1}): 1724.05 (C=O), 1685 (C=O), 1513 (N-O); HRMS (TOF MS ASAP-): m/z calculated for $C_{17}H_{12}NO_6^+$: requires 326.0659 for $[M+H]^+$, found 326.0695.

3-Methyl-7-propionyl-2H-chromen-2-one (**59**):

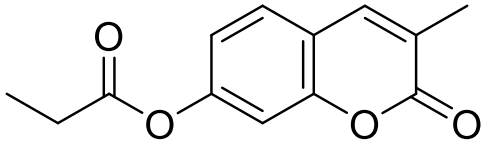

2,4-Dihydroxybenzaldehyde (3.0 g, 21.7 mmol), sodium propionate (4.5 g, 46.8 mmol), piperidine (0.4 mL) and propanoic anhydride (7.54 mL) were added to together and heated to reflux for 3 hrs. The resulting solution was poured into ice water (100 mL) and the precipitate filtered. The precipitate was taken up in ethyl acetate (50 mL), washed with 1 M HCl (50 mL) and water (3 x 50 mL). The solution was dried with $MgSO_4$ and concentrated in vacuo to afford the pure product **59** as a cream solid (1.5 g, 4.64 mmol, 30 %). M.p. 135-137 ˚C; ^{1}H NMR (500 MHz, $CDCl_3$) δ 7.49 (d, J = 1.7 Hz, 1H), 7.40 (d, J = 8.4 Hz, 1H), 7.07 (d, J = 2.2 Hz, 1H), 7.00 (dd, J = 8.5, 2.2 Hz, 1H), 2.61 (q, J = 7.5 Hz, 2H), 2.19 (d, J = 1.4 Hz, 3H), 1.27 (t, J = 7.5 Hz, 3H); ^{13}C NMR (126 MHz, $CDCl_3$) δ 172.38, 161.89, 153.68, 152.15, 138.69, 127.53, 125.15, 118.20, 117.30, 109.94, 27.70, 17.10, 8.90; IR (thin film) ν max (cm^{-1}) 1760.87, 1712.73 (C=O); FTMS (p ESI): m/z calculated for $C_{13}H_{12}O_4$ requires 233.080 for $[M+H]^+$, found 233.0807.

3-(Bromomethyl)-7-propionyl-2H-chromen-2-one (**60**):

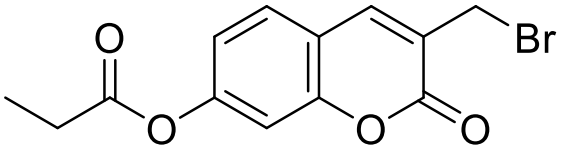

3-Methyl-7-propionyl-2H-chromen-2-one (**59**) (1.5 g, 6.46 mmol), N-bromosuccinimide (2.3 g, 12.9 mmol) and AIBN (0.11 g, 0.65 mmol) were added to acetonitrile and heated to reflux for 3 hrs. The reaction was cooled and concentrated in vacuo and diluted with DCM (50 mL) and washed with $NaHCO_3$ (50 mL), water (3 x 25 mL) and brine (50 mL). The solution was dried with $MgSO_4$ and solvent removed in vacuo to afford the product (**60**) as a white solid (0.99g, 3.1 mmol, 48 %). M.p. 118-120 ˚C; ^{1}H NMR (500 MHz, $CDCl_3$) δ 7.84 (d, J = 0.8 Hz, 1H), 7.51 (d, J = 8.4 Hz, 1H), 7.14 (d, J = 2.3 Hz, 1H), 7.08 (dd, J = 8.5, 2.2 Hz, 1H), 4.42 (d, J = 0.8 Hz, 2H), 2.63 (q, J = 7.5 Hz, 2H), 1.28 (t, J = 7.5 Hz, 3H); ^{13}C NMR (126 MHz, $CDCl_3$) δ 159.55, 154.33, 153.53, 141.32, 128.69, 124.84, 118.74, 116.56, 110.25, 27.73, 27.42, 25.16, 8.88. IR (thin film) ν max (cm^{-1}) 1761.92, 1722.78 (C=O); FTMS (p ESI): m/z calculated for $C_{13}H_{11}O_4Br$ requires 332.9733 for $[M+Na]^+$, found 332.9737.

(7-Acetyl-2-oxo-2H-chromen-3-yl)methyl acetate (**61**):

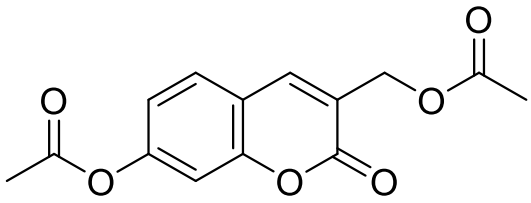

3-(Bromomethyl)-7-propionyl-2H-chromen-2-one (**60**) (0.8 g, 2.5 mmol) and sodium acetate (0.62 g, 7.5 mmol) were added to acetic anhydride (10 mL). The reaction was heated to reflux and monitored *via* TLC. Once complete, after 2 h, the reaction was cooled to 100 ºC and filtered while hot. Residual acetic anhydride was removed in vacuo and azeotroped with toluene to afford the final compound (**61**) as a brown solid (0.6 g, 2.17 mmol, 71 %). M.p. 140-142 ºC; ^{1}H NMR (500 MHz, $CDCl_3$) δ 7.74 (q, J = 1.0 Hz, 1H), 7.50 (d, J = 8.5 Hz, 1H), 7.13 (d, J = 2.2 Hz, 1H), 7.07 (dd, J = 8.5, 2.2 Hz, 1H), 5.06 (d, J = 1.2 Hz, 2H), 2.34 (s, 3H), 2.15 (s, 3H); ^{13}C NMR (126 MHz, $CDCl_3$) δ 170.49, 168.61, 159.88, 154.09, 153.12, 140.23, 128.69, 123.06, 118.59, 116.53, 110.21, 61.08, 21.10, 20.86; IR (thin film) ν max (cm^{-1}) 1758.51, 1741.63, 1712.10 (C=O); FTMS (p ESI): m/z calculated for $C_{14}H_{12}O_6$ requires 299.0526 for $[M+Na]^+$, found 299.0558.

7-Hydroxy-3-(hydroxymethyl)-2H-chromen-2-one (**62**):

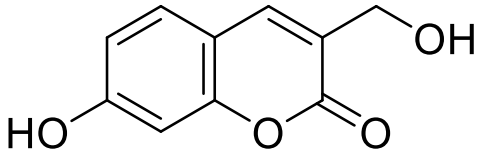

(7-Acetyl-2-oxo-2H-chromen-3-yl)methyl acetate (**61**) (1.5 g, 5.4 mmol) was dissolved in methanol (60 mL) and cooled to 0 ºC. Potassium acetate (2.3 g, 16.3 mmol) was added and the reaction was left for 1 hr. The solvent was removed in vacuo and diluted with water (20 mL). The resulting solution was acidified to pH 3 and the pure product (**62**) precipitated as a brown solid (1.1 g, 5.7 mmol, 90 %). M.p. 201-203 ºC; ^{1}H NMR (500 MHz, DMSO-d_6) δ 10.46 (s, 1H), 7.83 (s, 1H), 7.54 (d, J = 8.4 Hz, 1H), 6.77 (dd, J = 8.5, 2.3 Hz, 1H), 6.71 (d, J = 2.3 Hz, 1H), 5.31 (s, 1H), 4.29 (s, 2H); ^{13}C NMR (126 MHz, DMSO-d_6) δ 160.94, 160.61, 154.71, 138.38, 129.73, 124.72, 113.54, 111.94, 102.30, 58.57; IR (thin film) ν max (cm^{-1}) 3417.87 (O-H); FTMS (p ESI): m/z calculated for $C_{10}H_8O_4$ requires 215.0315 for $[M+Na]^+$, found 215.0307.

3-(Hydroxymethyl)-7-((4-(4,4,5,5-tetramethyl-1,3,2-dioxaborolan-2-yl)benzyl)oxy)-2H-chromen-2-one (**63**):

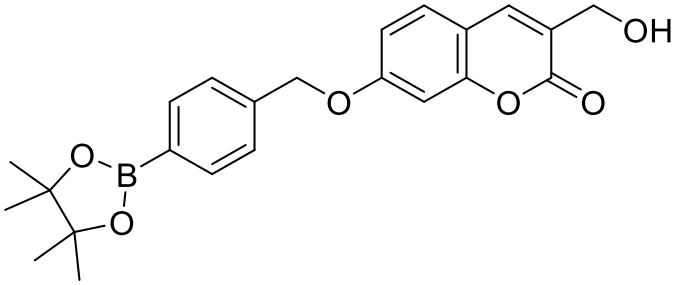

7-Hydroxy-3-(hydroxymethyl)-2H-chromen-2-one (**62**) (0.35 g, 1.82 mmol), 2-(4-(bromomethyl)phenyl)-4,4,5,5-tetramethyl-1,3,2-dioxaborolane (0.56 g, 1.91 mmol) and K_2CO_3 (0.50 g, 3.64 mmol) were added to DMF (5 mL) and stirred overnight. The reaction mixture was then diluted with EtOAc (25 mL), washed with water (3 x 50 mL) and brine (2 x 20 mL), dried with $MgSO_4$ and concentrated in vacuo. The final product was purified using column chromatography EtOAc: Pet Ether (40:60) to afford a white solid (**63**) (0.246 g, 0.74 mmol, 41 %). M.p. 198-200 ºC; ^{1}H NMR (500 MHz, $CDCl_3$) δ 7.86 – 7.82 (m, 2H), 7.66 (d, J = 1.4 Hz, 1H), 7.44 – 7.41 (m, 2H), 7.39 (d, J = 8.6 Hz, 1H), 6.92 (dd, J = 8.6, 2.4 Hz, 1H), 6.88 (d, J = 2.4 Hz, 1H), 5.15 (s, 2H), 4.58 (d, J = 1.2 Hz, 2H), 1.34 (s, 12H); ^{13}C NMR (126 MHz, $CDCl_3$) δ 161.68, 161.49, 154.92, 138.92, 138.77, 135.16, 128.79, 126.54, 124.38, 113.46, 112.85, 101.79, 83.89, 70.41, 61.32, 24.85; IR (thin film) ν max (cm^{-1}): 3407.94 (O-H), 1698.17 (C=O); FTMS (p ESI): m/z calculated for $C_{23}H_{25}BO_6$ requires 431.1640 for $[M+Na]^+$, found 431.1641.

2-Oxo-7-((4-(4,4,5,5-tetramethyl-1,3,2-dioxaborolan-2-yl)benzyl)oxy)-2H-chromene-3-carbaldehyde (**57**):

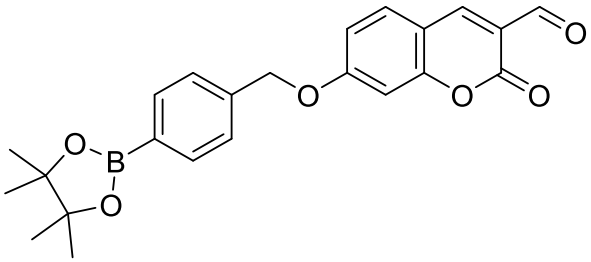

To a stirred solution of 3-(hydroxymethyl)-7-((4-(4,4,5,5-tetramethyl-1,3,2-dioxaborolan-2-yl)benzyl)oxy)-2H-chromen-2-one (**63**) (100 mg, 0.246 mmol) in dichloromethane (5 mL) was added (2,2,6,6-Tetramethylpiperidin-1-yl)oxyl or (2,2,6,6-tetramethylpiperidin-1-yl)oxidanyl (TEMPO) (7.6 mg, 0.049 mmol) and Bis(acetoxy)iodobenzene (BAIB) (118.9 mg, 0.369 mmol). The reaction was stirred for 16 hrs at rt, then the solvent was removed, and purification of the crude material was achieved by column chromatography EtOAc: Pet Ether (40:60) to yield the pure product (**57**) as an off-white powder (63 mg, 0.155 mmol, 63%). M.p. 178-181 ºC; ^{1}H NMR (500 MHz, $CDCl_3$) δ 10.20 (s, 1H), 8.36 (s, 1H), 7.85 (d, J = 8.2 Hz, 2H), 7.57 (d, J = 8.8 Hz, 1H), 7.42 (d, J = 8.1 Hz, 2H), 6.99 (dd, J = 8.7, 2.4 Hz, 1H), 6.90 (d, J = 2.4 Hz, 1H), 5.20 (s, 2H), 1.35 (s, 13H); ^{13}C NMR (126 MHz, $CDCl_3$) δ 187.75, 164.71, 160.52, 157.90, 145.63, 138.06, 135.26, 132.10, 126.58, 118.49, 114.74, 112.14, 101.96, 83.94, 70.79, 24.85; IR (thin film) ν max (cm^{-1}): 3069.75 (C=C=H), 1719.25 (C=O), 1596.44 (C=O); FTMS (p ESI): m/z calculated for $C_{23}H_{23}BO_6$ requires 42901484 for $[M+Na]^+$, found 429.1488.

4,7-Dihydroxy-2H-chromen-2-one (**77**):

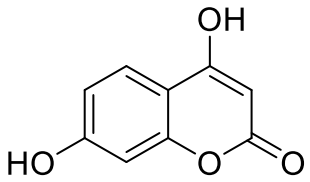

A mixture of resorcinol (5.5 g, 50 mmol), malonic acid (6.15 g, 59 mmol), anhydrous zinc chloride (22 g, 160 mmol), and phosphorus oxychloride (20 mL) was heated with stirring at 60-65 ℃ for 35 h. After cooling to RT the mixture was poured into ice-water and stirred. The crude product precipitate was collected and dissolved in 10% sodium carbonate. An oily by-product was removed, and acidification of the remaining solution gave the residues which were recrystallized from EtOAc to yield (**77**) (4.859 g, 27.3 mmol, 54 %). M.p. 277-280 °C; ^{1}H NMR (500 MHz, DMSOd_6) δ 12.25 (br, 1H), 10.49 (s, 1H), 7.61 (d, J = 8.7 Hz, 1H), 6.75 (d, J = 8.7 Hz, 1H), 6.55 (s, 1H), 5.37 (s, 1H); ^{13}C NMR (126 MHz, DMSOd_6) δ 167.0, 156.8, 140.1, 137.9, 131.6, 128.3, 127.9, 126.9, 119.8; I.R (thinfilm) ν max (cm^{-1}): 3238.46 (O-H), 3214.28 (O-H),1635.86 (C=O); HRMS (TOF MS ASAP^{+}): m/z calculated for $C_9H_6O_4$: requires 178.0266 for $[M-H]^-$, found 177.0216.

4-Chloro-7-hydroxy-2-oxo-2H-chromene-3-carbaldehyde (**73**):

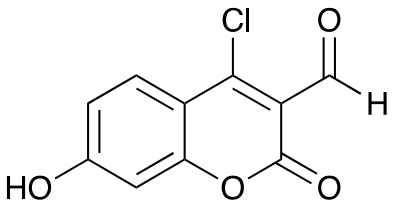

4,7-Dihydroxy-2H-chromen-2-one (**77**) (200 mg, 1.12 mmol) was dissolved in DMF (1 mL) and warmed to 30 °C for 5 minutes, phosphoryl chloride (0.26 ml, 3.05 mmol) was then added to the solution; stir continuously at 40 ℃ for 40 minutes. The mixture was then cooled to RT, poured into water (100 mL) and stirred for another hour. The precipitate was filtered, washed with water (30 mL) and dried *in vacuo* to obtain compound **73** as product (140 mg, 62 mmol, 56 %). M.p. 209-212 °C; ^{1}H NMR (500 MHz, Acetone-d_6) δ 10.24 (s, 1H), 8.06 (d, J = 8.9 Hz, 1H), 7.05 (d, J = 11.3 Hz, 1H), 6.85 (d, J = 2.3 Hz, 1H); ^{13}C NMR (126 MHz, Acetone-d_6) δ 166.75, 162.90, 162.22, 155.86, 124.87, 112.99, 108.14, 102.42, 88.26; I.R (thinfilm) ν max (cm^{-1}): 3224.95 (O-H), 1721.36 (C=O); HRMS (TOF MS ASAP^{+}): m/z calculated for $C_{10}H_5ClO_4$: requires 223.9876 for [M-H+Na]$^{-}$, found 245.9689.

6.3.2 Synthesis for Fluorescein probes

3'-Hydroxy-3-oxo-3H-spiro[isobenzofuran-1,9'-xanthen]-6'-yl trifluoromethanesulfonate (**91**):

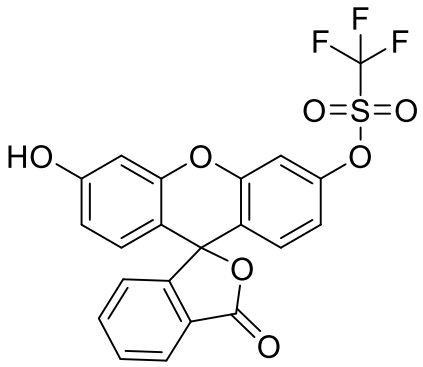

Fluorescein (4.00 g, 11.6 mmol) and N-Phenyl bis(trifluoromethanesulfonamide) (4.2 g, 11.6 mmol) were dissolved in anhydrous DMF (20 mL) and flushed with nitrogen. Diisopropylethylamine (7.4 mL) was then added and the reaction mixture was stirred for 48 h. The reaction mixture was quenched with 1 M HCl (200 mL) and extracted with EtOAc (3 x 200 mL). The combined organic layers were dried with $MgSO_4$ and concentrated in-vacuo to give crude material. The crude was purified *via* column chromatography EtOAc/ Pet Ether (30:70) and yielded the title compound (**91**) as a white solid (2.32 g, 4.81 mmol, 43 %). M.p. 139-142 ^{o}C; ^{1}H NMR (300 MHz, DMSO-d_6) d 10.30 (br. s., 1 H,), 8.05 (d, J = 7.0 Hz, 1 H), 7.87 - 7.67 (m, 4 H), 7.38 (d, J = 7.5 Hz, 1 H,), 7.24 (dd, J = 2.6, 8.9 Hz, 1 H), 7.02 (d, J = 8.9 Hz, 1 H), 6.78 - 6.72 (m, 1 H), 6.63 (s, 2 H); ^{13}C NMR (75.5 MHz, DMSO-d_6) d 168.8, 160.2, 152.4, 151.7, 151.6, 150.0, 136.3, 130.9, 129.6, 125.9, 125.3, 124.5, 120.7, 120.2, 117.6, 116.4, 113.8, 111.1, 109.1, 102.6, 81.6, 60.1; I.R (thinfilm) ν max (cm^{-1}): 3389.62 (O-H), 1736.19 (C=O); HRMS (TOF MS ASAP^{+}): m/z calculated for $C_{21}H_{11}F_3O_7S$: requires 465.0256 for $[M+H]^{+}$, found 465.0256.

3'-Hydroxy-6'-(4,4,5,5-tetramethyl-1,3,2-dioxaborolan-2-yl)-3H-spiro[isobenzofuran-1,9'-xanthen]-3-one (**92**):

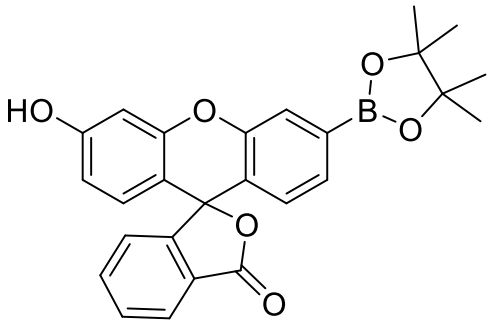

To a solution of 3'-hydroxy-3-oxo-3H-spiro[isobenzofuran-1,9'-xanthen]-6'-yl trifluoromethanesulfonate (**91**) (0.630 g, 1.36 mmol) in anhydrous DMF (10 mL) was added Bis(pinacolato) diboron (0.62 g, 2.44 mmol), KOAc (0.80 g, 8.15 mmol) and Pd(dppf)Cl_2.DCM (0.10 g, 0.14 mmol). The mixture was degassed with N_2 and heated at 95 ^oC under N_2 for 16 h. The reaction mixture was then cooled to rt and EtOAc (100 mL) and H_2O (100 mL) were added. The aqueous layer was extracted with EtOAc (2 x 100 mL). The combined organics were then washed with H_2O (2 x 100 mL), brine (100 mL) and dried ($MgSO_4$) and concentrated in-vacuo to afford the crude material. The crude material was purified *via* column chromatography EtOAc: Pet Ether (10:90 to 40:60) to afford the title compound (**92**) as a pale clear oil (0.15 g, 0.34 mmol, 25 %). ^{1}H NMR (500 MHz, $CDCl_3$ J = 7.3 Hz, 1 H), 7.73 (s, 1 H), 7.68 - 7.59 (m, 2 H), 7.43 (d, J = 7.8 Hz, 1 H), 7.14 (d, J = 7.3 Hz, 1 H), 6.81 - 6.76 (m, 2 H), 6.65 (d, J = 8.8 Hz, 1 H), 6.56 (dd, J = 2.2, 8.6 Hz, 1 H), 1.36 (s, 12 H); $_{13}$C NMR (125.75 MHz, $CDCl_3$) 170.0, 158.2, 153.4, 152.4, 150.7, 135.2, 129.8, 129.3, 129.2, 127.2, 126.3, 125.1, 123.9, 123.5, 121.4, 112.4, 110.6, 103.3, 84.3, 24.8, 24.8; I.R (thinfilm) ν max (cm^{-1}): 1746.51 (C=O); HRMS (TOF MS ASAP$^+$): m/z calculated for $C_{26}H_{23}BO_6$: requires 442.1702 for $[M+H]^+$, found 442.1700.

3'-((Tert-butyldimethylsilyl)oxy)-6'-(4,4,5,5-tetramethyl-1,3,2-dioxaborolan-2-yl)-3H-spiro[isobenzofuran-1,9'-xanthen]-3-one (**90**):

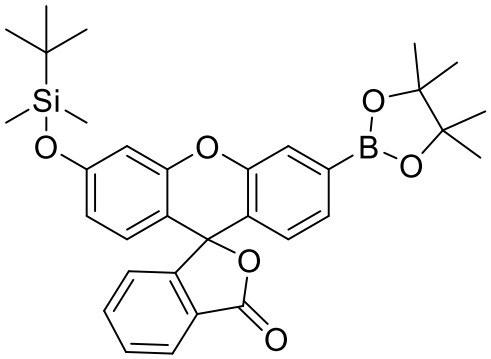

3'-Hydroxy-6'-(4,4,5,5-tetramethyl-1,3,2-dioxaborolan-2-yl)-3H-spiro[isobenzofuran-1,9'-xanthen]-3-one (**92**) (0.140 mg, 0.316 mmol) was dissolved in DCM (5 mL) and stirred at 0 °C. Imidazole (43 mg, 0.633 mmol) was added and stirred for 5 min. TBDMS-Cl (95 mg, 0.633 mmol) was added and the mixture was allowed to warm to RT over three hours. After this time, the reaction mixture was poured into brine (50 mL) and extracted with EtOAc (3 × 30 mL), dried over $MgSO_4$, filtered and concentrated *in vacuo*. The crude mixture was then purified *via* flash column chromatography EtOAc: Pet Ether (30:70) to yield the pure product **90** (0.75 g, 0.13 mmol, 42 %). M.p. 109-111 °C; ^{1}H NMR (500 MHz, CDCl3) δ 8.02 (ddd, J = 7.3, 1.3, 0.8 Hz, 1H), 7.74 (d, J = 1.0 Hz, 1H), 7.67 – 7.58 (m, 2H), 7.42 (dd, J = 7.8, 1.1 Hz, 1H), 7.15 – 7.11 (m, 1H), 6.80 (d, J = 7.8 Hz, 1H), 6.73 (d, J = 2.4 Hz, 1H), 6.67 (d, J = 8.6 Hz, 1H), 6.53 (dd, J = 8.6, 2.4 Hz, 1H), 1.34 (d, J = 1.4 Hz, 12H), 0.98 (s, 9H), 0.23 (d, J = 1.9 Hz, 6H); 13C NMR (125.75 MHz, CDCl3) δ 169.48, 157.67, 134.99, 129.66, 129.28, 128.80, 127.14, 126.26, 125.06, 123.82, 123.49, 121.54, 116.56, 111.78, 107.73, 84.15, 82.60, 29.68, 25.59, 25.01, 24.86, 24.82, 18.19, -4.41; I.R (thinfilm) ν max (cm^{-1}): 1743.63 (C=O); HRMS (FTMS-NSI): m/z calculated for $C_{32}H_{37}BO_6Si$: requires 557.2530 for $[M+H]^+$, found 557.2495.

3-Oxo-3'-(4,4,5,5-tetramethyl-1,3,2-dioxaborolan-2-yl)-3H-spiro[isobenzofuran-1,9'-xanthen]-6'-yl 2,4-dinitrobenzenesulfonate (**103**):

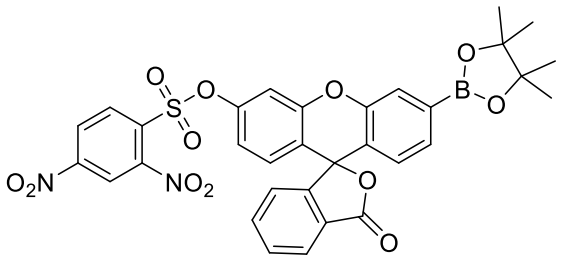

2,4-Dinitrobenzenesulfonyl chloride (0.089 g, 0.033 mmol) in DCM (3 mL) was added dropwise to a solution of 3'-hydroxy-6'-(4,4,5,5-tetramethyl-1,3,2-dioxaborolan-2-yl)-3Hspiro[isobenzofuran-1,9'-xanthen]-3-one (**92**) (0.15 g, 0.34 mmol) and NEt_3 (95 µL, 0.69 mmol) in DCM (5 mL) at 0 ^oC. The reaction mixture was stirred at 0 ^oC for 2 h before the addition of H_2O (15 mL) and DCM (15 mL). The organic layer was washed with H_2O (2 x 10 mL), brine (10 mL) and dried ($MgSO_4$) and concentrated in-vacuo to afford the crude material. The crude material was purified *via* column chromatography EtOAc:Pet Ether (30:70) to afford the title compound as a pale yellow solid (**103**) (0.115 g, 0.17 mmol, 52 %). M.p. 119-122 ^oC; ^1H NMR (500MHz, $CDCl_3$) δ 8.67 (d, J = 2.0 Hz, 1 H, ArH), 8.53 (dd, J = 2.0, 8.8 Hz, 1 H, ArH), 8.25 (d, J = 8.8 Hz, 1 H, ArH), 8.03 (d, J = 7.3 Hz, 1 H, ArH), 7.73 (s, 1 H, ArH), 7.69 - 7.62 (m, 2 H, ArH), 7.47 (d, J = 7.8 Hz, 1 H, ArH), 7.19 (d, J = 2.0 Hz, 1 H, ArH), 7.11 (d, J = 7.8 Hz, 1 H, ArH), 6.91 (dd, J = 2.2, 8.6 Hz, 1 H, ArH), 6.86 (d, J = 8.3 Hz, 1 H, ArH), 6.82 (d, J = 7.8 Hz, 1 H, ArH), 1.35 (s, 12 H, BPin); ^{13}C NMR (125.75 MHz, $CDCl_3$) 169.0, 153.0, 151.9, 151.1, 150.0, 149.5, 149.0, 135.4, 134.0, 133.3, 130.2, 130.2, 129.8, 127.0, 126.7, 125.6, 125.4, 123.7, 123.4, 121.0, 120.5, 119.2, 117.2, 111.0, 84.3, 24.9, 24.8, 24.8; I.R (thinfilm) ν max (cm^{-1}): 1766.44 (C=O); HRMS (FTMS-NSI): m/z calculated for $C_{32}H_{25}BN_2O_{12}S$: requires 672.1330 for $[M+H]^+$, found 672.1329.

3'-((4-Nitrobenzyl)oxy)-6'-(4,4,5,5-tetramethyl-1,3,2-dioxaborolan-2-yl)-3H-spiro[isobenzofuran-1,9'-xanthen]-3-one (**97**):

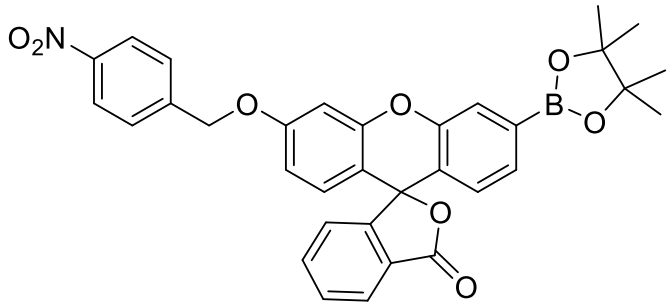

To a solution of 3'-hydroxy-6'-(4,4,5,5-tetramethyl-1,3,2-dioxaborolan-2-yl)-3Hspiro[isobenzofuran-1,9'-xanthen]-3-one (**92**) (89 mg, 0.20 mmol) in DCM (5 mL) was added 4-nitrobenzaldehyde (41.3 mg, 0.192 mmol) and NEt_3 (54 µL, 0.40 mmol). The reaction mixture was stirred at 0 ˚C for 3 hours, when TLC indicated completion. The solvent was removed from the reaction mixture and the crude material was purified *via* column chromatography EtOAc: Pet Ether (30:70) to yield the pure title compound (**97**) (72 mg, 0.124 mmol, 42%). M.p. 127-131 ºC; ^{1}H NMR (500 MHz, $CDCl_3$) δ 8.30 – 8.21 (m, 2H), 8.03 (dd, J = 6.6, 1.3 Hz, 1H), 7.73 (d, J = 0.8 Hz, 1H), 7.69 – 7.58 (m, 4H), 7.43 (dd, J = 7.8, 1.0 Hz, 1H), 7.11 (dd, J = 6.6, 0.9 Hz, 1H), 6.84 – 6.72 (m, 3H), 6.68 (dd, J = 8.8, 2.5 Hz, 1H), 5.20 (s, 2H), 1.34 (s, 12H); ^{13}C NMR (126 MHz, $CDCl_3$) δ 169.39, 159.78, 153.38, 152.36, 150.58, 147.70, 143.66, 135.07, 129.78, 129.52, 129.24, 127.63, 127.16, 126.20, 125.15, 123.90, 123.75, 123.41, 121.45, 111.96, 102.07, 84.20, 82.32, 68.89, 24.81; I.R (thinfilm) ν max (cm^{-1}): 1764.23 (C=O), 1521.98 (N-O), 1504.06 (N-O); HRMS (FTMS-NSI): m/z calculated for $C_{33}H_{28}BNO_8$: requires 577.1908 for $[M+H]^+$, found 578.1892.

2-Amino-3',6'-dihydroxyspiro[isoindoline-1,9'-xanthen]-3-one (**93**):

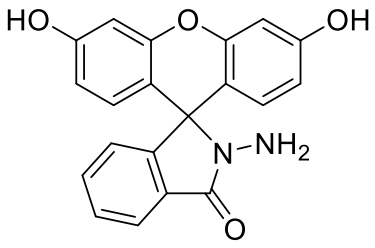

Fluorescein (4.00 g, 12.00 mmol) was dissolved in MeOH (250 mL). $NH_2NH_2.OH$ (20 mL) was then added and stirred vigorously. The solution was heated to reflux for 12 hours. The reaction was then cooled to rt and the solvent was removed in *vacuo*. The product was recrystallised from MeOH and DCM. The solid was then collected using Buchner filtration and dried to yield compound (**93**), an off white solid (3.90 g, 93.00%). ^{1}H NMR (500 MHz, DMSO-d_6) δ 9.05 (s, 1H), 7.91 (d, J = 7.1 Hz, 1H), 7.66 - 7.56 (m, 2H), 7.41 (dd, J = 6.8 Hz, 3.0 Hz, 2H), 7.34 (dd, J = 5.7 Hz, 1.7 Hz, 3H), 7.13 (d, J = 7.4 Hz, 1H), 6.66 (d, J = 2.3 Hz, 2H), 6.50 (d, J = 8.6 Hz, 2H), 6.45 (dd, J = 8.6 Hz, 2.3 Hz, 2H). ^{13}C NMR (DMSO, 125 MHz): δ 165.88, 158.86, 152.87, 151.99, 133.01, 129.79, 128.81, 128.32, 123.85, 122.76, 112.50, 110.20 and 102.82 ppm. ^{1}H and ^{13}C NMR agree with literature values. [1]

[1] X. Chen, H. Ma, *Anal. Chim, Acta.*, **2006**, *575*, 217-222.

(E)-2-(benzylideneamino)-3',6'-dihydroxyspiro[isoindoline-1,9'-xanthen]-3-one (**96**):

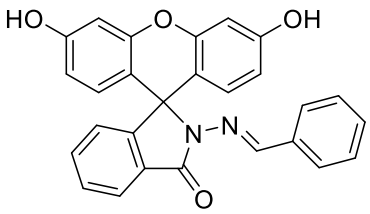

93 (358 mg, 1.03 mmol) and Benzaldehyde (109.68 mg, 1.03 mmol) was dissolved in EtOH (35 mL) and AcOH (35 µL) was added to the solution and heated to reflux for 12 hours. The reaction mixture was then cooled to rt and concentrated in *vacuo*. The product was recrystallized from MeOH and DCM and collected *via* filtration to produce (**96**) a beige solid (400 mg, 89.08%). ^{1}H NMR δ 9.88 (s, 2H), 9.04 (s, 2H), 7.90 (d, J = 5.0 Hz, 1H), 7.62 (td, J = 10 Hz, 1H), 7.58 (td, 1H), 7.41 (dd, 2H), 7.33 (dd, J = 5 Hz, 3H), 7.12 (d, J = 10 Hz, 1H), 6.65 (d, 2H), 6.50 – 6.43 (m, 4H). ^{13}C NMR (DMSO, 125 MHz): δ 164.06, 159.00, 152.69, 150.79, 149.64, 134.91, 134.43, 130.80, 129.53, 129.26, 128.46, 127.19, 127.27, 123.63, 112.74, 110.63 and 102.89 ppm. ^{1}H and ^{13}C NMR agree with literature values.[2]

[2] A. F. M. M. Rahman, S.-E. Park, A. A. Kadi and Y. Kwon, J. Med. Chem., 2014, 57, 9139–9151.

6.3.3 Synthesis of TCF probes

2-(3-Cyano-4,5,5-trimethylfuran-2(5H)-ylidene)malononitrile (**104**):

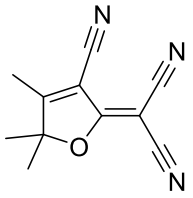

NaOEt (0.391 g, 5.75 mmol) was added to a solution of 3-hydroxy-3-methyl-2-butanone (4 mL, 38 mmol) and malonitrile (4.9 g, 74 mmol) in EtOH (10 mL) and stirred for 1.5 h. The reaction mixture was then refluxed for 1 h, which was then cooled to rt. The mixture was cooled, and the solid precipitate was filtered to afford the title compound (**104**) as a pale grey solid (4.92 g, 24.70 mmol, 65 %). M.p. 204 – 208 °C (decomp); ^{1}H NMR (500 MHz, $CDCl_3$) δ 2.37 (s, 3H), 1.64 (s, 6 H); ^{13}C NMR (75.5 MHz, $CDCl_3$) δ 182.6, 175.2, 111.1, 110.4, 109.0, 104.8, 99.8, 58.5, 24.4, 14.2; I.R (thinfilm) ν max (cm^{-1}): 2232.78, 2222.00 (CN); HRMS (FTMS-NSI): m/z calculated for $C_{11}H_9N_3O$: requires 200.0108 for $[M+H]^+$, found 200.0108.

(E)-2-(3-cyano-5,5-dimethyl-4-(4-(4,4,5,5-tetramethyl-1,3,2-dioxaborolan-2-yl)styryl)furan-2(5H)-ylidene)malononitrile (**114**):

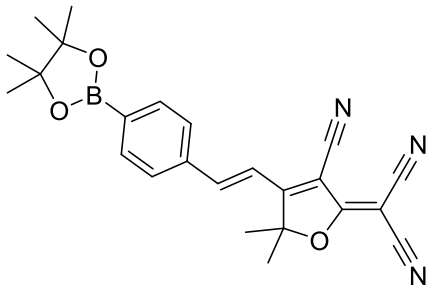

Two drops of Piperidine was added to a mixture of 4-(4,4,5,5-tetramethyl-1,3,2-dioxaborolan-2-yl)benzaldehyde (0.232 g, 1 mmol) and TCF (**104**) (0.288 g, 1.15 mmol) in EtOH (10 mL). The reaction mixture was heated in the microwave at 100 °C for 15 min. The reaction mixture was cooled and the solid was filtered off to afford the title compound (**114**) as an orange solid (0.310 g, 0.75 mmol, 75 %). M.p. 275 – 278 °C; ^{1}H NMR (300 MHz, CDCl3) δ 7.90 (d, *J* = 8.1 Hz, 2 H), 7.71 - 7.59 (m, 3 H), 7.11 (d, *J* = 16.4 Hz, 1 H), 1.82 (s, 6 H), 1.37 (s, 12 H); ^{13}C NMR (75.5 MHz, CDCl3) δ 175.2, 173.7, 147.3, 135.9, 135.7, 128.1, 115.6, 111.6, 110.8, 110.1, 100.6, 97.9, 84.4, 58.2, 26.5, 24.9; I.R (thinfilm) ν max (cm^{-1}): 2231.63 (CN); HRMS (FTMS-NSI): m/z calculated for $C_{24}H_{24}BN_3O_3$: requires 430.2285 for $[M+NH4]^+$, found 430.2287.

(E)-2-(3-cyano-4-(4-hydroxystyryl)-5,5-dimethylfuran-2(5H)-ylidene)malononitrile (**118**):

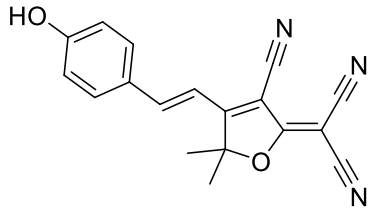

Two drops of Piperidine were added to a mixture of 4-hydroxybenzaldehyde (0.122 g, 1 mmol) and TCF (**104**) (0.228 g, 1.15 mmol) in EtOH (10 mL). The reaction mixture was heated in the microwave for 15 min at 100 °C, which was then cooled to rt. The solid precipitate was filtered off to afford the title compound (**118**) as an orange solid (0.218 g, 0.72 mmol, 72 %). M.p. 202 – 206 °C (decomp). ^{1}H NMR (300 MHz, DMSO-d_6) 7.95 - 7.73 (m, 3 H), 7.01 (d, *J* = 16.2 Hz, 1 H), 6.89 (d, *J* = 8.7 Hz, 2 H), 1.77 (s, 6 H); ^{13}C NMR (75.5 MHz, DMSO-d_6) δ 177.6, 176.2, 162.7, 148.7, 132.7, 126.0, 116.8, 113.3, 112.5, 112.0, 111.6, 99.4, 96.9, 53.5, 25.7; I.R (thinfilm) ν max (cm^{-1}): 3361.61 (O-H), 2224.73 (CN); HRMS (FTMS-NSI): m/z calculated for $C_{18}H_{13}N_3O_2$: requires 304.1081 for $[M+H]^+$, found 304.1084.

(E)-2-(3-cyano-5,5-dimethyl-4-(4-((4-(4,4,5,5-tetramethyl-1,3,2-dioxaborolan-2-yl)benzyl)oxy)styryl)furan-2(5H)-ylidene)malononitrile (**115**):

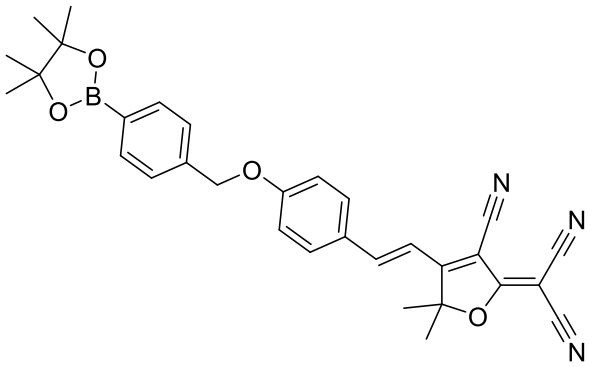

(E)-2-(3-cyano-4-(4-hydroxystyryl)-5,5-dimethylfuran-2(5H)-ylidene)malononitrile (**118**) (0.090 g, 0.297 mmol), 2-(4-(bromomethyl)phenyl)-4,4,5,5-tetramethyl-1,3,2-dioxaborolane (0.088 g, 0.297 mmol), K_2CO_3 (0.123 g, 0.89 mmol) and NaI (0.044 g, 0.297 mmol) in MeCN (5 mL) was stirred overnight at rt. The reaction mixture was partitioned with EtOAc (50 mL) and H_2O (50 mL). The organic layer was washed with H_2O (2 x 50 mL), Brine (50 mL) and dried ($MgSO_4$). The solvent was removed *in-vacuo* and the crude material was triturated (MeOH) to afford the title compound (**115**) as a red solid (0.073 g, 0.14 mmol, 47 %). M.p. 267 – 269 °C. ^{1}H NMR (500 MHz, $CDCl_3$) δ 7.88 - 7.82 (d, *J* = 8.3 Hz, 2 H), 7.67 - 7.57 (m, 3 H), 7.48 - 7.40 (d, *J* = 8.3 Hz, 2 H), 7.05 (d, *J* = 8.8 Hz, 2 H), 6.90 (d, *J* = 16.1 Hz, 1 H), 5.19 (s, 2 H), 1.79 (s, 6 H), 1.36 (s, 12 H); ^{13}C NMR (125.5 MHz, $CDCl_3$) δ 175.5, 174.0, 162.8, 147.2, 138.8, 135.2, 131.3, 126.9, 126.5, 116.0, 112.5, 111.8, 111.0, 110.4, 97.4, 83.9, 70.3, 26.5, 24.8; I.R (thinfilm) ν max (cm^{-1}): 2227.39 (CN); HRMS (FTMS-NSI): m/z calculated for $C_{31}H_{30}BN_3O_4$: requires 536.2704 for $[M+NH4]^+$, found 536.2699

(*E*)-2-(3-cyano-4-(3,5-dichloro-4-hydroxystyryl)-5,5-dimethylfuran-2(5H)-ylidene)malononitrile (**124**):

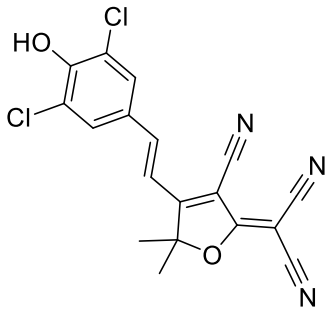

Two drops of piperidine were added to a mixture of 3,5-dichloro-4-hydroxybenzaldehyde (0.19 g, 1 mmol) and TCF (**104**) (0.20 g, 1.00 mmol) in EtOH (10 mL). The reaction mixture was heated in the microwave for 15 min at 100 °C, which was then cooled to rt. The solid precipitate was filtered off to afford the title compound (**124**) as a blue solid (0.19 g, 0.50 mmol, 50 %). M.p. > 300 °C; ^{1}H NMR (500 MHz, DMSO-d_6) δ 8.06 (s, 2 H), 7.76 (d, *J* = 16.1 Hz, 1 H), 7.19 (d, *J* = 16.1 Hz, 1 H), 1.77 (s, 6 H); ^{13}C NMR (125.75 MHz, DMSO-d_6) δ 177.5, 175.4, 153.2, 145.4, 130.4, 127.6, 123.3, 115.1, 113.2, 112.3, 111.2, 99.7, 25.6; I.R (thinfilm) ν max (cm^{-1}): 3356.50 (Br O-H), 2212.91 (CN); HRMS (ASAP+): m/z calculated for $C_{18}H_{11}Cl_2N_3O_2$: requires 372.0307 for $[M+H]^+$, found 372.0300

(*E*)-4-(2-(4-cyano-5-(dicyanomethylene)-2,2-dimethyl-2,5-dihydrofuran-3yl)vinyl)phenyl 2,4-dinitrobenzenesulfonate (**121**):

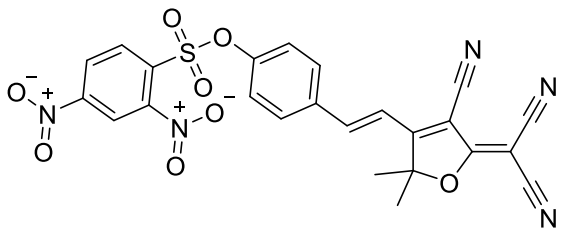

(E)-2-(3-cyano-4-(4-hydroxystyryl)-5,5-dimethylfuran-2(5H)-ylidene)malononitrile (**118**) (0.10 g, 0.33 mmol) was dissolved in DCM (5 mL) followed by the addition of NEt_3 (89 µL, 0.66 mmol). The reaction mixture was cooled to 0 ^oC and 2,4-dinitrobenzenesulfonylchloride (0.11 g, 0.40 mmol) in DCM (5 mL) was added dropwise to the reaction mixture. The reaction was allowed to warm to rt and was stirred for a further 4 hrs. The solvent was removed *in vacuo* and the crude product was purified *via* column chromatography - EtOAc:Pet ether (20:80 to 60:40). The title compound (**121**) was isolated as an orange solid (0.08 g, 0.15 mmol, 45 %). M.p. 236 – 238 ^oC; ^1H NMR (300 MHz, DMSO-d_6) δ 9.13 (d, *J* = 2.3 Hz, 1 H), 8.59 (dd, *J* = 2.3, 8.7 Hz, 1 H), 8.24 (d, *J* = 8.7 Hz, 1 H), 7.99 (d, *J* = 8.9 Hz, 2 H), 7.87 (d, *J* = 16.8 Hz, 1 H), 7.32 (d, *J* = 8.9 Hz, 2 H), 7.21 (d, *J* = 16.6 Hz, 1 H), 1.77 (s, 6 H); ^{13}C NMR (125. 75 MHz, Acetone-d6) δ 176.3, 174.4, 151.0, 144.7, 134.7, 134.0, 131.9, 131.1, 127.2, 123.0, 120.9, 117.0, 111.9, 111.2, 110.2, 101.4, 99.1, 25.0; I.R (thinfilm) ν max (cm^{-1}): 3100 (C-H sp^2), 2229.72 (CN); HRMS (FTMS-NSI): m/z calculated for $C_{24}H_{15}N_5O_8S$: requires 534.0714 for $[M+H]^+$, found 534.0720

(*E*)-2,6-dichloro-4-(2-(4-cyano-5-(dicyanomethylene)-2,2-dimethyl-2,5-dihydrofuran-3-yl)vinyl)phenyl 2,4-dinitrobenzenesulfonate (**122**):

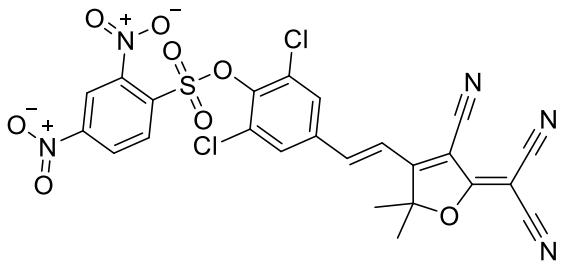

(*E*)-2-(3-cyano-4-(3,5-dichloro-4-hydroxystyryl)-5,5-dimethylfuran-2(5H)-ylidene)malononitrile (**124**) (0.17 g, 0.46 mmol) was dissolved in DCM (5 mL) followed by the addition of NEt_3 (124 µL, 0.92 mmol). The reaction mixture was cooled to 0 °C and 2,4- dinitrobenzenesulfonylchloride (0.146 g, 0.55 mmol) in DCM (5 mL) was added dropwise to the reaction mixture. The reaction was allowed to warm to rt and was stirred for a further 4 hrs. The solvent was removed *in vacuo* and the crude product was purified *via* column chromatography - EtOAc:Pet ether (60:40). The title compound (**122**) was isolated as a yellow solid (0.20 g, 0.33 mmol, 72 %). M.P. 268 -272 °C; ^{1}H NMR (500 MHz, DMSO-d^6) δ 9.12 (d, *J* = 2.4 Hz, 1 H), 8.70 (dd, *J* = 2.4, 8.8 Hz, 1 H), 8.49 (d, *J* = 8.8 Hz, 1 H), 8.34 (s, 2 H), 7.76 (d, *J* = 16.6 Hz, 1 H), 7.44 (d, *J* = 16.6 Hz, 1 H), 1.80 (s, 6 H); ^{13}C NMR (125.75 MHz, DMSO-d_6) δ 177.3, 174.2, 152.1, 148.2, 143.7, 142.6, 136.5, 133.6, 133.4, 130.5, 129.9, 128.3, 121.6, 119.7, 112.9, 112.1, 110.7, 102.4, 100.1, 56.0, 25.4; I.R (thinfilm) ν max (cm^{-1}): 3112.22 (C-H sp^2), 2225.72 (CN); HRMS (FTMS-NSI): m/z calculated for $C_{24}H_{13}C_{l2}N_5O_8S$: requires 623.9754 for $[M+Na]^+$, found 623.9761

7.0 Appendix

7.1 NMR Spectra

2-Oxo-7-((4-(4,4,5,5-tetramethyl-1,3,2-dioxaborolan-2-yl)benzyl)oxy)-2H-chromene-8-carbaldehyde (**42**):

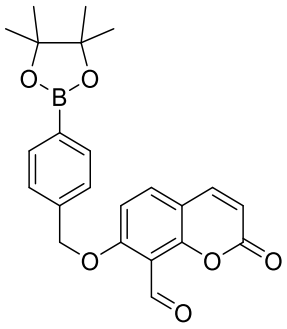

^{1}H Spectra:

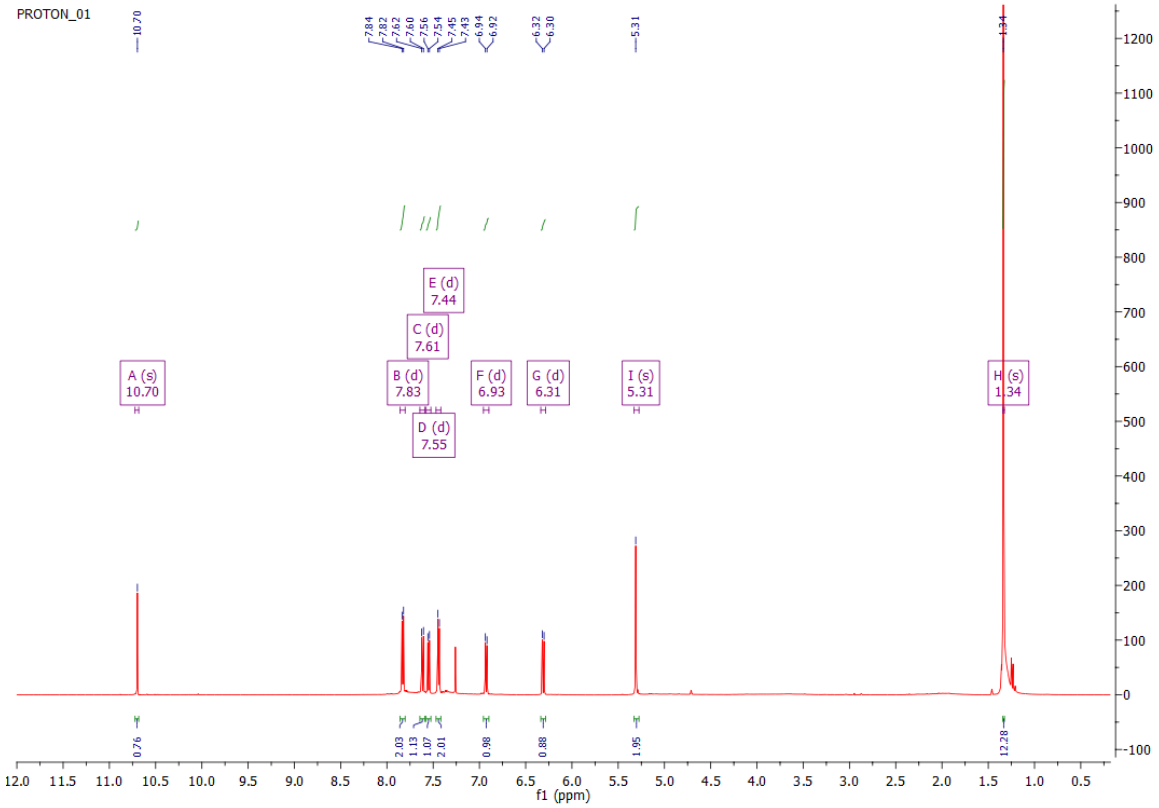

^{13}C Spectra:

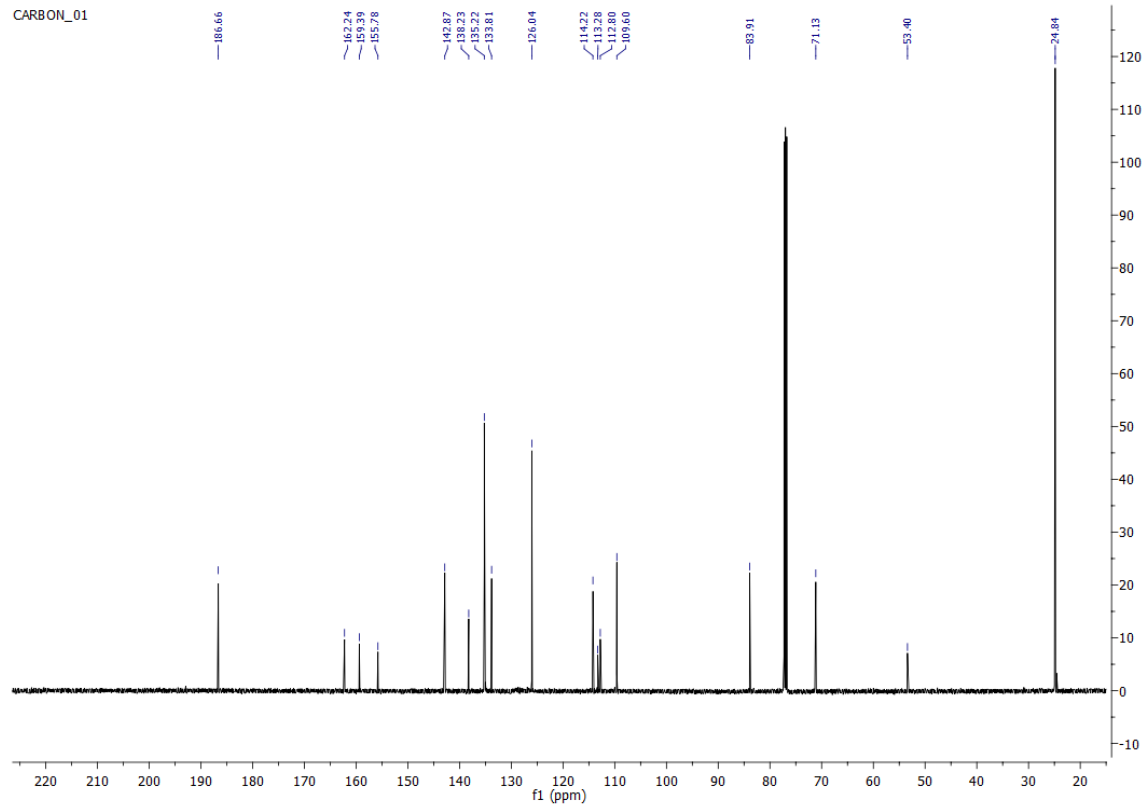
CARBON_01
186.66
162.24
159.39
155.78
142.87
138.23
135.22
133.81
126.04
114.22
113.28
112.80
109.60
83.91
71.13
53.40
24.84
f1 (ppm)

7-((4-Nitrobenzyl)oxy)-2-oxo-2H-chromene-8-carbaldehyde (**46**):

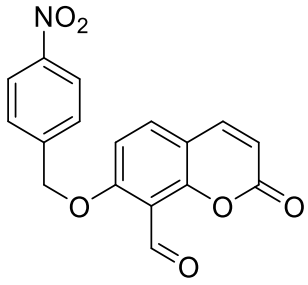

^{1}H Spectra:

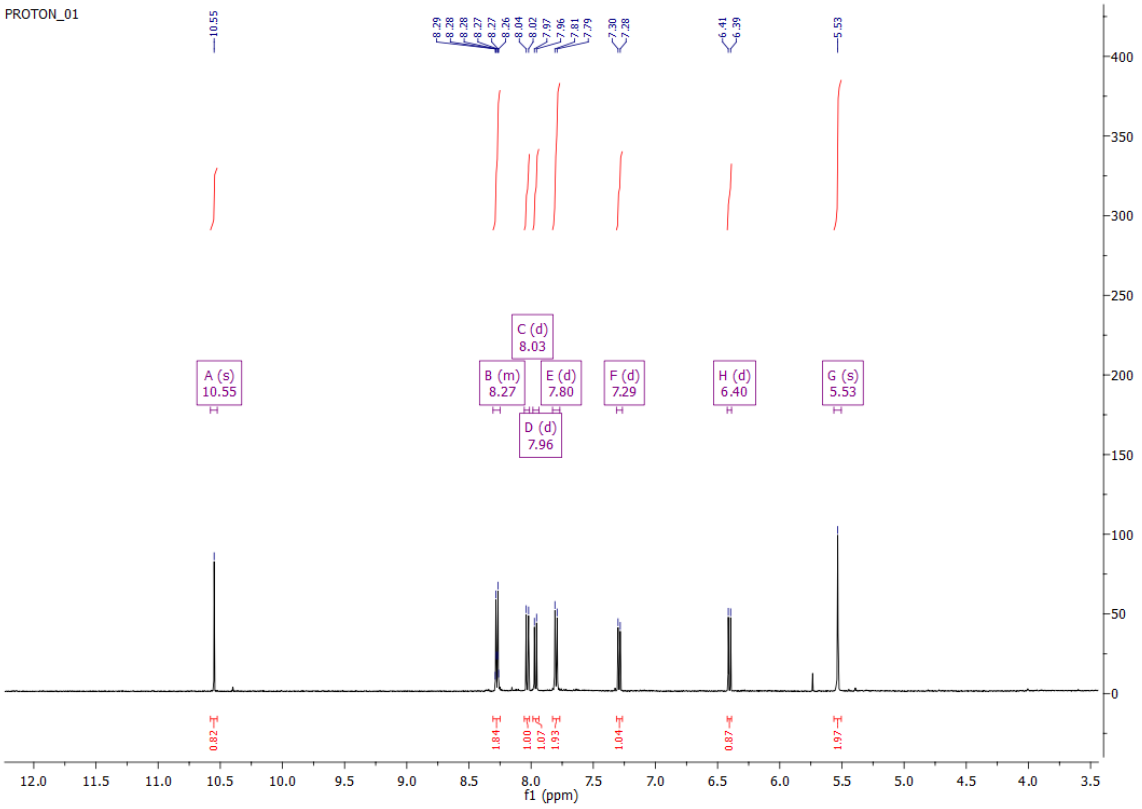

^{13}C Spectra:

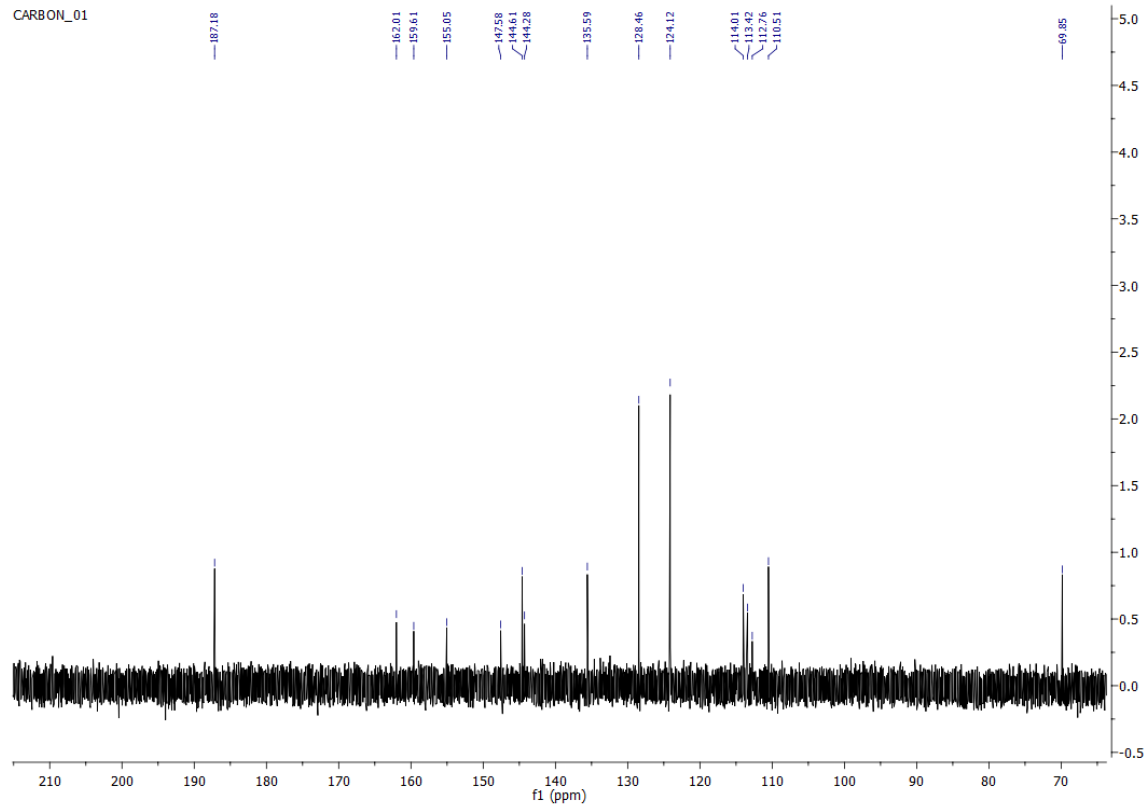
CARBON_01
187.18
162.01
159.61
155.05
147.58
144.61
144.28
135.59
128.46
124.12
114.01
113.42
112.76
110.51
69.85
f1 (ppm)

2-Oxo-7-((4-(4,4,5,5-tetramethyl-1,3,2-dioxaborolan-2-yl)benzyl)oxy)-2H-chromene-3-carbaldehyde (**57**):

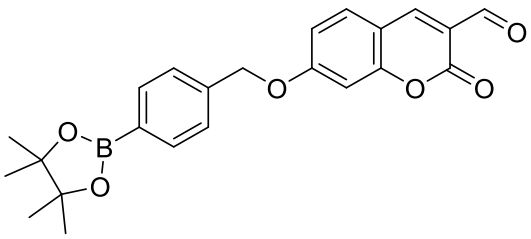

^{1}H Spectra:

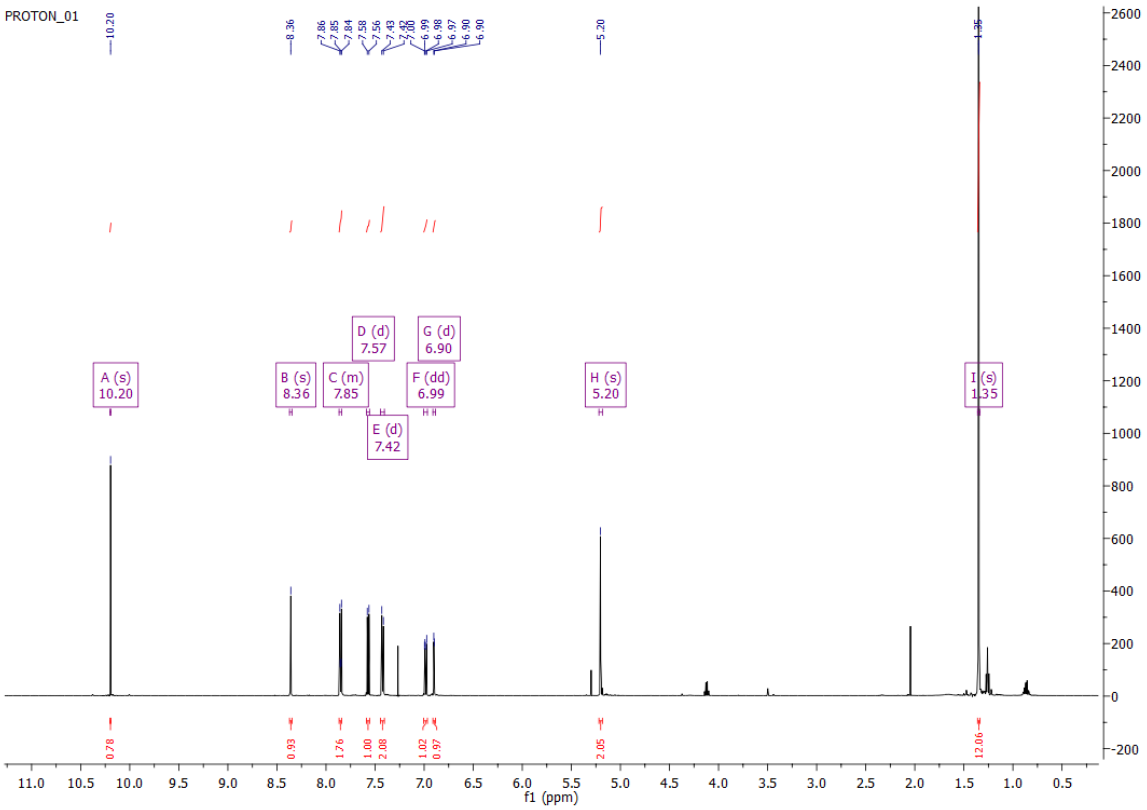

^{13}C Spectra:

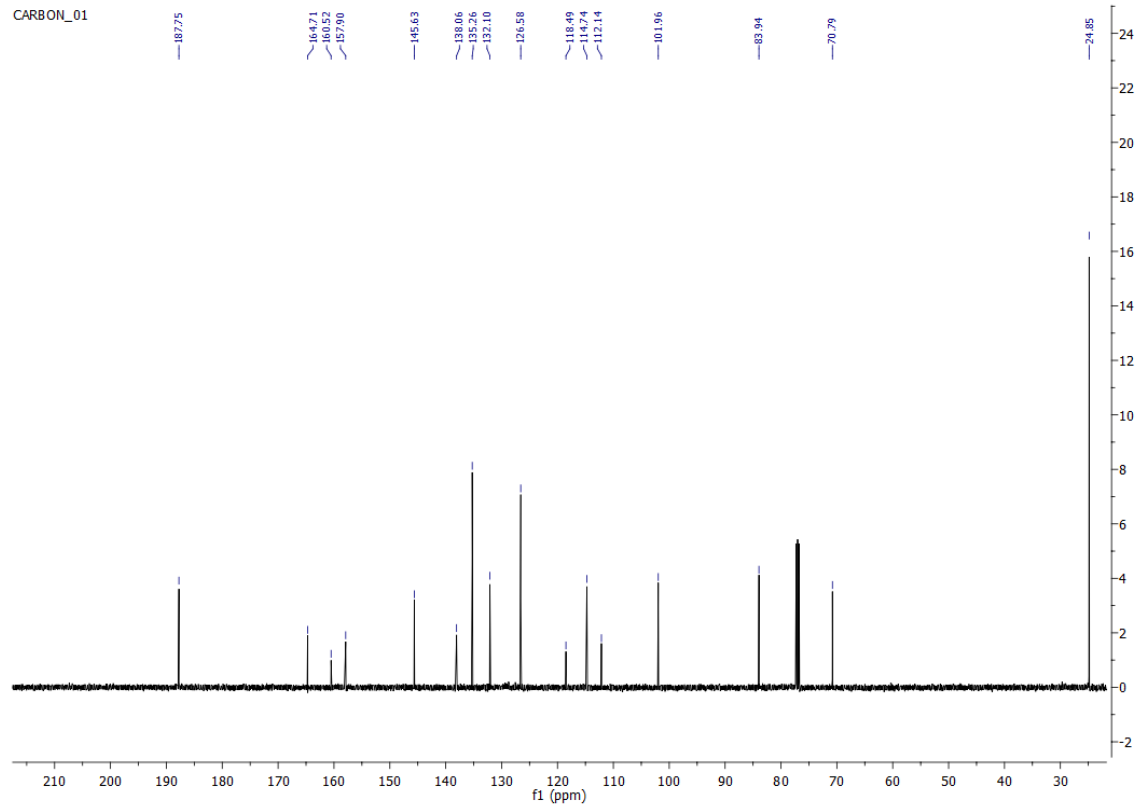
CARBON_01
187.75
164.71
160.52
157.90
145.63
138.06
135.26
132.10
126.58
118.49
114.74
112.14
101.96
83.94
70.79
24.85
f1 (ppm)

4-Chloro-7-hydroxy-2-oxo-2H-chromene-3-carbaldehyde (**73**):

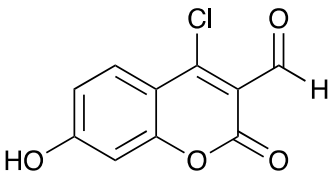

^{1}H Spectra:

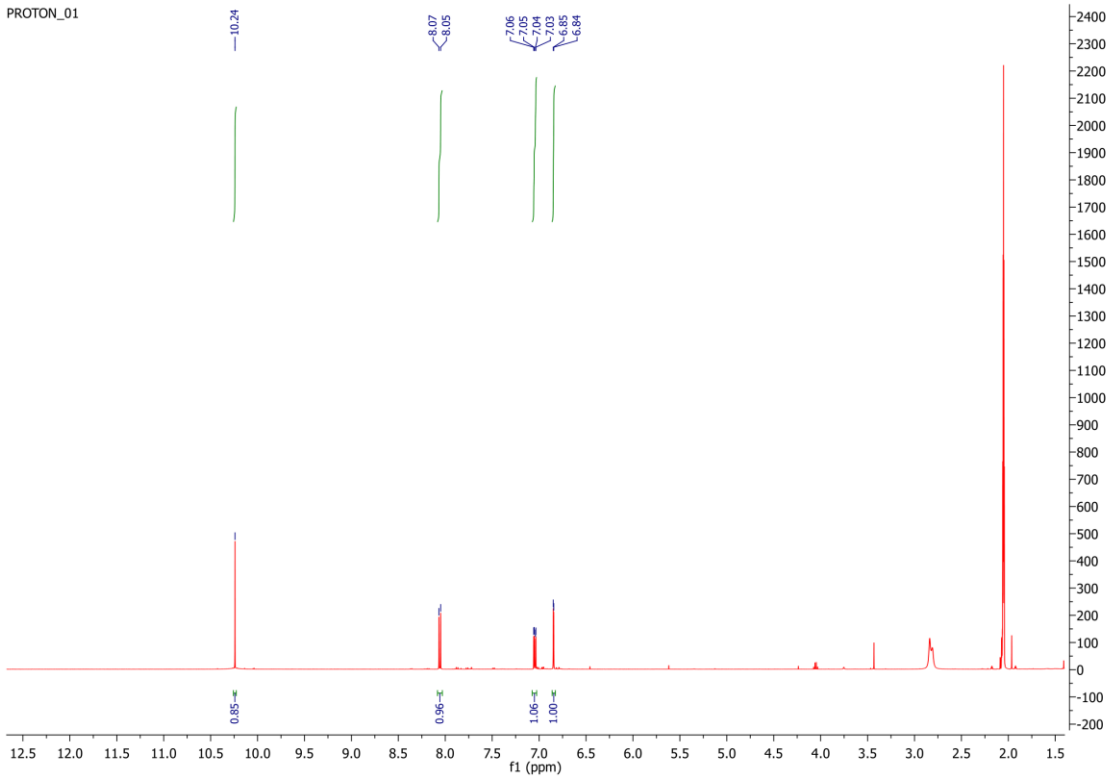

^{13}C Spectra:

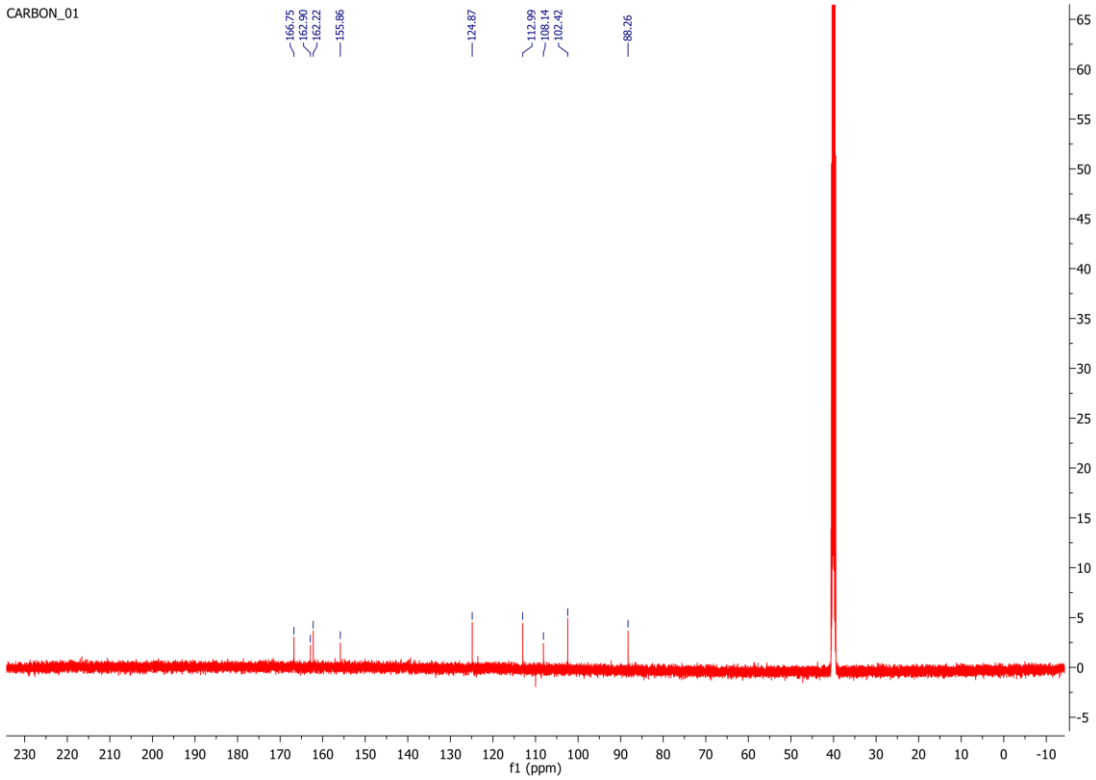
CARBON_01
166.75
162.90
162.22
155.86
124.87
112.99
108.14
102.42
88.26
f1 (ppm)

3-Oxo-3'-(4,4,5,5-tetramethyl-1,3,2-dioxaborolan-2-yl)-3H-spiro[isobenzofuran-1,9'-xanthen]-6'-yl 2,4-dinitrobenzenesulfonate (**103**):

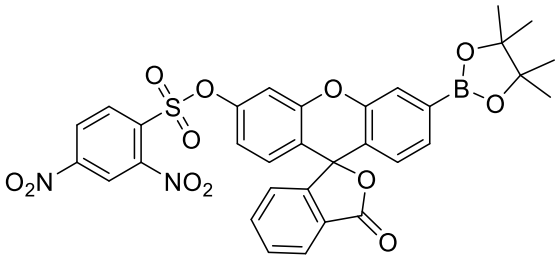

^{1}H Spectra:

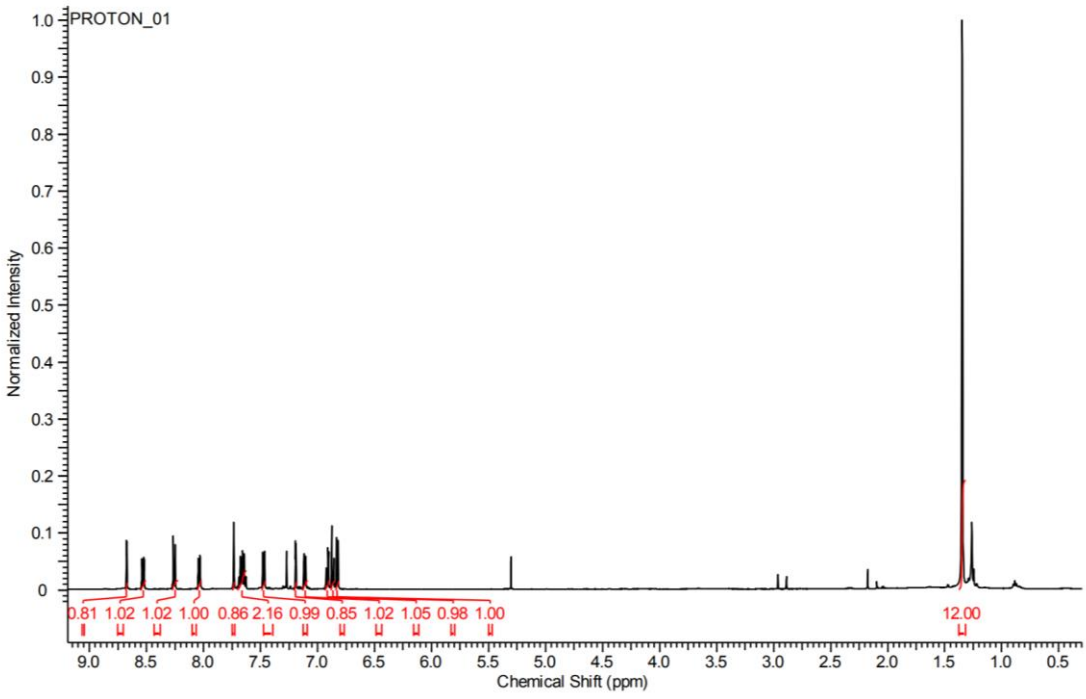

^{13}C Spectra:

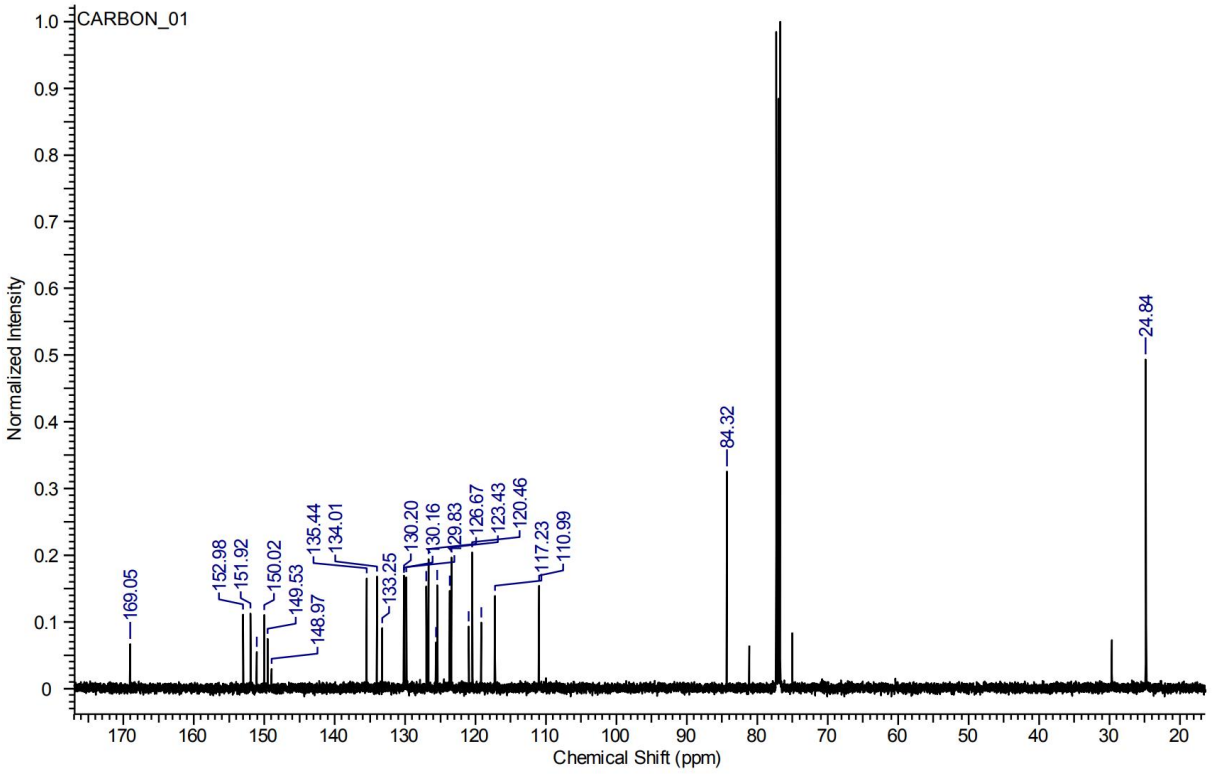
CARBON_01
Normalized Intensity
Chemical Shift (ppm)
169.05
152.98
151.92
150.02
149.53
148.97
135.44
134.01
133.25
130.20
130.16
129.83
126.67
123.43
120.46
117.23
110.99
84.32
24.84

3'-((4-Nitrobenzyl)oxy)-6'-(4,4,5,5-tetramethyl-1,3,2-dioxaborolan-2-yl)-3H-spiro[isobenzofuran-1,9'-xanthen]-3-one (**97**):

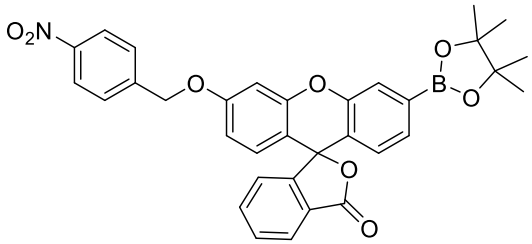

^{1}H Spectra:

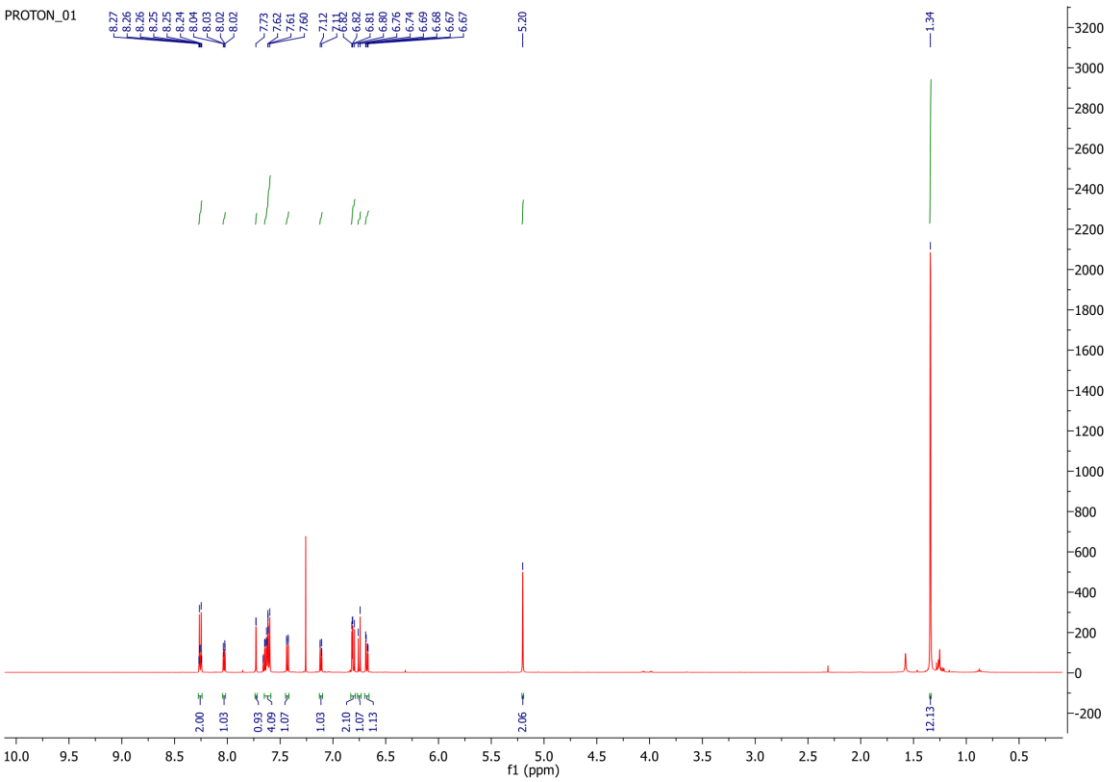

^{13}C Spectra:

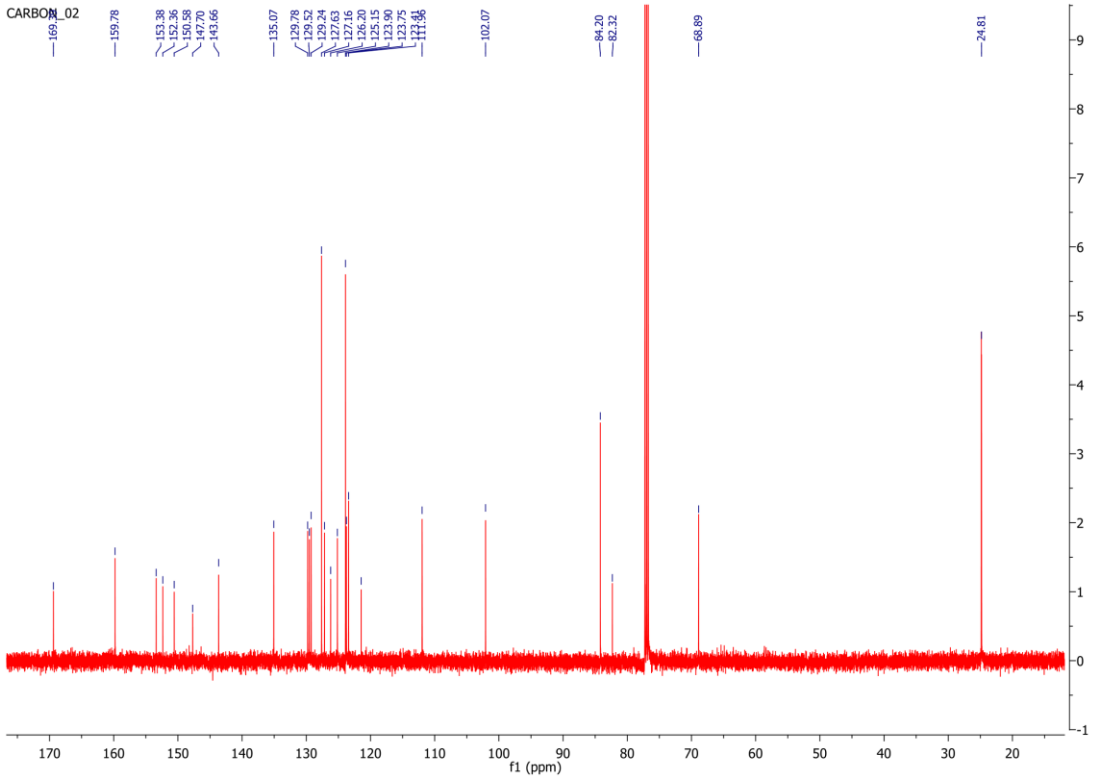
CARBON_02
169.78
159.78
153.38
152.36
150.58
147.70
143.66
135.07
129.78
129.52
129.24
127.63
127.16
126.20
125.15
123.90
123.75
111.96
102.07
84.20
82.32
68.89
24.81
f1 (ppm)

2-Amino-3',6'-dihydroxyspiro[isoindoline-1,9'-xanthen]-3-one (**93**):

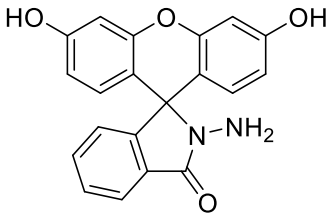

^{1}H Spectra:

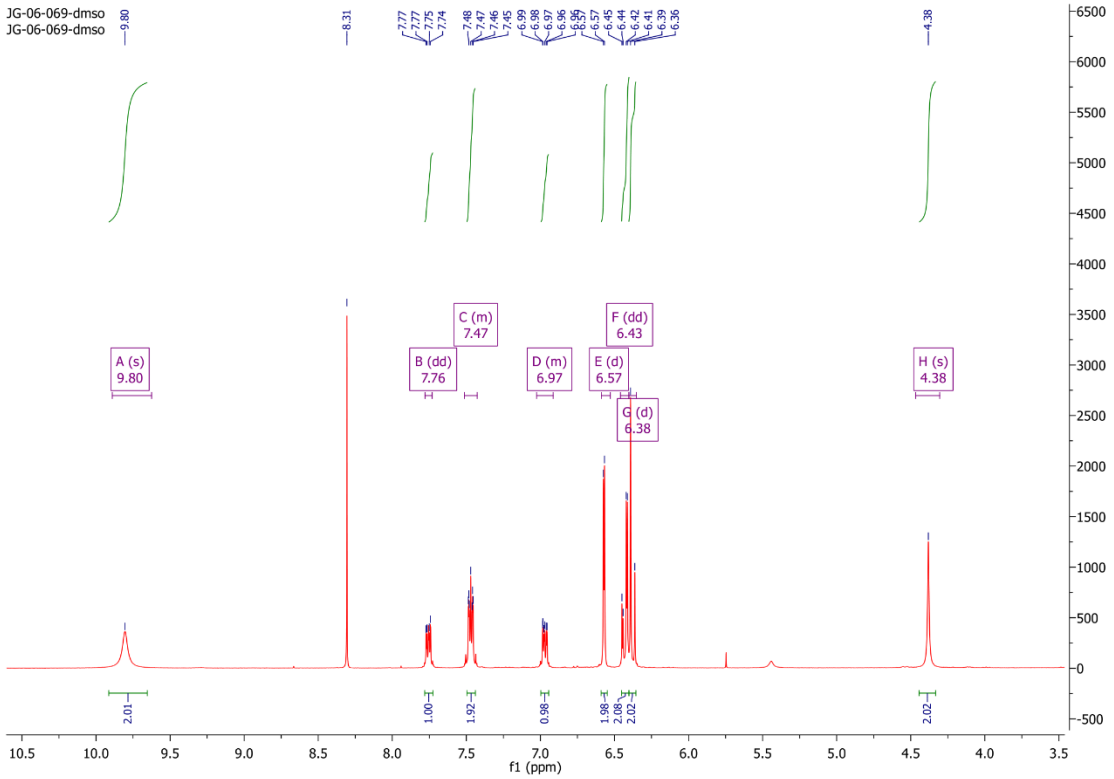

^{13}C Spectra:

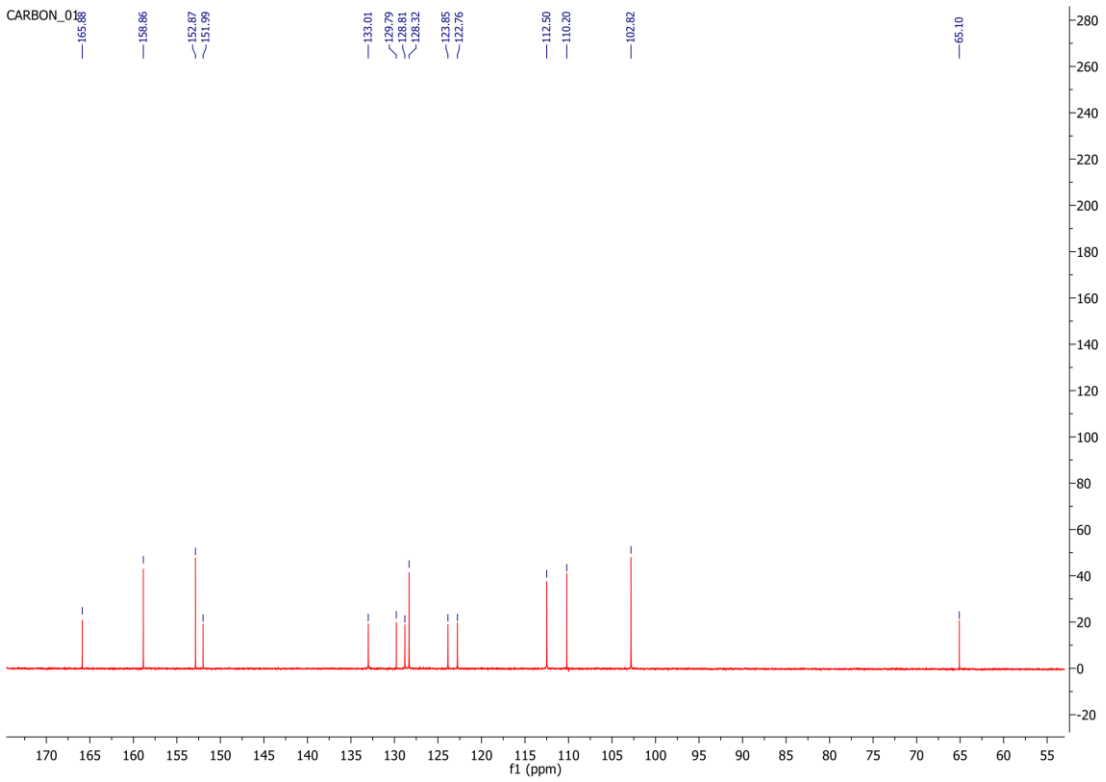

[1] X. Chen, H. Ma, *Anal. Chim, Acta.*, **2006**, *575*, 217-222.

(E)-2-(benzylideneamino)-3',6'-dihydroxyspiro[isoindoline-1,9'-xanthen]-3-one (**96**):

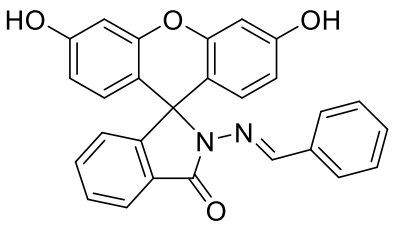

^{1}H Spectra:

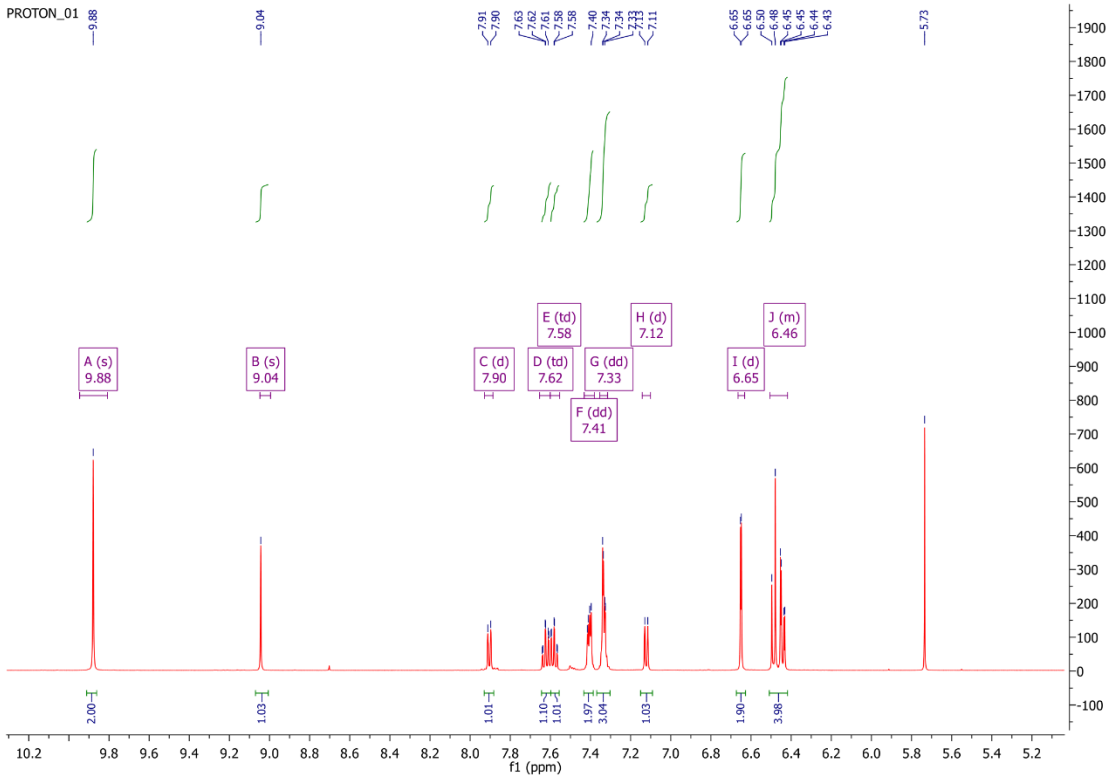

^{13}C Spectra:

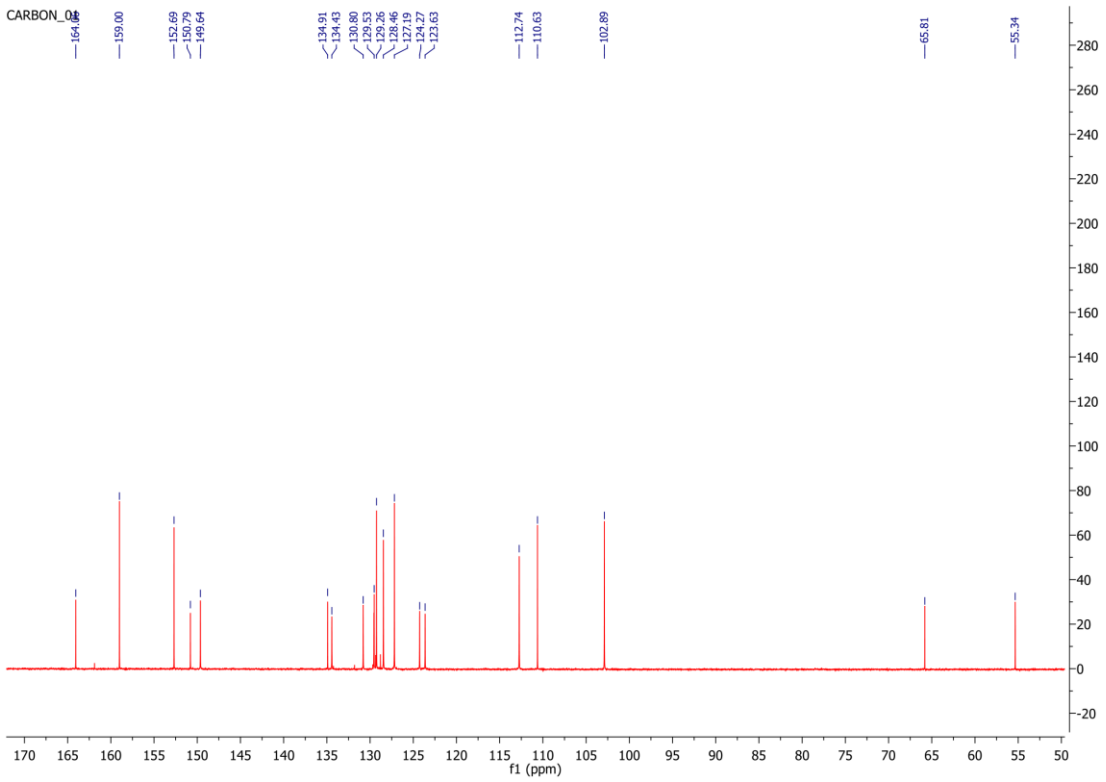

[2] A. F. M. M. Rahman, S.-E. Park, A. A. Kadi and Y. Kwon, J. Med. Chem., 2014, 57, 9139–9151.

(E)-2-(3-cyano-5,5-dimethyl-4-(4-(4,4,5,5-tetramethyl-1,3,2-dioxaborolan-2-yl)styryl)furan-2(5H)-ylidene)malononitrile (**114**):

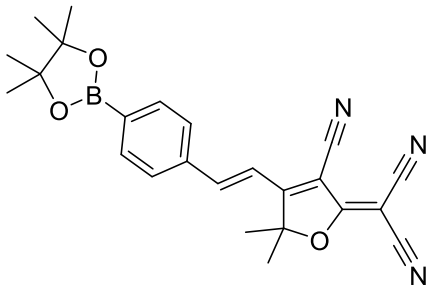

^{1}H Spectra:

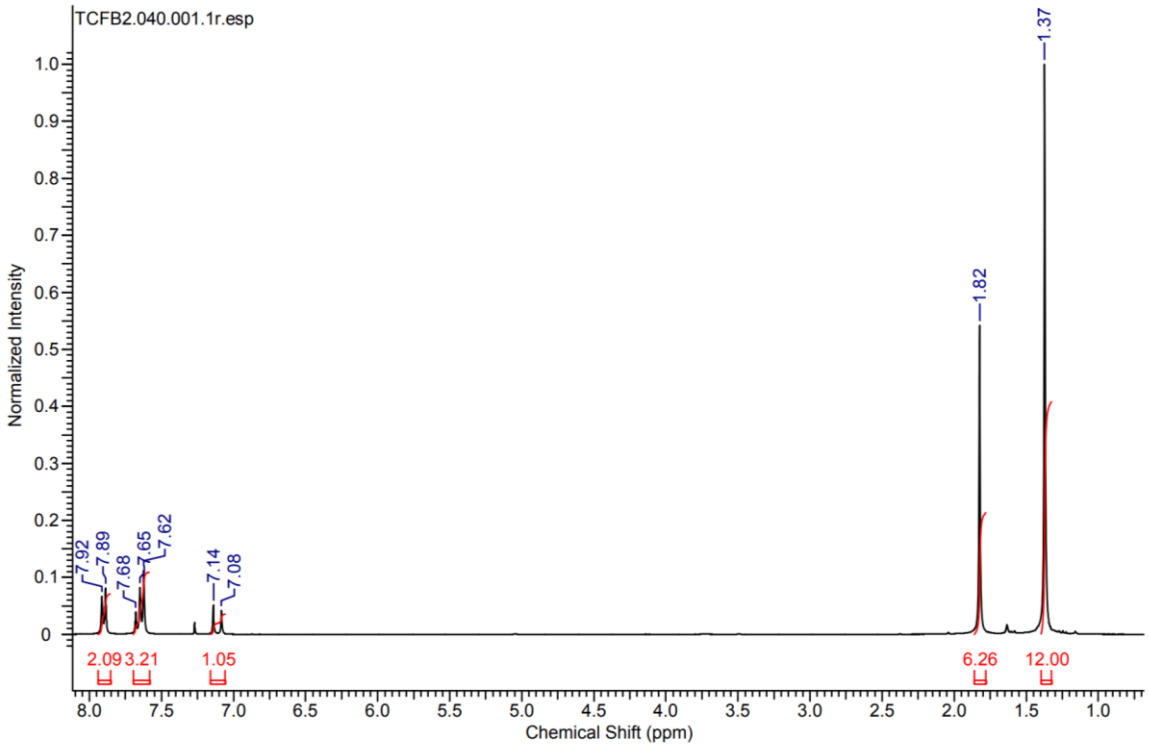

^{13}C Spectra:

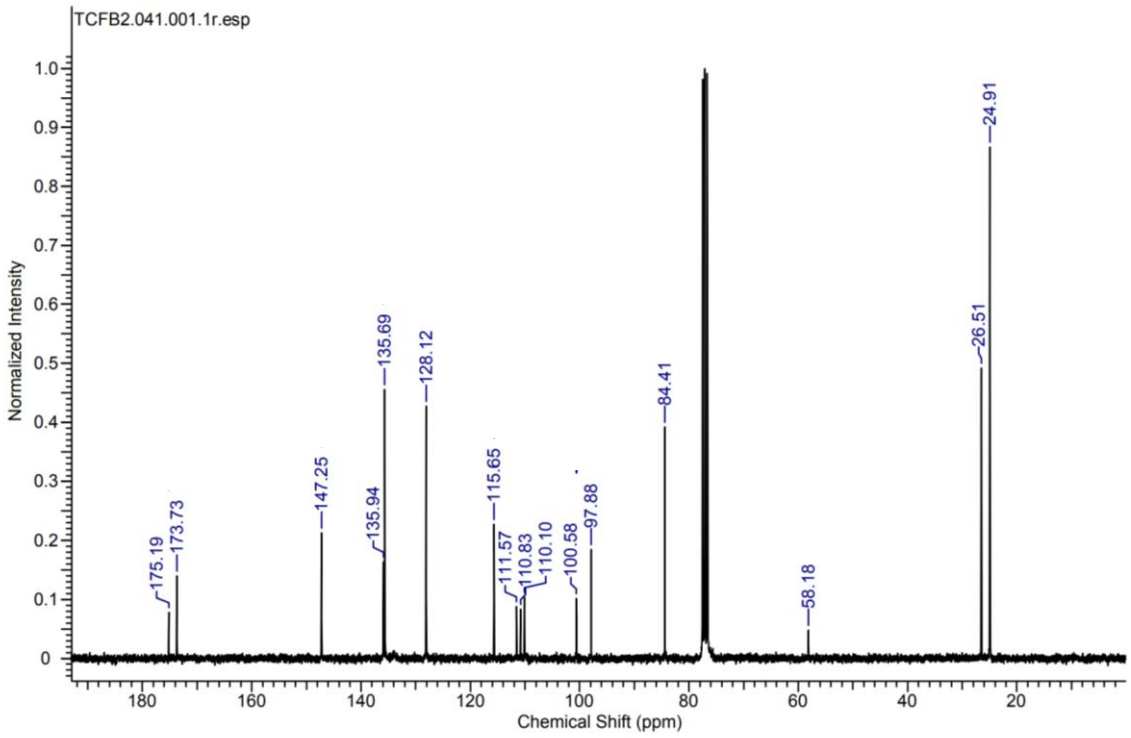
TCFB2.041.001.1r.esp
Normalized Intensity
Chemical Shift (ppm)
175.19
173.73
147.25
135.94
135.69
128.12
115.65
111.57
110.83
110.10
100.58
97.88
84.41
58.18
26.51
24.91

(E)-2-(3-cyano-5,5-dimethyl-4-(4-((4-(4,4,5,5-tetramethyl-1,3,2-dioxaborolan-2-yl)benzyl)oxy)styryl)furan-2(5H)-ylidene)malononitrile (**115**):

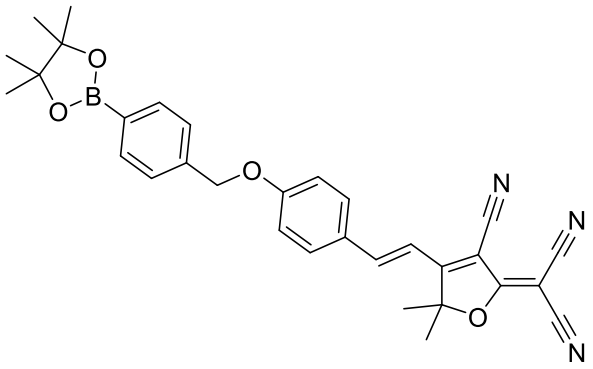

^{1}H Spectra:

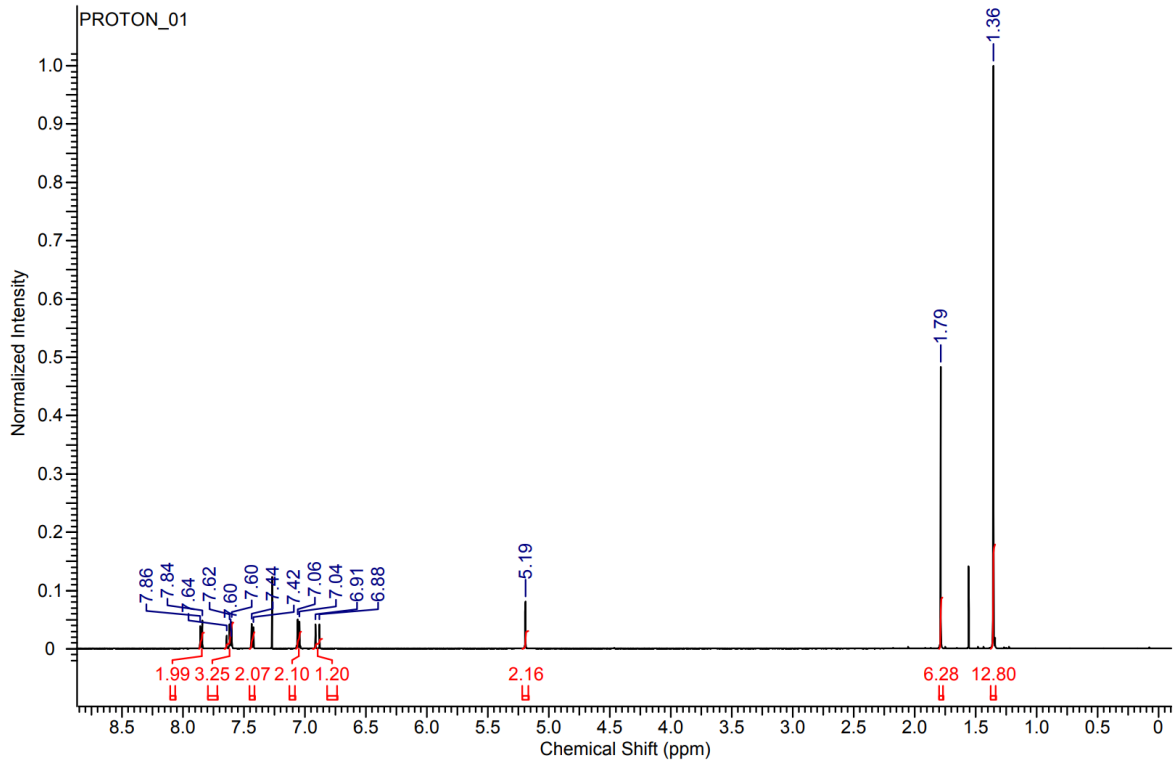

^{13}C Spectra:

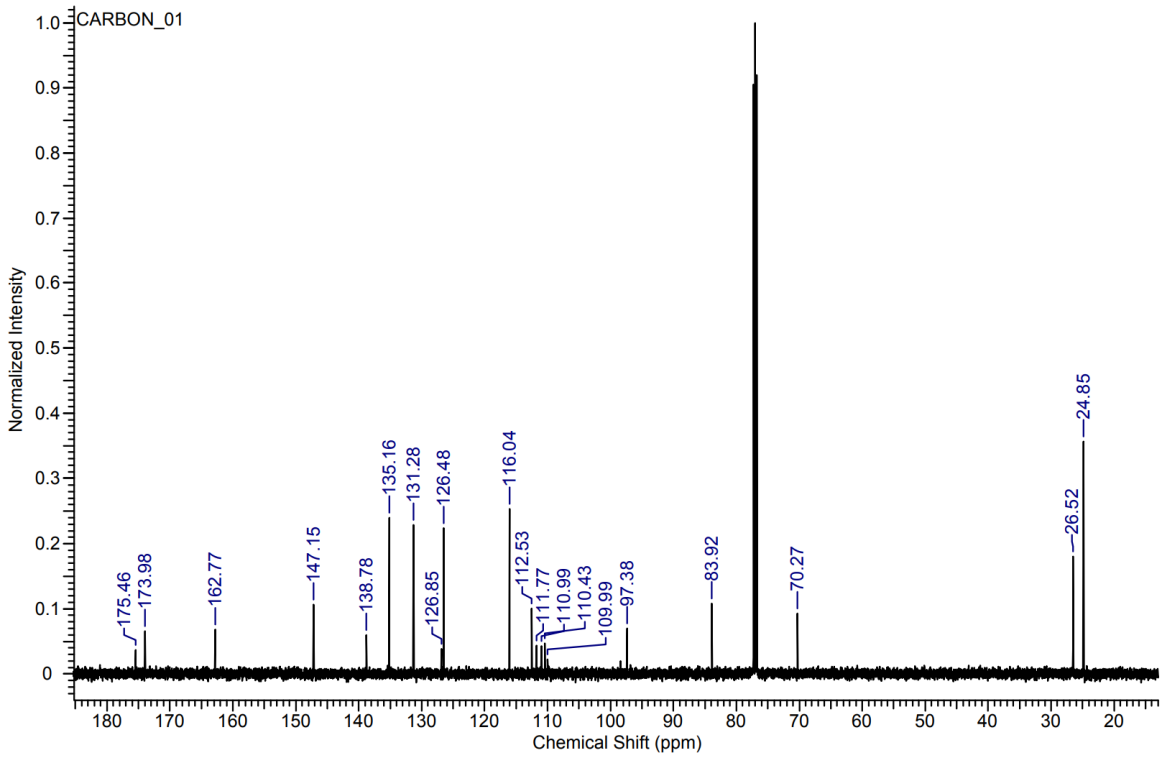
CARBON_01
Normalized Intensity
Chemical Shift (ppm)
175.46
173.98
162.77
147.15
138.78
135.16
131.28
126.48
126.85
116.04
112.53
111.77
110.99
110.43
109.99
97.38
83.92
70.27
26.52
24.85

(*E*)-4-(2-(4-cyano-5-(dicyanomethylene)-2,2-dimethyl-2,5-dihydrofuran-3yl)vinyl)phenyl 2,4-dinitrobenzenesulfonate (**121**):

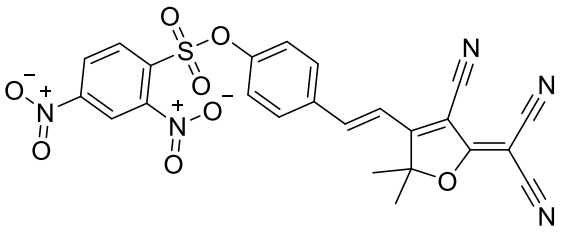

^{1}H Spectra:

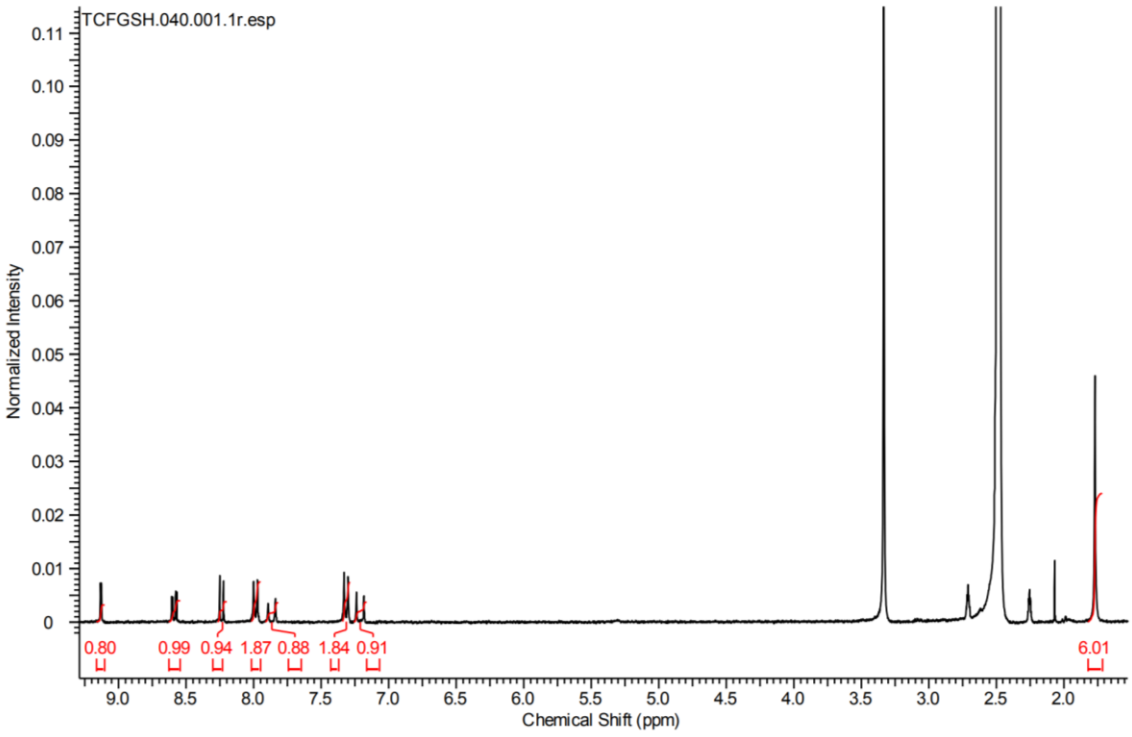

^{13}C Spectra:

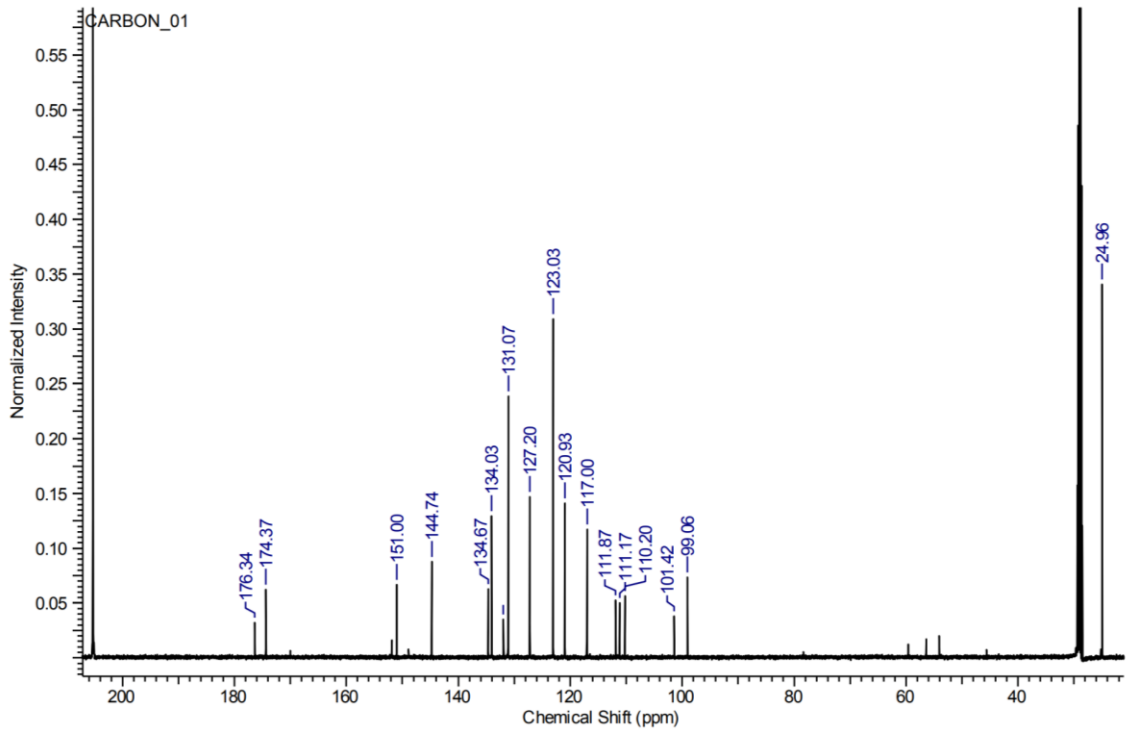
CARBON_01
Normalized Intensity
0.55
0.50
0.45
0.40
0.35
0.30
0.25
0.20
0.15
0.10
0.05
176.34
174.37
151.00
144.74
134.67
134.03
131.07
127.20
123.03
120.93
117.00
111.87
111.17
110.20
101.42
99.06
24.96
200
180
160
140
120
100
80
60
40
Chemical Shift (ppm)

(*E*)-2,6-dichloro-4-(2-(4-cyano-5-(dicyanomethylene)-2,2-dimethyl-2,5-dihydrofuran-3-yl)vinyl)phenyl 2,4-dinitrobenzenesulfonate (**122**):

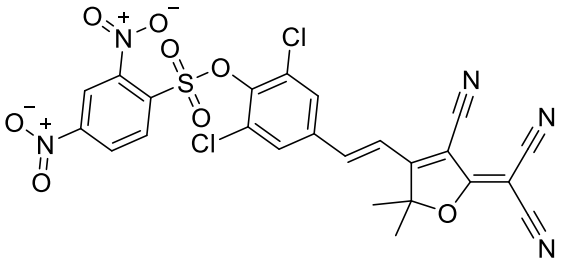

^{1}H Spectra:

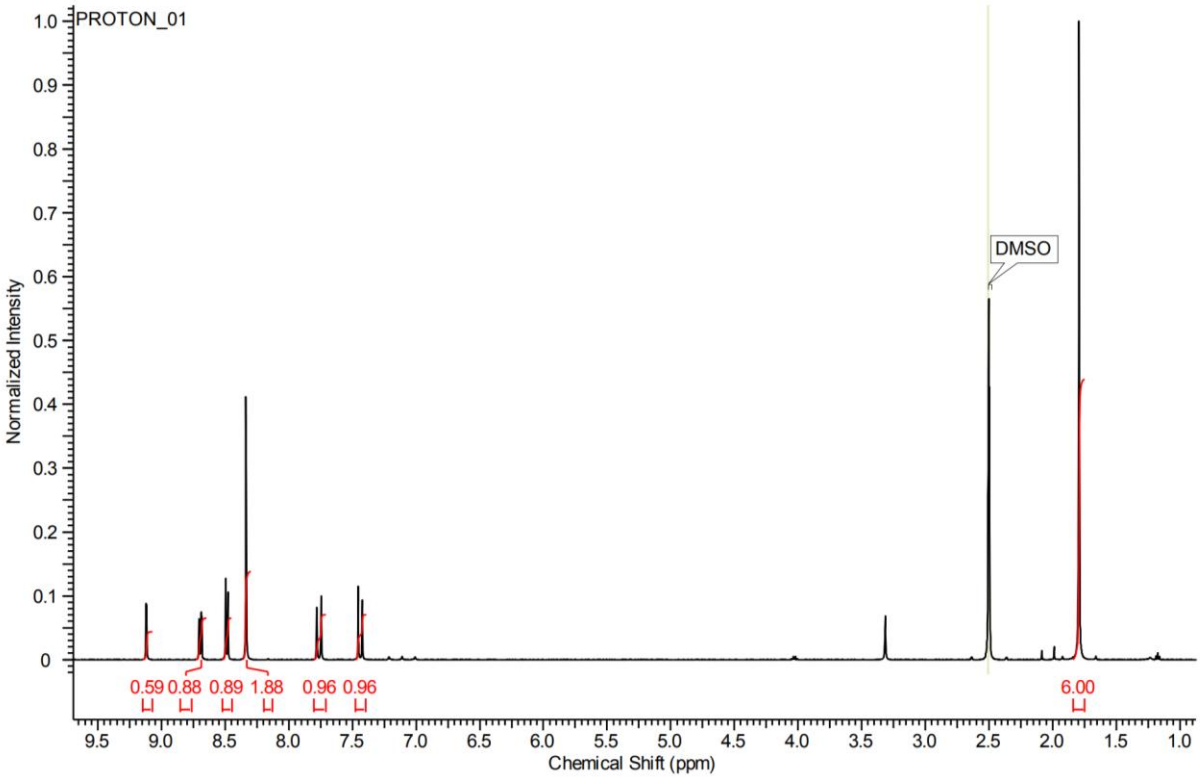

^{13}C Spectra:

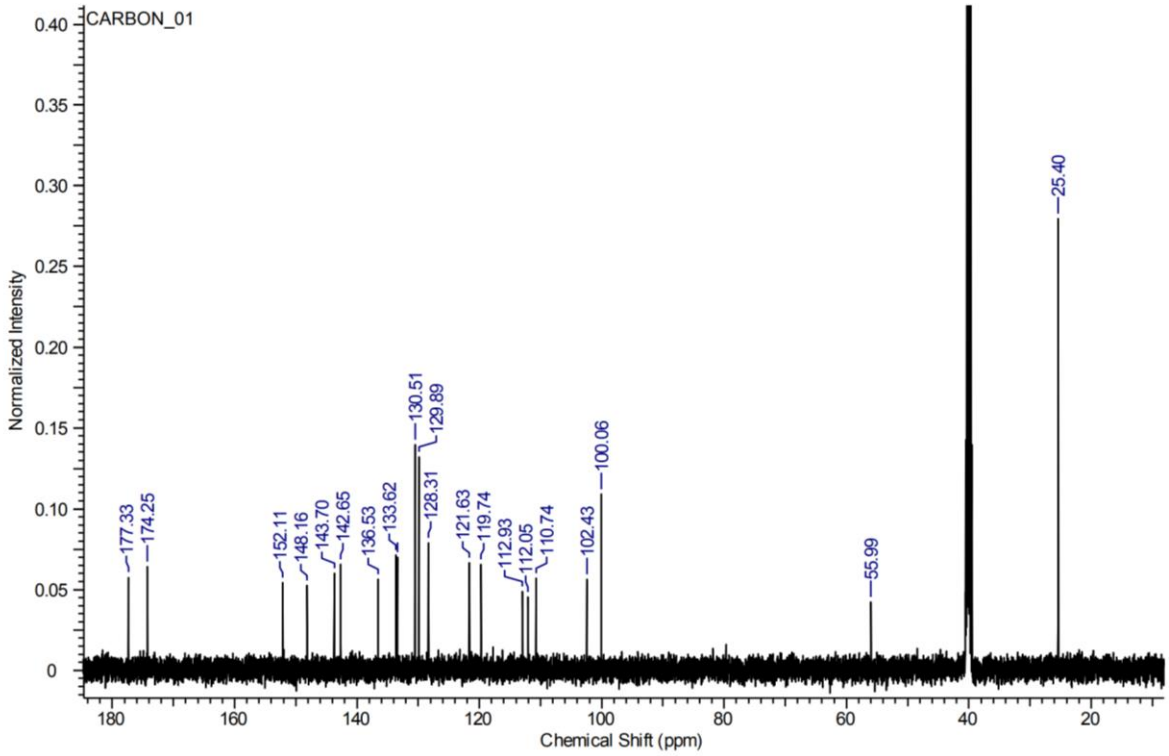
CARBON_01
Normalized Intensity
0.40
0.35
0.30
0.25
0.20
0.15
0.10
0.05
0
177.33
174.25
152.11
148.16
143.70
142.65
136.53
133.62
130.51
129.89
128.31
121.63
119.74
112.93
112.05
110.74
102.43
100.06
55.99
25.40
180
160
140
120
100
80
60
40
20
Chemical Shift (ppm)

7.2 Published Papers

Three papers have been published on some of the works contained within this thesis. They will be presented over the next few pages in their original formatting.

Chemical Science

EDGE ARTICLE

View Article Online
View Journal | View Issue

Cite this: *Chem. Sci.*, 2018, **9**, 3672

The development of a novel AND logic based fluorescence probe for the detection of peroxynitrite and GSH†

Adam C. Sedgwick, ‡*[a] Hai-Hao Han,‡[b] Jordan E. Gardiner,[a] Steven D. Bull,*[a] Xiao-Peng He*[b] and Tony D. James*[a]

We have developed a novel AND logic based fluorescence probe for the simultaneous detection of $ONOO^-$ and GSH (**GSH-PF3**). The **GSH-PF3** probe was synthesised over three steps starting from commercially available fluorescein. The probe was constructed by attaching the GSH reactive motif, 2,4-dinitrobenzenesulfonyl, to the previously reported boronate fluorescence based probe, **PF3**. **GSH-PF3** produced only a small fluorescence response towards the addition of GSH or $ONOO^-$ separately. However, when the probe was exposed to both analytes, there was a significant (40-fold) fluorescence enhancement. **GSH-PF3** demonstrated an excellent selectivity towards both GSH and $ONOO^-$. In cellular imaging experiments the probe was shown to be cell permeable with no 'turn-on' response observed for the addition of either GSH or $ONOO^-$ separately. However, in the presence of both analytes, a clear fluorescence response was observed in live cells. **GSH-PF3** was further able to monitor the co-existence of metabolically produced $ONOO^-$ and GSH by exogenous stimulation.

Received 13th February 2018
Accepted 10th March 2018

DOI: 10.1039/c8sc00733k

rsc.li/chemical-science

Peroxynitrite ($ONOO^-$), is a highly reactive nitrogen species that is formed *via* the diffusion controlled reaction between superoxide anion ($O_2^{\bullet-}$) and nitric oxide ($NO^{\bullet}$).[1,2] $ONOO^-$ acts as a signalling molecule *in vivo* for a number of pathways.[1,3] However, $ONOO^-$ is more commonly known for its deleterious properties, causing irreversible damage to a range of biological targets such as lipids, proteins and DNA.[4] Therefore, $ONOO^-$ has been implicated as a key pathogenic factor for a number of diseases, which include inflammation, cancer, ischemia-reperfusion and neurodegenerative diseases.[5–7] Glutathione (GSH) is a natural tripeptide (γ-L-glutamyl-L-cysteinyl-glycine), that exists in the thiol reduced form (GSH) and disulphide-oxidised (GSSG) form. GSH is the predominant form, existing at millimolar concentrations in most cells.[8] However, GSH can be directly oxidised by $ONOO^-$ therefore acting as a cellular defence by serving as an $ONOO^-$ scavenger. Elevated levels of GSH are common in cells under oxidative stress and the susceptibility of a cell towards $ONOO^-$ largely depends on the concentration of intracellular GSH.[1,9,10]

Therefore, with this work we set out to develop a fluorescence-based probe capable of monitoring the close relationship between $ONOO^-$ and GSH. Traditionally, most fluorescence probes require a single analyte to produce a fluorescence response.[11–19] However, in recent years a number of fluorescence based probes for dual or multi-analyte detection have been developed.[20–27] These types of fluorescence based probes have been used for the construction of molecular logic gates or for medical diagnostics.[28] AND logic based fluorescence probes require both analytes to be simultaneously present or work in tandem in order to elicit a fluorescence response. This method has a number of advantages including: being faster than serial measurements for different analytes within the same biological sample and can provide a method for monitoring bimolecular events, which may contribute to a specific disease.[20]

Currently, only a few reversible fluorescence based probes for the detection of $ONOO^-$ and GSH have been developed to monitor the relationship between these analytes.[29,30] These include a selenium based fluorescence probe, which is oxidised by $ONOO^-$ (turn "on") and reduced by GSH (turn "off"). The fluorescence of the CyPSe probe is initially quenched by a photoinduced electron transfer (PET) process. The presence of $ONOO^-$ results in the oxidation of selenium to CyPSe=O causing the fluorescence emission to be "turned on". Then in the presence of biological thiols such as cysteine and GSH, the CyPSe=O probe is reduced back to its non-fluorescent selenide

[a]*Department of Chemistry, University of Bath, Bath, BA2 7AY, UK. E-mail: a.c.sedgwick@bath.ac.uk; s.d.bull@bath.ac.uk; t.d.james@bath.ac.uk*

[b]*Key Laboratory for Advanced Materials and Joint International Research Laboratory of Precision Chemistry and Molecular Engineering, Feringa Nobel Prize Scientist Joint Research Center, School of Chemistry and Molecular Engineering, East China University of Science and Technology, 130 Meilong Rd., Shanghai 200237, China. E-mail: xphe@ecust.edu.cn*

† Electronic supplementary information (ESI) available: Additional figures, experimental section and original spectra of new compounds. See DOI: 10.1039/c8sc00733k

‡ These authors contributed equally.

form. A similar reversible NIR Tellurium-based fluorescence probe was later developed for monitoring the redox cycles between $ONOO^-$ and GSH. This probe was successfully applied for the visualisation of the redox cycles of $ONOO^-$ and GSH in live cells and animals.[29] The probes developed by Han *et al.* are turn "on" with $ONOO^-$ and "off" with GSH. As far as we are aware, there are currently no AND logic based fluorescence probes for GSH "and" $ONOO^-$.

With this research, we aimed to develop a GSH "and" $ONOO^-$ logic based fluorescence probe (Scheme 1). We identified a suitable mono-boronate fluorescein based fluorescence probe, **PF3** that had been previously developed by Chang *et al.*, shown in Scheme 2. As previously reported the reactivity of boronate based fluorescence probes with $ONOO^-$,[12,14,15] are significantly greater than hypochlorite (ClO^-) and H_2O_2.[31] Therefore, we anticipated that the attachment of a GSH reactive motif to **PF3** would produce a selective GSH-$ONOO^-$ AND logic based fluorescence probe, **GSH-PF3** (Scheme 2). **GSH-PF3** was readily synthesised in three steps. Fluorescein was triflated using *N*-phenyl bis(trifluoromethanesulfonamide) to afford fluorescein mono-triflate in good yield. Suzuki–Miyaura conditions were then carried out to provide fluorescein mono-boronate, **PF3**. The 2,4-dinitrobenzenesulfonyl unit was then attached to **PF3** using 2,4-dinitrobenzenesulfonyl chloride, CH_2Cl_2 and NEt_3 at 0 °C. Using these conditions **GSH-PF3** was prepared in a reasonable yield of 52%.

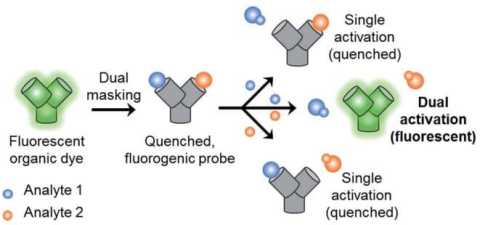

Scheme 1 Design concept for AND logic based fluorogenic probe. A fluorescence dye is masked by two functional groups, which respond to two different analytes. The fluorogenic probe requires both analytes to be present or to work in tandem in order to produce a response.

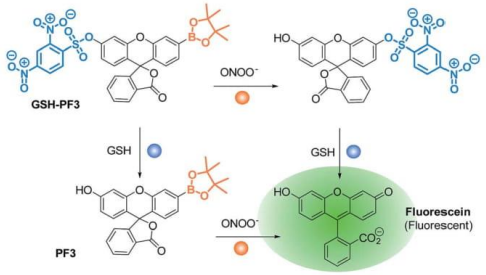

Scheme 2 Structure of the GSH-PF3 probe and proposed sensing mechanism for the simultaneous detection of $ONOO^-$ and GSH.

With **GSH-PF3** in hand, fluorescence experiments for the detection of GSH and $ONOO^-$ were performed. As shown in Fig. 1, **GSH-PF3** was initially non-fluorescent and with the addition of $ONOO^-$ (10 μM), a small fluorescence increase was observed. However, incremental additions of GSH resulted in a much larger increase in fluorescence intensity (>30-fold see ESI – Fig. S1†), clearly demonstrating the need for the addition of both GSH and $ONOO^-$ in order to achieve a full 'turn-on' response.

In order to demonstrate that **GSH-PF3** required both GSH and $ONOO^-$ for a complete 'turn-on' response, the fluorescence experiments were performed the other way around. Therefore, an excess of GSH (200 μM) was added to **GSH-PF3**, and the probe was incubated for 10 min. Remarkably, this only led to a small increase in fluorescence intensity and the subsequent additions of $ONOO^-$ resulted in a large fluorescence increase (Fig. 2 and ESI – Fig S2†). These results confirm that the probe requires both GSH and $ONOO^-$ for a full fluorescence 'turn-on' response.

The selectivity of **GSH-PF3** was then evaluated against a series of amino acids (L-cysteine, L-methionine, L-tryptophan, L-serine, L-lysine, L-leucine, L-glutamic acid, L-valine, L-arginine, L-histidine and L-aspartic acid) – see ESI Fig. S3.† Unsurprisingly, the probe responded to the other sulfhydryl containing amino acid cysteine. However, the biological concentrations of cysteine are low in cells.[32] More importantly, **GSH-PF3** displayed an excellent selectivity against other amino acids including serine, methionine and lysine. The probe demonstrated excellent selectivity for $ONOO^-$ over many other ROS including H_2O_2 (see ESI – Fig. S4†). The excellent selectivity for both GSH and $ONOO^-$ allowed us to evaluate **GSH-PF3** in cell imaging experiments.

The macrophage cell line – RAW264.7 (ATCC® TIB-71™; obtained from ATCC [American Type Culture Collection]) – was used for cell imaging experiments. The cells were incubated with **GSH-PF3**, followed by either treatment of SIN-1 (an $ONOO^-$ donor)[33] to produce intracellular $ONOO^-$ or by addition of

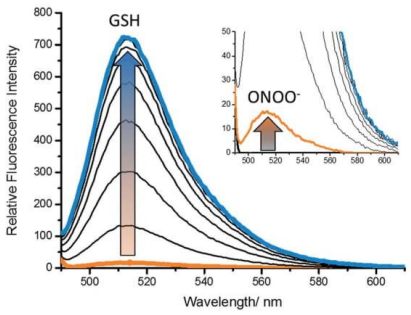

Fig. 1 Fluorescence spectra of **GSH-PF3** (0.5 μM) with addition of $ONOO^-$ (10 μM) (inset) followed by the addition of GSH (0–80 μM), 5 min wait between addition in buffer solution [52 wt% methanol] (pH = 8.21 at 25 °C). Fluorescence intensities were measured with λ_{ex} = 488 nm with slit widths ex slit: 5 nm and em slit: 2.5 nm.

View Article Online

Chemical Science

Edge Article

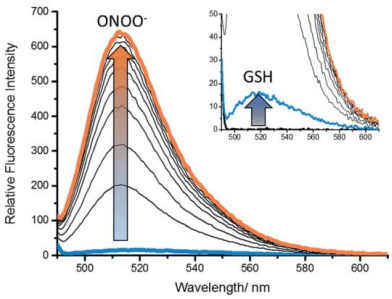

Fig. 2 Fluorescence spectra of **GSH-PF3** (0.5 μM) with addition of GSH (200 μM), 10 min wait (inset), then addition of $ONOO^-$ (0–10 μM) in buffer solution [52 wt% methanol] (pH = 8.21 at 25 °C). Fluorescence intensities were measured with λ_{ex} = 488 nm with slit widths ex slit: 5 nm and em slit: 2.5 nm.

exogenous GSH. As shown below in Fig. 3, addition of GSH separately resulted in no fluorescence response, whereas $ONOO^-$ led to a small fluorescence response in cells. This observation is believed to be due to the presence of a low levels of endogenous biological thiols in the cells, resulting in the activation of the probe's fluorescence. As predicted, treatment of cells with both GSH and SIN-1 led to a clear fluorescence increase in RAW264.7 cells with **GSH-PF3**, in clear agreement with the analytical data obtained on the fluorimeter.

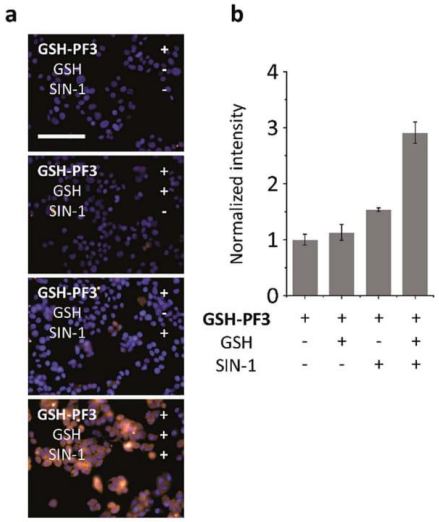

Fig. 3 Fluorescence imaging (a) and quantification (b) of RAW264.7 cells with **GSH-PF3** (10 μM) in the absence and presence of exogenously added GSH (50 μM) and/or SIN-1 (500 μM). Excitation channel = 460–490 nm, emission channel filtered = 530–590 nm. Cell nuclei were stained with Hoechst 33342. Scale bar = 100 μm. Error bars represent SD.

We then turned our attention to evaluate the ability of **GSH-PF3** for monitoring the co-existence of metabolically produced $ONOO^-$ by lipopolysaccharide (LPS) simulation[34] and GSH through a drug treatment.[35] It has been reported that LPS can elicit $ONOO^-$ in macrophage, which is a signature of inflammation, whereas caffeic acid (CA) is commonly used to treat inflammation through the augmentation of intracellular GSH. Consequently, treatment with LPS, followed by the addition of increasing CA (0–100 μM) led to a gradual enhancement in the fluorescence intensity of **GSH-PF3** (Fig. 4). This result is due to the co-existence of $ONOO^-$ produced by LPS stimulation as well as GSH elicited by CA. Interestingly, a further increase of the CA concentration (>100 μM) led to the suppression of probe's fluorescence, which is believed to be due to the production of an excess of GSH, resulting in quenching of the $ONOO^-$ (Fig. 4). To corroborate the presence of intracellular GSH in macrophage, a commercial GSH probe was used. The result suggested that both the exogenous addition of GSH and stimulation of metabolic GSH by treatment of CA/LPS activated the commercial probe's fluorescence (Fig. S5†). Furthermore, a cell proliferation assay indicated that **GSH-PF3** is not toxic for RAW264.7 cells (Fig. S6†).

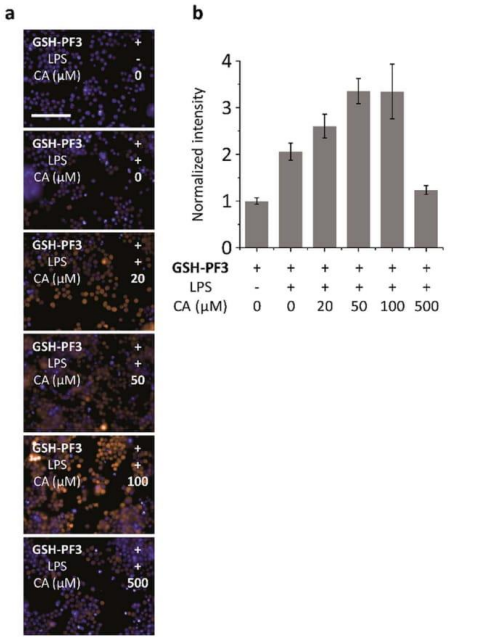

Fig. 4 Fluorescence imaging (a) and quantification (b) of RAW264.7 cells with **GSH-PF3** (10 μM) in the absence and presence of LPS (1 μg mL^{-1}), which elicits $ONOO^-$ and increasing caffeic acid (CA, a drug that elicits endogenous GSH to quench $ONOO^-$). Excitation channel = 460–490 nm, emission channel filtered = 530–590 nm. Cell nuclei were stained with Hoechst 33342. Scale bar = 100 μm. Error bars represent SD.

These results clearly demonstrate the potential of AND logic based fluorescence imaging probes for optimizing drug dosage in the treatment of inflammation and various other diseases. In addition this system could be used to help monitor the treatment of Alzheimer's disease (AD), since it is known that high levels of $ONOO^-$ correlate with oxidative stress and the progression of AD, while, high levels of GSH have been implicated in AD therapy.[36–39] Therefore, we believe that our **GSH-PF3** probe, which can detect GSH "and" $ONOO^-$ could potentially be used to monitor cellular resistance towards ROS and map therapeutic improvements in AD victims.

In summary, **GSH-PF3** is an easy-to-prepare fluorescence based probe providing a platform for the development of other novel AND logic based fluorescence imaging probes for use in medical diagnostics. We are currently exploring the use of 6-amino/carboxyfluorescein, which we believe could provide the opportunity to attach additional fluorophores in order to develop ratiometric fluorescence sensors[40] or for the attachment of targeting or therapeutic units.[41–43]

Conflicts of interest

No conflicts of interest.

Acknowledgements

We would like to thank the EPSRC and the University of Bath for funding. ACS and JEG thank the EPSRC for studentships. X.-P. He thanks the National Natural Science Foundation of China (21722801 and 21572058), the Science and Technology Commission of Shanghai Municipality (15540723800), the Fundamental Research Funds for the Central Universities (222201717003) and the Shanghai Rising-Star Program (16QA1401400) for financial support. TDJ wishes to thank the Royal Society for a Wolfson Research Merit Award and ECUST for a guest professorship. The Catalysis and Sensing for our Environment (CASE) network is thanked for research exchange opportunities. NMR characterisation facilities were provided through the Chemical Characterisation and Analysis Facility (CCAF) at the University of Bath (http://www.bath.ac.uk/ccaf). The EPSRC UK National Mass Spectrometry Facility at Swansea University is thanked for analyses. All data supporting this study are provided as Electronic Supplementary Information (ESI) accompanying this paper.

Notes and references

1 P. Pacher, J. S. Beckman and L. Liaudet, *Physiol. Rev.*, 2007, **87**, 315.
2 J. S. Beckman and W. H. Koppenol, *Am. J. Physiol. Cell Physiol.*, 1996, **271**, C1424.
3 A. Weidinger and A. V. Kozlov, *Biomolecules*, 2015, **5**, 472.
4 P. Ascenzi, A. di Masi, C. Sciorati and E. Clementi, *Biofactors*, 2010, **36**, 264.
5 H. Ischiropoulos and J. S. Beckman, *J. Clin. Invest.*, 2003, **111**, 163.
6 P. Sarchielli, F. Galli, A. Floridi and V. Gallai, *Amino Acids*, 2003, **25**, 427.
7 D. A. Wink, Y. Vodovotz, J. Laval, F. Laval, M. W. Dewhirst and J. B. Mitchell, *Carcinogenesis*, 1998, **19**, 711.
8 S. C. Lu, *Mol. Aspect. Med.*, 2009, **30**, 42.
9 K. A. Marshall, R. Reist, P. Jenner and B. Halliwell, *Free Radic. Biol. Med.*, 1999, **27**, 515.
10 J. P. Bolanos, S. J. R. Heales, J. M. Land and J. B. Clark, *J. Neurochem.*, 1995, **64**, 1965.
11 M. Li, X. M. Wu, Y. Wang, Y. S. Li, W. H. Zhu and T. D. James, *Chem. Commun.*, 2014, **50**, 1751.
12 S. Palanisamy, P. Y. Wu, S. C. Wu, Y. J. Chen, S. C. Tzou, C. H. Wang, C. Y. Chen and Y. M. Wang, *Biosens. Bioelectron.*, 2017, **91**, 849.
13 D. Cheng, Y. Pan, L. Wang, Z. B. Zeng, L. Yuan, X. B. Zhang and Y. T. Chang, *J. Am. Chem. Soc.*, 2017, **139**, 285.
14 A. C. Sedgwick, X. L. Sun, G. Kim, J. Yoon, S. D. Bull and T. D. James, *Chem. Commun.*, 2016, **52**, 12350.
15 X. Sun, Q. Xu, G. Kim, S. E. Flower, J. P. Lowe, J. Yoon, J. S. Fossey, X. Qian, S. D. Bull and T. D. James, *Chem. Sci.*, 2014, **5**, 3368.
16 J. Yin, Y. Kwon, D. Kim, D. Lee, G. Kim, Y. Hu, J. H. Ryu and J. Yoon, *J. Am. Chem. Soc.*, 2014, **136**, 5351.
17 Q. Xu, K.-A. Lee, S. Lee, K. M. Lee, W.-J. Lee and J. Yoon, *J. Am. Chem. Soc.*, 2013, **135**, 9944.
18 Z. Lei, X. Li, X. Luo, H. He, J. Zheng, X. Qian and Y. Yang, *Angew. Chem., Int. Ed.*, 2017, **56**, 2979.
19 Y. Kuriki, M. Kamiya, H. Kubo, T. Komatsu, T. Ueno, R. Tachibana, K. Hayashi, K. Hanaoka, S. Yamashita, T. Ishizawa, N. Kokudo and Y. Urano, *J. Am. Chem. Soc.*, 2018, **140**, 1767.
20 A. Romieu, *Org. Biomol. Chem.*, 2015, **13**, 1294.
21 L. Yu, S. L. Wang, K. Z. Huang, Z. G. Liu, F. Gao and W. B. Zeng, *Tetrahedron*, 2015, **71**, 4679.
22 G. C. Van de Bittner, C. R. Bertozzi and C. J. Chang, *J. Am. Chem. Soc.*, 2013, **135**, 1783.
23 L. Yuan, W. Y. Lin, Y. N. Xie, B. Chen and S. S. Zhu, *J. Am. Chem. Soc.*, 2012, **134**, 1305.
24 C. G. Dai, X. L. Liu, X. J. Du, Y. Zhang and Q. H. Song, *ACS Sens.*, 2016, **1**, 888.
25 S. Debieu and A. Romieu, *Org. Biomol. Chem.*, 2015, **13**, 10348.
26 L. Yi, L. Wei, R. Y. Wang, C. Y. Zhang, J. Zhang, T. W. Tan and Z. Xi, *Chem.–Eur. J.*, 2015, **21**, 15167.
27 C. Y. Ang, S. Y. Tan, S. J. Wu, Q. Y. Qu, M. F. E. Wong, Z. Luo, P. Z. Li, S. T. Selvan and Y. L. Zhao, *J. Mater. Chem. C*, 2016, **4**, 2761.
28 S. Erbas-Cakmak, S. Kolemen, A. C. Sedgwick, T. Gunnlaugsson, T. D. James, J. Yoon and E. U. Akkaya, *Chem. Soc. Rev.*, 2018, DOI: 10.1039/c7cs00491e.
29 F. B. Yu, P. Li, B. S. Wang and K. L. Han, *J. Am. Chem. Soc.*, 2013, **135**, 7674.
30 F. B. A. Yu, P. Li, G. Y. Li, G. J. Zhao, T. S. Chu and K. L. Han, *J. Am. Chem. Soc.*, 2011, **133**, 11030.
31 A. Sikora, J. Zielonka, M. Lopez, J. Joseph and B. Kalyanaraman, *Free Radic. Biol. Med.*, 2009, **47**, 1401.

32 G. Y. Wu, Y. Z. Fang, S. Yang, J. R. Lupton and N. D. Turner, *J. Nutr.*, 2004, **134**, 489.

33 X. Li, R. R. Tao, L. J. Hong, J. Cheng, Q. Jiang, Y. M. Lu, M. H. Liao, W. F. Ye, N. N. Lu, F. Han, Y. Z. Hu and Y. H. Hu, *J. Am. Chem. Soc.*, 2015, **137**, 12296.

34 A. Vazquez-Torres, J. Jones-Carson and E. Balish, *Infect. Immun.*, 1996, **64**, 3127.

35 M. Y. Moridani, H. Scobie, A. Jamshidzadeh, P. Salehi and P. J. O'Brien, *Drug Metab. Dispos.*, 2001, **29**, 1432.

36 M. A. Smith, P. L. R. Harris, L. M. Sayre, J. S. Beckman and G. Perry, *J. Neurosci.*, 1997, **17**, 2653.

37 E. Rojas-Gutierrez, G. Munoz-Arenas, S. Trevino, B. Espinosa, R. Chavez, K. Rojas, G. Flores, A. Diaz and J. Guevara, *Synapse*, 2017, **71**, e21990.

38 C. B. Pocernich and D. A. Butterfield, *Biochim. Biophys. Acta, Mol. Basis Dis.*, 2012, **1822**, 625.

39 I. Cacciatore, L. Baldassarre, E. Fornasari, A. Mollica and F. Pinnen, *Oxid. Med. Cell. Longevity*, 2012, 240146.

40 A. E. Albers, V. S. Okreglak and C. J. Chang, *J. Am. Chem. Soc.*, 2006, **128**, 9640.

41 M. H. Lee, J. Y. Kim, J. H. Han, S. Bhuniya, J. L. Sessler, C. Kang and J. S. Kim, *J. Am. Chem. Soc.*, 2012, **134**, 12668.

42 S. Bhuniya, S. Maiti, E. J. Kim, H. Lee, J. L. Sessler, K. S. Hong and J. S. Kim, *Angew. Chem., Int. Ed.*, 2014, **53**, 4469.

43 X.-P. He and H. Tian, *Chem*, 2018, **4**, 246.

ChemComm

COMMUNICATION

View Article Online
View Journal | View Issue

Cite this: *Chem. Commun.*, 2017, **53**, 12822

Received 10th October 2017,
Accepted 3rd November 2017

DOI: 10.1039/c7cc07845e

rsc.li/chemcomm

Long-wavelength fluorescent boronate probes for the detection and intracellular imaging of peroxynitrite†

Adam C. Sedgwick, *[a] Hai-Hao Han,[b] Jordan E. Gardiner,[a] Steven D. Bull,*[a] Xiao-Peng He*[b] and Tony D. James*[a]

Two boronate fluorescent probes have been developed for the detection of peroxynitrite (TCFB1 and TCFB2). TCFB1 was shown to have a low sensitvity towards peroxynitrite and have a poor solubility in aqueous solution whereas TCFB2 demonstrated high sensitivity towards peroxynitrite and mitochondria localisation with the ability to detect exogenous and endogenous peroxynitrite in live cells (Hep-G2, RAW 264.7, HeLa and A459).

Peroxynitrite ($ONOO^-$) is a highly reactive nitrogen species that is formed *via* the diffusion controlled reaction between superoxide ($^-O_2$) and nitric oxide (NO).[1,2] $ONOO^-$ acts as a signalling molecule *in vivo* for a number of pathways.[1,3] However, $ONOO^-$ is more commonly known for its deleterious properties, causing irreversible damage to a range of biological targets such as lipids, proteins and DNA.[4] Therefore, $ONOO^-$ has been implicated as a key pathogenic factor for a number of diseases, which include inflammation, cancer, ischemia-reperfusion and neurodegenerative diseases.[5–7] In biological systems, $ONOO^-$ is difficult to measure due to it being short-lived with a half-life ~10–20 ms.[1] Therefore, the development of powerful tools for the detection of $ONOO^-$ is of significant interest.

With our research, we are particularly interested in the development of small molecule fluorescent probes for the detection of biologically relevant analytes *in vivo* owing to their high sensitivity, selectivity and high spatial and temporal resolution. In the past few years, a number of $ONOO^-$ fluorescent probes have been developed for imaging in live cells and mice.[8–13] However, despite significant progress in this area of research, there is a lack of long-wavelength $ONOO^-$ fluorescent probes. The development of long wavelength/near infrared (NIR) probes is of particular interest because longer excitation/emission wavelengths allows deeper tissue penetration and minimalises background auto-fluorescence from proteins and photodamage to the biological samples.[14,15]

In the literature, Sikora *et al.* reported that the reaction rates of $ONOO^-$ with aromatic boronates are 200 times faster than hypochlorous acid ($HOCl/ClO^-$) and a million times faster than hydrogen peroxide (H_2O_2).[16] Therefore, a number of boronate fluorescent probes have been recently developed for the detection of $ONOO^-$.[8,17,18]

2-Dicyanomethylene-3-cyano-4,5,5-trimethyl-2,5-dihydrofuran (TCF)-based fluorophores have an internal charge transfer (ICT) donor-π-acceptor (D-π-A) structure with long emission wavelengths. As a result, TCF fluorophores have been used in many applications such as non-linear optic chromophores and molecular probes.[19–25] With this research, we developed two boronate TCF-based fluorescent probes for the detection of $ONOO^-$ (**TCFB1** and **TCFB2**). The TCF fluorophore unit was synthesised in one step using the reaction of 3-hydroxy-3-methyl-2-butanone, malonitrile and NaOEt in EtOH. With the TCF unit in hand, the (D-π-A) systems **TCFB1** and **TCFB2** were isolated in high yield using microwave reaction conditions.[26] The microwave irradiation of a mixture of piperidine (Cat.), TCF and 4-(4,4,5,5-tetramethyl-1,3,2-dioxaborolan-2-yl)benzaldehyde in EtOH followed by filtration led to the isolation of the desired **TCFB2**. For the synthesis of **TCFB1**, microwave irradiation of a mixture of piperidine (Cat.), TCF and 4-hydroxybenzaldehyde in EtOH followed by filtration led to the isolation of the intermediate TCF-OH. This was subsequently alkylated with 2-(4-(bromomethyl)phenyl)-4,4,5,5-tetramethyl-1,3,2-dioxaborolane using K_2CO_3 and NaI in MeCN to afford **TCFB1** in a reasonable yield (47%).

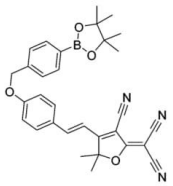

TCFB1

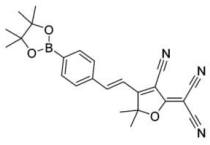

TCFB2

[a] *Department of Chemistry, University of Bath, Bath, BA2 7AY, UK. E-mail: t.d.james@bath.ac.uk, s.d.bull@bath.ac.uk*
[b] *Key Laboratory for Advanced Materials & Feringa Nobel Prize Scientist Joint Research Center, East China University of Science and Technology, 130 Meilong Rd., Shanghai 200237, P. R. China. E-mail: xphe@ecust.edu.cn*

† Electronic supplementary information (ESI) available. See DOI: 10.1039/c7cc07845e

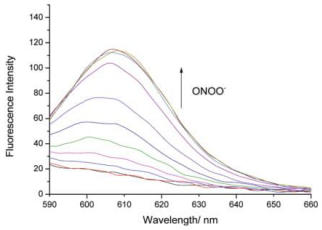

Fig. 1 Fluorescence spectra of **TCFB1** (10 μM) with addition of $ONOO^-$ (0–100 μM) in PBS buffer solution, 20% DMSO, pH 8.00 at 25 °C. λ_{ex} = 560 nm. Slit widths ex = 10 nm and em = 15 nm.

We initially evaluated the UV-Vis (Fig. S2, ESI†) and fluorescence behaviour (Fig. 1 and Fig. S3, ESI†) of **TCFB1**, in pH 8.0 buffer solution (20% DMSO). DMSO was required to improve the aqueous solubility of **TCFB1**. Under these conditions, **TCFB1** produced an up to 6.5-fold fluorescence "turn on" in the presence of $ONOO^-$ (0–100 μM). (Schemes S1, S2 and Fig. S1, ESI†) However, in comparison to our previously reported ESIPT probe, **TCFB1** was less sensitive towards $ONOO^-$ despite a larger "turn on" response.[8]

Subsequently, we evaluated the selectivity of **TCFB1** towards other ROS (Fig. S4, S5 and S11, ESI†). **TCFB1** demonstrated an excellent selectivity for $ONOO^-$, which permitted the evaluation of its ability to detect exogenous and endogenous $ONOO^-$ in live cells. Unfortunately, due to its poor aqueous solubility, large amounts of precipitate with **TCFB1** was observed (data not shown).

Therefore, we turned our attention towards the evaluation of the UV-Vis and fluorescence properties of **TCFB2**, which has previously been reported for the detection of ClO^-.[20] As previously reported for other aryl boronate fluorescent probes,[27,28] **TCFB2** was found to be initially non-fluorescent with no UV absorption beyond ~525 nm (Fig. S6, ESI†). The addition of $ONOO^-$ to **TCFB2** resulted in the appearance of a large emission peak at 606 nm (Fig. 2 and Fig. S7, ESI†). This was accompanied by a colorimetric response (yellow to pink) and the appearance of a large UV absorption peak at ~590 nm. **TCFB2** demonstrated high sensitivity and rapid reaction (Fig. S8, ESI†) with $ONOO^-$ and was able to detect very low concentrations (0–10 μM).

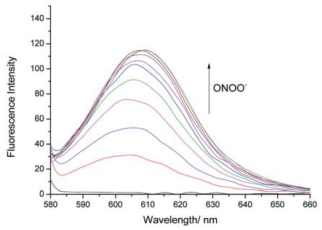

Fig. 2 Fluorescence spectra of **TCFB2** (10 μM) with addition of $ONOO^-$ (0–10 μM) in PBS buffer solution, 20% DMSO, pH 8.00 at 25 °C. λ_{ex} = 560 nm. Slit widths ex = 10 nm and em = 15 nm.

As predicted, both ClO^- and H_2O_2 also resulted in a fluorescence response (Fig. S9, S10 and S12, ESI†), however, larger concentrations and reaction times were required. These observations clearly, demonstrated the greater reactivity of the boronate towards $ONOO^-$.

Having determined the selectivity of **TCFB2**, we evaluated its ability to image endogenous and exogenous $ONOO^-$ in live cells. **TCFB2** was evaluated in a number of different cell lines (Hep-G2: human hepatoma, HeLa: human cervical cancer, RAW 264.7: mouse macrophage and A549 cells: human lung cancer), which were incubated with **TCFB2** (10 μM) for 30 minutes and washed with PBS buffer solution three times. As shown in Fig. 3, **TCFB2** demonstrated a clear "turn on" response with the addition of SIN-1 ($ONOO^-$ donor). No "turn on" response was observed when the cells were pre-treated with the $ONOO^-$ scavenger uric acid. **TCFB2** also provided a clear "turn on" response for the detection of stimulated $ONOO^-$. RAW 264.7 cells were used in which $ONOO^-$ was stimulated using lipopolysaccharide (LPS).[29] This led to the activation of the TCFB2 fluorescence intracellularly (Fig. 4). In contrast, no "turn on" response was observed in the presence of uric acid indicating the selectivity for $ONOO^-$ in cells. A cell proliferation assay showed that the compound was not toxic towards all the cell lines used with concentrations well above that used for imaging (Fig. S13, ESI†).

The production of superoxide occurs mainly through the mitochondrial electron transport pathway;[30] therefore the mitochondria are the main source of $ONOO^-$ in macrophages. Commercial Mito-tracker Green was used to localise in the mitochondrial compartments of RAW 264.7. We then used **TCFB2** to investigate the subcellular distribution of $ONOO^-$. The results indicated that the fluorescence of the probe co-localised with that

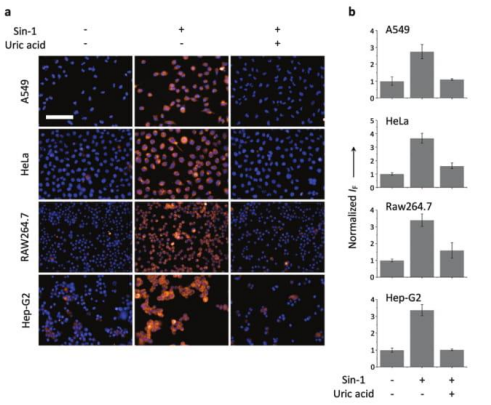

Fig. 3 (a) Fluorescence imaging (scale bar = 100 μm) (b) quantification of different cells incubated with **TCFB2** (10 μM) without (–/–) or with a subsequent addition of Sin-1 (500 μM, a $ONOO^-$ promoter) (+/–) or a subsequent addition of and uric acid (100 μM, a $ONOO^-$ quencher) and then Sin-1 (+/+). Excitation and emission wavelengths for **TCFB2** are 560–580 nm and 580–650 nm, respectively. The cell nuclei were stained by Hoechst 33342.

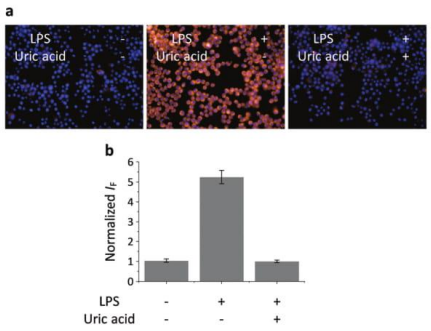

Fig. 4 (a) Fluorescence imaging (scale bar = 100 μm) (b) quantification of RAW 264.7 incubated with **TCFB2** (10 μM) without (−/−) or with a subsequent addition of lipopolysaccharide (LPS, 1 μg mL^{-1}) (+/−) or a subsequent addition of both LPS and uric acid (100 μM, a $ONOO^-$ quencher) (+/+). Excitation and emission wavelength for **TCFB2** are 560–580 nm and 580–650 nm, respectively. The cell nuclei were stained by Hoechst 33342.

of the tracker resulting in a Pearson coefficient of 0.84 (Fig. 5). We have also carried out an additional lysosome co-localisation assay, and the result showed that the probe did not co-localise well with lysosome (Pearson's correlation = 0.38) (Fig. S14, ESI†). This suggests that $ONOO^-$ was produced at the mitochondria.

In conclusion, we have developed two long-wavelength reaction based fluorescent probes for the detection of $ONOO^-$. Unfortunately, **TCFB1** had a low solubility in aqueous solution, which led to the observation of precipitates in cell imaging experiments. A glycosylation strategy[31,32] to improve the water solubility of the insoluble **TCFB1** is currently underway in our laboratories. However, **TCFB2** displayed selective and sensitive "turn on" with the addition of $ONOO^-$. The large fluorescence response observed for **TCFB2** facilitated its use in cell imaging experiments. Therefore, **TCFB2** was able to detect exogenous and endogenous $ONOO^-$ with a large fluorescence "turn on" over a range of cell lines (Hep-G2, RAW 264.7, HeLa and A459). Mitochondrial localisation of **TCFB2** was observed by co-localisation with Mito-Tracker Green. Overall, these results demonstrate that **TCFB2** is a useful tool to understand the role of $ONOO^-$ in biological systems and could lead to systems capable of disease diagnosis.

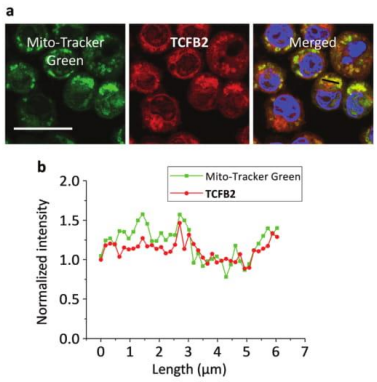

Fig. 5 (a) Fluorescence co-localisation of **TCFB2** (10 μM) with Mito-Tracker Green (1 μM) in RAW 264.7 cells (scale bar = 20 μm). (b) Fluorescence quantification of **TCFB2** and Mito-Tracker of a selected section (the black line in "Merged" panel) of a RAW 264.7 cell. Excitation wavelength for Mito-Tracker Green and **TCFB2** is 489 and 579 nm, respectively. Emission wavelength for Mito-Tracker Green and **TCFB2** is 506 and 603 nm, respectively. The cell nuclei were stained by Hoechst 33342.

We would like to thank the EPSRC and the University of Bath for funding. A. C. S. and J. E. G. thank the EPSRC for studentships. T. D. J. wishes to thank the Royal Society for a Wolfson Research Merit Award. NMR characterisation facilities were provided through the Chemical Characterisation and Analysis Facility (CCAF) at the University of Bath (www.bath.ac.uk/ccaf). The EPSRC UK National Mass Spectrometry Facility at Swansea University is thanked for analyses. X.-P. He thanks the National Natural Science Foundation of China (21722801 and 21572058), the Science and Technology Commission of Shanghai Municipality (15540723800), the Fundamental Research Funds for the Central Universities (222201717003) and the Shanghai Rising-Star Program (16QA1401400) (to X.-P. He) for financial support. The Catalysis And Sensing for our Environment (CASE) network is thanked for research exchange opportunities. T. D. J. thanks ECUST for a guest professorship. Professors Jia Li and Yi Zang are thanked for their helpful advice on the cellular experiments. All data supporting this study are provided as supplementary information accompanying this paper.

Conflicts of interest

There are no conflicts to declare.

Notes and references

1 P. Pacher, J. S. Beckman and L. Liaudet, *Physiol. Rev.*, 2007, **87**, 315.
2 J. S. Beckman and W. H. Koppenol, *Am. J. Physiol.: Cell Physiol.*, 1996, **271**, C1424.
3 A. Weidinger and A. V. Kozlov, *Biomolecules*, 2015, **5**, 472.
4 P. Ascenzi, A. di Masi, C. Sciorati and E. Clementi, *BioFactors*, 2010, **36**, 264.
5 H. Ischiropoulos and J. S. Beckman, *J. Clin. Invest.*, 2003, **111**, 163.
6 P. Sarchielli, F. Galli, A. Floridi and V. Gallai, *Amino Acids*, 2003, **25**, 427.
7 D. A. Wink, Y. Vodovotz, J. Laval, F. Laval, M. W. Dewhirst and J. B. Mitchell, *Carcinogenesis*, 1998, **19**, 711.
8 A. C. Sedgwick, X. L. Sun, G. Kim, J. Yoon, S. D. Bull and T. D. James, *Chem. Commun.*, 2016, **52**, 12350.
9 Z. N. Sun, H. L. Wang, F. Q. Liu, Y. Chen, P. K. H. Tam and D. Yang, *Org. Lett.*, 2009, **11**, 1887.
10 X. Li, R.-R. Tao, L.-J. Hong, J. Cheng, Q. Jiang, Y.-M. Lu, M.-H. Liao, W.-F. Ye, N.-N. Lu, F. Han, Y.-Z. Hu and Y.-H. Hu, *J. Am. Chem. Soc.*, 2015, **137**, 12296.
11 F. B. A. Yu, P. Li, G. Y. Li, G. J. Zhao, T. S. Chu and K. L. Han, *J. Am. Chem. Soc.*, 2011, **133**, 11030.
12 F. B. Yu, P. Li, B. S. Wang and K. L. Han, *J. Am. Chem. Soc.*, 2013, **135**, 7674.
13 D. Cheng, Y. Pan, L. Wang, Z. B. Zeng, L. Yuan, X. B. Zhang and Y. T. Chang, *J. Am. Chem. Soc.*, 2017, **139**, 285.

14 L. Yuan, W. Y. Lin, K. B. Zheng, L. W. He and W. M. Huang, *Chem. Soc. Rev.*, 2013, **42**, 622.
15 R. Weissleder, *Nat. Biotechnol.*, 2001, **19**, 316.
16 A. Sikora, J. Zielonka, M. Lopez, J. Joseph and B. Kalyanaraman, *Free Radical Biol. Med.*, 2009, **47**, 1401.
17 X. Sun, Q. Xu, G. Kim, S. E. Flower, J. P. Lowe, J. Yoon, J. S. Fossey, X. Qian, S. D. Bull and T. D. James, *Chem. Sci.*, 2014, **5**, 3368.
18 S. Palanisamy, P. Y. Wu, S. C. Wu, Y. J. Chen, S. C. Tzou, C. H. Wang, C. Y. Chen and Y. M. Wang, *Biosens. Bioelectron.*, 2017, **91**, 849.
19 Y. H. Yang, J. L. Liu, H. Y. Xiao, Z. Zhen and S. H. Bo, *Dyes Pigm.*, 2017, **139**, 239.
20 W. Shu, L. G. Yan, Z. K. Wang, J. Liu, S. Zhang, C. Y. Liu and B. C. Zhu, *Sens. Actuators, B*, 2015, **221**, 1130.
21 Y. J. Wang, Y. Shi, Z. Y. Wang, Z. F. Zhu, X. Y. Zhao, H. Nie, J. Qian, A. J. Qin, J. Z. Sun and B. Z. Tang, *Chem. – Eur. J.*, 2016, **22**, 9784.
22 Y. R. Wang, L. Feng, L. Xu, Y. Li, D. D. Wang, J. Hou, K. Zhou, Q. Jin, G. B. Ge, J. N. Cui and L. Yang, *Chem. Commun.*, 2016, **52**, 6064.
23 B. C. Zhu, H. Kan, J. K. Liu, H. G. Liu, Q. Wei and B. Du, *Biosens. Bioelectron.*, 2014, **52**, 298.
24 C. Y. Li, M. Li, Y. Li, Z. S. Shi, Z. J. Li, X. B. Wang, J. Sun, J. W. Sun, D. M. Zhang and Z. C. Cui, *J. Mater. Chem. C*, 2016, **4**, 8392.
25 T. Yu, G. X. Yin, P. Yin, Y. Zeng, H. T. Li, Y. Y. Zhang and S. Z. Yao, *RSC Adv.*, 2017, **7**, 24822.
26 M. Ipuy, C. Billon, G. Micouin, J. Samarut, C. Andraud and Y. Bretonniere, *Org. Biomol. Chem.*, 2014, **12**, 3641.
27 E. W. Miller, A. E. Albers, A. Pralle, E. Y. Isacoff and C. J. Chang, *J. Am. Chem. Soc.*, 2005, **127**, 16652.
28 B. C. Dickinson, C. Huynh and C. J. Chang, *J. Am. Chem. Soc.*, 2010, **132**, 5906.
29 A. Vazquez-Torres, J. Jones-Carson and E. Balish, *Infect. Immun.*, 1996, **64**, 3127.
30 M. D. Brand, C. Affourtit, T. C. Esteves, K. Green, A. J. Lambert, S. Miwa, J. L. Pakay and N. Parker, *Free Radical Biol. Med.*, 2004, **37**, 755.
31 X.-P. He, Y. Zang, T. D. James, J. Li, G.-R. Chen and J. Xie, *Chem. Commun.*, 2017, **53**, 82.
32 J. Zhang, Y. Fu, H.-H. Han, Y. Zang, J. Li, X.-P. He, B. L. Feringa and H. Tian, *Nat. Commun.*, 2017, **8**, 987.

ChemComm

COMMUNICATION

View Article Online
View Journal | View Issue

Cite this: *Chem. Commun.*, 2018, 54, 4786

Received 28th February 2018,
Accepted 16th April 2018

DOI: 10.1039/c8cc01661e

rsc.li/chemcomm

Long-wavelength TCF-based fluorescence probes for the detection and intracellular imaging of biological thiols†

Adam C. Sedgwick, *[a] Jordan E. Gardiner,[a] Gyoungmi Kim,[b] Maksims Yevglevskis,[c] Matthew D. Lloyd,[c] A. Toby A. Jenkins,[a] Steven D. Bull, *[a] Juyoung Yoon *[b] and Tony D. James *[a]

Two 'turn on' TCF-based fluorescence probes were developed for the detection of biological thiols (TCF-GSH and TCFCl-GSH). TCF-GSH was shown to have a high sensitivity towards glutathione (GSH) with a 0.28 μM limit of detection. Unfortunately, at higher GSH concentrations the fluorescence intensity of TCF-GSH decreased and toxicity was observed for TCF-GSH in live cells. However, TCFCl-GSH was shown to be able to detect GSH at biologically relevant concentrations with a 0.45 μM limit of detection. No toxicity was found for TCFCl-GSH and a clear 'turn on' with good photostability was observed for the exogenous addition of GSH, Cys and HCys. Furthermore, TCFCl-GSH was used to evaluate the effects of drug treatment on the levels of GSH in live cells.

Glutathione (GSH), cysteine (Cys) and homocysteine (HCys) play a vital role in maintaining the biological redox homeostasis.[1,2] GSH is a natural tripeptide (γ-L-glutamyl-L-cysteinyl-glycine), which exists in the thiol reduced form (GSH) and disulphide-oxidised (GSSG) form.[2] GSH is the predominant form, which exists in millimolar concentrations in most cells where it functions as an antioxidant.[3] Elevated levels of GSH are common in the presence of oxidative stress and the susceptibility of a cell towards reactive oxygen or nitrogen species (ROS/RNS) largely depends on the concentration of intracellular GSH.[4–7] Therefore, the change in the level of GSH concentration has been associated with a number of diseases such as AIDS, liver damage, cancer and neurodegenerative disease (Alzheimer's disease).[6,7] Interestingly, it was reported that at early stages of cell proliferation (S, G_2 and M phases), GSH was found to localise at the nucleus. This was believed to prevent apoptosis and provide a reduced environment for transcription factors to bind to DNA.[8]

[a] *Department of Chemistry, University of Bath, Bath, BA2 7AY, UK. E-mail: t.d.james@bath.ac.uk, s.d.bull@bath.ac.uk*
[b] *Department of Chemistry and Nano Science, Ewha Womans University, Seoul 120-750, Korea. E-mail: jyoon@ewha.ac.kr*
[c] *Drug & Target Development, Department of Pharmacy & Pharmacology, University of Bath, Claverton Down, Bath, BA2 7AY, UK*

† Electronic supplementary information (ESI) available: All data supporting this study. See DOI: 10.1039/c8cc01661e

With our research, we are interested in the development of reaction based fluorescent probes for the detection of biologically relevant species to be used as powerful tools for the understanding of diseases.[9–13] Currently, a number of fluorescent probes exist for the detection of biological thiols.[14–20] However, long excitation/emission wavelength fluorescent probes are highly desirable as they allow deeper tissue penetration, minimal background auto-fluorescence from proteins and photodamage to the biological samples. Therefore, in this work we looked to develop TCF-based systems for the long wavelength detection of GSH.[11]

TCF-based fluorophores have an internal charge transfer (ICT) donor–π–acceptor (D–π–A) structure with long emission wavelengths (see ESI† – Scheme S1). As a result, TCF fluorophores have been used in many applications such as non-linear optic chromophores and fluorescent probes.[21–25] Hilderbrand *et al.* previously developed a 'turn on' sulfonamide based TCF fluorescent probe for the detection of biological thiols.[26] However, a PEG unit was required to provide aqueous solubility and cell permeability. The probe was successfully shown to detect biological thiols in 3T3 cells. We believed the synthesis of the analogous sulfonate ester would overcome the need for a PEG unit and provide a much simpler synthesis. The TCF fluorophore unit was synthesised as previously reported using the reaction of 3-hydroxy-3-methyl-2-butanone, malonitrile and NaOEt in EtOH. With the TCF unit in hand, the (D–π–A) systems **TCF-OH** and **TCFCl-OH** were isolated in high yield using microwave reaction conditions.[27] The **TCF** phenols were then reacted with 2,4-dinitrobenzenesulfonylchloride to afford the desired fluorescent probes **TCF-GSH** and **TCFCl-GSH** in satisfactory yields (55% and 64%) (Fig. 1).

On the addition of GSH, both probes **TCF-GSH** and **TCFCl-GSH** change colour from yellow to purple (see ESI† – Fig. S1 and S2). We evaluated the fluorescence behaviour of **TCF-GSH**, in pH 8.0 buffer solution (20% v/v DMSO) (see ESI†–Fig. S3 and S4). Interestingly, 20% v/v DMSO was required for the reaction between the probe and the chosen biological thiol to take place. We then evaluated **TCF-GSH** for the detection of GSH, given that it is the most predominant biological thiol in cells.

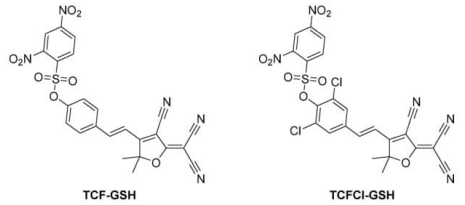

Fig. 1 TCF-based fluorescent probes for the detection of biological thiols (**TCF-GSH** and **TCFCl-GSH**).

Remarkably, **TCF-GSH** was very sensitive towards GSH producing a full 'turn on' fluorescence response in the presence of 25 μM GSH. Unfortunately, at concentrations >50 μM the fluorescence intensity of **TCF-GSH** began to drop dramatically. This is due to attack of the TCF fluorophores by nucleophiles (Fig. 2)[28] (see ESI† – Fig. S5–S11).

We then evaluated the selectivity of **TCF-GSH** towards other biologically relevant thiols and amino acids (see ESI† – Fig. S12 and S13). As predicted, **TCF-GSH** reacted with the other sulphydryl (R-SH) compounds, Cys and HCys with Cys producing the largest fluorescent response. However, the overall concentrations of both Cys and HCys are low in comparison to GSH in cells.[29,30] **TCF-GSH** demonstrated an excellent selectivity for GSH against other amino acids. This excellent selectivity permitted the evaluation of **TCF-GSH** for the detection of exogenous and endogenously generated thiols in live cells. Sadly, despite **TCF-GSH** being sensitive towards GSH, we only observed a clear 'off–on' response for the exogenous addition of Cys in HeLa cells. Furthermore, **TCF-GSH** was shown to have toxicity in cell viability experiments (see ESI† – Fig. S16 and S17). **TCF-GSH** is therefore unsuitable for cell imaging experiments for the detection of biothiols. Interestingly, cellular imaging experiments did not require any additional additives to compensate for the 20% v/v DMSO required in the *in vitro* experiments.

We therefore turned our attention towards the fluorescence properties of **TCFCl-GSH**. In order to produce a fluorescence

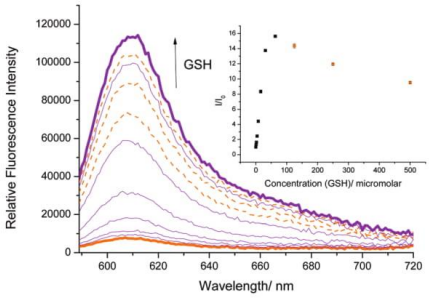

Fig. 2 Fluorescence spectra of **TCF-GSH** (5 μM) with addition of GSH (0–500 μM) and 15 min wait between additions in PBS buffer solution, 20% v/v DMSO, pH 8.00 at 25 °C. λ_{ex} = 560 ± 15 nm. Orange dashed lines indicate fluorescence decrease at high GSH concentrations.

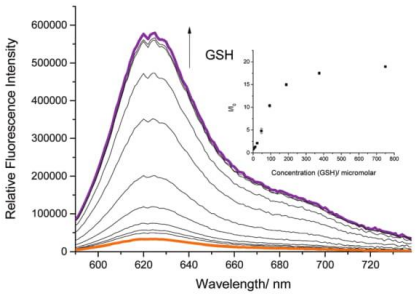

Fig. 3 Fluorescence spectra of **TCFCl-GSH** (5 μM) with addition of GSH (0–750 μM) and 15 min wait between additions in PBS buffer solution, 20% v/v DMSO, pH 8.00 at 25 °C. λ_{ex} = 560 ± 15 nm.

response, **TCFCl-GSH** also required pH 8.0 buffer solution (20% v/v DMSO). However, **TCFCl-GSH** was shown to be less sensitive towards the biological thiols and no decrease in fluorescence intensity was observed at higher concentrations (Fig. 3).

We then evaluated the selectivity of **TCFCl-GSH** towards other biologically relevant thiols and amino acids (see ESI† – Fig. S14 and S15). As for **TCF-GSH**, **TCFCl-GSH** reacted with the R-SH containing amino acids Cys and HCys. While excellent selectivity for GSH was observed against other amino acids. This permitted the evaluation of **TCFCl-GSH** for the detection of exogenous and endogenous thiols in live cells. As shown in

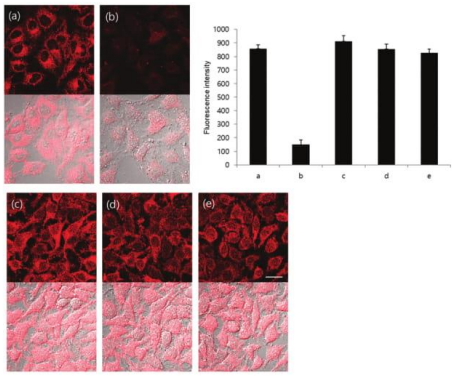

Fig. 4 Fluorescence imaging in live cells. HeLa cells were preincubated with 0.2 mM NMM for 20 min and washed with Dulbecco's phosphate-buffered saline (DPBS) and incubated with 200 μM cysteine, homocysteine and GSH-MEE for 20 min. After washing with DPBS, cells were stained with 20 μM **TCFCl-GSH** for 20 min and fluorescence images acquired by confocal microscopy. (a) Only **TCFCl-GSH**, (b) NMM + **TCFCl-GSH**, (c) NMM + cysteine + **TCFCl-GSH**, (d) NMM + homocysteine + **TCFCl-GSH** and (e) NMM + GSH-MEE + **TCFCl-GSH**. Top: Fluorescence image (ex. 559 nm/em. 575–675 nm), bottom: merged image with DIC. Scale bar: 20 μm. Quantitative data of fluorescence intensity was calculated by FV10-ASW 4.0 software and measured per one cell. Results are expressed as mean ± standard deviation of three independent experiments.

Fig. 4 (see ESI† – Fig. S18 and S19 for **TCF-GSH**), **TCFCl-GSH** displayed an already strong fluorescence response in live cells Fig. 4(a). This observation was due to the presence of endogenous thiols reacting with **TCFCl-GSH**. However, pre-treatment of HeLa cells with the thiol reactive *N*-methylmaleimide (NMM) led to the reduction of endogenous thiols and therefore low fluorescence intensity was observed when **TCFCl-GSH** was added Fig. 4(b). The addition of 200 μM of an exogenous thiol (Cys, HCys, or GSH-Methyl ester) led to a clear change in fluorescence intensity demonstrating the ability of **TCFCl-GSH** to detect thiols in cells.

We then evaluated the ability of **TCFCl-GSH** to detect changes in the concentration levels of endogenous thiols through the addition of drugs and reactive oxygen species (ROS) such as H_2O_2. It is well known that GSH protects against drug induced toxicity and acts as a ROS scavenger. Therefore in Fig. 5 and 6 (see ESI† – Fig. S20 and S21 for **TCF-GSH**), the addition of H_2O_2 (500 μM) or Cisplatin (200 μM) resulted in the depletion of the endogenous thiols and consequently reduced fluorescence was observed when **TCFCl-GSH** was added. Subsequently, the addition of the GSH producing drug *N*-acetylcysteine[31] recovered the GSH levels resulting in a large increase in fluorescence intensity.

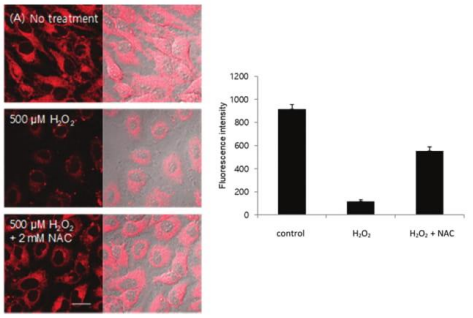

Fig. 5 Intracellular fluorescence change caused by drug treatment. (A) HeLa cells were incubated with 500 μM H_2O_2 with or without 2 mM NAC for 6 h and stained with 20 μM **TCFCl-GSH** for 20 min. Quantitative data of fluorescence intensity was calculated by FV10-ASW 4.0 software and measured per one cell. Results are expressed as mean ± standard deviation of three independent experiments. Ex. 559 nm/em. 575–675 nm. Scale bar: 20 μm.

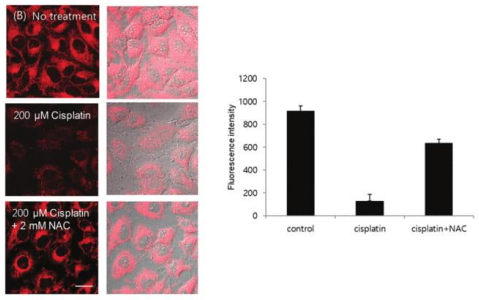

Fig. 6 Intracellular fluorescence change caused by drug treatment. (B) HeLa cells were incubated with 200 μM cisplatin with or without 2 mM NAC for 6 h and stained with 20 μM **TCFCl-GSH** for 20 min. Quantitative data of fluorescence intensity was calculated by FV10-ASW 4.0 software and measured per one cell. Results are expressed as mean ± standard deviation of three independent experiments. Ex. 559 nm/em. 575–675 nm. Scale bar: 20 μm.

In summary, two 'turn on' TCF-based fluorescent probes have been developed for the detection of biological thiols (**TCF-GSH** and **TCFCl-GSH**). **TCF-GSH** was shown to have a high sensitivity towards glutathione (GSH). Unfortunately, at higher GSH concentrations the fluorescence intensity of **TCF-GSH** decreased and toxicity was observed in live cells making it unsuitable for cellular imaging. However, **TCFCl-GSH** was shown to be able to detect GSH at biological relevant concentrations. Also, no toxicity was observed for **TCFCl-GSH** and a clear 'turn on' response was observed upon the exogenous addition of GSH, Cys and HCys. Furthermore, **TCFCl-GSH** was able to evaluate the effects of drug treatment and the addition of ROS (H_2O_2) on live cells, both of which resulted in a depletion of cellular GSH levels and a reduced fluorescence intensity. Subsequent, addition of NAC increased the GSH levels and enhanced the observed fluorescence intensity.

We would like to thank the EPSRC, the University of Bath and Prostate Cancer UK (PG14-009) for funding. ACS and JEG thank the EPSRC for studentships. TDJ wishes to thank the Royal Society for a Wolfson Research Merit Award. NMR characterisation facilities were provided through the Chemical Characterisation and Analysis Facility (CCAF) at the University of Bath (www.bath.ac.uk/ccaf). The EPSRC UK National Mass Spectrometry Facility at Swansea University is thanked for analyses. JY thanks the support from the National Research Foundation of Korea (NRF), which was funded by the Korea government (MSIP) (No. 2012R1A3A2048814). ACS, MY, MDL and TDJ are members of the Cancer Research@Bath (CR@B) network.

Conflicts of interest

No conflicts of interest.

Notes and references

1 L. B. Poole, *Free Radical Biol. Med.*, 2015, **80**, 148–157.
2 G. Y. Wu, Y. Z. Fang, S. Yang, J. R. Lupton and N. D. Turner, *J. Nutr.*, 2004, **134**, 489–492.
3 S. C. Lu, *Mol. Aspects Med.*, 2009, **30**, 42–59.
4 J. S. Armstrong, K. K. Steinauer, B. Hornung, J. M. Irish, P. Lecane, G. W. Birrell, D. M. Peehl and S. J. Knox, *Cell Death Differ.*, 2002, **9**, 252–263.
5 M. Valko, D. Leibfritz, J. Moncol, M. T. D. Cronin, M. Mazur and J. Telser, *Int. J. Biochem. Cell Biol.*, 2007, **39**, 44–84.
6 C. B. Pocernich and D. A. Butterfield, *Biochim. Biophys. Acta*, 2012, **1822**, 625–630.
7 N. Ballatori, S. M. Krance, S. Notenboom, S. J. Shi, K. Tieu and C. L. Hammond, *Biol. Chem.*, 2009, **390**, 191–214.
8 J. Markovic, C. Borras, A. Ortega, J. Sastre, J. Vina and F. V. Pallardo, *J. Biol. Chem.*, 2007, **282**, 20416–20424.
9 A. C. Sedgwick, R. S. L. Chapman, J. E. Gardiner, L. R. Peacock, G. Kim, J. Yoon, S. D. Bull and T. D. James, *Chem. Commun.*, 2017, **53**, 10441–10443.
10 A. C. Sedgwick, X. L. Sun, G. Kim, J. Yoon, S. D. Bull and T. D. James, *Chem. Commun.*, 2016, **52**, 12350–12352.

11 A. C. Sedgwick, H. H. Han, J. E. Gardiner, S. D. Bull, X. P. He and T. D. James, *Chem. Commun.*, 2017, **53**, 12822–12825.
12 A. C. Sedgwick, H.-H. Han, J. E. Gardiner, S. D. Bull, X.-P. He and T. D. James, *Chem. Sci.*, 2018, **9**, 3672–3676.
13 A. C. Sedgwick, A. Hayden, B. Hill, S. D. Bull, R. B. P. Elmes and T. D. James, *Front. Chem. Sci. Eng.*, 2018, DOI: 10.1007/s11705-017-1697-0.
14 D. Wu, A. C. Sedgwick, T. Gunnlaugsson, E. U. Akkaya, J. Yoon and T. D. James, *Chem. Soc. Rev.*, 2017, **46**, 7105–7123.
15 S. Q. Wang, S. L. Shen, Y. R. Zhang, X. Dai and B. X. Zhao, *Chin. J. Org. Chem.*, 2014, **34**, 1717–1729.
16 L. L. Yin, Z. Z. Chen, L. L. Tong, K. H. Xu and B. Tang, *Chin. J. Anal. Chem.*, 2009, **37**, 1073–1081.
17 Y. M. Yang, Q. Zhao, W. Feng and F. Y. Li, *Chem. Rev.*, 2013, **113**, 192–270.
18 Y. Qi, Y. Huang, B. W. Li, F. Zeng and S. Z. Wu, *Anal. Chem.*, 2018, **90**, 1014–1020.
19 J. Li, Y. Kwon, K. S. Chung, C. S. Lim, D. Lee, Y. K. Yue, J. Yoon, G. Kim, S. J. Nam, Y. W. Chung, H. M. Kim, C. X. Yin and J. H. Ryu, *Theranostics*, 2018, **8**, 1411–1420.
20 L. Chen, J.-S. Park, D. Wu, C.-H. Kim and J. Yoon, *Sens. Actuators, B*, 2018, **262**, 306–312.
21 Y. J. Wang, Y. Shi, Z. Y. Wang, Z. F. Zhu, X. Y. Zhao, H. Nie, J. Qian, A. J. Qin, J. Z. Sun and B. Z. Tang, *Chem. – Eur. J.*, 2016, **22**, 9784–9791.
22 W. Shu, L. G. Yan, Z. K. Wang, J. Liu, S. Zhang, C. Y. Liu and B. C. Zhu, *Sens. Actuators, B*, 2015, **221**, 1130–1136.
23 Y. H. Yang, J. L. Liu, H. Y. Xiao, Z. Zhen and S. H. Bo, *Dyes Pigm.*, 2017, **139**, 239–246.
24 T. Yu, G. X. Yin, P. Yin, Y. Zeng, H. T. Li, Y. Y. Zhang and S. Z. Yao, *RSC Adv.*, 2017, **7**, 24822–24827.
25 B. C. Zhu, H. Kan, J. K. Liu, H. G. Liu, Q. Wei and B. Du, *Biosens. Bioelectron.*, 2014, **52**, 298–303.
26 J. Bouffard, Y. Kim, T. M. Swager, R. Weissleder and S. A. Hilderbrand, *Org. Lett.*, 2008, **10**, 37–40.
27 M. Ipuy, C. Billon, G. Micouin, J. Samarut, C. Andraud and Y. Bretonniere, *Org. Biomol. Chem.*, 2014, **12**, 3641–3648.
28 W. L. Wu, Z. Y. Wang, X. Dai, J. Y. Miao and B. X. Zhao, *Sci. Rep.*, 2016, **6**, 25315.
29 R. Banerjee, *J. Biol. Chem.*, 2012, **287**, 4397–4402.
30 P. Ganguly and S. F. Alam, *J. Nutr.*, 2015, **14**, 6.
31 S. Y. Sun, *Cancer Biol. Ther.*, 2010, **9**, 109–110.